UK UNLIMITED

ATOMIC WEAPONS ESTABLISHMENT

AWE Report No. O 4/94

Seismic Source Discrimination at Teleseismic Distances using Radiation Patterns: Concepts and Feasibility Study

R G Pearce*
R M Rogers†

*Department of Geology and Geophysics, University of Edinburgh, Grant Institute, West Mains Road, Edinburgh, EH9 3JW

†Now at: Computing Services, PO Box 335, Staffordshire University Beaconside, Stafford, ST18 0DP

Recommended for issue by: A Douglas, Group Leader, Seismic Detection Group.

Approved for issue by: H P S Powell, Manager, Systems Engineering Division.

CONTENTS

SUMMARY

We examine how to extract the maximum information about the seismic source from teleseismic *P*-wave seismograms which may be close to the detection threshold. It is concluded that the most basic measurements which can be utilised are the relative amplitudes and polarities of *P* and the surface reflections *pP* and *sP*, which are governed by the form of the *P*- and *S*-wave source radiation patterns. We first present some concepts and definitions, borrowed in part from the relative amplitude method for determining earthquake focal mechanisms, which has been applied successfully to presumed double-couple sources. We then present a theoretical study of the probability of observing different *P*-wave seismograms ranging through all relative amplitudes of *P*, *pP* and *sP*, given a specified type of source, with unknown orientation but with all orientations assumed to be equally likely. The full range of source types described by the moment tensor are considered, including the compensated linear vector dipole (CLVD), negative CLVD, tensile crack and vector dipole, as well as the double-couple earthquake and the explosion. The form of these probability density functions is examined on a specially designed graphical display referred to as a "compatibility plot", to investigate the potential for using this relative amplitude information as a source discriminant. Numerically generated probability density functions are presented for a wide range of source types "observed" at a range of teleseismic distances. These provide a basis for quantifying the extent to which relative amplitude data can be used to discriminate between particular types of source. The best situation for discriminating between different types of source occurs if they create seismogram probability density functions which are mutually exclusive — i.e. any seismogram observed could only have been generated by one of the possible types. It is found that this ideal situation only occurs for a few unimportant source types. However, it is found that, for every source type, large ranges of seismograms are predicted to be either prohibited or highly unexpected. This means that relative amplitude data can in principle provide clear discrimination in some circumstances. This is of special interest, since such a discriminant is independent of spectral or magnitude data used by some other discriminants, and utilises radiation pattern information in a systematic way. Finally we consider how this method might be applied, in particular to earthquake/explosion discrimination.

1. INTRODUCTION

It has been recognised that the relative amplitudes of seismic phases observed at teleseismic distances provide sufficient information to estimate the source radiation pattern, and hence determine the source mechanism of a presumed earthquake ([1] and [2]). An attempt has also been made to quantify the information on the source radiation pattern which these relative amplitude measurements contain [3]. Here we present a theoretical study of the relation between the relative amplitudes and polarities of the phases *P*, *pP* and *sP* (figure 1) which may be observed on a seismogram, and the *P*- and *S*-wave radiation patterns characteristic of various types of seismic source. The motivation for this is to establish the extent to which relative amplitude information may be useful in discriminating between different source types. We have been encouraged by previous success in determining earthquake source mechanisms from relative amplitudes, and by the success achieved using relative amplitudes to discriminate between earthquake seismograms and those resulting from multiple explosions.

The problem of discriminating between seismic sources is central to the verification of any treaty banning underground nuclear tests. It requires evidence from as diverse a range of discriminants as possible to minimise ambiguity and uncertainty. Sometimes a seismic source cannot be identified by conventional seismic discriminants such as the m_b:M_S criterion, either because the source is too small and distant from recording sites for surface waves to be detected, or (exceptionally) because its surface waves give an anomalous m_b:M_S ratio despite being well recorded. Usually, short period *P*-wave seismograms then constitute the only data available; we must identify all those characteristics of such seismograms which relate to the source, and we must then establish how these characteristics can be measured and interpreted most effectively. Methods which do not take full account of the radiation pattern fail in both of these aims.

One of the early empirical discriminants was the "complexity criterion", which assumes that the teleseismically recorded *P*-wave seismogram from an earthquake is more complicated than that from a comparable explosion. Complex explosion signals (e.g. from LONGSHOT which was fired over the structural

complexities of a subduction zone) and simple earthquake records, which conspired to render this discriminant unreliable, are now partly understood. We now know, for example, that signals derived from the passage of surface reflected phases through structures above the source contribute to the relative complexity of earthquake seismograms, since earthquakes are in general deeper than explosions. Radiation pattern studies can explain why sometimes we do not get surface reflections at all — one explanation of a simple earthquake seismogram.

If radiation pattern information were found to offer a useful discriminant, then it would contribute to the diversity of discriminants, and may be the only seismic discriminant for some smaller sources. The directional dependence of the seismic source radiation is utilised to some extent by other discriminants such as the *P*-wave first motion method, the complexity criterion and the ratio of body wave and surface wave magnitudes (the m_b:M_S criterion). The explicit application of radiation patterns to earthquake/explosion discrimination cannot be attempted until the overall behaviour of radiation pattern information is investigated systematically, and that is achieved in this report using the relative amplitude method.

We first summarise the relative amplitude method and its relevance to the utilisation of radiation pattern information obtained from seismograms (section 2). In section 3 some quantities useful in the analysis of radiation pattern information are defined, and some special terminology is introduced. Some of these ideas are taken or adapted from the relative amplitude method of determining earthquake focal mechanisms previously introduced. (A glossary of special terms used in this report is given in Appendix A.) In section 4 the "compatibility plot" which represents all possible *P*, *pP* and *sP* relative amplitudes is described. We examine theoretically the likelihood of observing a *P*-wave seismogram exhibiting different relative amplitudes of *P*, *pP* and *sP* from different types of source. In section 5 results are presented for many types of single seismic source at non-zero depth, including the double couple. The analysis in section 5 provides sufficient information to evaluate relative amplitudes as a means of discrimination; the additional power of discrimination achievable by combining the results for individual stations is considered qualitatively in section 6. Conclusions are drawn in section 7.

2. THE RELATIVE AMPLITUDE METHOD AND ITS RELEVANCE TO SOURCE DISCRIMINATION — PROGRAMS FALT, RAMP AND GRAM

Amplitude measurements relating the three phases *P*, *pP* and *sP* form the basis of a method to determine the orientations of presumed double-couple earthquakes, as described in [1] and [2]; the computer program FALT [4] was developed for this purpose. Examples of the application of this method are given in the references. The method has been applied to many earthquakes in a variety of situations (see also [5] to [13]). Some of the earthquakes were large, but many were only just above the teleseismic detection threshold.

The method has since been generalised to constrain five of the six independent components of the moment tensor ([14] and [15]). These five components describe the type of source model in addition to its orientation (but exclude its overall size, which corresponds to the sixth moment tensor component and which cannot be determined from relative amplitudes). This generalisation removes the double-couple assumption, and is embodied in a computer program RAMP [16]. Additional examples using this generalisation of the method appear in [17] to [19].

An alternative version of the method has been developed which differs from RAMP only in its treatment of uncertainties in the observed relative amplitudes. In FALT and RAMP, each amplitude is assumed to lie with equal likelihood anywhere between specified upper and lower bounds. In some circumstances it is justifiable to assume that amplitudes near the midpoint between these limits are more likely to represent the true value. To allow for this, the uniform likelihood is replaced by a Gaussian likelihood function in amplitude. This approach is referred to as the Gaussian relative amplitude method (GRAM) and is described in [16] and [20]. A consequence of this approach is that a single 'best-fit' solution is always obtained, rather than a zone of equally likely source mechanisms.

The moment tensor is used as the basis for defining the set of source types which we may wish to discriminate. It is widely used, and includes the common source types such as the double couple and explosion. However, it excludes sources whose equivalent force systems, and hence radiation patterns, are of a higher angular order than two. There is no evidence that such complex sources are important in practice, and even if they were, seismological observations would usually be insufficient to resolve such complexity.

The relative amplitude method and its generalisation to non-double-couple sources is described adequately elsewhere ([1], [2], [4], [14] to [16] and [20]). The method has been used to determine the mechanism of a known or assumed earthquake. Here, however, we explore its ability to discriminate between sources; we therefore need to minimise the *a priori* assumptions about the source. The relative amplitude method may be better able to do this than other discrimination methods because radiation patterns differ in a major way between different types of source. While other methods of determining earthquake focal mechanisms may assume that the source is a double couple, here we aim to test observations against a range of possible sources in different orientations, to establish which, if any, of their radiation patterns is consistent with the observed relative amplitude and polarity data.

P-wave seismograms within the teleseismic range contain information about the source which is, in essence, simple in form. The direct *P* wave is followed closely by surface reflected *P* and *S* waves, *pP* and *sP* respectively (figure 1). These phases originate from diverse points on the upper and lower focal hemispheres, and comparison of their amplitudes provides information on the angular dependence of both the *P*- and *S*-wave radiation. The phase identifications themselves are made on the seismograms with due regard to mutual compatibility of surface reflection arrival times at different stations.

The full exploitation of these intrinsically simple observations is important because the amplitudes and polarities of these three phases represent most of the information relating to the source type and its orientation which is contained within a single *P*-wave seismogram observed at teleseismic distances. It is essential to extract this information without relying on the absolute amplitude of the signals, which carries a large uncertainty introduced by the attenuation of seismic waves during propagation. This uncertainty affects the determination of radiation pattern much more than in the determination of magnitude, because magnitude can be averaged over observations at several stations, and is proportional to the log of the amplitude.

Application of the relative amplitude method to a wide range of sources has already given us valuable experience in dealing with the practical aspects of translating poor signal-to-noise ratio relative amplitude observations into focal mechanism solutions with appropriate confidence limits. Relative amplitudes have been used successfully to determine the mechanisms of presumed double-couple (earthquake) sources, and to compute earthquake moment tensors with the double-couple assumption relaxed (see above references). Because the polarities and relative amplitudes of *P* and its surface reflections may constitute the only information about the source which is measurable at teleseismic distances, this information becomes crucial in the discrimination of smaller sources. Relative amplitude and polarity information relates not to spectral characteristics of the source, or to its magnitude, but to the form of the *P* and *S* radiation patterns alone. We shall consider how this residual information can best be exploited when the available signals are close to the noise level, and we show that it should be possible to derive something about the form of the radiation even for the smallest of teleseismically recorded sources.

3. DEFINITIONS, TERMINOLOGY AND BASIC RELATIONS

3.1 Essential features of the source model — "source type" and "source orientation"; the "vectorplot"

We describe the seismogenic mechanism, for example the double couple, as the "source type", and its orientation with respect to the Earth's surface as the "source orientation". Any sources with the same source type thus have identical radiation patterns when appropriately reoriented. This approach has the advantage of revealing the source type explicitly.

A variety of approaches may be used to define a range of source types. We use the conventional diagonalised moment tensor for this purpose in section 3.4. The source orientation can always be defined by three angles. We use the three angles δ, σ and ψ as defined in figure 2. For the double-couple source these angles correspond respectively to the dip and strike of the fault plane, and the slip angle in the fault plane.

The definition of these angles follows [1]. For the double couple ψ corresponds to the slip of the foot wall of the fault if the dip is less than 90°. This definition was chosen to agree with that adopted in the synthetic seismogram program of Douglas et al [21] but this convention is opposite to that used by other authors, who define the slip angle (or "rake") with respect to the hanging wall (see for example Aki and

Richards [22] page 106). Most moment tensor publications (for example references [23] to [25]) use the Aki and Richards convention. The range of the three angles, following [1], are 0 to 180° for δ and ψ, and 0 to 360° for σ. Aki and Richards [22] use 0 to 90° for the dip angle, and $-180°$ to 180° for slip angle (rake).

We represent a source orientation as a vector on a vectorplot as described for the double couple in [1]. A range of orientations therefore plots as a series of vectors corresponding to the equivalent points in the search mesh. A vectorplot is shown in figure 3. It can similarly be used to plot orientations of any source type other than the double couple, as described in [14], and if only a limited range of orientations is of interest, the vectorplot need not cover the whole range in slip angle and dip.

3.2 The "class" of a seismogram — 27 classes of *P*-wave seismogram

For simple shallow sources observed at teleseismic distances the explicit information in the *P*-wave seismogram relating to the source radiation pattern is the relative amplitudes (i.e. the amplitude ratios) and polarities of *P*, *pP* and *sP*. Consequently we use the relative amplitudes and polarities of these three phases to define the seismogram "class". We shall not in general assign quantitative limits to the amplitude ratios of a particular class of seismogram, but for the study of relations between seismogram class and the source radiation pattern which governs it, the separation of seismograms into a discrete number of classes each comprising a specific range of ratios is helpful. We therefore adopt the convention of [2], in which each of the three phases *P*, *pP* and *sP* is classified as either "large and positive", or "large and negative" or "small", giving thirteen possible classes of seismogram, which are defined in figure 4, using the numbering convention of [2].

In [2] the definitions do not take into account the polarity of the complete seismogram. Moreover, only the double couple is considered, and its radiation pattern has the special property that it is unchanged, apart from a 90° rotation about its null axis, if its polarity in all directions is reversed. It follows that a population of randomly oriented double couples has identical properties if the polarity of the radiation pattern is reversed. This means that the likelihood of observing two seismograms which are the same except for an inversion of polarity is identical in the case of a double couple. Hence, when such probabilities are displayed for such a source, no distinction needs to be made between two seismograms which are identical except for the polarity of the whole waveform. This behaviour is not generally true for other source types. We therefore introduce here (by convention) the suffix "positive", or "+ve" for classes describing seismograms where the first "large" phase is positive, and suffix "negative", or "–ve" for classes describing seismograms

in which it is negative. Both sets of classes are shown in figure 4. If the suffix is omitted, this implies reversion to the previous definition covering either case.

We also introduce the "class 0" seismogram, in which all three phases are "small". For relative amplitude data this class strictly does not exist, since if all amplitudes are similar and observed, then they would be regarded as "large". However, the class is of practical importance because there are circumstances in which we might deduce that all three phases are indeed small (i.e. they have all emerged from near to a node in the radiation pattern or have a small surface reflection coefficient). The most important of these circumstances is when we observe an emergent or characterless coda, perhaps with an anomalously low body-wave magnitude compared with other stations. This would suggest that the seismogram is dominated by scattered energy rather than by geometric phases such as *P*, *pP* and *sP*, giving a signal which is conspicuously complex compared with those at other stations. The information implied by a class 0 seismogram has now been incorporated into the relative amplitude method.

It is important to remember that the quantitative limits imposed on each seismogram class in figure 4 have no special significance and do not constitute a rigorous division of seismograms into equal-sized non-overlapping classes. For situations in which it is useful to have a formal definition of "small" and "large" when referring to relative amplitude values, we point out that a uniform division of seismograms into classes based on relative amplitudes should ideally have the effect of dividing the space of relative amplitude values into contiguous and non-overlapping zones, each of equal size in the sense that they all contain the same range of amplitude ratios. Such a condition must be achieved by defining limits on the three amplitude ratios, rather than on the individual amplitudes as is done in figure 4. It is shown in section 4.5 that the numerical values used in figure 4 result in a complete coverage of relative amplitude values, but with overlapping zones of unequal size in relative amplitude space. In fact, a division into equal contiguous non-overlapping areas is

not possible using fixed bounds on amplitude ratios, and our choice of numerical limits represents a close approximation.

3.3 Information content of a seismogram — "quality" and "significance"

Given a teleseismic *P*-wave recording from which a set of *P*, *pP* and *sP* relative amplitude measurements has been made with appropriate confidence limits, it is important to be able to quantify what these measurements can tell us about the source radiation. This is what we broadly define as the "information content" of the seismogram, and it is central to the discrimination capability of relative amplitude measurements.

There are two factors which determine the information content. The first is the accuracy to which the true radiated amplitude at the source can be inferred from the amplitude of that phase observed on the seismogram. More precisely, for each pair of seismic phases we are placing a constraint on the ratio of the signal amplitude radiated in two directions from the source, based upon a constraint imposed on the relative amplitude of two phases measured on the seismogram (figure 1). The severity of this constraint depends upon the width of the amplitude bounds placed upon each phase, and this yields a corresponding permitted range of amplitude ratios for each pair of phases. Clearly, a seismogram for which no constraint can be placed on these amplitude ratios has zero information content. A seismogram for which polarities are certain, and for which amplitudes are closely constrained, has a high information content. Ability to constrain the relative amplitudes is restricted by complex pulse shape, seismic noise and other uncertainties. We refer to these factors collectively as determining the seismogram "quality"; a higher quality seismogram is therefore one from which a higher degree of constraint can be placed on the observed relative amplitudes, and from which more polarities are measurable with certainty. This measure of quality can be defined quantitatively in terms of the proportion of relative amplitude values contained within a given relative amplitude observation. This quantitative treatment is introduced in section 4.1, and determines the shape of the compatibility plot (section 4).

The second factor which determines the information content of a seismogram as defined above is the extent to which a given increment in relative amplitude value constrains the form of the source radiation. The proportion of all possible source types and orientations which is compatible with a relative amplitude observation is strongly dependent upon the relative amplitude value itself — that is, upon the seismogram class. It is this which makes some relative amplitude values much more powerful in constraining the source moment tensor than others.

A measure of the constraint imposed on the source radiation by a given relative amplitude observation can only be defined with respect to a finite population of possible source models, source orientations or other source characteristics, since without *a priori* assumptions the range of possibilities is infinite and the constraint is zero, unless information about the source is total. Our use of the moment tensor itself implies an *a priori* restriction on the source model to a finite range as explained in section 2: the moment tensor defines the source as equivalent to some combination of three mutually orthogonal dipoles. A yet more restricted range might be one source type from within the moment tensor set, such as the double couple, with change in source orientation providing the only variation in radiation permissible. The proportion of radiation patterns compatible with the relative amplitude observation will always be a strong function of the relative amplitude value - that is, of the seismogram class. Depending upon the range of source models being tested, a given class of seismogram may be compatible with a large proportion, a small proportion, or with none of the range, implying different information content relating to the source.

Seismogram quality and seismogram class therefore combine to determine the information content of a relative amplitude observation. Seismograms of a given class will always yield higher information content if they are of higher quality, and information content will vary widely for seismograms of the same quality but different class. For an earthquake, the assumption of a double couple would enable us to reduce the total population of source models to the possible orientations of a single source type - the double couple. If we then asked: "What proportion of presumed double-couple orientations is compatible with a given relative amplitude observation?" then the answer would provide us with an inverse measure of the information content of that seismogram in relation to the chosen population of source models; this measure takes care of both the quality of the seismogram and its class.

In [2], the term "significance" is defined as the proportion of orientations of a presumed double couple which is incompatible with a relative amplitude observation or set of observations; seismograms with a significance approaching 1.0 have a high information content and those approaching zero contain little or no information. Using this definition, the significance is formally shown in equation 3 of [4] to be given by

$$S = 1 - \frac{\sum_{\text{all acceptable orientations}} \sin\delta}{N < \sin\delta >}, \quad 0 < \delta < \pi \qquad (1)$$

where N is the total number of orientations in the search mesh and δ is the dip of the fault plane (figure 2(a)), or its equivalent for source types other than the double couple. The quantity $<\sin\delta>$ is $\sin\delta$ averaged over the angular range of the search which, for the complete range of orientations, is 0 to π and is equal to $2/\pi$. (There is an error in the printing of our equation 1 as it appears in equation 1 of [2] and equation 3 of [4].)

Thus the significance corresponds to one minus that proportion of the solution space which is compatible with the data. A significance of 1.0 (no orientations compatible) indicates that the data are incompatible with the model. This implies either that the observation is in error, or that *a priori* assumptions (e.g. of source type) are incorrect (although *a priori* assumptions may, of course, also be erroneous if the significance is not unity). A significance of 0.0 implies that all the solution space is compatible, and the seismogram contains no information.

It is useful to generalise the definition of "significance" to situations where the source type is not fixed, or where only a subset of orientations is considered. Significance is then defined as the proportion of the chosen source parameter space which is incompatible with a relative amplitude observation or set of observations; this source parameter space may include different source types (section 3.4) and/or orientations, or would be equally valid if some other means of parameterising the source were adopted.

When defining a search mesh the significance measure corresponding to each point must be weighted to compensate for possible unequal spacing of the points within the parameter space. For the three orientation parameters, uniformity of spacing is defined on the basis that all orientations are equally probable. The weighting required for each point in the (δ,σ,ψ) parameter space of figure 3 is embodied in equation 1 and is the origin of the $\sin\delta$ term (see [2] or [4]). The equivalent weighting of source-type parameters requires first a definition of "equal spacing" in these parameters and this is given in section 3.4.

We have now considered how the quality and the class of a seismogram both affect its information content. An amplitude ratio observed on a seismogram relates to a ratio of amplitudes radiated in two directions from the source. This relation is itself dependent upon several aspects of the source-receiver geometry and Earth structure, and these dependencies are considered in section 3.6.

3.4 Classification of source types — the moment tensor, T and k, and the "source-type plot"

To use radiation patterns for discrimination, the *a priori* assumption must be widened to include not only the double-couple source but the range of possible source types which are physically plausible, including the explosion. The range of source models should ideally include the possibility of multiple events, either superposed or spread in time or space. Multiple events could for example be multiple explosions, or an explosion plus tectonic release. As explained in section 2, we include here any source with an equivalent force system corresponding to three mutually orthogonal force dipoles; this corresponds to the conventional moment tensor. We do this for two reasons. First, it represents the most relaxed and physically reasonable assumption that can be contemplated with currently available seismic data at teleseismic or regional distances. Secondly, the superposition of multiple sources which are so close in space and time as not to be resolvable on seismograms, will appear as a single source with a moment tensor corresponding to the sum of the constituent sources — and so is implicitly included in this range of source types. Multiple sources which are more separated will have additional seismic phases to those expected, and the relative amplitude method should help to reveal this by showing that the relative amplitude data are incompatible with expected source types when the seismic phases are incorrectly interpreted.

For a single source we follow [14] and [15], and express the source type as a diagonalised moment tensor, the three diagonal elements corresponding to the sizes of the three orthogonal dipoles comprising the source. To diagonalise the moment tensor we must express it in an appropriately oriented coordinate system which makes the off-diagonal elements of the tensor zero. The coordinate system re-orientation required to achieve this is expressed in terms of the same three angles (δ, σ and ψ) which are used to define the orientation of the double-couple source (see section 3.1 and [1] and [2]). The double couple then simply becomes one of a range of source types. By defining the source type in terms of the diagonalised moment tensor components, and its orientation in terms of the orientation of the corresponding coordinate system, we ensure that the source type and its orientation are expressed separately and explicitly.

We do not use the sizes of the three orthogonal dipoles as the explicit three parameters defining source type. Instead we define an equivalent set of three parameters which is more useful than the dipole sizes because it isolates aspects of the source type which are of special interest. We use k, which is the proportion of the source which is isotropic (i.e. explosive or implosive); T, which describes the form of the constant-volume component of the source, and M, the absolute size of the source (i.e. its scalar moment). This third parameter is simply a scaling factor for the three tensor elements and does not relate to the source type itself. Moreover, it cannot be determined from relative amplitudes. So we ignore M, and assume that the sizes of the three dipoles, or principal moments, are normalised. The definitions of our T and k in terms of the sizes of the three dipoles, referred to as the normalised principal moments M_x, M_y and M_z, are then given by:

$$\begin{bmatrix} M_x \\ M_Y \\ M_z \end{bmatrix} = M \begin{bmatrix} Min\ (2, 2-T) & 0 & 0 \\ 0 & Max\ (-2, -(2+T)) & 0 \\ 0 & 0 & T \end{bmatrix} (1-|k|) + 2Mk \begin{bmatrix} 1 & 0 & 0 \\ 0 & 1 & 0 \\ 0 & 0 & 1 \end{bmatrix} \quad (2)$$

(from equation 1 of [14], with the inclusion of M). Here the principal moments are normalised so that the one with the largest absolute value is equal to $2M$; this ensures that T and k both range between plus and minus unity. The detailed reasons for choosing T and k as explicit variables for source type are given in [14] and [15].

A range of compatible source types can be plotted on a "source-type plot" (see [14]) whose shape is chosen so that a uniform population of source types appears with uniform density on the display. Here "uniform density" of source types is defined to mean that the three principal moments of the source are independent and each uniformly distributed between zero and some arbitrary upper limit, the value of which is irrelevant since with T and k we are concerned only with ratios of the moments. Figure 5 shows the resulting shape of the source-type plot, which is derived in [15].

The above definition of "uniform density of source types" gives us the weighting in T and k which must be applied to each source-type element when calculating significance values for a search mesh which includes a range of source types, as discussed in section 3.3. By analogy with equation 1, the significance S of a single matrix element in T and k is given by

$$S = (1 - |k|) \cdot \psi(\tau, k) \quad (3)$$

where $\tau = T(1 - |k|)$, and $\psi(\tau,k)$ is the combined distribution function in τ and k, which is given in equations 33 *et seq.* of [15].

The positions on the source-type plot of some important source types are shown in figure 5(a). In table 1 the values of the normalised principal moments, and of T and k, are given for these source types. Sources which are effectively superposed in space and time, with respect to the wavelength of signal on the seismogram, will be superposed to give a single composite source type. Treatment of separated multiple sources would rely on the correct identification of the discrete phases derived from each source.

3.5 *P*- and *S*-wave radiation patterns

Each source type has a characteristic radiation pattern for *P*-waves and *S*-waves. Figures 5(b) and (c) show *P*-wave nodal surfaces on a lower focal hemisphere for two orientations of a range of source

types: (b) is for a 45° dip slip with northerly strike (or its equivalent for non-double-couple sources), and (c) is for a vertical strike slip or equivalent with northerly strike. This type of plot shows the zones of alternate polarity but not the angular variation of amplitude, for which a polar diagram or vector display is required (see below). The familiar double-couple radiation pattern has planar nodal surfaces separating four alternate polarity quadrants. Moving along the T axis, the quadrants of one polarity begin to merge at the null axis, until at extreme T values the radiation pattern consists of a dipole encircled by a toroid of opposite polarity to the dipole, giving conical nodal surfaces. For $T=-1$ (CLVD), the toroid is negative, and for $T=1$ (negative CLVD) the toroid is positive. Moving along the k axis, a uniform positive or negative value is added to the radiation pattern, with the result that the toroid at $T=+1$ or -1 becomes larger or smaller with respect to the dipole until a value of k is reached where the radiation is all of one polarity. The amplitude is however not uniform until one of the extreme values of k is reached, corresponding either to the implosion or to the explosion. The loci along which the nodal surfaces disappear and the radiation is all of one polarity are shown in figure 5(a). Also shown is the locus along which the nodal surfaces are planar.

Figure 5(d) shows S-wave radiation patterns for the five values of T illustrated in (b) and (c). The focal sphere is shown in isometric view oriented for a vertical dip-slip fault, or equivalent. Separate S wave displays are not shown for different values of k because the S-wave radiation pattern does not change with k except for its amplitude relative to that of P. Since the S-wave is a vector, these radiation patterns are displayed by vectors on an isometric view of the focal sphere (a sphere concentric with the source). Vectors are plotted on the surface of the focal sphere to indicate the amplitude and particle motion direction of initial far-field S radiation along each emergent angle. The (far field) S radiation has transverse particle motion, lying in some direction in the plane normal to the ray direction (i.e. in the plane tangential to the focal sphere). Its amplitude and polarisation direction are again indicated by an arrow.

This method of plotting radiation patterns (introduced for the double couple in [2] and [4]) is much more helpful than polar diagrams, especially for the S-wave which, being a vector, is usually resolved into two components which are plotted on separate polar diagrams, with consequent failure to display explicitly the two all-important properties of the S wave — its absolute amplitude and its polarisation direction.

These radiation patterns have been generated using the Fortran computer program SRAD [26], which can also be used to display P-wave radiation patterns in a similar way.

3.6 Relations between seismogram class and source radiation pattern

The polarities and relative amplitudes of P, pP and sP observed on a seismogram (i.e. the seismogram class) depend upon three factors:

(i) the direction of emergence from the source for each phase observed on the seismogram;

(ii) the relative attenuation of the phases along their paths;

(iii) the source type and its orientation — that is, the source radiation pattern itself.

Factors (i) and (ii) relate to the source-receiver geometry, velocity structure and raypath effects. Taking into account the teleseismic ray geometry of figure 1, and various practical considerations, we can reexpress these two factors in terms of variables convenient to our study, as suggested in [2].

For any single seismogram, factor (i) corresponds to the take-off angles of P, pP and sP, and the azimuth of the station. Ignoring the orientation of the source, this dependence effectively reduces to the relative positions of the three phases on the focal sphere; that is, upon the angles subtended by the take-off angles of P, pP and sP at the source (see figures 1 and 2(b)). This is equivalent to a dependence mainly upon epicentral distance; the P-wave take-off angle decreases with increasing epicentral distance, and the relationship between this and the take-off angles of pP and sP is fixed for a given Poisson's ratio. For intracrustal sources the angles between these emergent rays depend also upon the source layer velocity, particularly at closer range. Also, there is a small change with source depth for sources below the crust. These effects can be allowed for, but for application to discrimination we are concerned only with shallow sources, so this dependence can be

neglected. The main variable needed to account for variations of take-off angle at the source is therefore simply epicentral distance.

Factor (ii) is only the loss of amplitude of *pP* and *sP* due to energy partitioning within the above-source structure, since the phases effectively traverse the same path outside the source region if the source is shallow. Assuming an above-source structure, the total amplitude losses to *pP* and *sP* above the source are related to each other. For practical purposes these amplitude losses can therefore be quantified by a related pair of parameters, which can be estimated given an above-source velocity structure. An allowance for any anelastic attenuation or scattering above the source can also be included if required.

Factor (iii) corresponds to the source type and its orientation, which together comprise its moment tensor. The source type is defined by the two variables T and k, following section 3.4, and the orientation is defined by the three angles δ, σ and ψ (dip, strike, and slip angle respectively, or their equivalent), following section 3.1.

For the results presented in section 5, we assume that the source orientation is unknown, with all orientations equally likely. The orientation part of factor (iii) can thus be ignored. The factors upon which the probability density functions depend are now effectively reduced to three: epicentral distance; a related pair of structure parameters; and source type.

Figure 6 shows significance against take-off angle of each of the classes of seismogram defined in figure 4, computed for the double-couple source, and assuming that the near-source velocity structure is simply a halfspace. This figure is reproduced from [2]. For each seismogram class, significance is plotted linearly as a function of take-off angle (representing roughly an inverse measure of epicentral distance). Because the double-couple source is used, only 13 curves need to be shown as values remain the same if the complete seismogram is inverted (section 3.2). Although for most classes the significance changes a lot with take-off angle, the range of take-off angles corresponding to the teleseismic range of distances is rather small.

The form of these curves is explained in section 5.3 using probability density functions on compatibility plots. The most important feature of these curves is that a wide range of significance values is obtained for different classes. It is this which makes some classes of seismogram very valuable in source discrimination.

4. THE DISPLAY OF SEISMOGRAM CLASS ON A "COMPATIBILITY PLOT"

4.1 Shape of the compatibility plot, and the need for a pair of plots

The "compatibility plot" is a display which maps all possible values of the relative amplitudes of *P*, *pP* and *sP*; that is, all seismogram classes as defined in section 3.2 are distributed upon it. Any given seismogram is therefore represented by a point or a zone according to how well its relative amplitudes can be determined. If one or more polarities cannot be measured then the seismogram is represented by two or more zones. A series of seismograms is represented by more zones corresponding to each seismogram.

Since there are only two independent amplitude ratios corresponding to the three phases *P*, *pP* and *sP*, the plot is two dimensional. We choose, by convention alone, that the horizontal axis be used for the *pP/P* amplitude ratio, and the vertical axis for the *sP/P* amplitude ratio. For any chosen combination the relative amplitude of *sP/pP* is then fixed. We impose a condition that the plot must be "equal area" in terms of the information content of a seismogram; that is, any seismograms which are deemed to embody the same amount of information relating to the relative amplitudes and polarities of the three phases must occupy the same proportion of the total area of the plot. Following Pearce et al [27] we define "equal information" in this context using the *a priori* assumption that the amplitudes of the three phases are independent, and that each has a probability which is uniform within the range between an arbitrary negative and positive limit. The numerical values of these limits are unimportant because only amplitude ratios are used. This definition of equal information gives a precise meaning to the "quality" of a seismogram, which was introduced in section 3.3.

The resulting shape of the compatibility plot is derived in [27] and is shown here in figure 7(a). The lines of equal *pP/P* and *sP/P* amplitude ratio are not exactly horizontal and vertical respectively over the whole plot, so that the plot is not strictly Cartesian. This is an inevitable consequence of our imposed equal area condition, and is explained in [27]. The lines of equal *sP/pP* amplitude ratio follow from those of the other two ratios and describe curved paths as shown in the figure (they are shown pecked for clarity). Similar plots presented in [3] did not satisfy the above equal area definition, so the plots in that reference have a different shape.

In constructing the compatibility plot, the polarity of the whole seismogram is neglected in [27]. This is only possible when consideration is restricted to the double-couple source, whose radiation pattern does not change in form if the signal polarity is reversed (section 3.2). For the same reason the polarity of the complete seismogram was ignored when seismogram classes were defined in [2]. In order to allow for non-double-couple sources the scheme for defining discrete seismogram classes was extended in section 3.2 to identify separately the polarity of the complete seismogram. We must also ensure that such seismograms are discriminated on a compatibility plot. To achieve this, a pair of plots is required in order to represent a complete population of *P*-wave seismograms. We divide the data into one plot with "*P*-negative" and another with "*P*-positive". These correspond to separate compatibility plots for seismograms with a negative direct *P* wave and those with a positive direct *P* wave. The term "compatibility plot" implies such a pair of plots where appropriate.

For source types which have no nodal surfaces (i.e. the *P* radiation has the same polarity in all directions) one of the pair of compatibility plots always has zero probability density throughout, since a radiation pattern wholly of one polarity can never yield a direct *P* wave of the other polarity. For all other source types, both the *P*-negative and the *P*-positive plots need to be presented, since they yield different probability density functions, except in the case of the double couple, where the functions are identical for *P*-negative and *P*-positive.

Any variable which is a function of seismogram class can be contoured or otherwise represented on a pair of compatibility plots. In section 5 we use them to display the probability density of seismogram class which is predicted theoretically under a variety of initial assumptions. Before that we describe in a general way how these density functions, and seismograms themselves, are displayed. The way in which single seismograms with different *P*, *pP* and *sP* relative amplitudes and polarities occupy different zones on the compatibility plot is explained in section 4.2, and the plotting of single seismograms is described. Section 4.3 shows how several seismograms, or a whole population, can be represented. Section 4.4 describes the ways in which a continuous function which varies with seismogram class can be displayed. The 27 classes of seismogram defined in figure 4 are displayed in section 4.5, and the true way in which the definitions of figure 4 divide seismograms into classes is revealed. Reference is made to computer programs, described elsewhere, which generate compatibility plots and the data to display on them.

4.2 Representation of a single seismogram on a compatibility plot

Figure 7(b) shows schematically the locations of different classes of seismogram on the pair of compatibility plots, and figure 7(c) summarises the polarities of each of the three phases in the four quadrant of each of the two plots. A *P*-wave seismogram comprising the phases *P*, *pP* and *sP*, if measured to perfect accuracy, would be represented by a single point in one of the quadrants. For a real seismogram there is always an uncertainty in the measurement of the amplitude of each phase, and hence in the relative amplitude of each pair of phases. Also, one or more of the polarities may be unknown, or only defined relative to the polarity of another phase.

The uncertainty in the amplitude of a phase is expressed as upper and lower bounds within which the true amplitude is deemed certain to lie; this implies that all amplitudes have equal likelihood within this range. It follows that the probability density of amplitude ratios is also uniform when shown on a compatibility plot, since this uniformity is the criterion used to define the shape of the plot (section 4.1). The seismogram therefore has an equal likelihood of lying anywhere within a curvilinear polygon on the compatibility plot, with a perimeter formed by the intersection of, in general, six lines corresponding to the upper and lower limits on each of the three amplitude ratios *pP/P*, *sP/P* and *sP/pP*. The form these lines take can be seen from figure 7(a), and figure 7(d) shows an example of a seismogram represented by its corresponding curvilinear polygon.

If one or more polarities are unknown, or are only measurable relative to the polarities of other phases, then similar curvilinear polygons appear in more than one of the eight quadrants. Where the *P*-wave polarity is unknown, then up to eight polygons will appear in either or both of the "*P*-negative" and "*P*-positive" plots. The proportion of the compatibility plot occupied by the seismogram increases with decreasing seismogram quality — a seismogram containing no information occupies the entire area of the pair of plots.

We have so far assumed that the amplitudes of phases on a seismogram are simply assigned upper and lower bounds; this corresponds to the scheme used in the relative amplitude method as implemented in programs FALT and RAMP, (see section 2). In [16] and [20] it is proposed that, in the presence of noise or other uncertainties, it may be more appropriate to express the amplitude of each observed phase by some likelihood function other than the uniform likelihood implied by the use of fixed upper and lower amplitude bounds. It is argued that some tapered function such as a Gaussian might be more realistic in some circumstances, since it makes amplitude values close to the centre of the range more likely, leading to a peaked probability density function in the representation of a seismogram on the compatibility plot. This is the scheme used in the program GRAM, also introduced in section 2. A seismogram described in this way is represented by a non-uniform density function rather than by one or more bounded zones. It can be plotted using one of the methods for the representation of density functions described in section 4.4.

A Fortran program, CPLT, generates compatibility plots and displays the data upon them [26]. The program includes facilities to display zones as curvilinear polygons corresponding to specified relative amplitude observations, or as dot-density distributions.

4.3 Representation of more than one seismogram on a compatibility plot

More than one seismogram is normally available, and to see these seismograms independently, the several curvilinear polygons corresponding to all of them may be overlaid on one pair of plots. Since each seismogram may have up to eight polygons, each polygon must be identified according to the seismogram it represents. This can be achieved either by using different boundary styles or character labels for the polygons associated with each seismogram, or by shading the polygons of each seismogram differently. Examples are given in [26].

Alternatively, the combined density function of seismogram class corresponding to a population of seismograms can be shown. If the curvilinear polygons for a number of seismograms are overlaid, the number contributing to each point on the plot may be counted, to yield a continuous density function which corresponds to the occurrence of each class of seismogram within the population of seismograms under consideration. In this case, again one of the methods described in section 4.4 for displaying a continuous density function on a compatibility plot may be used, and all the display features mentioned above provided by the program CPLT [26] are available.

One use for this would be for making a direct comparison of a population of observed seismograms with a population of predicted seismograms generated assuming a chosen source model. This might be useful for assessing the discriminating power of samples of seismograms, and might be used to determine, for example, trends in seismogram class for particular stations or source locations. It would reveal, for example, local bias in source orientation distributions. Such studies could also be used to assess the significance, in addition to the class, of seismograms which would be observed for particular stations or sources.

However, although the effect of any number of seismograms may be superposed or combined on a compatibility plot, the plot is normally only able to display a variable which depends upon single seismograms independently. The class combinations of several seismograms expected at different stations given a particular source type, depend additionally upon the relative positions of the stations on the focal sphere, and so would introduce additional dimensions into the plot. Calculations would have to be repeated for each station distribution. The constraint imposed by more than one seismogram is always much greater than that imposed by each seismogram independently. Statistical studies may be carried out on the observed occurrence probabilities of different seismogram types by superposing a population of them on one compatibility plot — perhaps for comparison with theoretical predictions for different source types. But in doing this we are considering the effect of single seismograms. The use of more than one station is discussed further in section 6.

4.4 Representation of continuous functions on a compatibility plot — the "dot-density display" and the "matrix-element display"

We need to be able to display on the compatibility plot any continuous function which depends upon seismogram class. This might be a predicted probability density of seismogram class for a given source type and population of source orientations. It might be the total count of a number of seismograms overlaid on the plot as described in section 4.3. It might be a single seismogram whose amplitudes are described by a Gaussian function rather than upper and lower bounds (section 4.2). In section 5 the probability density of seismograms of different classes is represented as a continuous function on compatibility plots, given various assumptions about the source. If any seismogram is represented on such a plot by means of its curvilinear polygon(s), then the total probability measure within the polygon(s), when subtracted from unity, gives the significance of the seismogram under the corresponding source assumptions (section 4.2).

Any such continuous function can be represented by contours, and this type of representation was used in [3]. Here we use two other methods of representing a continuous function. The first we call a "dot-density display"; this gives an immediate visual but qualitative impression of the distribution of probability measure on the compatibility plot. The second we call a "matrix-element display"; this gives a quantitative representation of the function.

For the matrix-element display, the square joining the four corners of the compatibility plot is divided into a 48x48 grid of bins, or "matrix elements", into which the continuous probability measure is divided. One third of the matrix elements are within the compatibility plot; the remainder are in the four regions which are within the square but outside the plot, and so contain no measure. The diagonal boundaries of the plot cut through matrix elements; these elements consequently contain a smaller probability measure than if they were wholly within the plot.

The values within all the matrix elements are scaled such that the element containing the largest probability measure is set to 100.0; this scaling will in general be different for every plot. The resulting value in each matrix element is then integerised by rounding. This procedure is adopted to optimise the values and precision of the matrix elements, given that only two significant figures can be clearly shown on the display: numerical values are thus limited to integers between 0 and 100, and 100 is denoted by two asterisks (**).

When a matrix-element display is used, and the probability measure is distributed between the *P*-negative and *P*-positive compatibility plots, the two plots are separately scaled so that a peak value of 100 appears on each of the pair. Moreover, the probability measure is not in general equally distributed between the *P*-negative and *P*-positive plots. In the case of randomly chosen orientations as used in this report, the ratio of the total probability measures on the two plots is equal to the corresponding ratio of *P*-negative and *P*-positive directions in the radiation pattern corresponding to the source type; i.e. it depends upon T and k.

A consequence of the above two effects is that a scaling factor (characteristic of a particular plot and different for the *P*-negative and *P*-positive plots) must be applied to each displayed matrix element value to convert it to true probability measure. On each plot, this scaling factor is normally quoted as "scaling factor to convert matrix elements to probability". After this scaling factor has been applied to the displayed matrix elements they should sum to unity across the *P*-negative and *P*-positive plots.

The matrix elements which lie within the curvilinear polygon(s) corresponding to an observed seismogram may be identified by overlaying the polygons on the pair of plots. The elements can be summed to give the total probability measure corresponding to that seismogram. Hence, once a probability distribution for a particular set of assumptions has been calculated and displayed, the same plots can be used for any observed seismogram appropriate to that density function.

In addition to the scaling factor, the matrix-element displays in this report also give "total measure with elements scaled to make the largest equal to 100.0", and "total measure when scaled elements are integerised". Neither of these parameters is important when using the plot, but the discrepancy between them is a measure of the effect of scaling and integerising the matrix elements. In plots where the probability measure is very broadly distributed, this discrepancy is larger, and the scaling results in only certain integer values appearing. These are artefacts which are unimportant in practice.

Where a dot-density display is used in this report, the same number of dots is plotted on the *P*-negative and *P*-positive plots irrespective of the distribution of total probability between the two plots. The absolute number of points plotted has no numerical significance, but is chosen in an attempt to show the maximum range of different values in the function without compressing them together towards either too high or too low a density of points. The plots are generated using the program CPLT [26] introduced in section 4.2.

4.5 The 27 classes of *P*-wave seismogram on a pair of compatibility plots

Figure 8 shows the 27 classes of seismogram defined in figure 4, on a *P*-negative and a *P*-positive compatibility plot. As explained in section 3.2, the classes do not correspond to a non-overlapping and contiguous set. Every point on the pair of plots is covered by at least one class, although there is in general some overlap. This means that the classification includes all possible seismograms. If the overlaps were reduced by narrowing the bounds in the definitions of each class shown in figure 4, then some parts of the plot would no longer be covered by a class.

For the classes in which one of the phases is "small" (classes 5 to 10 +ve and –ve), curvilinear polygons appear in two quadrants because the small phase can be of either polarity; in each of classes 7 to 10 +ve and –ve the two polygons join at quadrant boundaries, effectively forming a single polygon. Classes which have two "small" phases (11 to 13 +ve and –ve) plot in four quadrants because the two small phases can each assume either polarity. Of these, classes 11 and 12 +ve and –ve each join at quadrant boundaries, resulting in two polygons, and for each of classes 13 +ve and –ve, the four polygons join to form one polygon across the centre of the plot. In general, the classes defined in figure 4 which have a suffix "+ve" plot on the *P*-positive plot and those with suffix "–ve" plot on the *P*-negative plot. However, for classes where the direct *P* wave is defined in figure 4 as "small" (5, 6, 11 and 12 +ve and –ve), the seismogram can have either a positive or a negative direct *P* wave, whereas the class is assigned suffix "+ve" or "−ve" according to the polarity of the first phase which is not "small". Hence these classes have polygons on both the *P*-positive and *P*-negative plots. Classes with the same number of "small" and "large" phases occupy the same total area on the plot. The class 0 seismogram is not shown because it covers all of both plots — its information content in terms of relative amplitudes is zero (see section 3.2).

Figure 8 should be compared with figure 4, to which it is equivalent. In section 5.3 the wide variation of significance between different seismogram classes, evident in figure 6, will be explained by the examination of probability density functions of seismogram classes for the double couple, with reference to figure 8.

5. CATALOGUE OF COMPATIBILITY PLOTS — DESCRIPTION AND INTERPRETATION

5.1 Purpose of the catalogue

The catalogue shows the likelihood of observing different classes of seismogram, for a variety of source types at different distances and with different above-source structures. The information is presented by showing probability density functions on compatibility plots, for chosen combinations of these three variables. The behaviour of these probability density functions is analysed and compared. The potential for using relative amplitudes as a source discriminant can thereby be assessed. The probability of observing any particular seismogram under chosen assumptions can be determined by measuring the total probability contained within the zone(s) representing that seismogram on the chosen plot.

We make simple and realistic assumptions in choosing the cases for which probability density functions are generated. For each source type a selection of epicentral distances is fixed implicitly by choosing appropriate *P*-wave take-off angles, and the above-source structure parameter is fixed to values typical of crustal events. The orientation of the source is assumed to be unknown, with uniform probability over all orientations. A particular pair of plots therefore shows the predicted relative occurrence of every class of seismogram, assuming the appropriate source type, above-source structure and epicentral distance.

The probability density functions shown here are generated using the computer program FINF, which is described in [26]. This is a development of the program FALT, which has been generalised from the double-couple source to include any source type represented by the moment tensor. In the program FINF,

no relative amplitude data corresponding to specific seismogram observations are required. Instead, for the chosen source type, (and epicentral distance and above-source structure parameter) the relative amplitude values corresponding to all orientations in the search grid are computed, and are made available to the program CPLT, for plotting a dot-density or matrix-element display on a compatibility plot. To avoid artefacts arising from the use of a regular search mesh, this can be replaced by a set of randomly chosen orientations; this latter option is used throughout this report.

5.2 Summary of catalogue and notes on its use

We first present plots (in sections 5.3 and 5.4) for the double-couple source type for several epicentral distances and above-source structures. These demonstrate that within relevant limits the above-source structure parameter has only a secondary effect upon the probability density function. Similarly, the effect of epicentral distance is not strong until the *P*-wave take-off angle increases to values which correspond to the closest teleseismic distances. The teleseismic range of take-off angles is quite small; it lies between about 5° and 30°, with 0° to 5° corresponding to the phases *PKIKP* and *PKP*, which traverse the core. We shall see that between 0° and about 25° the features of the probability density generally remain similar, with some distortion or small shifting of the key features. Normally the epicentral distance is known; the consequences of uncertainty in this variable are therefore of little importance. It turns out that in most circumstances the probability density function is not strongly dependent upon the above-source structure within geologically reasonable limits, although its effect is significant. This dependence can be important since the above-source structure is usually poorly known.

Section 5.5 describes the variation of probability density with source type, for fixed epicentral distance and structure parameter. By contrast with the insensitivity to epicentral distance and structure parameter, it is found that source type has a considerable effect upon the probability density function, with mutually exclusive density functions being obtained for some pairs of source types. This variation is essential to the ability of relative amplitudes to discriminate between source types.

Each probability density function is shown in two forms on the pair of compatibility plots: a dot-density display is shown to give a visual impression of the distribution of probability measure, and a matrix of probability elements (matrix-element display) is given for quantitative work. These plots follow the descriptions given in section 4.4. If the curvilinear polygon(s) corresponding to the relative amplitudes observed on a seismogram are overlaid on the plots, the probability measure included within the polygon(s) can be summed to give the probability of observing such a seismogram, given the assumptions used in the generation of the chosen plot. This procedure is described in section 4.4. It is important first to rescale the probability measures as explained in section 4.4. When the probability measure is subtracted from unity the significance of the seismogram (section 3.3) is obtained. This operation forms the basis of quantitative calculations which can be carried out using these probability density functions.

5.3 Variation with epicentral distance for the double couple source

Figures 9 to 12 show a series of compatibility plots for a range of take-off angles (i.e. epicentral distances) for a double-couple source in a half-space. For a double couple the *P*-negative and *P*-positive compatibility plots are identical when they show data from a randomly oriented population of sources, so only one is shown. For a take-off angle of zero, which corresponds to a *PKIKP* observation at the antipole, the result is trivial and comprises a delta function of probability measure at the point (–1,0); this is shown in figure 9. This result arises because a vertical take-off angle implies sampling of two points directly opposed on the focal sphere, which gives equal amplitude and opposite polarity *P* and *pP* for <u>all</u> orientations when allowance is made for the change in polarity of *pP* at the free surface. Since the free surface reflection coefficient of *sP* is zero, the amplitude of *sP* is zero irrespective of the amplitude and polarisation direction of the upward travelling *S* wave. We conclude that all seismograms in these circumstances should be of class 10.

A delta function would be observed for any source type which presents the same radiation along opposing directions; this includes all source types derived from the moment tensor formulation. Hence, if the source is a single event, a *PKIKP* observation can tell us nothing about either its source type or its orientation. For *PKIKP* we therefore have the paradoxical situation that only one seismogram class is expected, implying that all other classes would be "suspicious", while there are no alternative source types

(within our range of models) which could be invoked to explain other types of observation.

In [27] three compatibility plots for the double-couple source in a halfspace, and observed at different epicentral distances are presented. Figures 10 to 12 are similar. The form of these plots is discussed in [27]. We mention here several important features.

First, as the take-off angle deviates from zero the probability measure spreads out from the delta function at $(-1,0)$ along a narrow ridge passing also through the points $(-\infty,\infty)$, $(0,-1)$ and $(\infty,-\infty)$. This encompasses seismograms of classes 6, 8, 11 and 12, as well as 10. With increasing take-off angle more of the probability measure migrates along the ridge, and at a take-off angle of 20° the ridge begins to become more diffuse, though it continues to dominate throughout the teleseismic range of take-off angles. When a take-off angle of about 30° is reached, most of the probability is clustered in the lower end of the ridge. If the *pP/P* and *sP/P* relative amplitudes were plotted on a linear scale, then this probability ridge would appear as a straight line. It is also seen that the ridge migrates slightly as the take-off angle increases; its intersection with the abscissa moves to the left. The existence and behaviour of this ridge has been verified analytically by Pearce et al [27]. It is the most important feature of compatibility plots for the double-couple source type, because it shows that most seismograms observed from a double-couple source are expected to be of a very restricted range of classes. This at once suggests a potential for discriminating between source types, especially if we can show that other source types have restricted probability zones which are different from this one.

Secondly, we can see that for take-off angles of less than 30°, 95% of the total probability is contained within less than 25% of the area of the plot. This is also an important result, because although seismograms are not totally prohibited outside this area, the probability measure is sufficiently small for any single seismogram which plots entirely in the other 75% of the plot to merit close examination. We should also point out that the further the seismogram is from the zone of high probability, the more anomalous the observation becomes.

Thirdly, it becomes clear for take-off angles of 15° and larger, that there is a large zone on the left side of the plot and above the main probability ridge, where the probability is identically zero. Within such an area we can confidently say that an observed seismogram is inconsistent with the double-couple source type. This boundary is later shown (section 5.5) to persist in different forms for other source types, and we call it the "characteristic boundary". The prohibited zone for the double couple source type corresponds generally to seismograms of class 2, which have all three phases large, and which have the polarity of *pP* opposite to that of the other two phases (see figure 8).

Referring to figures 7(b) and 8, we can draw another conclusion of practical importance: the ridge previously referred to, which contains most of the probability measure, contains no seismogram classes in which all three phases are "large". Thus we find that any seismogram which has large *P*, *pP* and *sP* (i.e. classes 1, 2, 3 or 4) is very unlikely to arise from a double-couple source, irrespective of the polarity or relative polarity of the phases. This fact was recognised by Pearce [2] and the compatibility plot enables it to be expressed in a quantitative way. In fact the same result would be expected for many other source types, bearing in mind that large *sP* amplitudes generally arise near to a node of *pP*. This kind of general conclusion is of particular importance when dealing with low signal-to-noise ratio records, for which polarity observations are unlikely to be measurable with confidence, while relative amplitude information may still be retrievable.

Using figures 9 to 12 we can now relate the probability density functions covering seismogram classes, to the significance curves shown in figure 6 for the 27 classes of seismogram defined in figures 4 and 8. The pair of compatibility plots shown in figure 8, upon which the classes of seismogram have been plotted, can be overlaid upon any of the probability density functions given in figures 9 to 12. From section 4.4 we know that if the probability measure contained within the polygon(s) representing a particular seismogram class is subtracted from unity (after appropriate rescaling of the matrix-element values), this gives the significance of that seismogram assuming a double-couple source in a half-space. This is equivalent to one point on one of the curves in figure 6. We see that the form of the curves relates to the features of the probability density functions displayed on the compatibility plots.

The compatibility plot is a more comprehensive and preferable means of displaying the data than the curves of figure 6 because it is independent of any arbitrary choice of the amplitude bounds defining

each class, and because the significance of any seismogram of any quality can be examined. In particular, the increase in significance of the class 10 seismogram away from a vertical take-off angle in figure 6 is related to the progressive spreading out of the probability measure away from the delta-function at the point (–1,0), seen in figures 9 to 12. It can also be seen that in some cases the significance obtained in figure 6 is rather misleading as it represents probability measure towards the edge of the polygon, and so is highly dependent upon the exact choice of numerical bounds for each class.

5.4 Variation with above-source structure for the double-couple source

We now compare the compatibility plots presented in figures 9 to 12 with equivalent plots computed with a typical above-source structure shown in table 2 (taken from [27]). The effect of any above-source structure is to reduce the amplitudes of *pP* and *sP* with respect to that of *P*, whether by energy partitioning at abrupt interfaces above the source, or by anelastic attenuation above the source, or by some combination of these two effects. For both effects the reduction in amplitude is more pronounced for *sP* than for *pP*: anelastic attenuation has more effect on *S* waves than on *P* waves, and the amplitude of *sP* type reflections at near-normal incidence is very sensitive to angle. The exact velocity structure in any particular case is of less importance than the overall loss of amplitude that a realistic velocity structure creates. The amplitudes of *pP* and *sP* may be reduced to about two thirds of the size they would be if only reflection at the free surface were considered. Figure 13(a) and (b) show the effect of a realistic velocity structure on the compatibility plots; these can be compared with those computed for a halfspace in figures 9 and 12 respectively.

As before, the compatibility plot for zero take-off angle is trivial (figure 13(a)). The amplitude of *sP* is always zero as before, and the reduction in *pP* amplitude results in a displacement of the delta-function of probability towards the right, away from the point (–1,0). In general the displacement is to the point $(x,0)$, where x is the new *pP*/*P* amplitude ratio resulting from the loss of *pP* amplitude.

Within the teleseismic range of take-off angles (between 5° and about 30°) we see similar changes in behaviour with a tendency for the distribution to become more diffuse. Figure 13(b) shows the compatibility plot for a take-off angle of 30° (modified from [27]). For larger take-off angles it is not easy to explain the locus of the ridge of probability, because a number of factors become important: the three phases no longer emerge from opposite points on the focal sphere; *sP* emerges at a steeper angle than *pP*, and the *sP* reflection coefficient depends upon the *S*-wave polarisation direction at the source for each orientation, as well as upon the angle of incidence of *sP* at the surface. For a takeoff angle of 30° the ridge crosses the abscissa to the left of the corresponding ridge for the halfspace, rather than to the right as for small take-off angles.

The main conclusion is that there is no substantial change in the probability density function for any teleseismic epicentral distance when the effect of the velocity structure is included; this indicates that an absence of accurate knowledge of the above-source structure does not introduce large uncertainties in the mapping of relative amplitude from seismogram to source, although the effect may be significant enough to warrant increasing the width of amplitude bounds when making measurements on observed seismograms. In principle, if the velocity structure is unknown, then a probability density function generated using a random variation of the structure within the range of uncertainty should be used. This would incorporate the uncertainty in above-source structure into the probability density on the compatibility plot. An approximate indication of the maximum broadening of the distribution that would be obtained for a given take-off angle is given by superposing the corresponding pair of plots given here for the halfspace and layered structures.

5.5 Variation with source type for fixed epicentral distance and above-source structure

To summarise the differences between the seismogram probability density functions for different source types, we show in figure 14 a composite diagram containing miniaturised compatibility plots for a representative range of source types, spaced schematically around a source-type plot. To create sufficient space the source-type plot is split into three parts across three pages. The form of *P* and *S* source radiations for each source type selected can be seen by reference to figure 5(b)-(d). In this summary all the compatibility plots are computed for a *P*-wave take-off angle of 15° in a halfspace, and we show only dot-density displays. A number of general features of these plots are now described.

First, as shown analytically in [15], all parts of the source-type plot outside the area between the two parallel dotted lines in figure 5 correspond to source types with no P nodal surfaces. For this range of source types the P radiation is either all positive (upper zone) or all negative (lower zone). This results in either the P-positive or the P-negative compatibility plot containing zero probability measure; these zero compatibility plots are omitted.

Secondly, the probability density functions are identical except for an interchange of the P-positive and P-negative plots, if the polarities of both T and k are changed. (Differences in the individual dots are due to the random sampling.) This behaviour can be explained as follows with reference to the radiation patterns shown in figure 5(b)-(d). If the polarity of T is changed for a source type with k=0, then the radiation pattern is identical except for a reversal of its polarity and a change of 90° in its orientation (compare, for example, the CLVD and negative CLVD). Because the probability density functions assume a uniform sample of orientations, a change in orientation of the radiation pattern with respect to the coordinate system in which it is defined has no effect. However, the reversal in its polarity results in the interchange of the P-positive and P-negative density functions because such a reversal results in seismograms which are themselves reversed in polarity. For source types with non-zero k, a change of the polarity of T must be accompanied by a change in that of k if the radiation pattern is to remain identical except for a change in its polarity. The observed symmetry between the probability density functions is therefore as expected.

Thirdly, some features of the double-couple plots are seen to persist in some form for other source types. Comparing the plots, we see that the narrow ridge of probability measure identified previously for the double-couple source type exists in a modified form for a wide range of source types. Also, the existence of a characteristic boundary (section 5.3) within which the probability is identically zero, is seen to represent a special case of a behaviour common to all source types: there is a boundary which dominates the shape of the probability density function, and whose location on the compatibility plot migrates with source type. For source types with only one polarity of P-wave radiation this characteristic boundary is closed, and all probability measure lies within it. For the vector dipole all the probability measure lies on the characteristic boundary. For source types which have both positive and negative P-wave lobes in their radiation patterns the behaviour is more complicated. Except for the double couple, the boundary is closed only along the edge of the compatibility plot. For the double couple all probability measure lies outside the boundary. Otherwise, the probability measure lies on both sides of the boundary, but in most cases it is distributed in such a way that most, or all, of the measure appears on one side of the boundary on each of the P-positive and P-negative plots.

For all source types, probability measure is mainly or entirely restricted to the lower left half of the compatibility plot. This behaviour therefore includes linear combinations of source types, such as a double couple with an explosive component, since such linear combinations are equivalent to another single source type. It follows that any observed seismogram which plots towards the upper right-hand corner of the plot is unlikely to come from a single source of any type; the observance of such a seismogram would suggest that phase identifications were incorrect, for example because the source comprises multiple separated events. This argument becomes stronger as the observation plots closer to the top right hand corner.

There is also virtually no probability measure for any source type in the bottom left hand extreme of the plot, which is therefore another area where observations are not expected to plot. The classes of seismogram corresponding to these two areas of the plot are 1, 5, 7 and 9 (see figures 4 and 8). In summary, these zones comprise any seismogram which has either all three phases or any two of them large, with all the large phases of the same polarity.

Further examination of the plots reveals that no seismograms with three large phases, irrespective of their polarity, are expected for most source types, (as previously noted for the case of the double couple), though there are some exceptions.

The probability density function for the explosion source has a trivial form. Like all other source types it yields a delta function at the point $(-1,0)$ for a take-off angle of 0.0° in a halfspace. Since the P-wave radiation pattern of the explosion is radially symmetric, and it produces no S-waves, the explosion also yields a delta-function for all other take-off angles, and this migrates towards the origin along the X-axis as the take-off angle increases.

We now consider the extent to which these plots can provide discrimination between different source types. The most important feature here is the characteristic boundary noted above. The special case of the vector dipole, previously referred to, is noteworthy. Although all the probability measure lies on the characteristic boundary, the locus includes a wide range of ratios, i.e. a large number of classes. If the uncertainty in, for example, structure parameter is taken into account, the ribbon spreads out with a much greater proportional increase in area than would be the case if it were in a cluster. In fact for practical purposes it would be more restrictive, and hence more powerful, if the probability measure were restricted to a small region of the plot, rather than along a very thin but extended ribbon of similar area, which consequently covers a wider variety of seismograms.

The disposition of probability measure with respect to the characteristic boundary for different source types offers one means of discriminating between source types. For absolute values of k larger than 0.5, the restriction of probability measure to within the characteristic boundary eliminates a large proportion of possible seismogram classes. Moreover, there is good discrimination between the positive and negative zones of large k, since all the probability measure is mutually exclusive, being in either the P-positive or P-negative plots. This corresponds to saying that the observed P polarity is always the same for any radiation pattern with no nodal surfaces. We conclude, therefore, that this type of relative amplitude data offers a high potential for discrimination between sources that have a large positive isotropic (i.e. explosive) component and those which have a large negative isotropic (i.e. implosive) component. This is to be expected. It also has potential for discriminating between these two ranges of source types and those with little or no isotropic component.

The above behaviour exploits a dependence which is mainly upon k rather than upon T. By comparison, we see that the probability densities for different values of T, with similar values of k, show no striking differences, at least for small values of k. This indicates that this type of relative amplitude data is not as good at discriminating between different types of constant volume component. More data derived from the S-wave radiation pattern are required to do this effectively.

The fact that P-wave relative amplitudes are better at resolving the proportion of isotropic component than they are at discriminating between different types of constant volume component was recognised in [14]. The argument relies on the fact that the P-wave nodal surfaces migrate rapidly as k changes, and that the entire nodal surfaces migrate. By contrast, as T varies, the migration of the nodal surfaces occurs mainly near the intermediate axis (i.e. the null vector). For S waves the position is different; S waves are unable to discriminate between different proportions of isotropic component because the S wave radiation pattern is independent of k. However, S waves are better able to discriminate between different values of T than are P waves. The evidence presented here is quite specific in its illustration of these points: we can see from the compatibility plots that the data offer a special ability to discriminate between source types which have P nodal surfaces (i.e. which have P wave radiation covering both polarities) and those which do not.

Of special note is the double couple. The probability density plot for this source type has a characteristic boundary which is similar in shape and position to those of all source types with large absolute k value, but it has all of the probability measure outside rather than inside the boundary. This implies a very strong capacity to discriminate between the double couple and all source types with large positive or negative k. This is particularly important since we know that most earthquakes radiate as double couples. An explosive or implosive source, or a double couple plus an explosive or implosive component, should therefore be well-discriminated with relative amplitudes. Of course, near to vertical incidence this discrimination capability diminishes because all source types, not only the explosion, have the same amplitude and polarity radiation in opposing directions; this causes the convergence of probability towards a single point on the plot as a vertical take-off angle is approached.

In figures 15 to 106 we show full size compatibility plots for the source types represented in the composite plot of figure 14. The source types represented include the double couple, the compensated linear vector dipole (CLVD), the tensile crack, and the vector dipole. For each source type three successive figures show compatibility plots for a take-off angle of 5°, 15° (as in figure 14) and 30°, corresponding to a range of teleseismic epicentral distances as seen in figure 6. A halfspace is assumed, so that no allowance is made for any loss of amplitude of the surface-reflected phases except at the surface. A fourth figure shows

plots for a take-off angle of 30° with allowance for a typical velocity structure as shown in table 2. In each case both a dot-density plot (a) and a matrix-element display (b) are shown.

These figures show in much more detail the behaviour summarised in figure 14. For each source type, plots for the three take-off angles indicate the range of behaviour appropriate to the range of take-off angles corresponding to teleseismic distances, and the inclusion of matrix-element plots provides this information in quantitative form. The main purpose of these figures is to act as a reference for determining the significance of individual seismograms for a given source type. This can be done by drawing the polygon(s) corresponding to the relative amplitudes observed on a seismogram (either using the program CPLT or manually using figure 7(a)), and overlaying them on the appropriate matrix-element plot. The significance can then be determined by the procedure described in section 4.4.

6. THE INCLUSION OF MORE THAN ONE STATION

We have concentrated on presenting data which show the ability of relative amplitude information to discriminate between different source types given a single seismogram. This has partly been done for simplicity, to minimise the number of variables to be considered, and partly to make the point that one station alone can offer valuable information. Of course, the discriminating power of any number of single stations recording one event can be examined independently in this way, but we can expect that if a given radiation pattern were required to satisfy relative amplitude observations at more than one station simultaneously, then in general this would impose a much stricter condition on the allowable source types and orientations. If we have relative amplitude observations at two or more stations, and ask the question "What range of source types is compatible with these observations simultaneously?" then the range will be dramatically reduced, compared with the range that will be compatible with any one station, or with all the stations treated individually.

Relative amplitude moment tensor determinations (i.e. with the double-couple assumption relaxed) have been made for a number of known earthquakes (see [14], and [16] to [19]), and in many cases the source type has been closely constrained to a double couple. However, most of those events which have been processed assuming a generalised source type have been of large magnitude; for large shallow earthquakes, whose surface reflections interfere, the *P*-wave information is usually limited to the direct *P*-wave polarity and so is usually augmented by that from three component direct *S* waves. This type of data is of no relevance to discrimination between sources at small magnitudes, because *S*-waves are not recorded at teleseismic distances from smaller sources.

More information is required on the ability of a number of small teleseismic short period *P*-wave seismograms to discriminate between source types using this method, before we can decide on optimum station distribution and required station numbers and data quality. Pearce and Rogers [14] compute a moment tensor solution for an earthquake in East Kazakhstan using three teleseismic observations. They find that the data give good discrimination in k (the proportion of volume change component) but less in T (the type of constant volume component). The reason for this is the same as has been concluded for a single station in section 5.5 — the *P*-wave nodal surfaces migrate rapidly around the focal sphere as the proportion of explosive component in the source is changed, whereas a change in the type of constant volume component has more effect on the *S*-wave radiation. Conversely, a change in explosive component has no effect on the *S* waves. Hence, we conclude that for discrimination studies which are particularly concerned with the recognition of any explosive component in the source, the *P*-wave relative amplitude information is most sensitive. Moreover, a number of observations placed around the focal sphere serve to restrict the range of explosive components which are compatible, by pinning down the positions of the nodal surfaces. The positions of the nodal surfaces can be pinned down even if all direct *P* waves are of the same polarity, if the relative amplitude observations are of good quality.

The additional constraint on source type which can be imposed by the simultaneous use of data from multiple stations depends upon the relative positions of these stations on the focal sphere. This is in addition to the dependence on seismogram class and quality identified for single stations in sections 3.3 and 3.6. We might expect that maximum discriminating power would be achieved by a homogeneous distribution of stations on the focal sphere, but this is not necessarily so.

To estimate the effect of station distribution we first consider single point observations of the radiation pattern on the focal sphere. (We recall that relative amplitude data always compare the radiation in two directions separated vertically on the focal sphere, so one direction cannot impose a constraint, except by means of a polarity.) A set of observations which are directionally well-separated contain information on low-order directional variations over a large part of the focal sphere, while clustered observations contain information on higher order directional variations but over a limited range of directions. Thus our conclusion about the relative value of these two extreme cases depends entirely upon the nature of the *a priori* constraints imposed upon the form of the radiation pattern — assuming that data quality and all other factors are similar.

In general, the fewer prior assumptions that we make about the form of the radiation pattern, the more useful it is to have a uniform station distribution. With few prior assumptions, widely distributed low order information is more likely to provide useful discrimination between different source types than high order information with large gaps; low order variations usually dominate the form of the radiation in any case. However, if we impose restrictive prior assumptions — for example because we only wish to discriminate between two source types, or we simply wish to determine the orientation of a source type which is presumed known — then restricted directional coverage may be sufficient to do this, since the form of the low order directional dependence of the radiation is already fixed. The higher order information contained in closely spaced observations may then be sufficient to fix the orientation of the radiation pattern more accurately than could be done with the lower order data. A simple example of this effect is the use of two observations closely spaced either side of a nodal surface (i.e. across a polarity change in the *P*-wave radiation).

The related phases *P* and *pP*, or *P* and *sP*, always sample widely spaced directions, in excess of 90° apart on the focal sphere. This means that some low order data are assured, at least in the *P* radiation, whatever is the station distribution. However, a uniform station distribution around the Earth will map to a distribution of teleseismic points on the focal sphere which is heavily biased towards the vertical axis, giving some higher order information close to the upward and downward verticals.

We do not show quantitative data here for more than one station, since they are highly dependent upon the station distribution and range of source types chosen. Computations can be carried out for specific cases using the methods employed here for the single station, and using the computer programs FINF and CPLT described in [26].

7. CONCLUSIONS

In section 5 we have presented formally the data required to establish the degree to which small teleseismically recorded seismic sources can be discriminated on the basis of their radiation patterns. We have then identified the circumstances in which it may be possible to discriminate between seismic source types, using observations from single stations, or from a number of independent stations, and we have indicated how this can be extended to analyse observations from a number of stations treated together (section 6).

For single station observations, the results of our analysis of the potential for discriminating between source types using radiation patterns are given in sections 5.3 to 5.5. Sections 5.3 and 5.4 show that the effects of typical uncertainties in epicentral distance and above-source velocity structure do not constitute major impediments, while section 5.5 provides the means to answer the central question — what source types can best be discriminated? We find that relative amplitude data are more successful at discriminating between sources with a different proportion of volumetric component, than they are in discriminating between different types of constant volume source.

The main conclusions of section 5 may be summarised as follows, with references given to parts of section 5 for more detail:

1 For a single source, a seismogram observed at the antipole (corresponding to vertical emergence of *P*, *pP* and *sP* from the source) can contain no information on source type or orientation except for polarity, and all such seismograms are expected to be of class 10 (section 5.3).

2 The distribution of seismogram occurrence probability across the compatibility plot is dominated by a narrow ridge which intersects only a small number of seismogram classes. For the double couple this ridge runs from top left to bottom right of the plot. To its right is a region, defined by a "characteristic boundary" where the probability is identically zero (section 5.3). For other source types the characteristic boundary takes different forms, becoming a closed loop with no lateral spread of probability measure in the case of the vector dipole (section 5.5).

3 It follows from 2 that seismograms observed at teleseismic distances from a double-couple source are almost completely restricted to a small number of classes, and classes having *P*, *pP* and *sP* all large are very unlikely to occur (section 5.3). The predominant classes change with source type, and the extent of these differences determine the ability of relative amplitudes to discriminate between the respective source types. However, the scarcity of seismograms with all three phases large is predicted for most, but not all, source types (section 5.5).

4 For all source types, probability measure is generally concentrated towards the lower left of the plot, but not in the extreme lower left, so that seismogram classes towards the upper right of the plot and at the extreme lower left are not expected at all for correctly interpreted seismograms from single sources (section 5.5).

5 Variation of the distribution of seismogram probability (and hence class) with epicentral distance is significant but not substantial within the teleseismic range of take-off angles (section 5.3). Variation within the realistic range of above-source velocity structures is generally small (section 5.4), so that uncertainty in the above-source structure need not seriously affect the validity of relative amplitude observations.

6 Certain symmetries between the plots of seismogram occurrence probability for different source types have been identified and explained (section 5.5).

7 Relative amplitudes have a high ability to discriminate between sources which have a large implosive component, a large explosive component, and no volume change component. They are particularly good at discriminating between sources with a large implosive or explosive component and the double couple. They are less good at discriminating between different constant volume source types; more information on the *S* wave radiation pattern is usually required to do this effectively (section 5.5).

8 The inclusion of more than one station is predicted to increase the power to discriminate between source types considerably (section 6).

A specific question of interest is whether relative amplitude data are potentially useful for earthquake/explosion discrimination. This question is not a simple one to answer because one is not in practice presented with a simple choice between these two source types when using such data. The use of relative amplitudes presupposes the correct identification of surface-reflected phases, and inherent in these identifications is a determination of focal depth. If discrete surface reflections are identified, then the source is probably too deep to be an explosion. In this situation the problem is one of demonstrating either that the phase identifications are correct (which would be evidenced by the data fitting a double couple) or that the identifications are incorrect (which failure to fit a double couple would support). This second possibility raises the further question as to what the observed waveforms do represent. For example, they could represent multiple explosions [28]. These problems are considered in detail elsewhere. In this report it has been shown that this minimum information retrievable from small teleseismic *P* wave signals can hold important information on the *P* and *S* wave radiation patterns in certain circumstances, and the means have been presented by which observed seismograms can be tested against different source types.

8. ACKNOWLEDGEMENTS

This work has benefited greatly from discussions with Professor A Douglas. The authors much appreciate having his many helpful suggestions.

REFERENCES

1 R G Pearce: "Fault plane solutions using relative amplitudes of *P* and *pP*". Geophys J R astr Soc, **50**, 381-394 (1977).

2 R G Pearce: "Fault plane solutions using relative amplitudes of *P* and surface reflections: further studies". Geophys J R astr Soc, **60**, 459-488 (1980).

3 R G Pearce: "The information content of relative amplitude observations". AWRE Report No. O 32/83, HMSO (1984).

4 R G Pearce: "Earthquake focal mechanisms from relative amplitudes of *P*, *pP* and *sP*: method and computer program". AWRE Report No. O 41/79, HMSO (1979).

5 R G Pearce, H Bainbridge, J B Young & P F Key: "The 1977 earthquake sequence in Uzbekistan: focal mechanisms determined using the relative amplitude method". AWRE Report No. O 26/80, HMSO (1980).

6 R G Pearce: "Complex *P* seismograms from a Gulf of Aden earthquake". Geophys J R astr Soc, **64**, 187-200 (1981).

7 C I Pooley, A Douglas & R G Pearce: "The seismic disturbance of 1976 March 20, E Kazakhstan: Earthquake or Explosions?". Geophys J R astr Soc, **74**, 621-631 (1983).

8 A Douglas, R C Stewart & L Richardson: "Comments on 'Analysis of broad band seismograms from the Chile-Peru area' by R Kind & D Seidl". Bull Seism Soc Am, **74**, 773-777 (1984).

9 H Trodd, P Warburton & C I Pooley: "The great British earthquake of 1984 seen from afar". Geophys J R astr Soc, **83**, 809-812 (1985).

10 R C Stewart: "A seismic event on August 20, 1983: double explosion or a single earthquake". Phys Earth Planet Inter, **46**, 381-383 (1987).

11 R G Pearce: "The relative amplitude method applied to 19 March 1984 Uzbekistan earthquake and its aftershocks". Phys Earth Planet Inter, **47**, 137-149 (1987).

12 R A Clark & A Graham: "Focal mechanism of the 20 August 1983, Caspian Sea earthquake". Phys Earth Planet Inter, **55**, 135-143 (1989).

13 P D Marshall, R C Stewart & R C Lilwall: "The seismic disturbance on 1986 August 1 near Novaya Zemlya: a source of concern?". Geophys J, **98**, 565-573 (1989).

14 R G Pearce & R M Rogers: "Determination of earthquake moment tensors from teleseismic relative amplitude observations". J Geophys Res, **94**, 775-786 (1989).

15 J A Hudson, R G Pearce & R M Rogers: "Source-type plot for inversion of the moment tensor". J Geophys Res, **94**, 765-774 (1989).

16 R M Rogers: "Earthquake moment tensors from teleseismic relative amplitudes". PhD thesis, University of Wales (1989).

17 R M Rogers & R G Pearce: "Application of the relative amplitude moment-tensor program to three intermediate-depth IASPEI earthquakes". Phys Earth Planet Inter, **47**, 93-106 (1987).

18 I G Stimpson & R G Pearce: "Moment tensors and source processes of three deep Sea of Okhotsk earthquakes". Phys Earth Planet Inter, **47**, 107-124 (1987).

19 I G Stimpson: "The relative amplitude moment tensor method applied to the IASPEI deep earthquakes". Phys Earth Planet Inter, **47**, 150-158 (1987).

20 R M Rogers & R G Pearce: "Use of the relative amplitude method to compute 'best-fit' earthquake moment tensors". J Geophys Res, **97**, 14083-14095 (1992).

21 A Douglas, J A Hudson & C Blamey: "A quantitative evaluation of seismic signals at teleseismic distances — III. Computed *P* and Rayleigh wave seismograms". Geophys J R astr Soc, **28**, 385-410 (1972).

22 K Aki & P G Richards: "Quantitative seismology: theory and methods" Vol. I. Freeman, San Francisco, 557pp (1980).

23 A M Dziewonski, T-A Chou & J H Woodhouse: "Determination of earthquake source parameters from waveform data for studies of global and regional seismicity". J Geophys Res, **86**, 2825-2852 (1981).

24 S A Sipkin: "Estimation of earthquake source parameters by the inversion of waveform data: global seismicity 1981-83". Bull Seism Soc Am, **76**, 1515-1541 (1986).

25 R A Strelitz: "Moment tensor inversions and source models". Geophys J R astr Soc, **52**, 359-364 (1978).

26 R G Pearce: "FORTRAN computer programs for use in seismic discrimination by radiation pattern measurements". AWE Report in preparation.

27 R G Pearce, J A Hudson & A Douglas: "On the use of *P*-wave seismograms to identify a double-couple source". Bull Seism Soc Am, **78**, 651-671 (1988).

28 R A Clark & R G Pearce: "Identification of multiple underground explosions using the relative amplitude method". Bull Seism Soc Am, **78**, 885-897 (1988).

APPENDIX A

GLOSSARY

This glossary explains particularly those terms which have been given a special meaning by the authors in the context of this and related work. If appropriate a reference is made to the section in this report where the term is introduced or explained more fully.

Characteristic boundary (sections 5.3 and 5.5). A feature of the probability density display of seismogram class when shown on a compatibility plot. The boundary has the appearance of a curved line or closed loop depending upon source type. It is related to the distribution of probability measure in different ways according to the source type; probability measure may be restricted to one side of the boundary, it may lie predominantly on one side of the boundary with a discontinuity in density at the boundary, or it may be confined to the boundary itself.

Class (of a seismogram) (section 3.2). Description of a seismogram according to the values of the relative amplitudes of the direct *P* and surface reflections *pP* and *sP*, and their polarities on that seismogram. The range of possible values has been divided arbitrarily into 27 classes, and any *P* seismogram observed at teleseismic distance can be described as belonging to one of these classes (or to any of a number of classes if the observation is of poor quality or lies near a boundary between classes). (There is some overlap in relative amplitude values between some classes, but this is unimportant.)

Compatibility plot (sections 4.1 to 4.4). A display showing all possible combinations of *P*, *pP* and *sP* relative amplitudes and polarities (i.e. all seismogram classes). There are only two independent amplitude ratios obtainable from three amplitudes, so the plot is two-dimensional. The ratio of the amplitudes of *sP* and *P* is the ordinate, and the ratio of the amplitudes of *pP* and *P* is the abscissa. However, the plot is not Cartesian. The shape of the plot is a consequence of imposing an equal-area condition. This is specified such that a random selection of relative amplitude observations plot with uniform density over the whole compatibility plot. A random set of relative amplitude observations is defined as having each of the three phases independent and uniformly distributed in amplitude up to some upper limit, the value of which is unimportant because ratios of amplitudes are always taken. To cover all combinations of polarities of the three phases, a pair of plots is required; these are referred to as the *P*-negative and the *P*-positive plots, according to the polarity of direct *P*. Relative amplitude measurements corresponding to particular seismograms can be displayed in the form of curvilinear polygons representing the parts of the plot whose relative amplitudes lie within the confidence of the amplitude measurements. Any parameter which varies with relative amplitude value can be plotted using either a dot-density display or a matrix-element display, as alternatives to conventional contouring.

Compensated linear vector dipole (CLVD). A seismic source comprising a positive vector dipole plus an implosion whose magnitude is just sufficient for the combined source to represent no volume change. Its *P*-wave radiation pattern has the form of a positive dipole with a negative toroid concentric with the dipole.

Constant volume component (of a seismic source) (section 3.4). That component of the seismic source which remains after any explosive or implosive component is removed. An explosive or implosive component implies a volume change. The constant volume component is therefore sometimes called the non-volumetric component. A constant volume component has directional variation, so implies shear.

Dot-density display (section 4.4). An alternative to contouring, used on the compatibility plot as a means of displaying any parameter which varies with the relative amplitudes of *P*, *pP*, *sP* and their polarities. The density of dots varies with the value of the parameter to provide a qualitative but easily interpreted display of the variation of parameter value across the compatibility plot.

Double couple. A seismic source corresponding to shear displacement along a fault plane. It is the usual source type assumed for earthquakes, and has no volume change.

Explosion. A directionally uniform seismic source representing a sudden gain in volume. It contains no constant-volume component (i.e. no shear).

Implosion. A directionally uniform seismic source representing a sudden loss of volume. It contains no constant-volume component (i.e. no shear).

k (section 3.4). Parameter used to indicate the proportion of volumetric component in a seismic source. Its value can range from –1 (pure implosion) through 0 (no volumetric component) to +1 (pure explosion).

Matrix-element display (section 4.4). An alternative to contouring, devised specifically for use on the compatibility plot as a means of displaying any parameter which varies with the relative amplitudes of *P pP*, *sP* and their polarities. The plot is divided into square bins (the matrix elements), and in each bin the value of the parameter integrated over the bin is plotted. This gives a quantitative measure of the variation of the parameter across the compatibility plot.

Negative compensated linear vector dipole (negative CLVD). A seismic source comprising a negative vector dipole plus an explosion whose magnitude is just sufficient for the combined source to represent no volume change. Its *P*-wave radiation pattern has the form of a negative dipole with a positive toroid concentric with the dipole.

Quality (of a seismogram) (section 3.3). A term describing the power of a seismogram to discriminate between source types and orientations using its relative amplitudes and polarities. The quality depends upon (1) the precision with which the relative amplitudes can be measured (and whether or not unambiguous polarities can be measured) — this is governed by signal-to-noise ratio and related factors — and (2) the class of the seismogram, since this also affects the degree of discrimination between sources which can be achieved.

Relative amplitude method (section 2). A method of determining seismic source mechanisms from the relative amplitudes and polarities of different seismic phases (raypaths) observed at the same station. In this report teleseismic observations of the direct *P* wave and the surface reflections *pP* and *sP* are implied.

Significance (of a relative amplitude observation or set of observations) (section 3.3). A quantitative measure of the extent to which the observation or observations constrain the source type and/or orientation, given a predefined set of possibilities. Its value can range from 0.0 (implying no constraint) to 1.0 (implying total constraint). For real data the significance can approach arbitrarily close to 1.0, but if it reaches 1.0, this implies that the observations are compatible with none of the possibilities.

Source orientation (section 3.1). The orientation of a seismic source, expressed in terms of three angles, which for the double-couple source correspond to the dip δ and strike σ of the fault plane, and the angle of slip ψ in the fault plane. The orientation is thus expressed with respect to a particular set of axes in which the source type is defined.

Source type (section 3.1). The type of seismic source, defined in terms of the type of constant-volume component, T, the proportion of volumetric component, k, and (olptionally) the absolute size of the source (i.e. scalar moment), M.

Source-type plot (section 3.4). A two-dimensional plot of the values of T and k, upon which source types compatible with a given set of relative amplitude observations can be identified. Using different size circles, the number of compatible orientations of different source types can be displayed, or different degrees of compatibility with the data can be shown. The shape of the plot is a consequence of imposing an equal area condition. The shape is specified such that a random population of different source types plot with uniform density. A random population of source types is defined such that each of the three principal moments (or orthogonal dipoles) comprising the source is independent and uniformly distributed in amplitude up to some limit, the value of which is unimportant since we are not considering the absolute size of the source.

T (section 3.4). Parameter used to describe the type of constant-volume component of a seismic source. Its value can range from −1.0 (CLVD) through 0.0 (double couple) to +1.0 (negative CLVD).

Tensile crack. A seismic source corresponding to the opening of a crack. The stress in the direction normal to the crack must be an absolute tension.

Vector dipole. A seismic source represented by equal and opposite forces acting along a single axis.

Vectorplot (section 3.1). A means of displaying the values of a discrete, three dimensional function where at least one of the dimensions is an angle. A grid of points is used to represent two of the dimensions, and the angle about the grid points is used to represent the third dimension. Vectors with lengths corresponding to the parameter value are drawn from the grid points. Here the vectorplot is used to display all possible orientations of a seismic source, defined in terms of fault plane dip δ, strike σ, and angle of slip ψ in the fault plane. (For non-double-couple sources the "fault plane" has no physical significance.) Those orientations of a chosen source type which are compatible with all (or a certain proportion of) a given set observations are plotted. The discrete values of the points correspond to the sampling used in computation.

Volumetric component (of a seismic source) (section 3.4). That component of a seismic source which represents a volume change. It is alternatively referred to as the explosive or implosive component, or the isotropic component since it is independent of direction.

TABLE 1

Values of the normalised principal moments (M_x,M_y and M_z), constant volume parameter (T), and proportion of isotropic component (k) for important source types

Source type	M_x	M_y	M_z	T	k
Explosion	2	2	2	undef.	1
Implosion	−2	−2	−2	undef.	−1
Double couple	2	−2	0	0	0
Dipole	0	0	2	−1	1/3
CLVD	−1	−1	2	−1	0
Negative CLVD	1	1	−2	1	0
Tensile crack	2/3	2/3	2	−1	5/9

The values of the principal moments are shown normalised so that the absolute value of the largest moment is equal to 2.0, following equation 2.

For the explosion and implosion T is undefined; there is no constant volume component.

For the tensile crack, the values of the parameters, and hence the radiation pattern, depend upon Poisson's ratio. Here the values are shown for a medium with a Poisson's ratio of 0.25.

CLVD Compensated linear vector dipole.

TABLE 2

Velocity structure used for the compatibility plots presented for sources in a layered structure

	P-wave velocity (km/sec)	Density (gm/cm^3)	Thickness (km)
Layer 1	3.0	2.7	0.5
Layer 2	4.6	2.7	3.0
Layer 3 (source layer)	6.1	2.8	

Layer thicknesses are not used. In all cases, the S-wave velocity is set to $1/\sqrt{3}$ times the P-wave velocity.

Structure taken from [27].

TABLE 3

Summary of assumptions in figures 15 to 106

Source type		Take-off angle			
T	k	5° (halfspace)	15° (halfspace)	30° (halfspace)	30° (velocity structure)
−1.0	5/9	Fig. 15	Fig. 16	Fig. 17	Fig. 18
−1.0	0.5	Fig. 19	Fig. 20	Fig. 21	Fig. 22
0.0	0.5	Fig. 23	Fig. 24	Fig. 25	Fig. 26
1.0	0.5	Fig. 27	Fig. 28	Fig. 29	Fig. 30
−1.0	1/3	Fig. 31	Fig. 32	Fig. 33	Fig. 34
−1.0	0.25	Fig. 35	Fig. 36	Fig. 37	Fig. 38
−0.5	0.25	Fig. 39	Fig. 40	Fig. 41	Fig. 42
0.0	0.25	Fig. 43	Fig. 44	Fig. 45	Fig. 46
0.5	0.25	Fig. 47	Fig. 48	Fig. 49	Fig. 50
1.0	0.25	Fig. 51	Fig. 52	Fig. 53	Fig. 54
−1.0	0.0	Fig. 55	Fig. 56	Fig. 57	Fig. 58
−0.5	0.0	Fig. 59	Fig. 60	Fig. 61	Fig. 62
0.0	0.0	Fig. 63	Fig. 64	Fig. 65	Fig. 66
0.5	0.0	Fig. 67	Fig. 68	Fig. 69	Fig. 70
1.0	0.0	Fig. 71	Fig. 72	Fig. 73	Fig. 74
−1.0	−0.25	Fig. 75	Fig. 76	Fig. 77	Fig. 78
−0.5	−0.25	Fig. 79	Fig. 80	Fig. 81	Fig. 82
0.0	−0.25	Fig. 83	Fig. 84	Fig. 85	Fig. 86
0.5	−0.25	Fig. 87	Fig. 88	Fig. 89	Fig. 90
1.0	−0.25	Fig. 91	Fig. 92	Fig. 93	Fig. 94
−1.0	−0.5	Fig. 95	Fig. 96	Fig. 97	Fig. 98
0.0	−0.5	Fig. 99	Fig. 100	Fig. 101	Fig. 102
1.0	−0.5	Fig. 103	Fig. 104	Fig. 105	Fig. 106

In figures 15 to 34 the P-negative compatibility plot contains no probability measure so is not shown. In figures 95 to 106 the P-positive compatibility plot contains no probability measure so is not shown.

LIST OF FIGURE CAPTIONS

FIGURE 1. Ray geometry for the phases *P*, *pP* and *sP* at teleseismic distances.

FIGURE 2. Source and ray geometries. (a) The three angles used to define the orientation of the source. For the double couple the angles have a physical significance: δ, σ and ψ are the fault plane (or auxiliary plane) dip, its strike, and the slip angle respectively. (For comparison between this and the convention used by some other authors see section 3.1.) (b) Definition of station azimuth and take-off angles of *P*, *pP* and *sP*.

FIGURE 3. The vectorplot, used for displaying ranges of compatible source orientations. Each vector drawn on such a plot is equivalent to one fault plane solution plotted on a conventional stereographic projection. Note that in this figure only, shaded quadrants are negative.

FIGURE 4 The 27 classes of *P*-wave seismogram defined according to whether each of the phases *P*, *pP* and *sP* is "large and positive", "large and negative" or "small". The definitions are taken from [2], extended to distinguish between seismograms which are of the same class except for a polarity reversal of the whole seismogram; by convention, suffixes "+ve" and "–ve" denote seismograms on which the first large phase is positive and negative respectively. Another addition is the "class 0" seismogram (see section 3.2).

FIGURE 5. The source-type plot (from [14] with additional detail). The plot shows all possible source types defined in terms of the variables *T* and *k*, which describe the type of constant-volume component and the proportion of volume-change component respectively (see section 3.4). The shape of the plot results from the imposition of the condition that the plot display uniform probability density of source types, given no *a priori* constraint on the moment tensor (see section 3.4 and [15]). (a) shows the positions of specific source types on the plot. The limits between which the *P*-wave radiation pattern includes both polarities (i.e. there are nodal surfaces) are shown dotted. The dashed line shows the locus along which these nodal surfaces are planar (see [14] and [15]). (b) and (c) show the form of the *P* nodal surfaces for a north-striking 45° dip-slip (thrust) fault (or equivalent for non-double-couple sources) and a north-striking vertical dextral strike-slip fault (or equivalent) respectively. Shaded quadrants are positive. (d) shows *S* wave radiation patterns for a series of *T* values, presented in isometric view by the method of section 3.5, and oriented as shown. The *S* wave radiation pattern is independent of *k*, except in its amplitude relative to that of *P*.

FIGURE 6. The significance of each of the classes of *P*-wave seismogram defined in figure 4, computed for the double-couple source type (T=0, k=0) for a presumed halfspace in the source region (from [2]). For each class, the significance is plotted as a function of increasing take-off angle (which relates to decreasing epicentral distance Δ). For the double-couple source the significance value does not change if the complete seismogram is inverted (see section 3.2), so then only 13 curves need be shown.

FIGURE 7. The compatibility plot (from [27]). The plot shows all possible values of the relative amplitudes of *P*, *pP* and *sP*. The shape of the plot results from the imposition of the condition that the plot be uniform in seismogram quality (see section 4.1 and [27]). In general, two plots are required to distinguish between seismograms with negative direct *P* and positive direct *P* (see section 4.1). (a) shows the locus of different relative amplitude values on the plots. The near-vertical lines join points of equal *pP*/*P* relative amplitude, and the near-horizontal lines join those of equal *sP*/*P* relative amplitude. Lines joining equal values of *sP*/*pP* relative amplitude are also shown (pecked for clarity), but this is not an independent variable — its value is fixed for each combination of the other two ratios. (b) shows schematically those parts of the plot occupied by seismograms whose phases have different relative amplitudes — i.e. seismograms of different class. (c) summarises the polarity of each phase in each of the eight quadrants. (d) shows an example of how a real seismogram plots. The amplitude of each phase is assigned upper and lower bounds to allow for uncertainties, so the seismogram occupies a curvilinear polygon whose perimeter segments correspond to the limits on each of the three amplitude ratios. Depending upon knowledge of the polarity of each phase, there may be similar polygons in any of the eight quadrants.

FIGURE 8. The 27 classes of *P*-wave seismogram defined in figure 4, plotted on a pair of compatibility plots (see section 4.5). The information presented is equivalent to that in figure 4.

FIGURE 9. Compatibility plot showing the probability density of seismogram classes observed for a *P*-wave take-off angle of 0° (*PKIKP* observation at the antipole) for a double-couple source whose orientation is unknown, but with uniform probability over all orientations. The source is assumed to be in a halfspace, so that the only correction applied to *pP* and *sP* for structure above the source is the effect of reflection at the free surface. This is a trivial case in that all probability measure is concentrated at two points, one on each of the *P*-negative and *P*-positive plots. For the double couple the *P*-negative and *P*-positive plots are identical so only one is shown, and the equivalent dot-density display and matrix-element display are shown side by side. For an explanation of the normalisation of the matrix-element display see section 4.4.

FIGURE 10. The same as figure 9, except that the *P*-wave take-off angle is 5°.

FIGURE 11. The same as figure 9, except that the *P*-wave take-off angle is 15°.

FIGURE 12. The same as figure 9, except that the *P*-wave take-off angle is 30°.

FIGURE 13. Repeat of (a) figure 9, and (b) figure 12, with the inclusion of the effect of a typical velocity structure above the source (table 2).

FIGURE 14. Summary of compatibility plots for a selection of source types, computed for a take-off angle of 15° and the source in a halfspace. The compatibility plots are arranged schematically around a source-type plot which is split between three pages to provide sufficient space.

FIGURES 15 - 106. Compatibility plots for the source types summarised in figure 14, computed for a range of takeoff angles. Source types are ordered according to their appearance on the source-type plot (see figure 14). That is, for each successive value of k (beginning with the largest), figures are ordered with increasing T. For each source type four successive figures appear. The first three show plots for take-off angles of 5°, 15° and 30° respectively, in a halfspace so that no correction is made to the amplitude of the surface reflections except for reflection at the free surface. This covers the typical range for teleseismic observations. The fourth figure shows plots for a takeoff angle of 30° with allowance for the effect on the surface-reflected phases of the velocity structure shown in table 2. In general, each figure shows P-negative and P-positive dot-density plots, followed by the equivalent pair of matrix-element displays on the following page. In cases where either the P-negative or P-positive plot contains zero probability measure, the blank plot is not shown, so the single dot-density display and its equivalent matrix-element display are shown on the same page. For the double couple the P-negative and P-positive plots are identical, but both are shown, to allow separate plotting of seismograms with negative and positive P. The assumptions in each of these figures are summarised in table 3. For a more detailed description, in particular of the matrix-element display, see section 4.4. The use of these plots to determine the significance of individual seismograms is also described in section 4.4.

seismograph
P
pP
sP
short period
seismogram
~10 sec.
shallow
earthquake
pP
sP
P

FIGURE 1

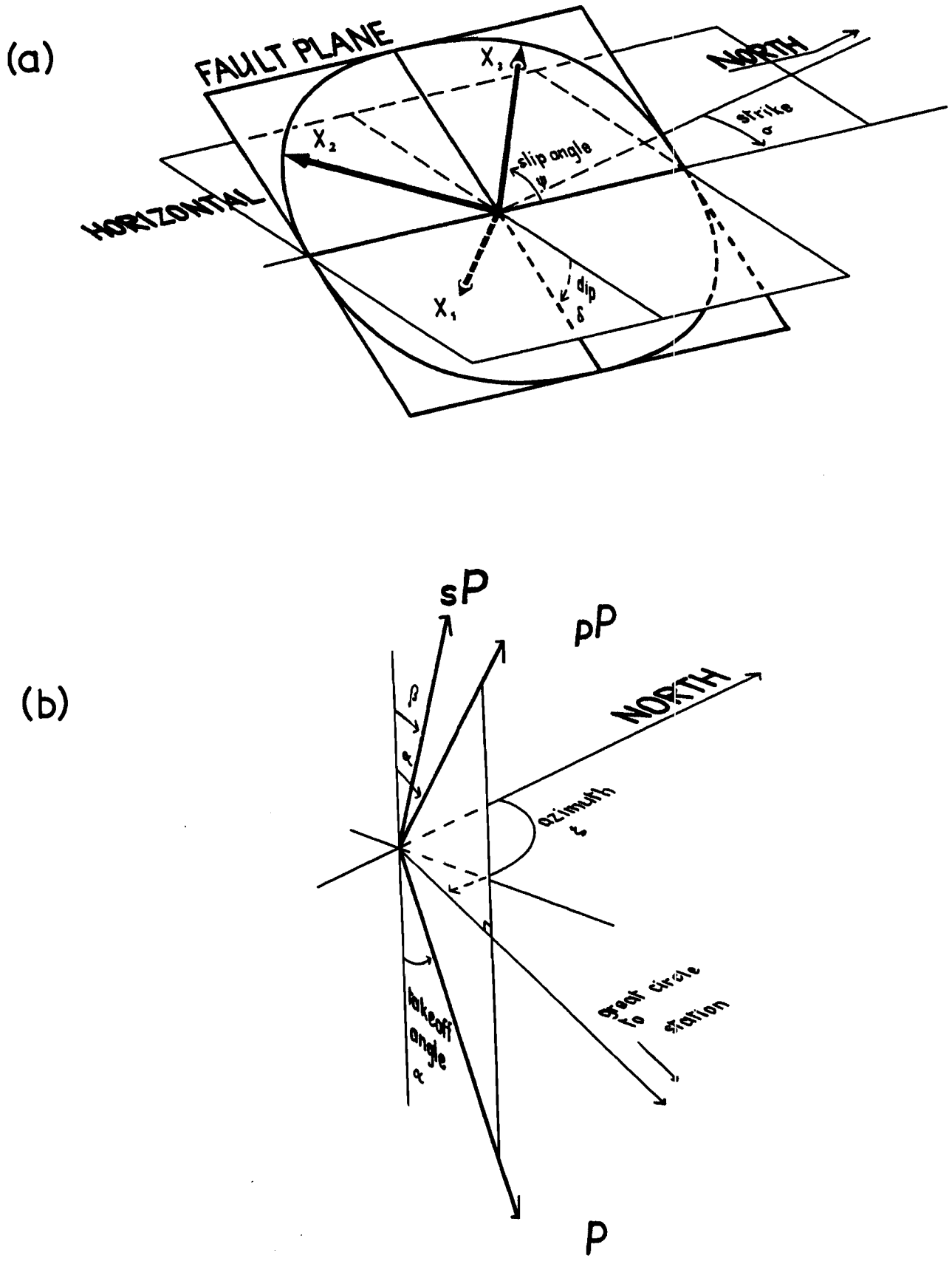
(a)
FAULT PLANE
NORTH
HORIZONTAL
X_3
X_2
X_1
slip angle
ψ
strike
σ
dip
δ
(b)
sP
pP
P
NORTH
β
azimuth
ξ
takeoff angle
α
great circle to station

FIGURE 2

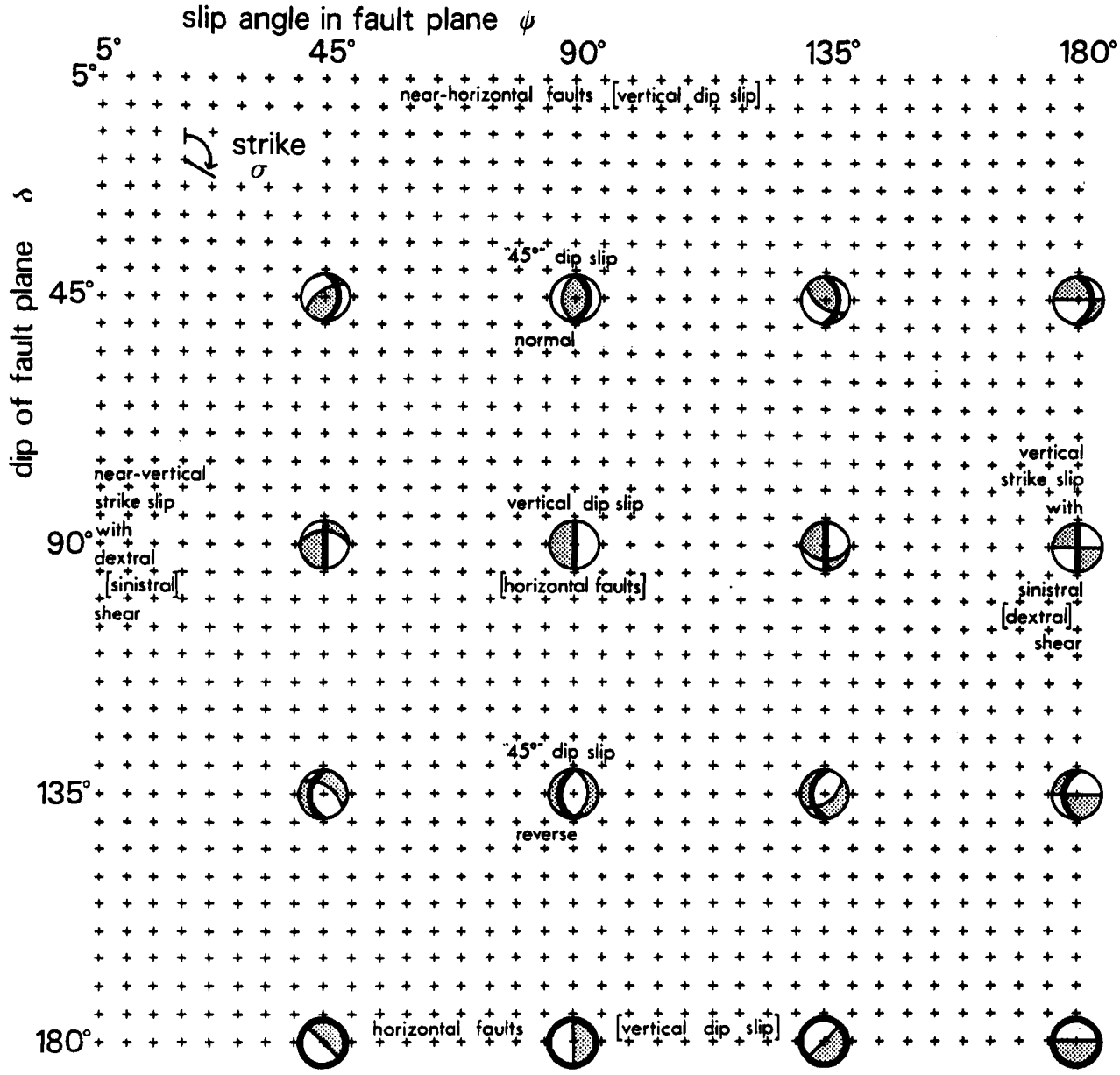

Method of representing acceptable fault plane orientations in terms of slip direction ψ, dip δ and strike σ.

Acceptable orientations are plotted as vectors from the Cartesian point defining ψ and δ, in the direction of the strike σ. Lower hemisphere stereographic projections indicate the type of fault plane orientation represented by various combinations of ψ and δ, and are shown oriented for strike $\sigma = 360°$ (northerly). In each case the fault plane is shown by a thick line ——; the auxiliary plane by a thin line ——. Shaded quadrants ▒ are negative. Different parts of the plot characterize various fault types, and some of these are shown. Where the interchange of fault and auxiliary planes yields a different fault type, this is shown in square brackets [ ].

FIGURE 3

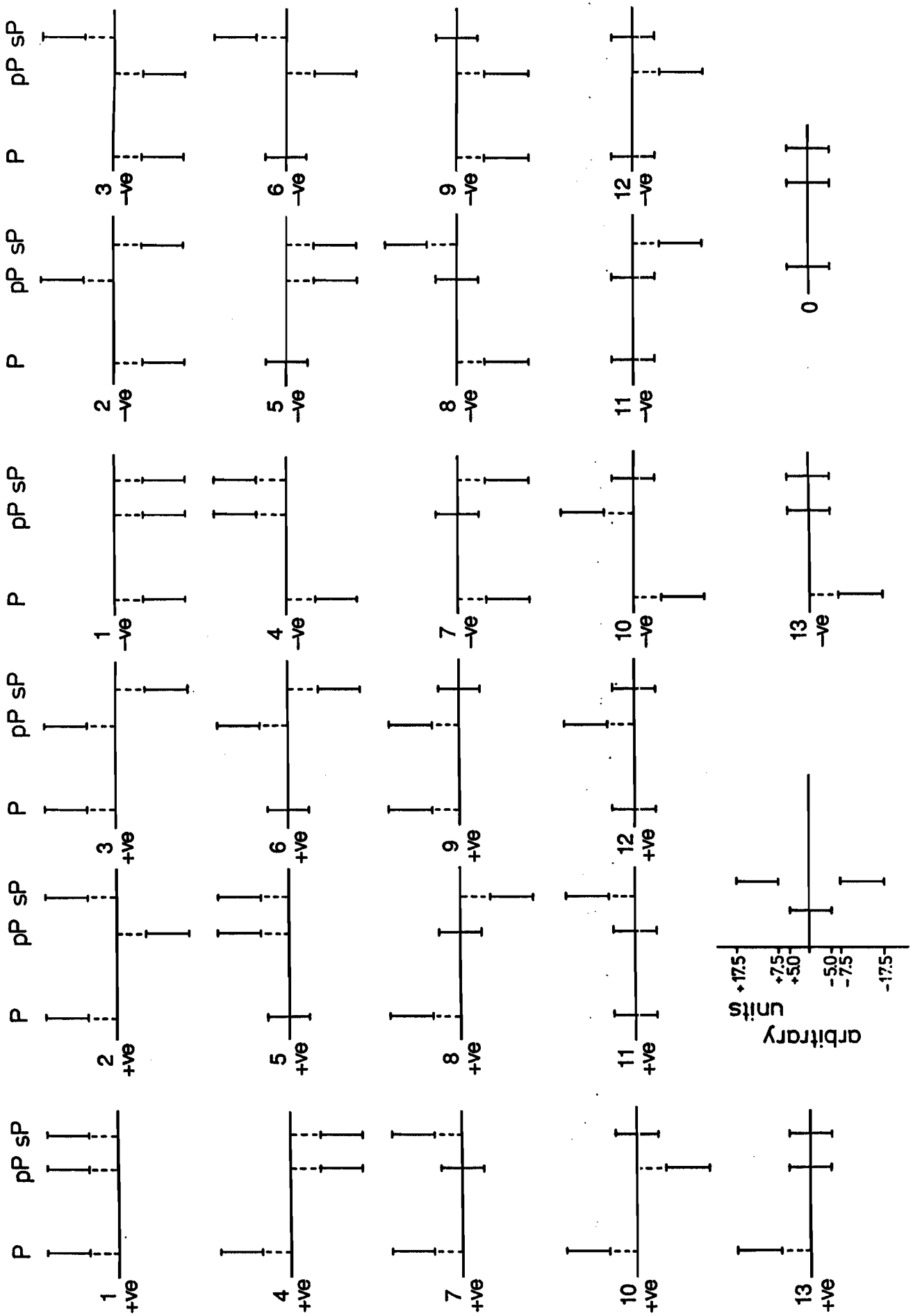
P
pP
sP
1 +ve
2 +ve
3 +ve
4 +ve
5 +ve
6 +ve
7 +ve
8 +ve
9 +ve
10 +ve
11 +ve
12 +ve
13 +ve
1 -ve
2 -ve
3 -ve
4 -ve
5 -ve
6 -ve
7 -ve
8 -ve
9 -ve
10 -ve
11 -ve
12 -ve
13 -ve
0
+17.5
+7.5
+5.0
-5.0
-7.5
-17.5
arbitrary units

FIGURE 4

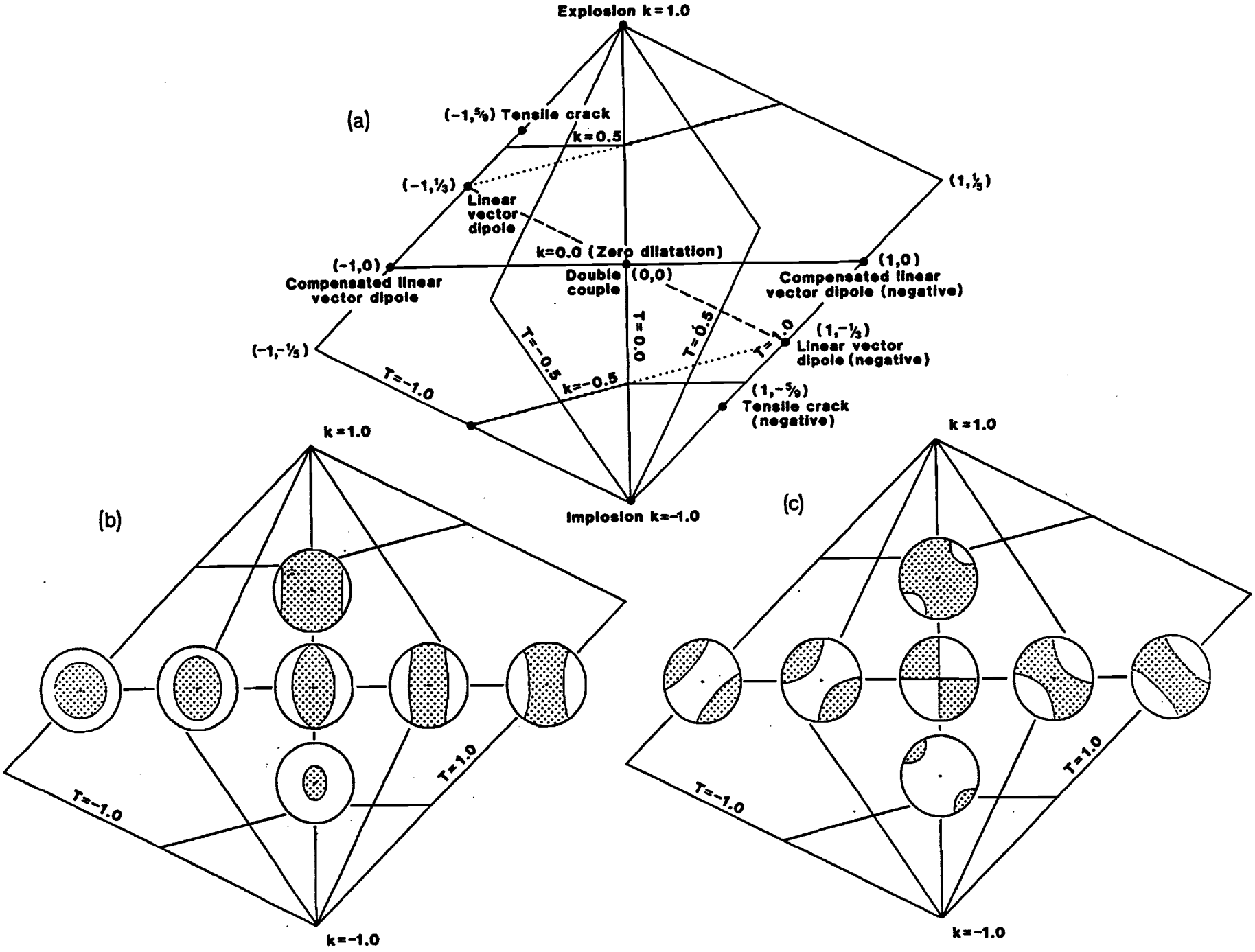
Explosion k = 1.0
(a)
(−1,5/9) Tensile crack
k = 0.5
(−1,1/3)
(1,1/3)
Linear vector dipole
k=0.0 (Zero dilatation)
(−1,0)
Compensated linear vector dipole
Double couple
(0,0)
(1,0)
Compensated linear vector dipole (negative)
T=0.0
T=0.5
T=1.0
T=−0.5
(1,−1/3)
Linear vector dipole (negative)
(−1,−1/3)
T=−1.0
k=−0.5
(1,−5/9)
Tensile crack (negative)
Implosion k=−1.0
k = 1.0
(b)
T=−1.0
T=1.0
k=−1.0
k = 1.0
(c)
T=−1.0
T=1.0
k=−1.0

FIGURE 5 (1)

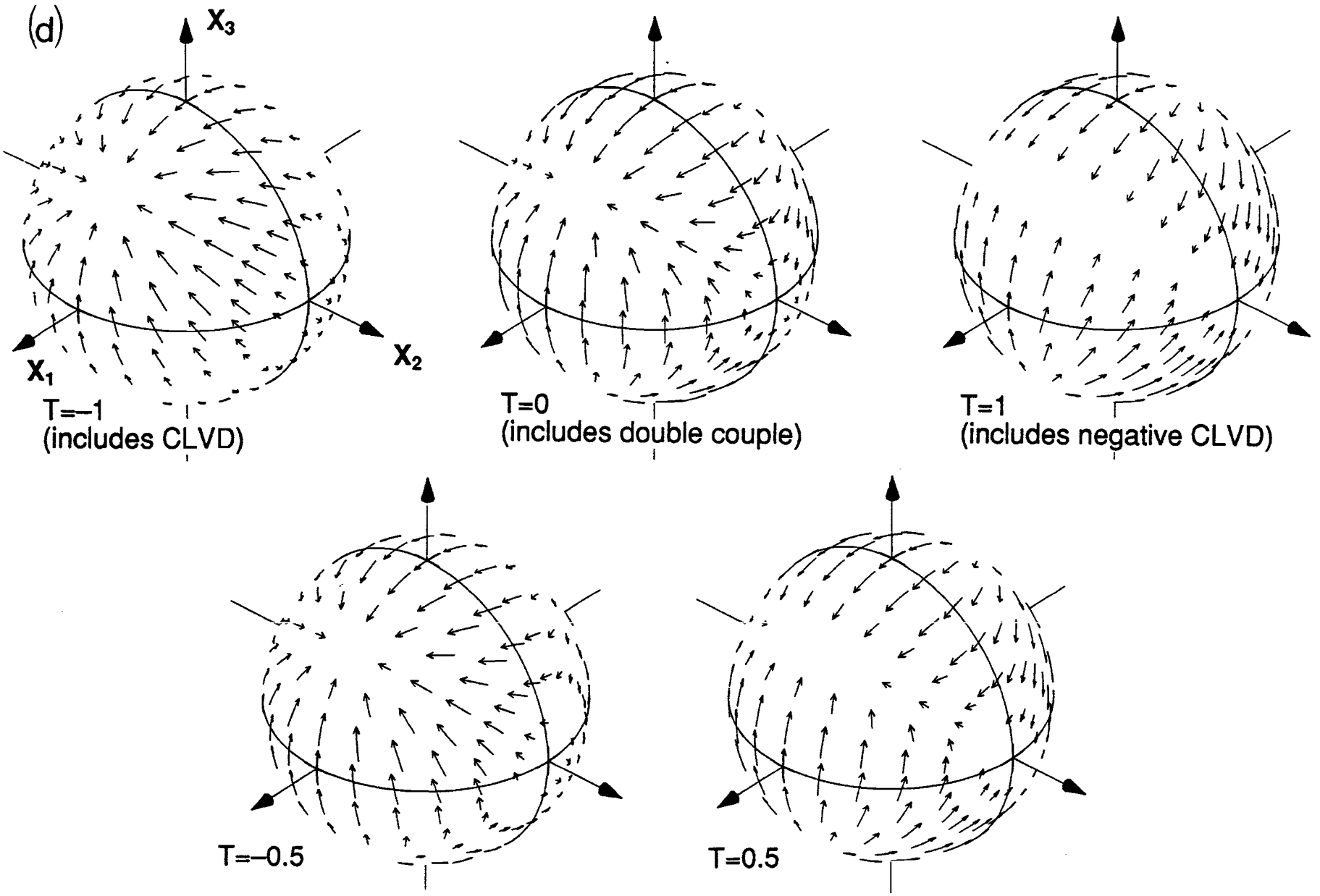
(d)
X3
X1
X2
T=–1
(includes CLVD)
T=0
(includes double couple)
T=1
(includes negative CLVD)
T=–0.5
T=0.5

FIGURE 5 (2)

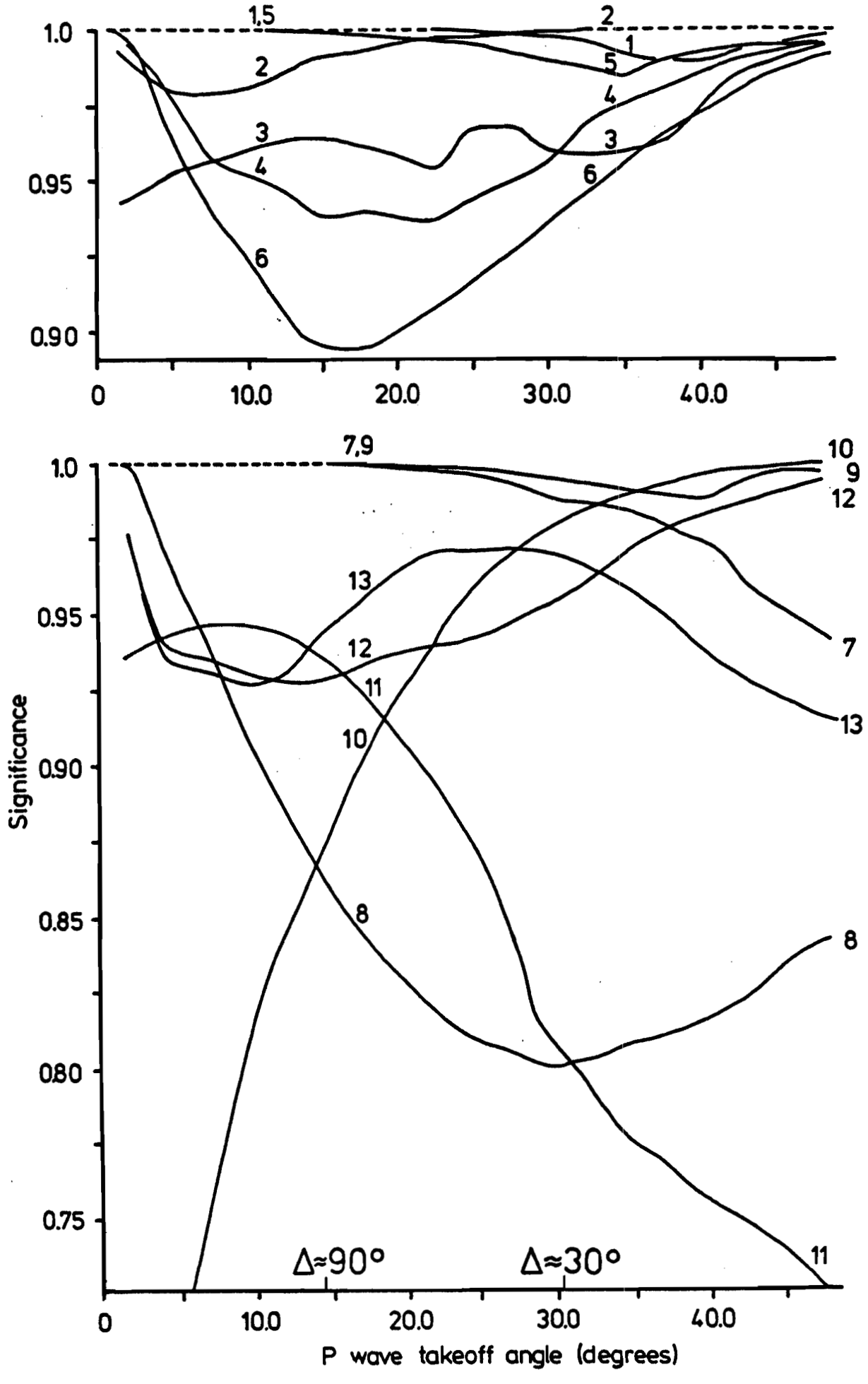
1.0
0.95
0.90
0
10.0
20.0
30.0
40.0
1,5
2
1
5
2
4
3
3
4
6
6
7,9
10
9
12
1.0
0.95
0.90
0.85
0.80
0.75
Significance
13
12
11
10
8
7
13
8
11
Δ≈90°
Δ≈30°
0
10.0
20.0
30.0
40.0
P wave takeoff angle (degrees)

FIGURE 6

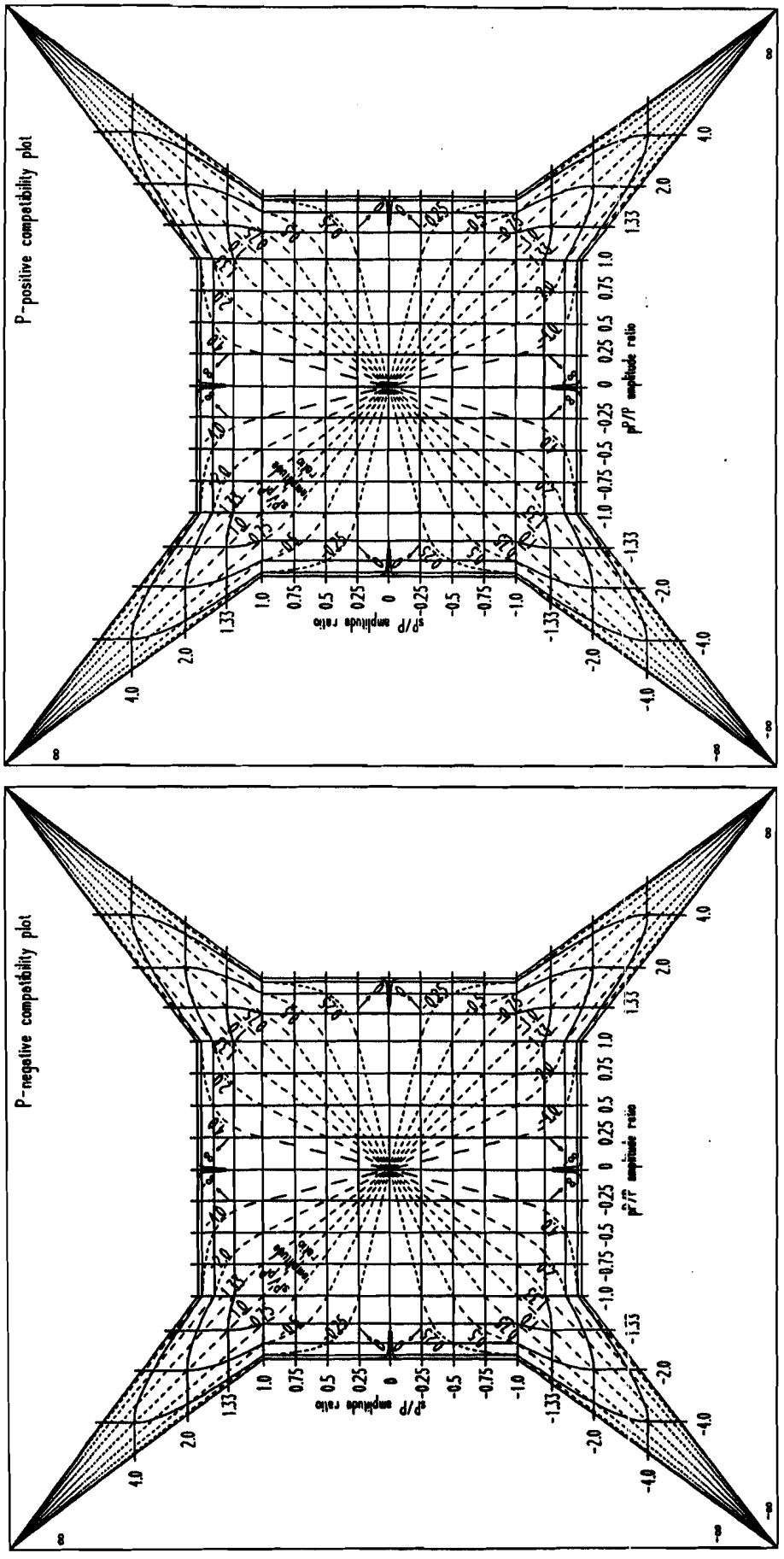
P-positive compatibility plot
P-negative compatibility plot
sP/P amplitude ratio
pP/P amplitude ratio

FIGURE 7(a)

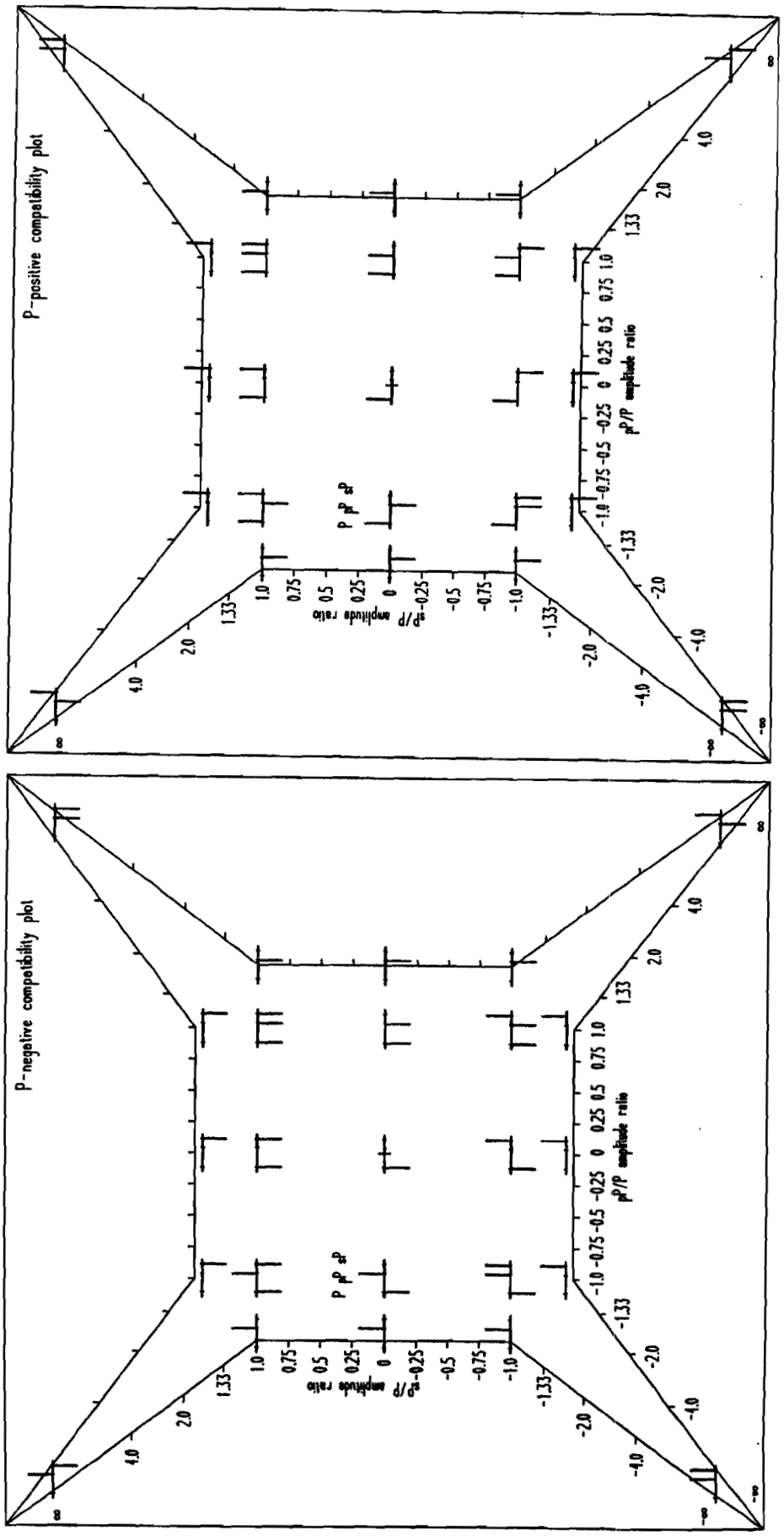
P-positive compatibility plot
P-negative compatibility plot
P pP sP
sP/P amplitude ratio
pP/P amplitude ratio
8
4.0
2.0
1.33
1.0
0.75
0.5
0.25
0
-0.25
-0.5
-0.75
-1.0
-1.33
-2.0
-4.0
-8

FIGURE 7(b)

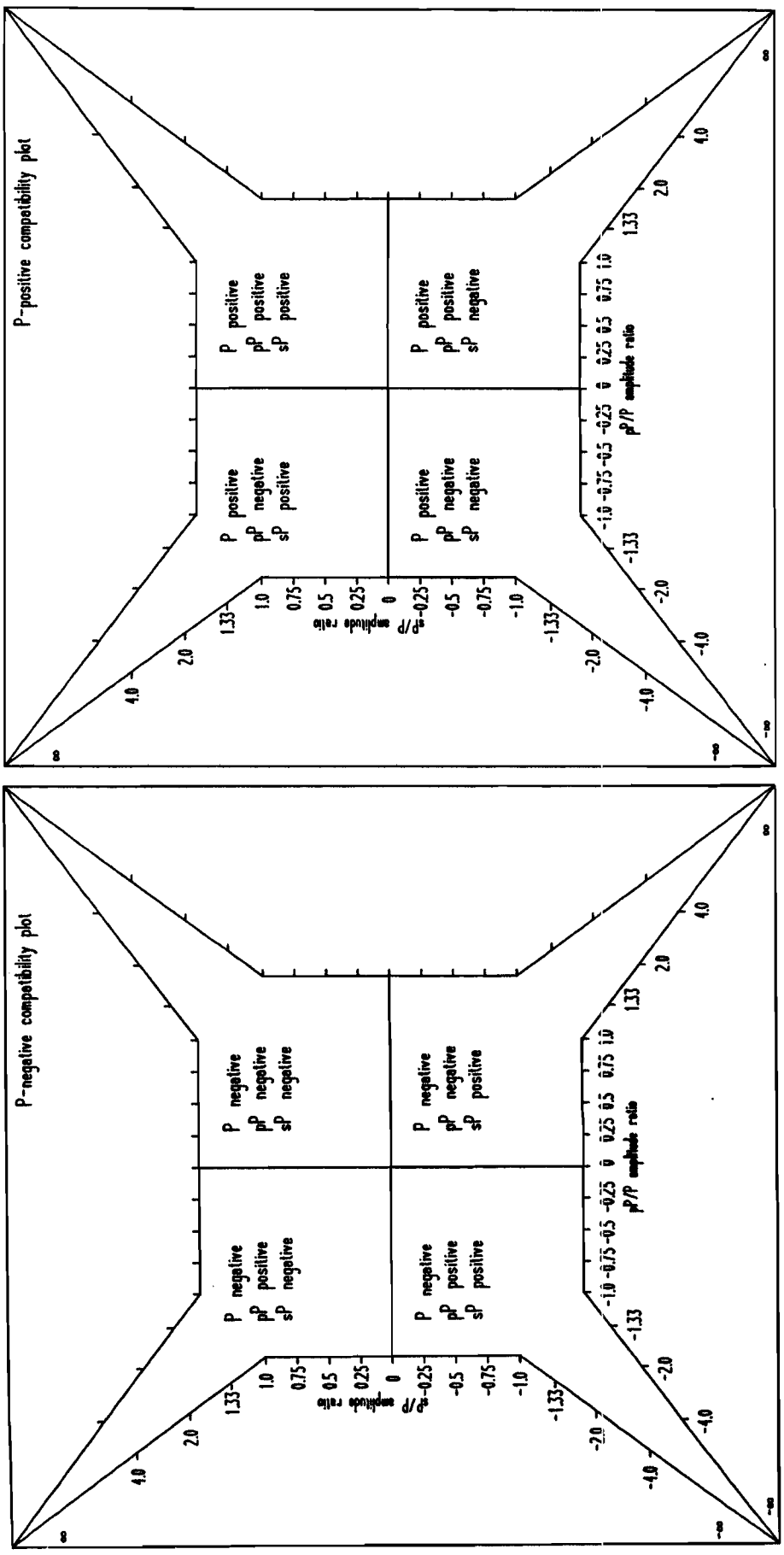
P-positive compatibility plot
P positive
pP positive
sP positive
P positive
pP negative
sP positive
P positive
pP positive
sP negative
P positive
pP negative
sP negative
pP/P amplitude ratio
P-negative compatibility plot
P negative
pP negative
sP negative
P negative
pP positive
sP negative
P negative
pP negative
sP positive
P negative
pP positive
sP positive
pP/P amplitude ratio

FIGURE 7(c)

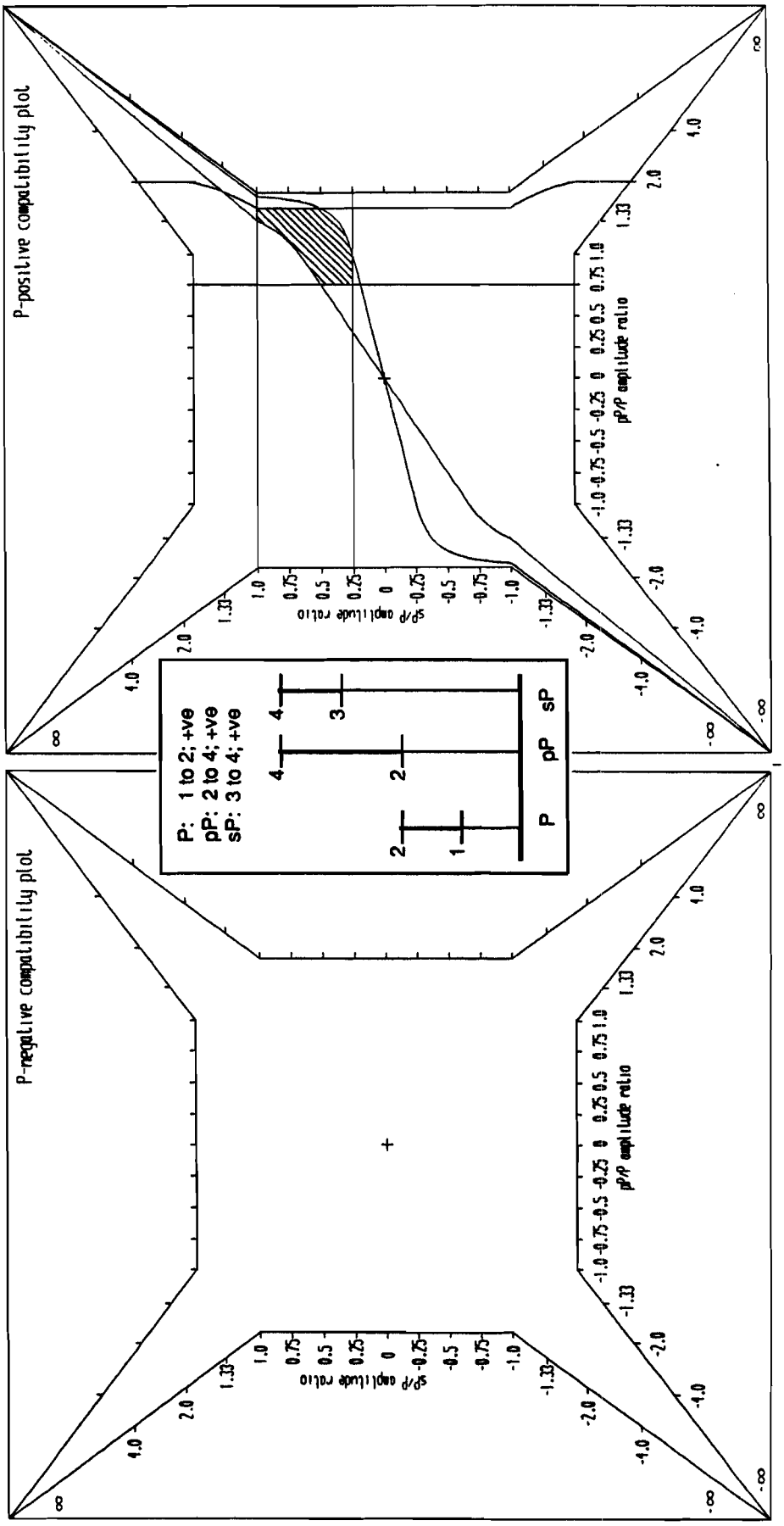
P-positive compatibility plot
P-negative compatibility plot
P: 1 to 2; +ve
pP: 2 to 4; +ve
sP: 3 to 4; +ve
P
pP
sP
sP/P amplitude ratio
pP/P amplitude ratio

FIGURE 7(d)

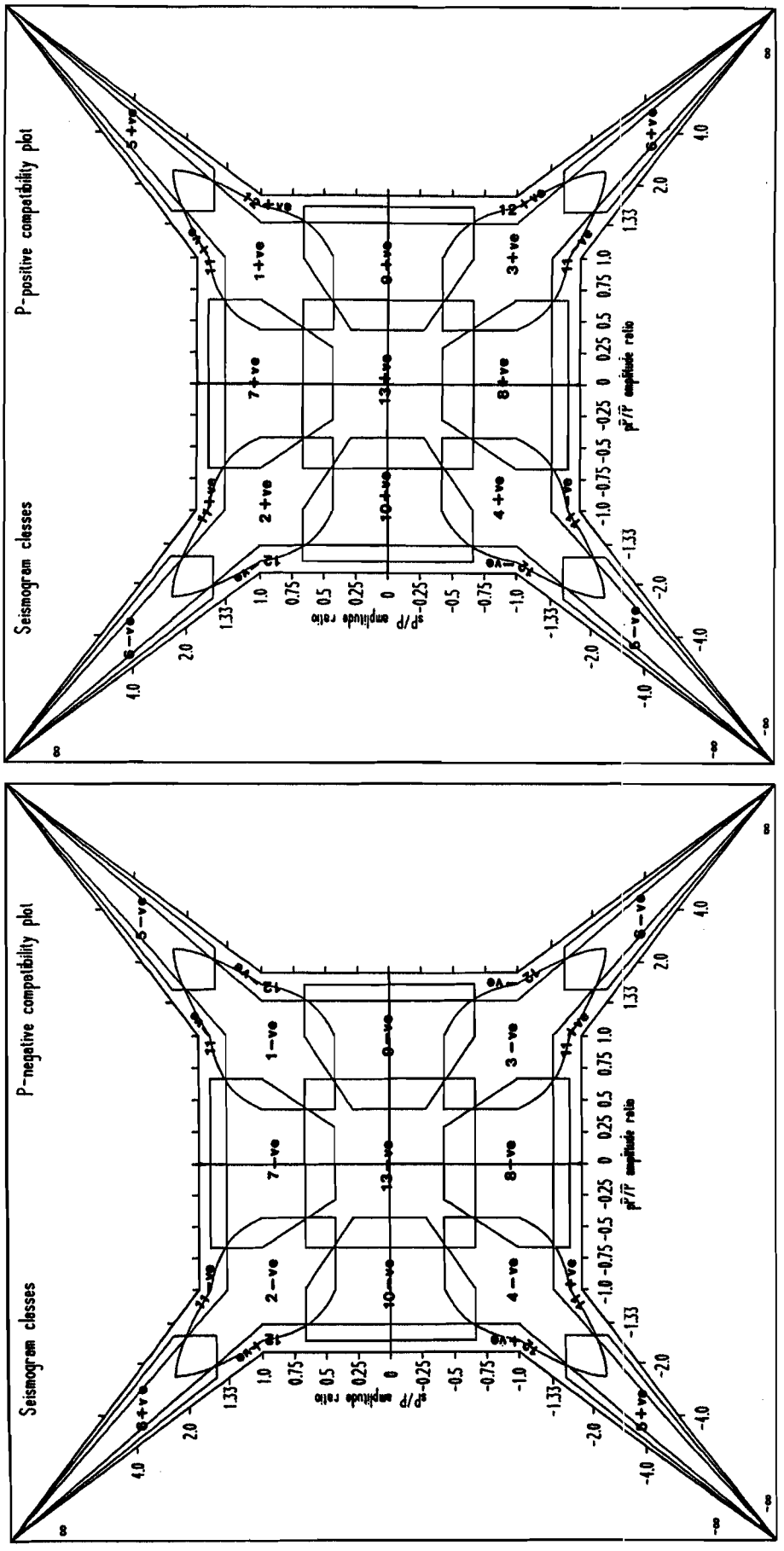
P-positive compatibility plot
Seismogram classes
P-negative compatibility plot
Seismogram classes

FIGURE 8

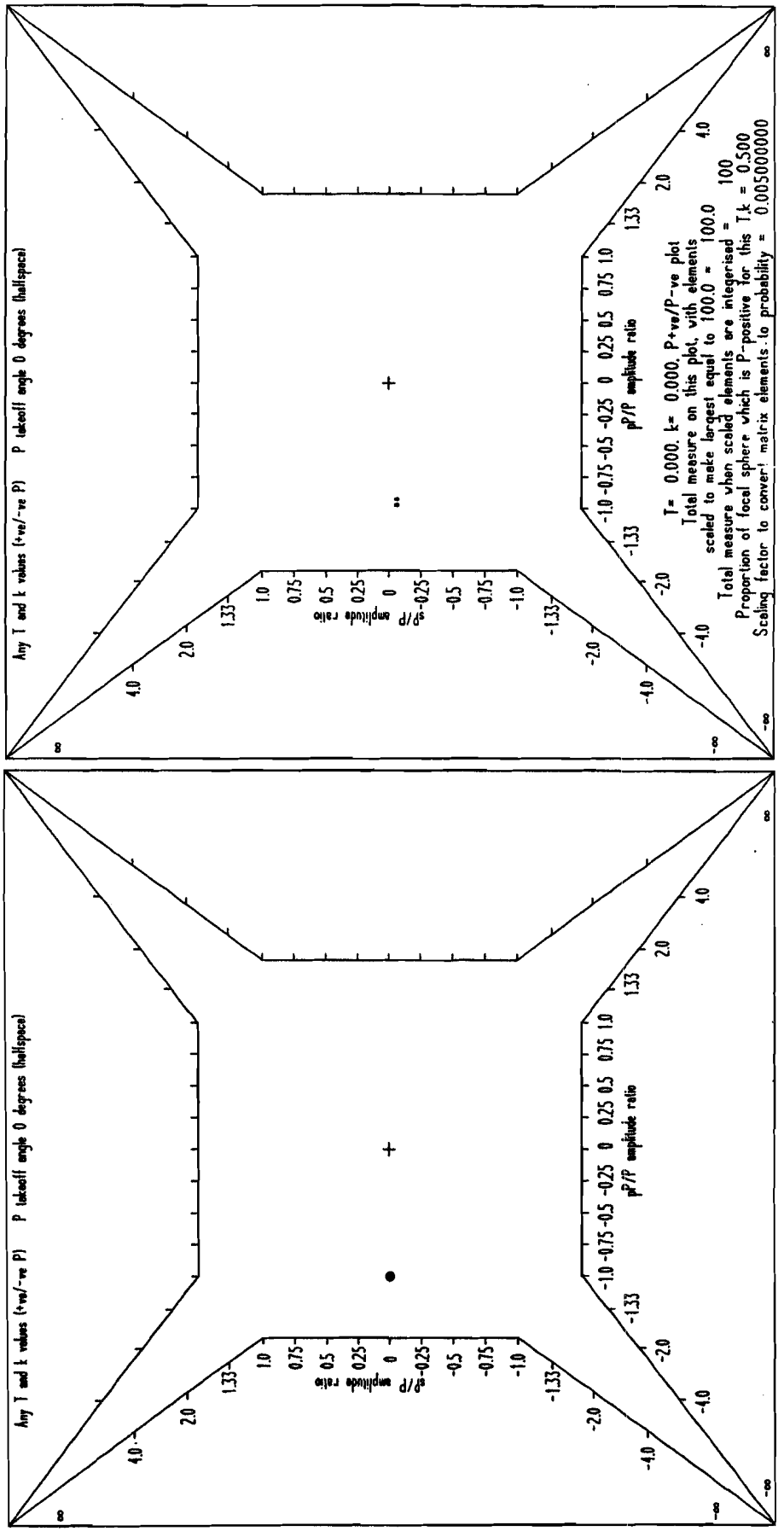
Any T and k values (+ve/-ve P)
P takeoff angle 0 degrees (halfspace)
p^s/p^p amplitude ratio
p^p/p^p amplitude ratio
T= 0.000, k= 0.000, P+ve/P-ve plot
Total measure on this plot, with elements
scaled to make largest equal to 100.0 = 100.0
Total measure when scaled elements are integerised = 100
Proportion of focal sphere which is P-positive for this T,k = 0.500
Scaling factor to convert matrix elements to probability = 0.005000000

FIGURE 9

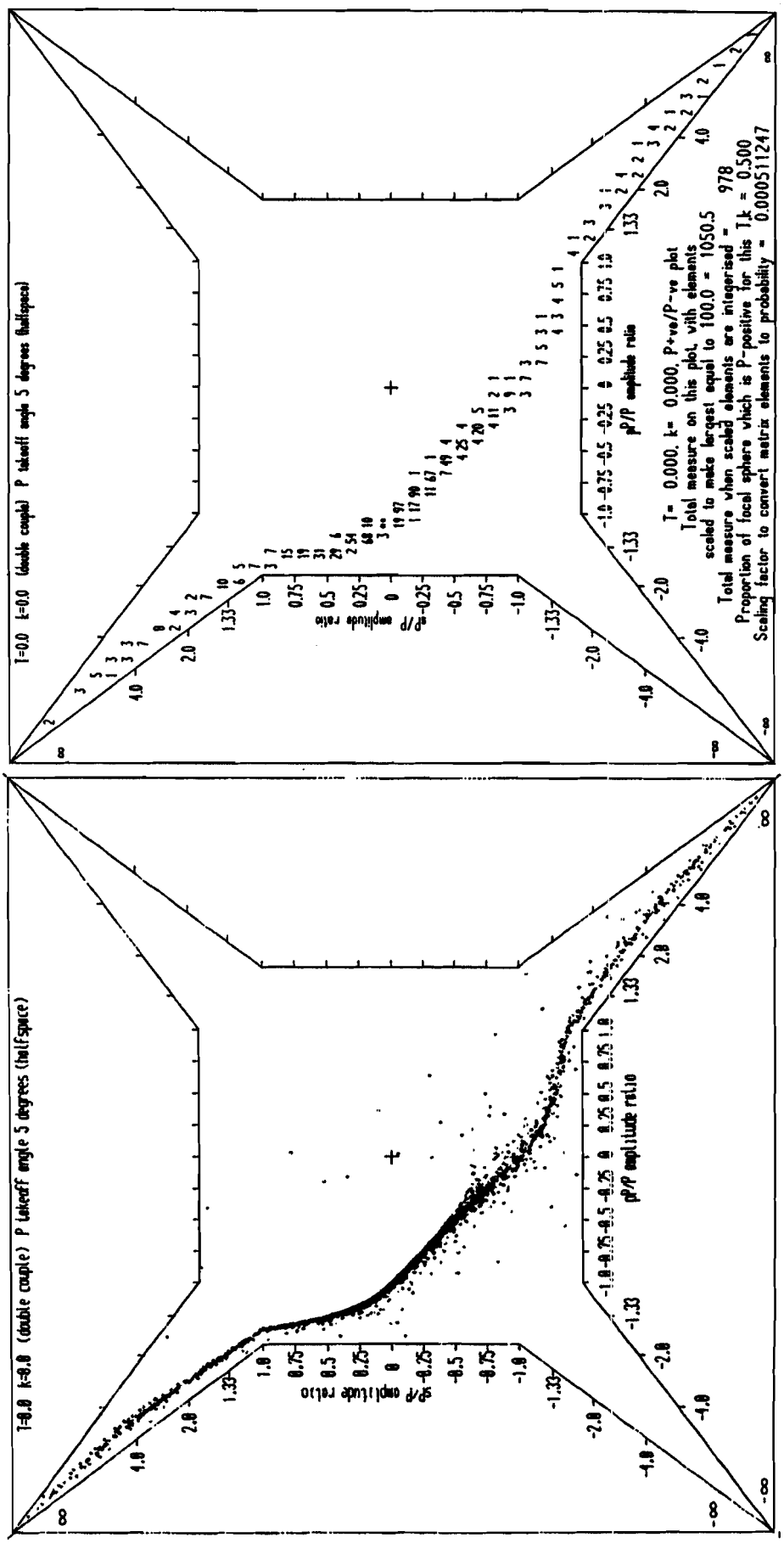
T=0.0 k=0.0 (double couple) P takeoff angle 5 degrees (halfspace)
T= 0.000, k= 0.000, P+ve/P-ve plot
Total measure on this plot with elements
scaled to make largest equal to 100.0 = 1050.5
Total measure when scaled elements are integerised = 978
Proportion of focal sphere which is P-positive for this Tk = 0.500
Scaling factor to convert matrix elements to probability = 0.000511247
sP/P amplitude ratio
pP/P amplitude ratio
T=-0.0 k=-0.0 (double couple) P takeoff angle 5 degrees (halfspace)

FIGURE 10

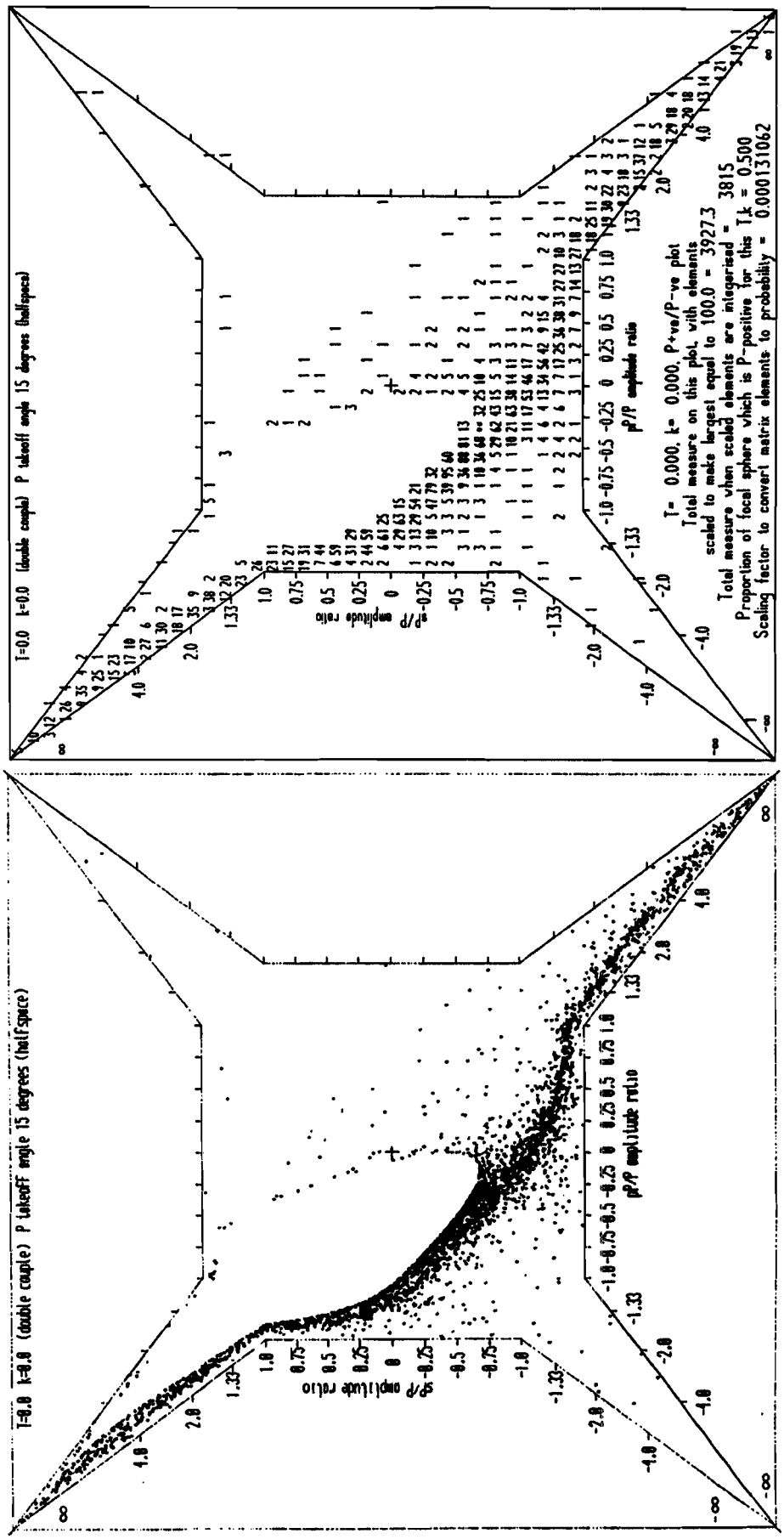
I=0.0 k=0.0 (double couple) P takeoff angle 15 degrees (halfspace)
sp/p amplitude ratio
p*/p amplitude ratio
T= 0.000, k= 0.000, P+ve/P-ve plot
Total measure on this plot with elements
scaled to make largest equal to 100.0 = 3927.3
Total measure when scaled elements are integerised = 3815
Proportion of focal sphere which is P-positive for this T,k = 0.500
Scaling factor to convert matrix elements to probability = 0.000131062

FIGURE 11

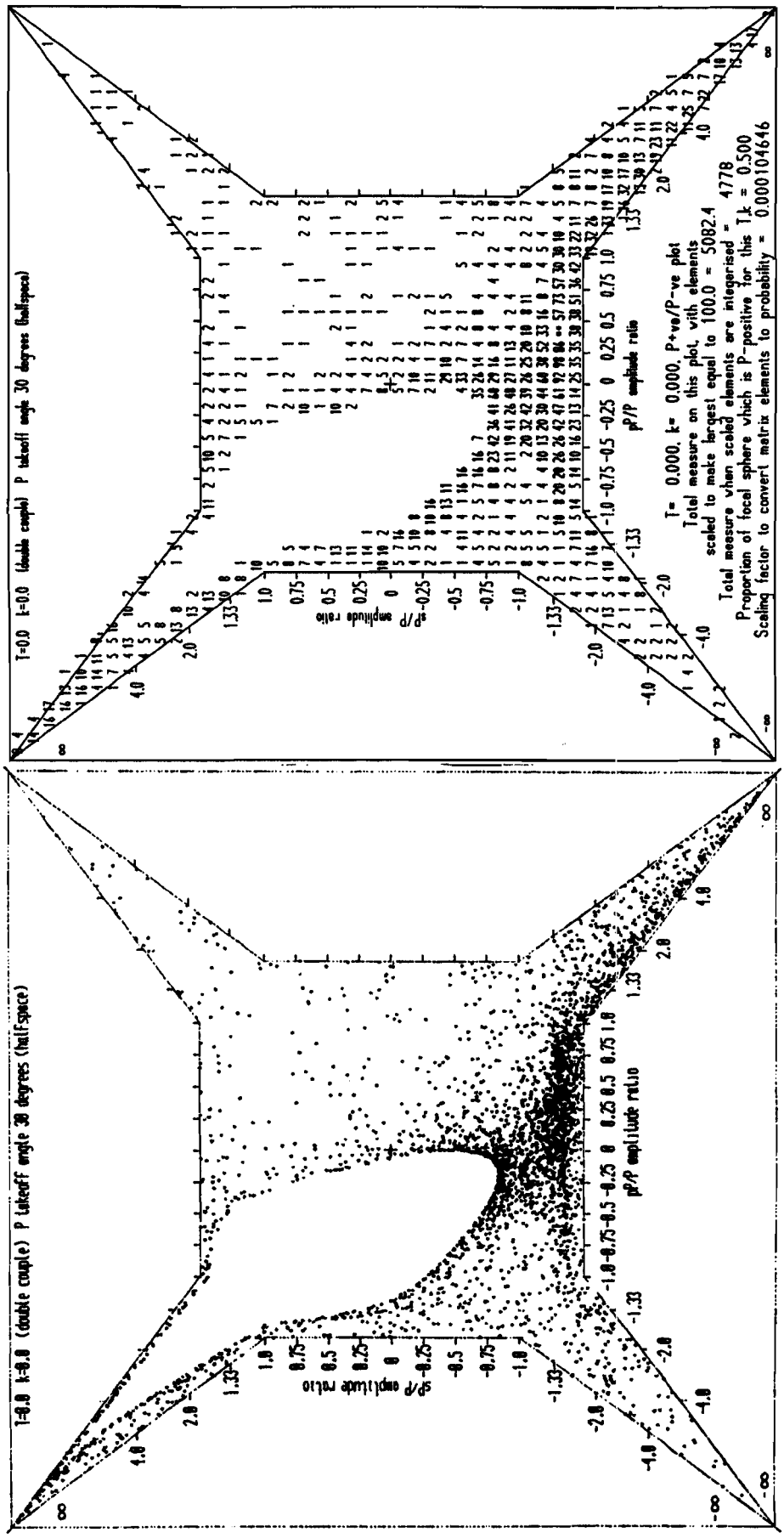
T=0.0 k=0.0 (double couple) P takeoff angle 30 degrees (halfspace)
sP/P amplitude ratio
pP/P amplitude ratio
T= 0.000, k= 0.000, P+ve/P-ve plot
Total measure on this plot, with elements
scaled to make largest equal to 100.0 = 5082.4
Total measure when scaled elements are integerised = 4778
Proportion of focal sphere which is P-positive for this T,k = 0.500
Scaling factor to convert matrix elements to probability = 0.000104646

FIGURE 12

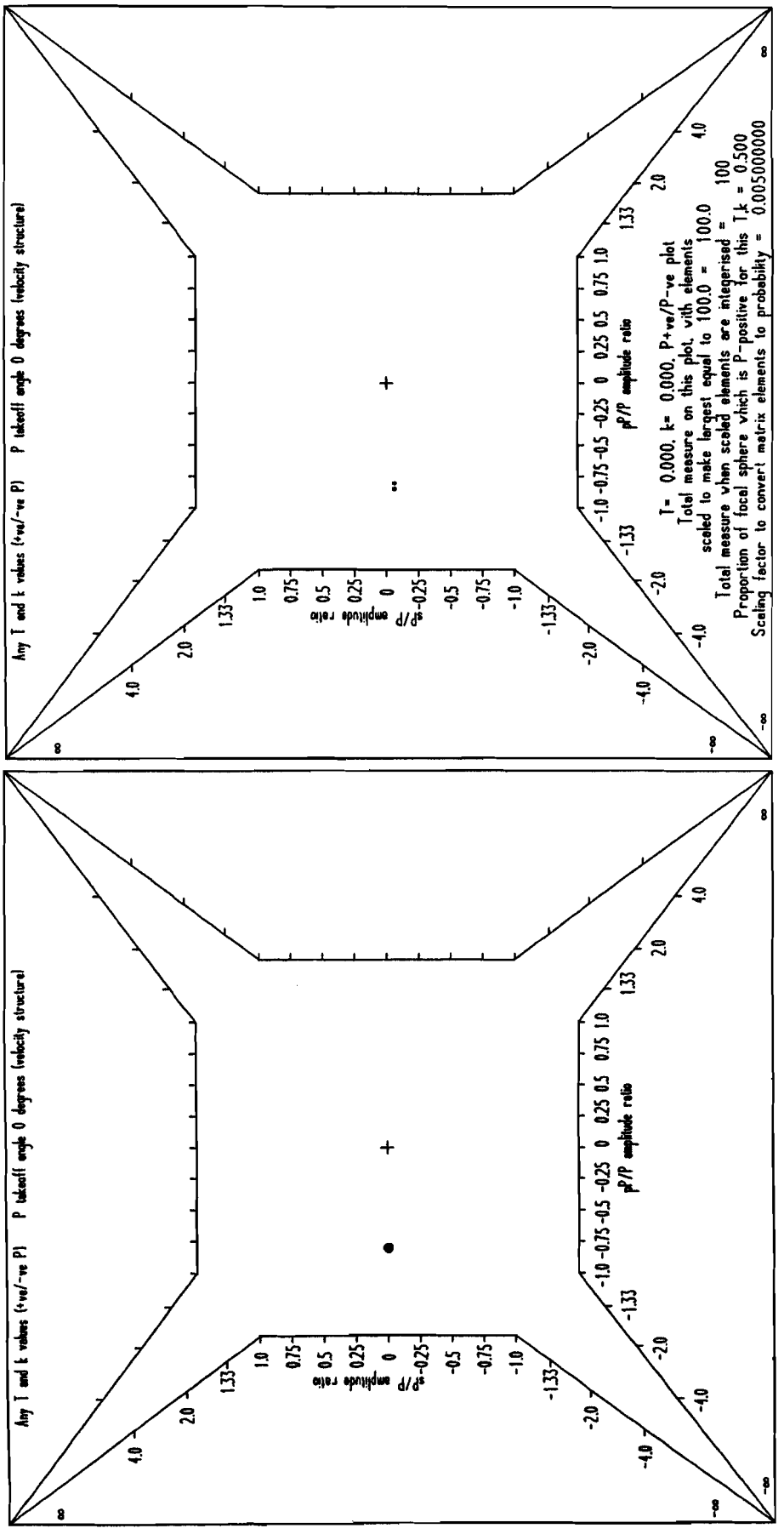
Any T and k values (+ve/-ve P)
P takeoff angle 0 degrees (velocity structure)
sP/P amplitude ratio
pP/P amplitude ratio
T= 0.000, k= 0.000, P+ve/P-ve plot
Total measure on this plot, with elements
scaled to make largest equal to 100.0 = 100.0
Total measure when scaled elements are integerised = 100
Proportion of focal sphere which is P-positive for this T,k = 0.500
Scaling factor to convert matrix elements to probability = 0.005000000

FIGURE 13(a)

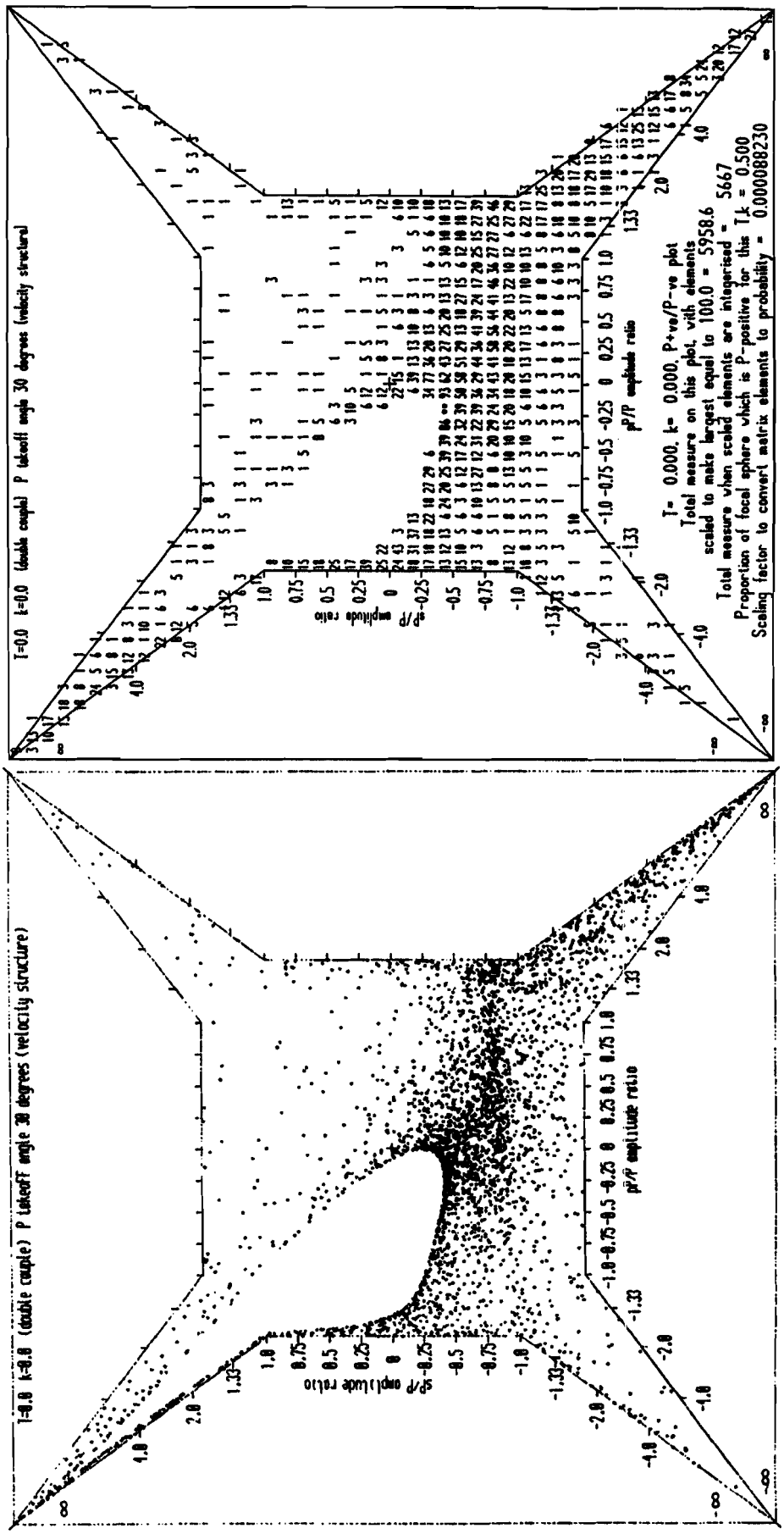
T=0.0 k=0.0 (double couple) P takeoff angle 30 degrees (velocity structure)
sP/P amplitude ratio
pP/P amplitude ratio
T= 0.000, k= 0.000, P+ve/P-ve plot
Total measure on this plot, with elements
scaled to make largest equal to 100.0 = 5958.6
Total measure when scaled elements are integrated = 5667
Proportion of focal sphere which is P-positive for this T,k = 0.500
Scaling factor to convert matrix elements to probability = 0.000088230
T=0.0 k=0.0 (double couple) P takeoff angle 30 degrees (velocity structure)
sP/P amplitude ratio
pP/P amplitude ratio

FIGURE 13(b)

T=1.0 k=0.5
P +ve
T=1.0 k=0.25
P +ve
T=1.0 k=0.25
P –ve
T=0.5 k=0.25
P +ve
T=0.5 k=0.25
P –ve
T=0.0 k=0.5
P +ve
T=0.0 k=0.25
P +ve
T=0.0 k=0.25
P –ve
T=–1.0 k=5/9
(tensile crack)
P +ve
T=–0.5 k=0.25
P +ve
T=–0.5 k=0.25
P –ve
T=–1.0 k=0.5
P +ve
T=–1.0 k=1/3
(vector dipole)
P +ve
T=–1.0 k=0.25
P +ve
T=–1.0 k=0.25
P –ve
Explosion k=1.0
T=1.0
T=0.5
k=0.5
k=0.0
k=–0.5
k=–1.0
T=–1.0
Tensile crack
Linear vector dipole

FIGURE 14(a)

T=1.0 k=0.0
(negative clvd)
P +ve
T=1.0 k=0.0
(negative clvd)
P –ve
T=0.5 k=0.0
P +ve
T=0.5 k=0.0
P –ve
T=0.0 k=0.0
(double couple)
P +ve & –ve
T=–0.5 k=0.0
P +ve
T=–0.5 k=0.0
P –ve
T=–1.0 k=0.0
(clvd)
P +ve
T=–1.0 k=0.0
(clvd)
P –ve
T=1.0
T=0.5
T=0.0
T=–0.5
T=–1.0
k=0.0
Compensated linear vector dipole (negative)
Double couple
Compensated linear vector dipole

FIGURE 14(b)

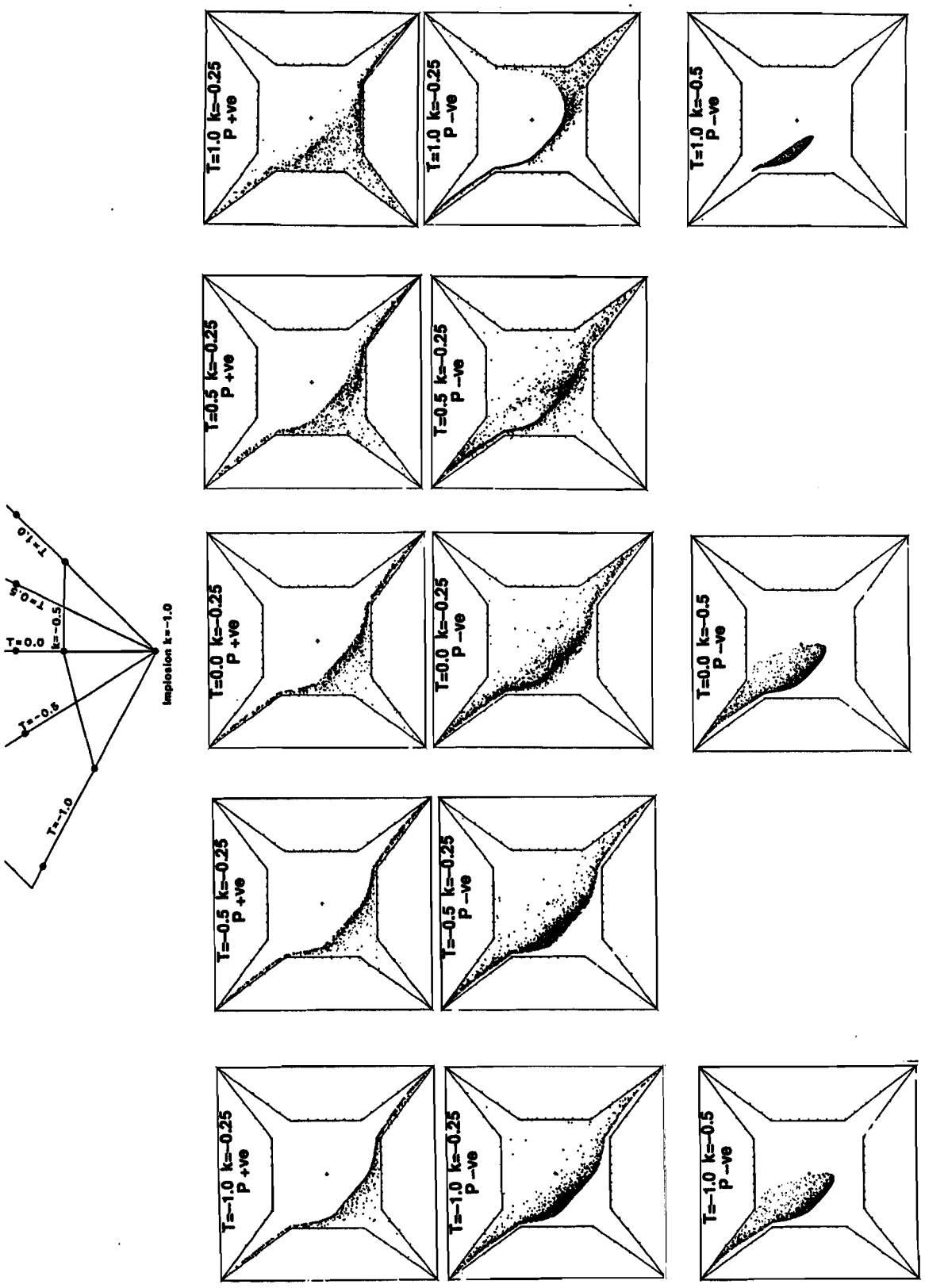
T=1.0
T=0.5
T=0.0
T=-0.5
T=-1.0
Implosion k=-1.0
T=1.0 k=-0.25 P +ve
T=1.0 k=-0.25 P -ve
T=1.0 k=-0.5 P -ve
T=0.5 k=-0.25 P +ve
T=0.5 k=-0.25 P -ve
T=0.0 k=-0.25 P +ve
T=0.0 k=-0.25 P -ve
T=0.0 k=-0.5 P -ve
T=-0.5 k=-0.25 P +ve
T=-0.5 k=-0.25 P -ve
T=-1.0 k=-0.25 P +ve
T=-1.0 k=-0.25 P -ve
T=-1.0 k=-0.5 P -ve

FIGURE 14(c)

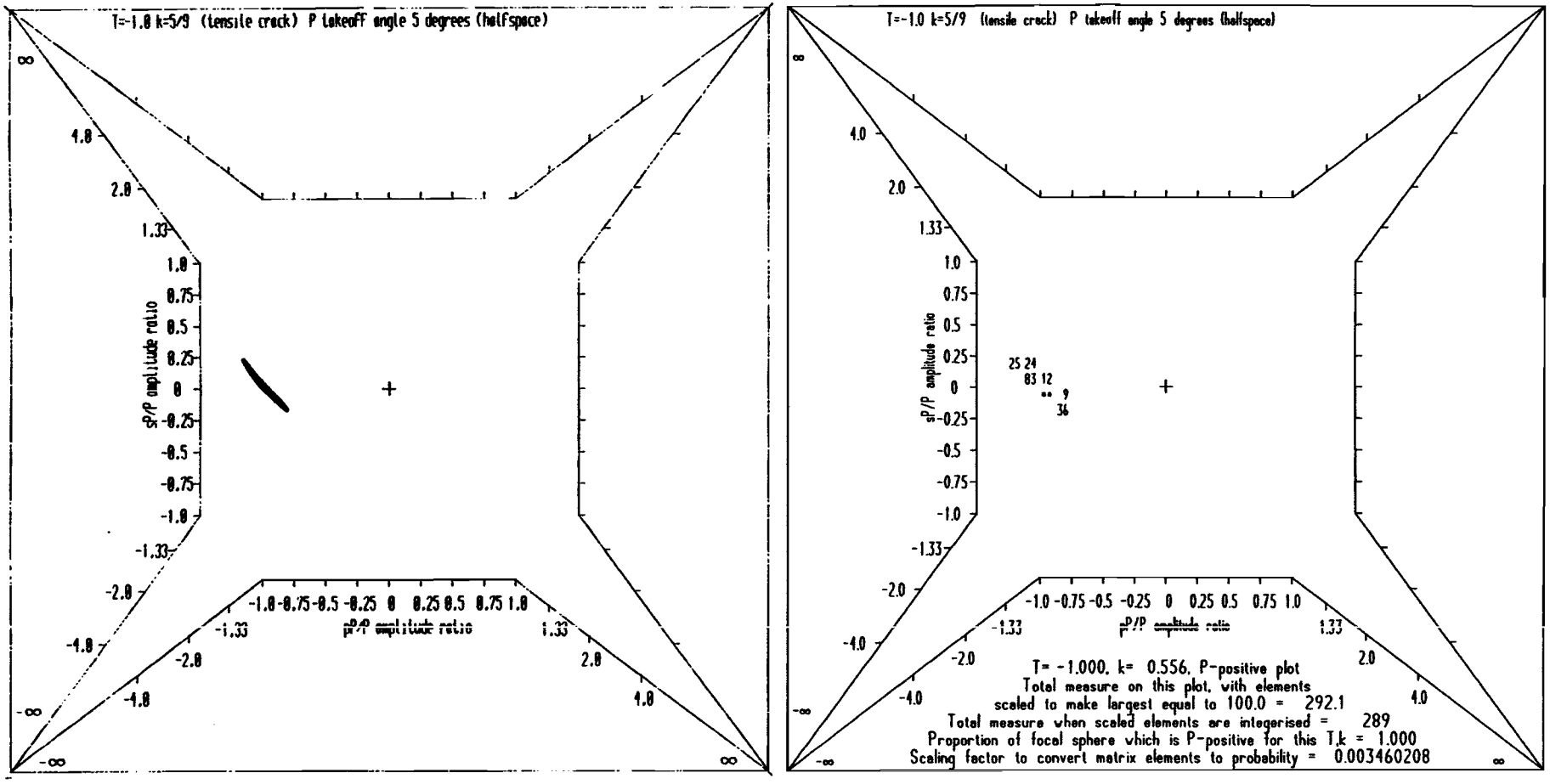
T=-1.0 k=5/9 (tensile crack) P takeoff angle 5 degrees (halfspace)
sP/P amplitude ratio
pP/P amplitude ratio
T=-1.0 k=5/9 (tensile crack) P takeoff angle 5 degrees (halfspace)
sP/P amplitude ratio
pP/P amplitude ratio
T= -1.000, k= 0.556, P-positive plot
Total measure on this plot, with elements
scaled to make largest equal to 100.0 = 292.1
Total measure when scaled elements are integerised = 289
Proportion of focal sphere which is P-positive for this T,k = 1.000
Scaling factor to convert matrix elements to probability = 0.003460208

Figure 15

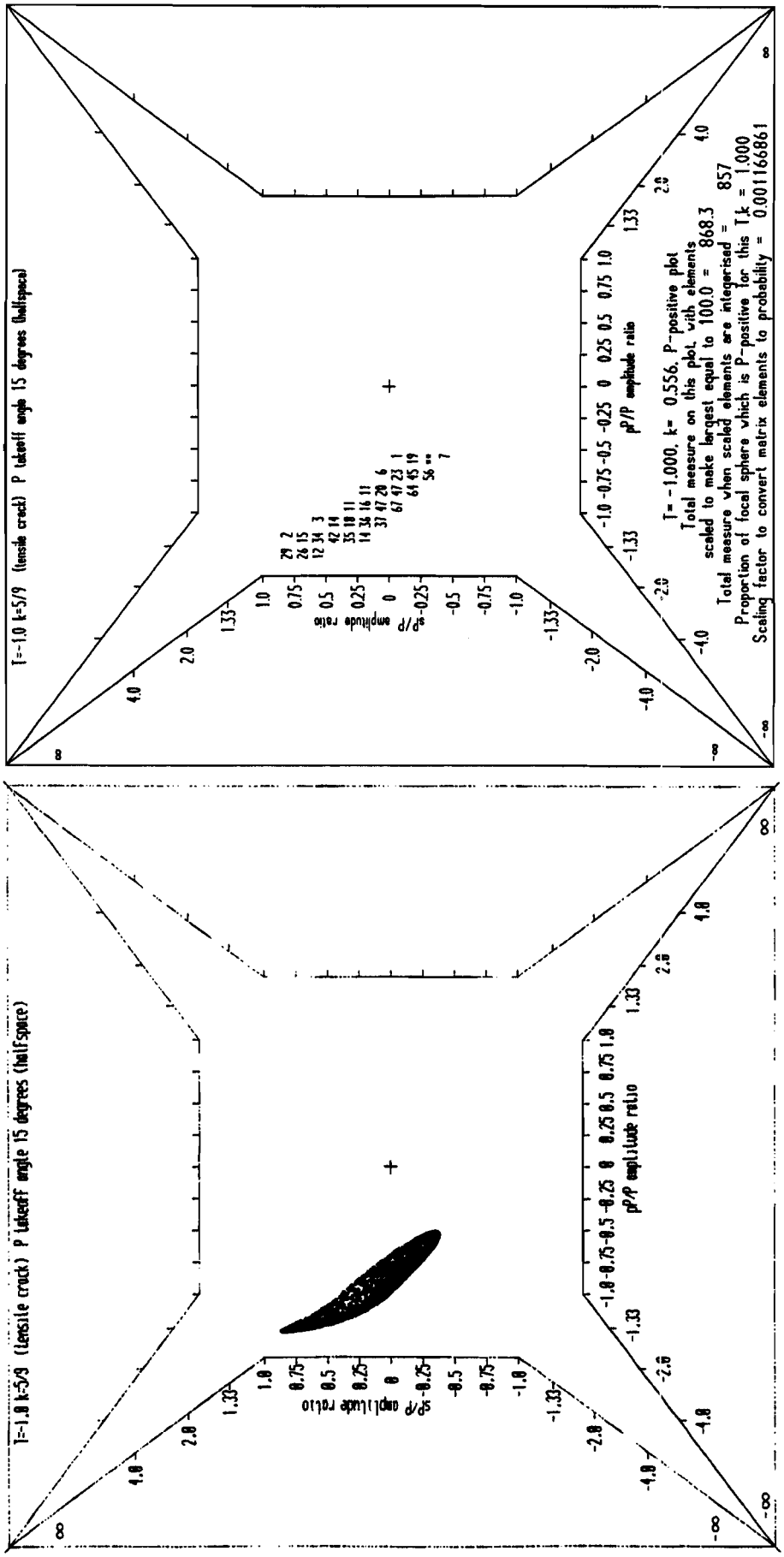
T=-1.0 k=5/9 (tensile crack) P takeoff angle 15 degrees (halfspace)
sP/P amplitude ratio
pP/P amplitude ratio
T=-1.000, k= 0.556, P-positive plot
Total measure on this plot, with elements
scaled to make largest equal to 100.0 = 868.3
Total measure when scaled elements are integerised = 857
Proportion of focal sphere which is P-positive for this Tk = 1.000
Scaling factor to convert matrix elements to probability = 0.001166861

Figure 16

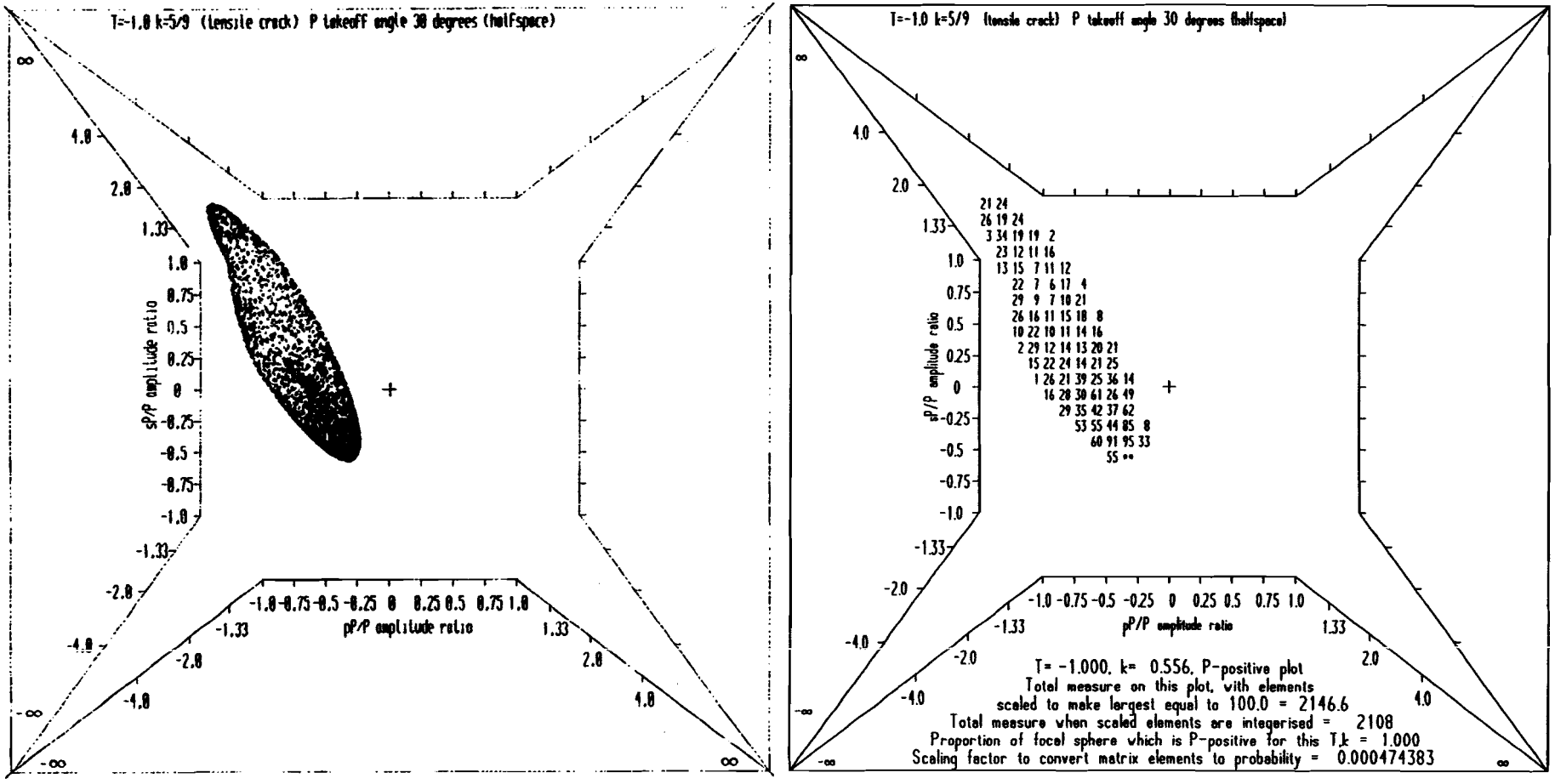
T=-1.0 k=5/9 (tensile crack) P takeoff angle 38 degrees (halfspace)
sP/P amplitude ratio
pP/P amplitude ratio
T=-1.0 k=5/9 (tensile crack) P takeoff angle 30 degrees (halfspace)
sP/P amplitude ratio
pP/P amplitude ratio
T= -1.000, k= 0.556, P-positive plot
Total measure on this plot, with elements
scaled to make largest equal to 100.0 = 2146.6
Total measure when scaled elements are integerised = 2108
Proportion of focal sphere which is P-positive for this T,k = 1.000
Scaling factor to convert matrix elements to probability = 0.000474383

Figure 17

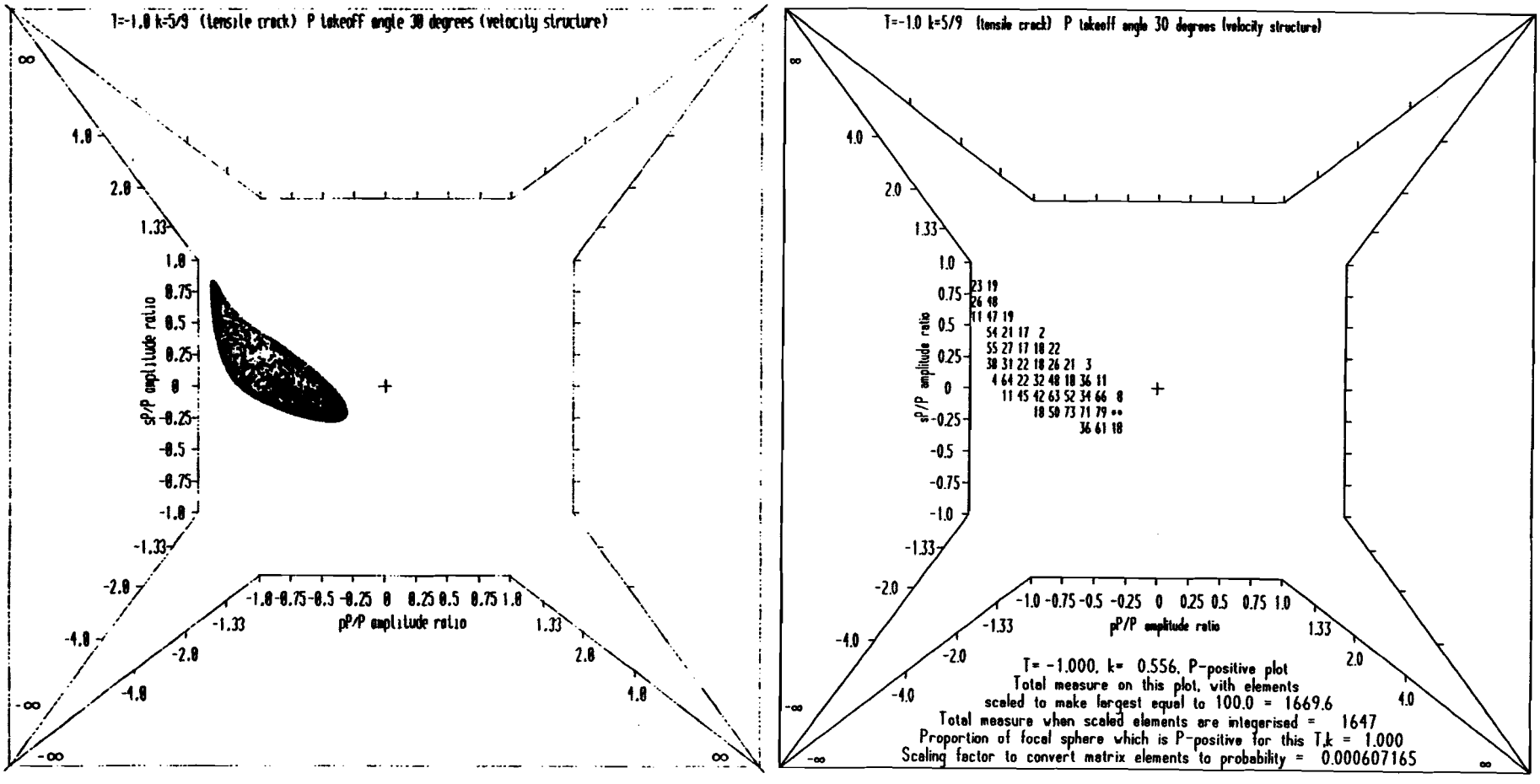
T=-1.0 k=5/9 (tensile crack) P takeoff angle 30 degrees (velocity structure)
sP/P amplitude ratio
pP/P amplitude ratio
T=-1.0 k=5/9 (tensile crack) P takeoff angle 30 degrees (velocity structure)
sP/P amplitude ratio
pP/P amplitude ratio
T= -1.000, k= 0.556, P-positive plot
Total measure on this plot, with elements
scaled to make largest equal to 100.0 = 1669.6
Total measure when scaled elements are integerised = 1647
Proportion of focal sphere which is P-positive for this T,k = 1.000
Scaling factor to convert matrix elements to probability = 0.000607165

Figure 18

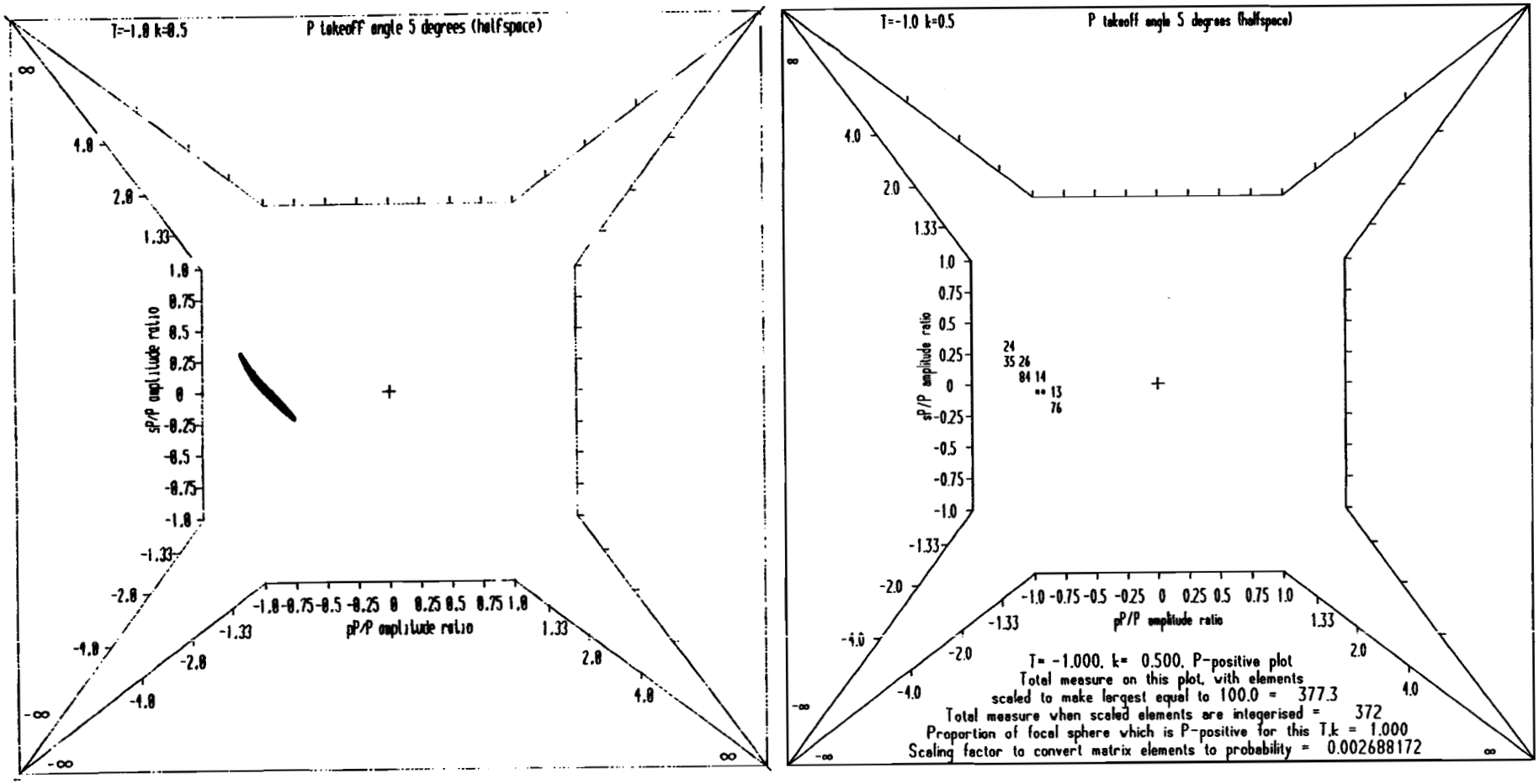
T=-1.0 k=0.5
P takeoff angle 5 degrees (halfspace)
sP/P amplitude ratio
pP/P amplitude ratio
T= -1.000, k= 0.500, P-positive plot
Total measure on this plot, with elements
scaled to make largest equal to 100.0 = 377.3
Total measure when scaled elements are integerised = 372
Proportion of focal sphere which is P-positive for this T,k = 1.000
Scaling factor to convert matrix elements to probability = 0.002688172

Figure 19

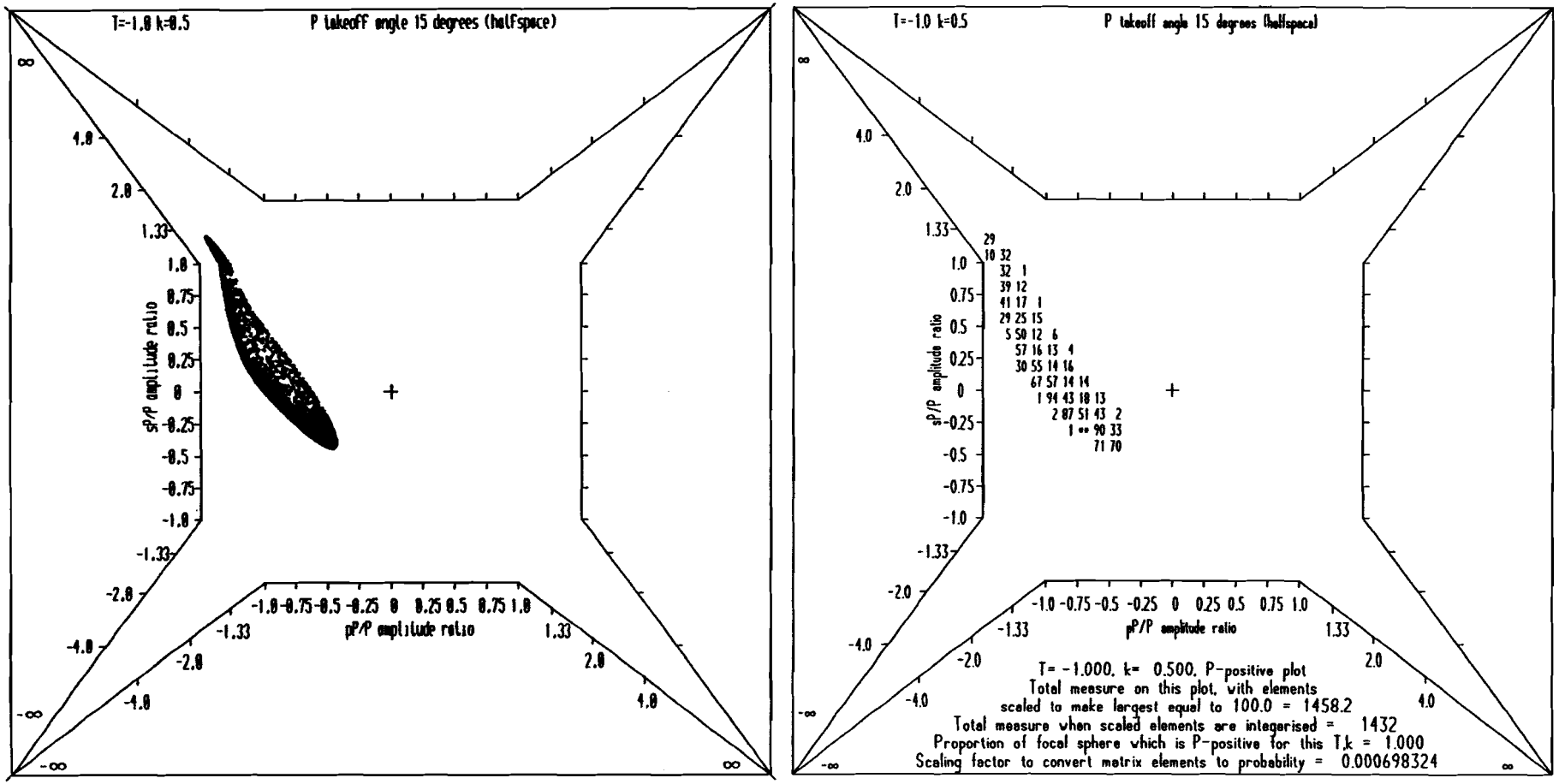
T=-1.0 k=0.5
P takeoff angle 15 degrees (halfspace)
sP/P amplitude ratio
pP/P amplitude ratio
T=-1.0 k=0.5
P takeoff angle 15 degrees (halfspace)
sP/P amplitude ratio
pP/P amplitude ratio
T= -1.000, k= 0.500, P-positive plot
Total measure on this plot, with elements
scaled to make largest equal to 100.0 = 1458.2
Total measure when scaled elements are integerised = 1432
Proportion of focal sphere which is P-positive for this T,k = 1.000
Scaling factor to convert matrix elements to probability = 0.000698324

Figure 20

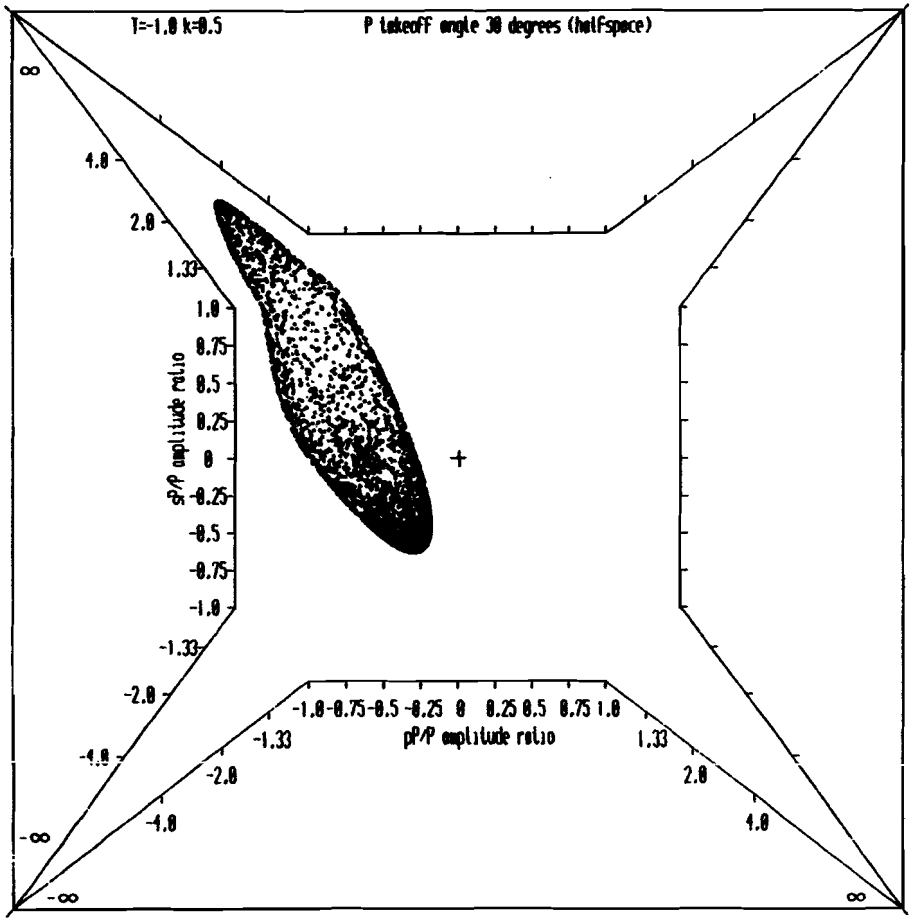
T=-1.0 k=0.5
P takeoff angle 30 degrees (halfspace)
sP/P amplitude ratio
pP/P amplitude ratio

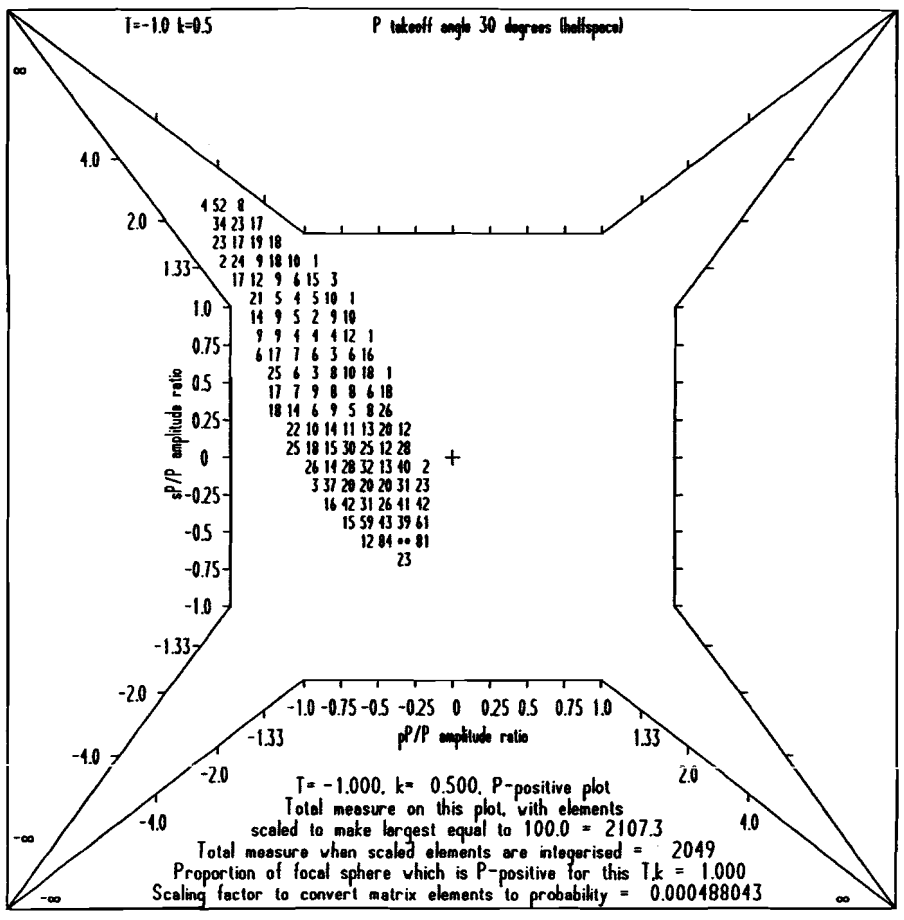
T=-1.0 k=0.5
P takeoff angle 30 degrees (halfspace)
sP/P amplitude ratio
pP/P amplitude ratio
T= -1.000, k= 0.500, P-positive plot
Total measure on this plot, with elements
scaled to make largest equal to 100.0 = 2107.3
Total measure when scaled elements are integerised = 2049
Proportion of focal sphere which is P-positive for this T,k = 1.000
Scaling factor to convert matrix elements to probability = 0.000488043

Figure 21

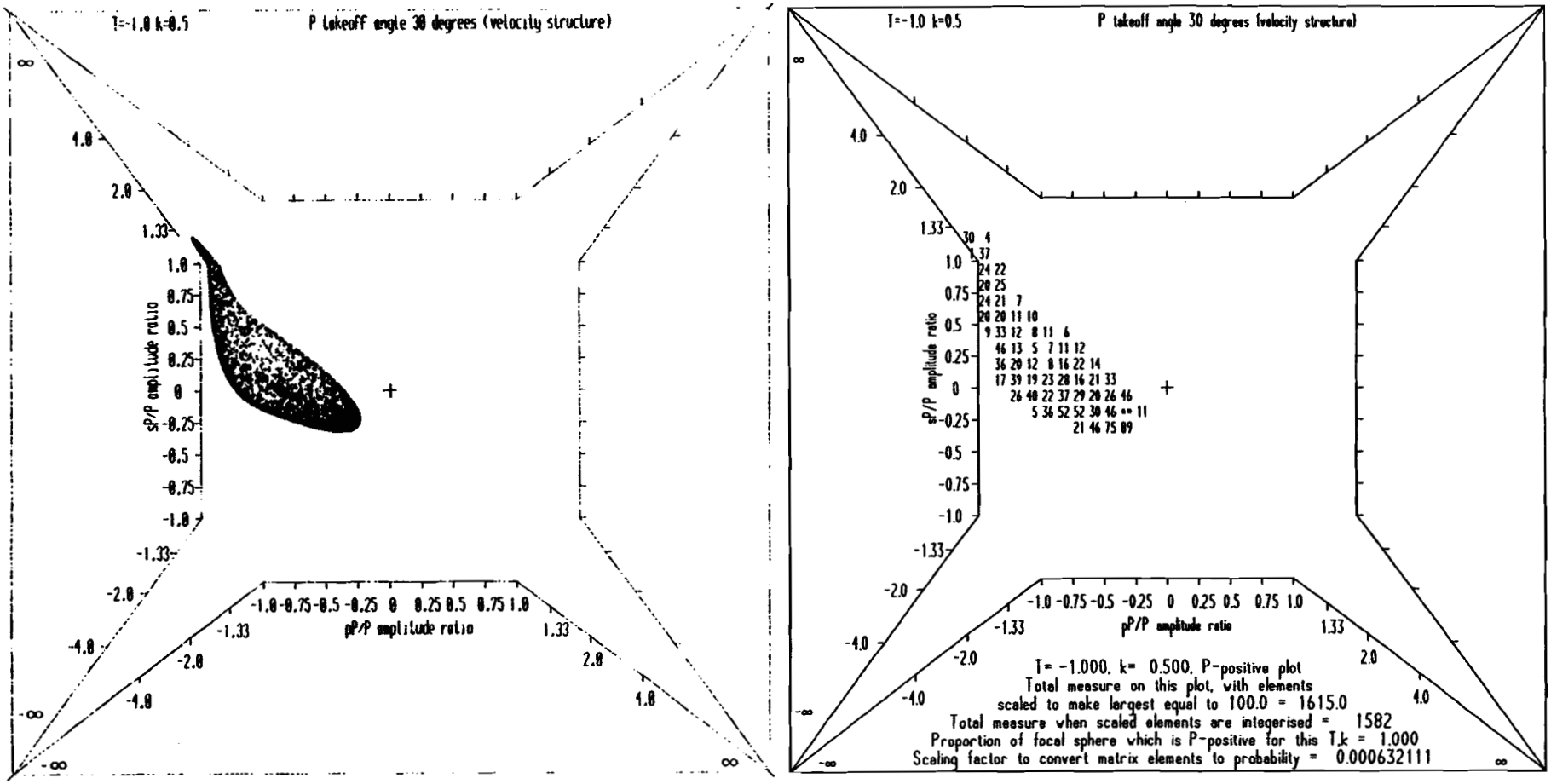
T=-1.0 k=0.5
P takeoff angle 30 degrees (velocity structure)
sP/P amplitude ratio
pP/P amplitude ratio
T= -1.000, k= 0.500, P-positive plot
Total measure on this plot, with elements
scaled to make largest equal to 100.0 = 1615.0
Total measure when scaled elements are integerised = 1582
Proportion of focal sphere which is P-positive for this T,k = 1.000
Scaling factor to convert matrix elements to probability = 0.000632111

Figure 22

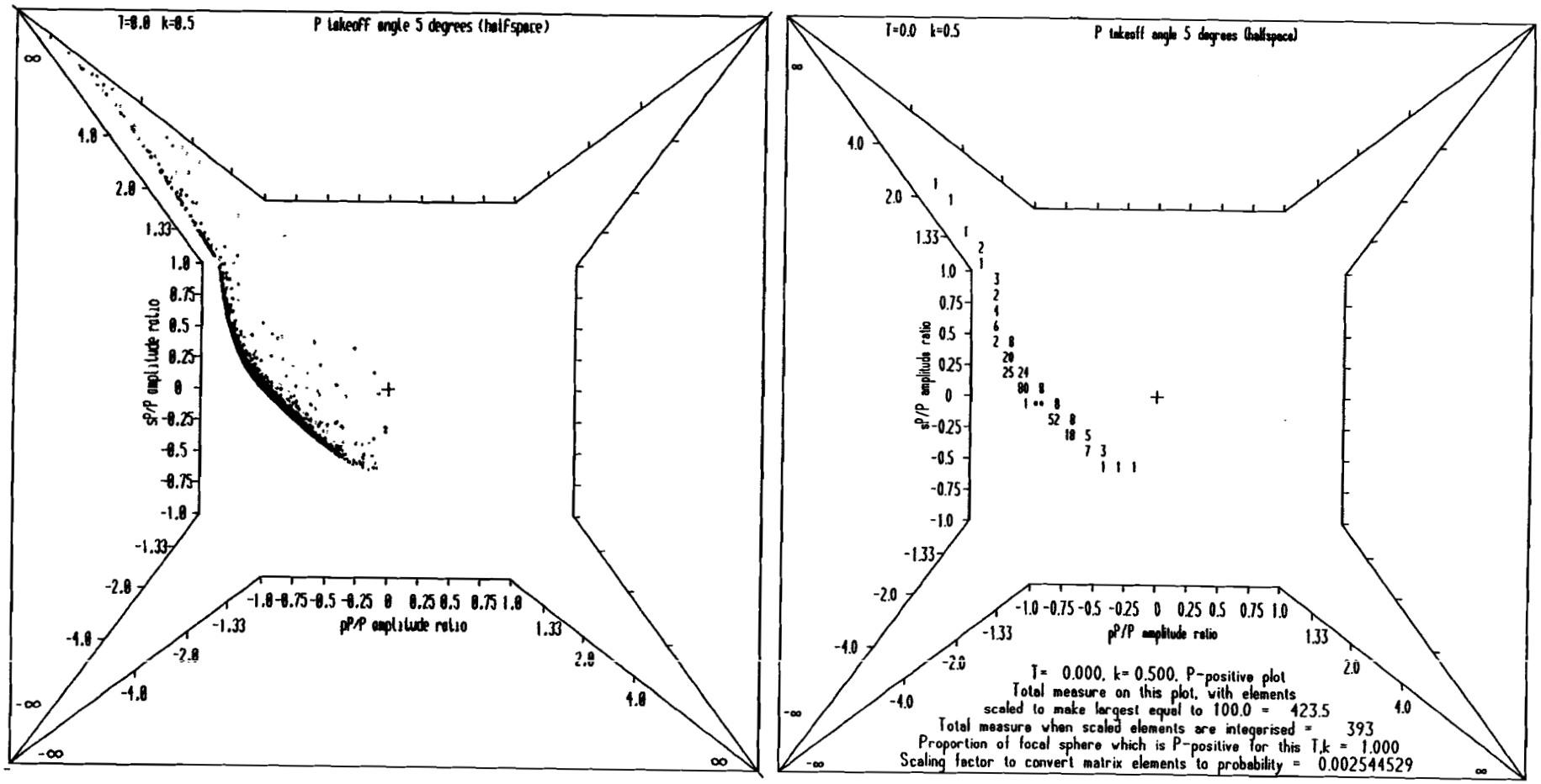
T=0.0 k=0.5
P takeoff angle 5 degrees (halfspace)
sP/P amplitude ratio
pP/P amplitude ratio
T=0.0 k=0.5
P takeoff angle 5 degrees (halfspace)
sP/P amplitude ratio
pP/P amplitude ratio
T= 0.000, k= 0.500, P-positive plot
Total measure on this plot, with elements
scaled to make largest equal to 100.0 = 423.5
Total measure when scaled elements are integerised = 393
Proportion of focal sphere which is P-positive for this T,k = 1.000
Scaling factor to convert matrix elements to probability = 0.002544529

Figure 23

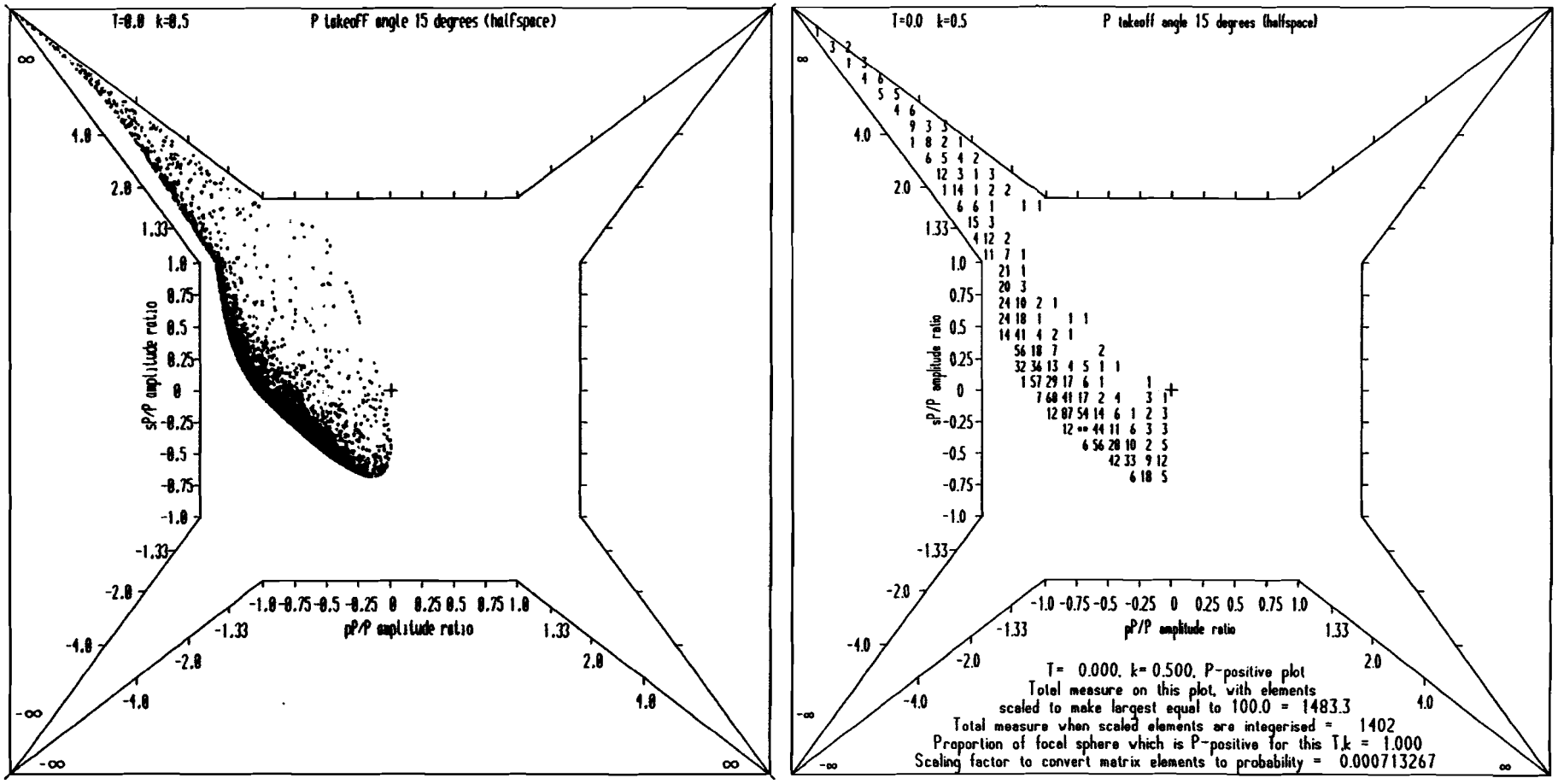
T=0.0 k=0.5
P takeoff angle 15 degrees (halfspace)
sP/P amplitude ratio
pP/P amplitude ratio
T= 0.000, k= 0.500, P-positive plot
Total measure on this plot, with elements
scaled to make largest equal to 100.0 = 1483.3
Total measure when scaled elements are integerised = 1402
Proportion of focal sphere which is P-positive for this T,k = 1.000
Scaling factor to convert matrix elements to probability = 0.000713267

Figure 24

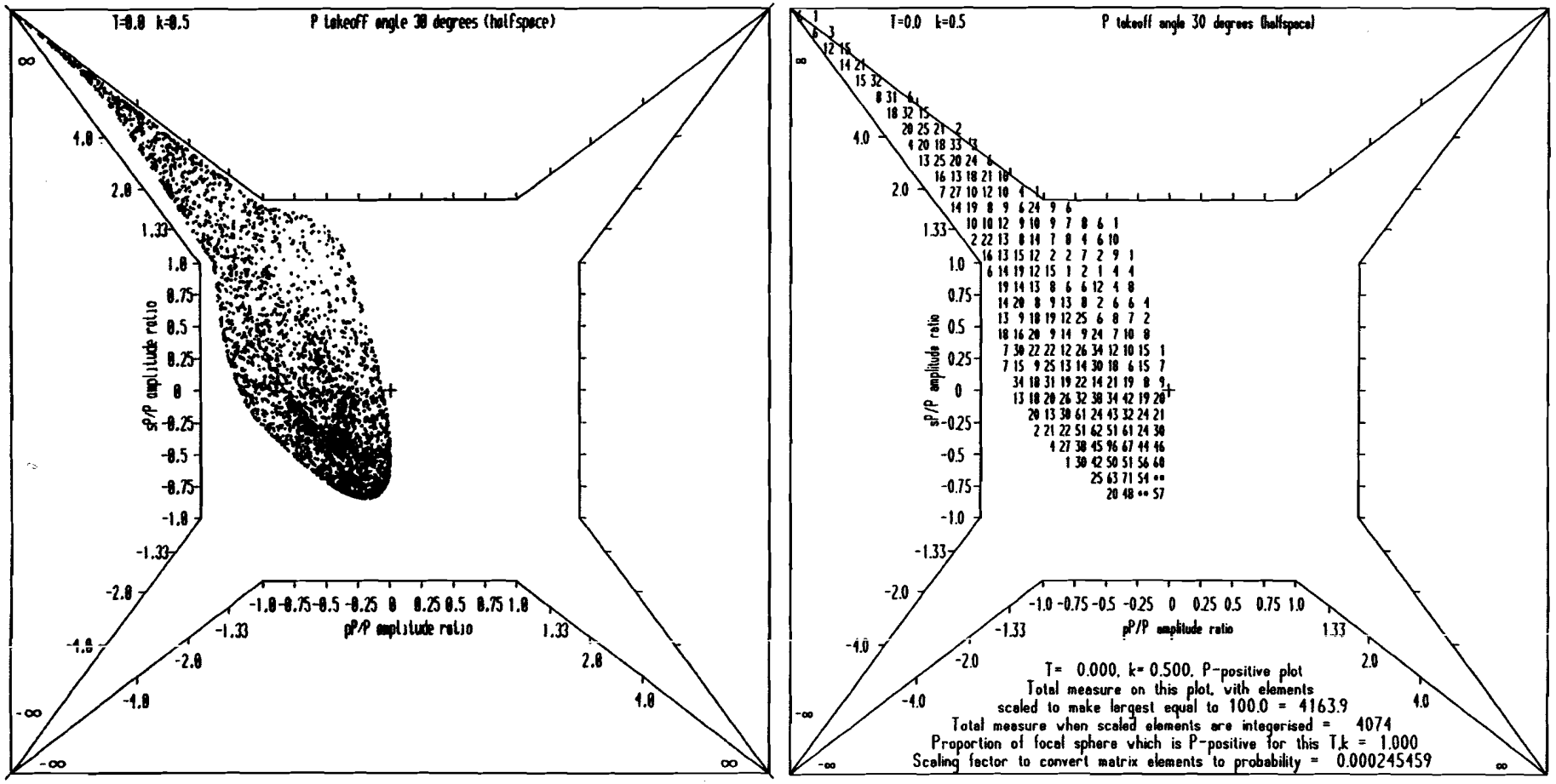
T=0.0 k=0.5
P takeoff angle 30 degrees (halfspace)
sP/P amplitude ratio
pP/P amplitude ratio
T= 0.000, k= 0.500, P-positive plot
Total measure on this plot, with elements
scaled to make largest equal to 100.0 = 4163.9
Total measure when scaled elements are integerised = 4074
Proportion of focal sphere which is P-positive for this T,k = 1.000
Scaling factor to convert matrix elements to probability = 0.000245459

Figure 25

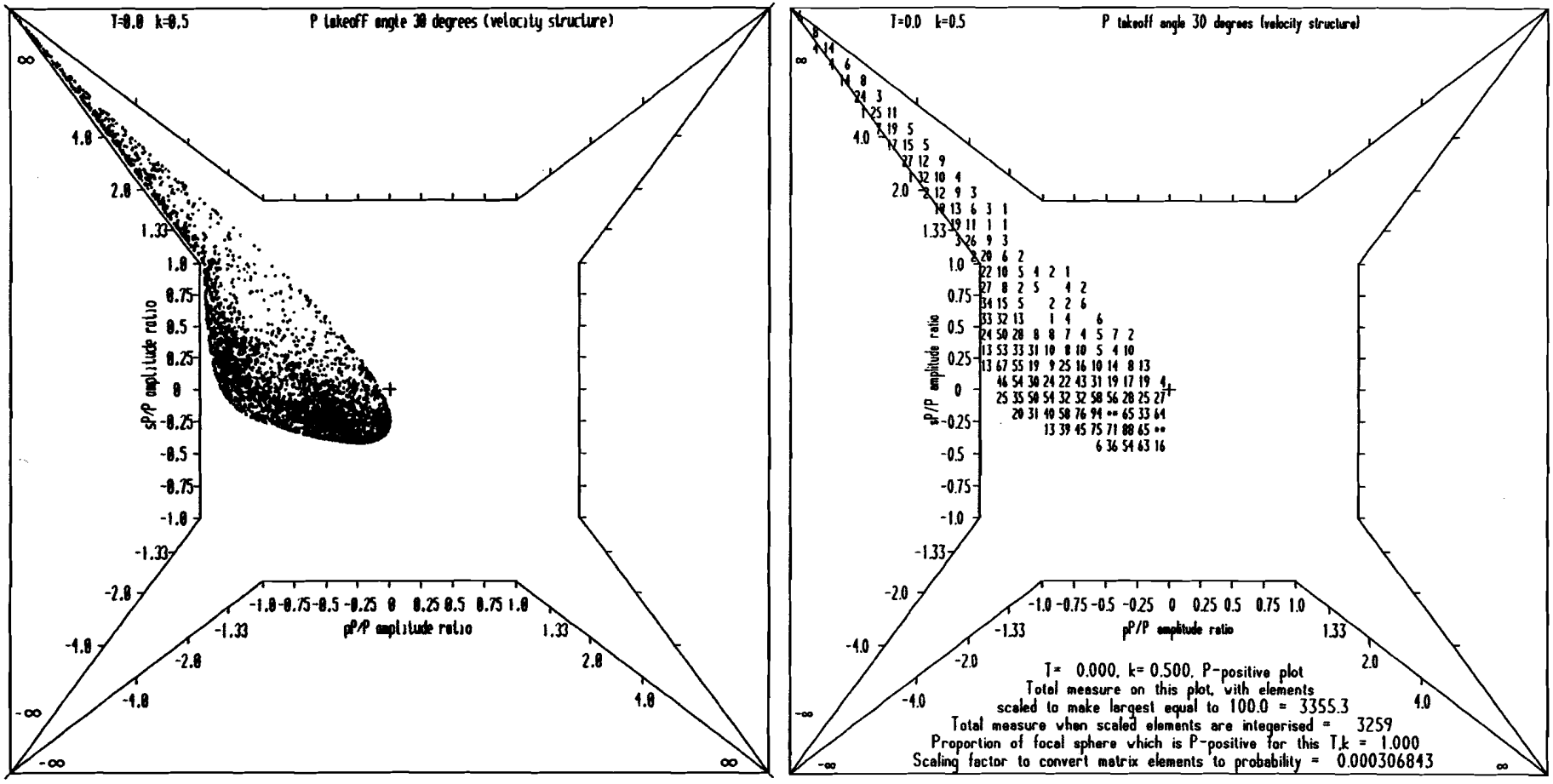
T=0.0 k=0.5
P takeoff angle 30 degrees (velocity structure)
sP/P amplitude ratio
pP/P amplitude ratio
T= 0.000, k= 0.500, P-positive plot
Total measure on this plot, with elements
scaled to make largest equal to 100.0 = 3355.3
Total measure when scaled elements are integerised = 3259
Proportion of focal sphere which is P-positive for this T,k = 1.000
Scaling factor to convert matrix elements to probability = 0.000306843

Figure 26

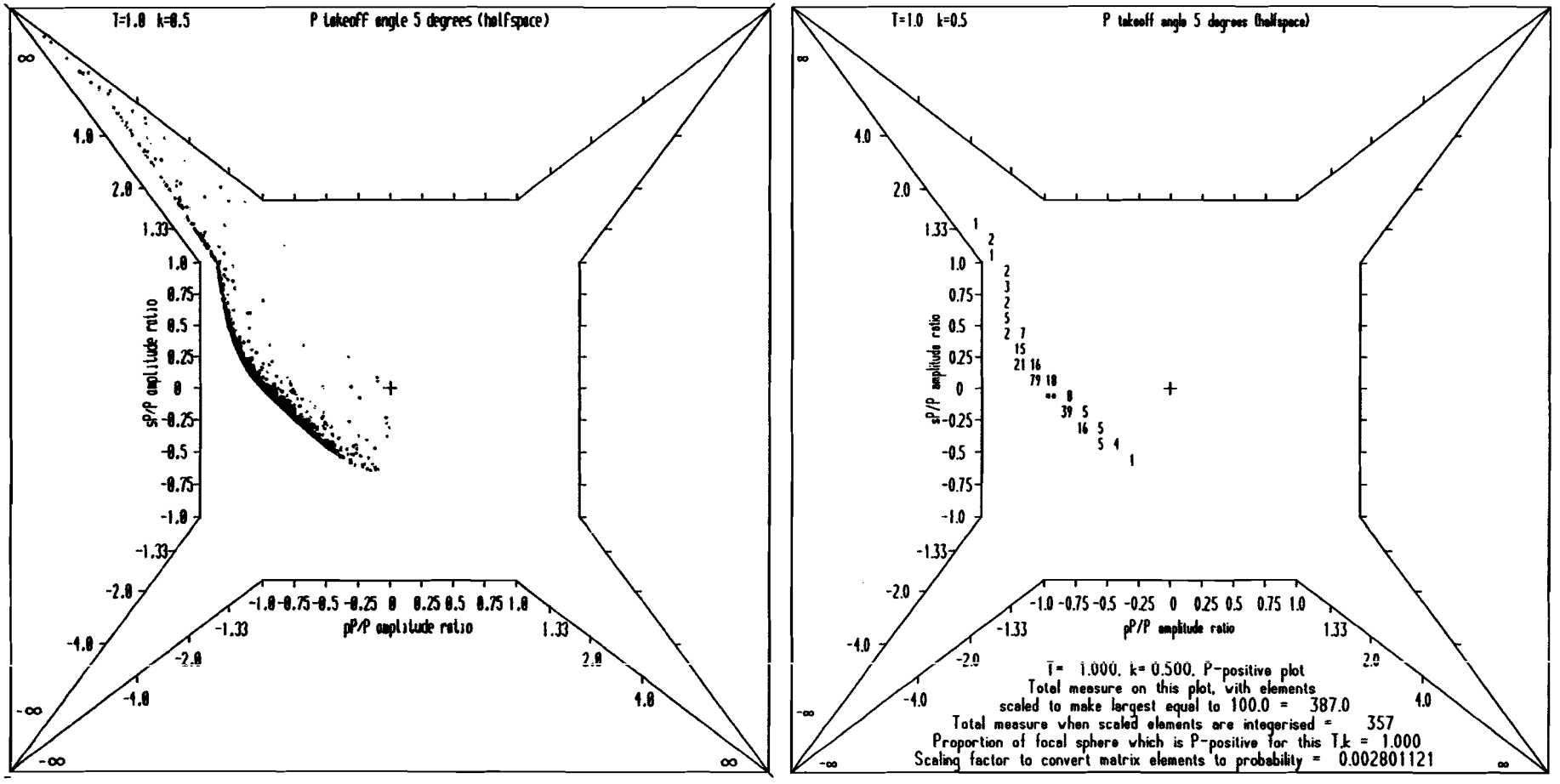
T=1.0 k=0.5
P takeoff angle 5 degrees (halfspace)
sP/P amplitude ratio
pP/P amplitude ratio
T= 1.000, k= 0.500, P-positive plot
Total measure on this plot, with elements
scaled to make largest equal to 100.0 = 387.0
Total measure when scaled elements are integerised = 357
Proportion of focal sphere which is P-positive for this T,k = 1.000
Scaling factor to convert matrix elements to probability = 0.002801121

Figure 27

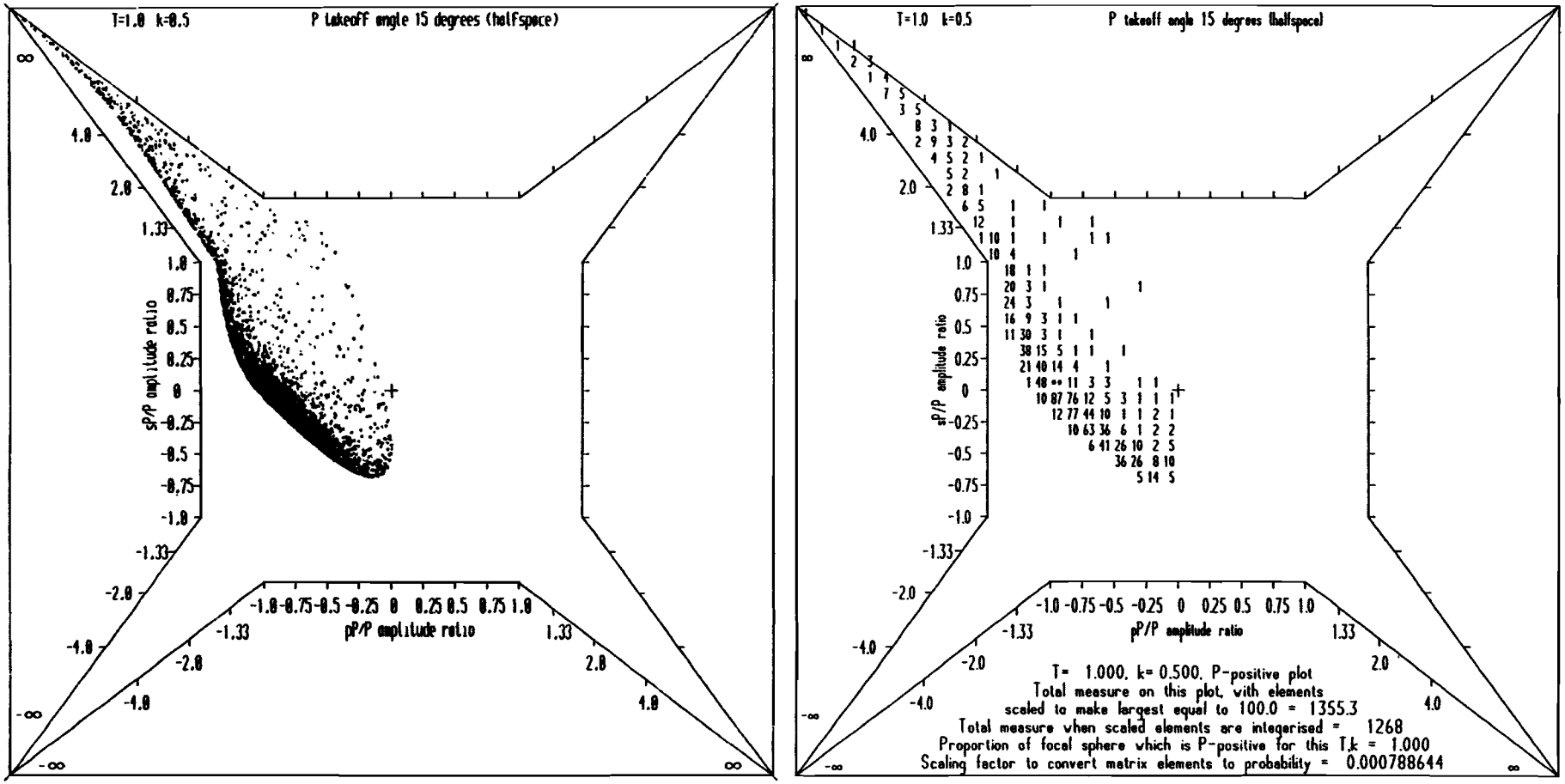
T=1.0 k=0.5
P takeoff angle 15 degrees (halfspace)
sP/P amplitude ratio
pP/P amplitude ratio
T=1.0 k=0.5
P takeoff angle 15 degrees (halfspace)
sP/P amplitude ratio
pP/P amplitude ratio
T= 1.000, k= 0.500, P-positive plot
Total measure on this plot, with elements
scaled to make largest equal to 100.0 = 1355.3
Total measure when scaled elements are integerised = 1268
Proportion of focal sphere which is P-positive for this T,k = 1.000
Scaling factor to convert matrix elements to probability = 0.000788644

Figure 28

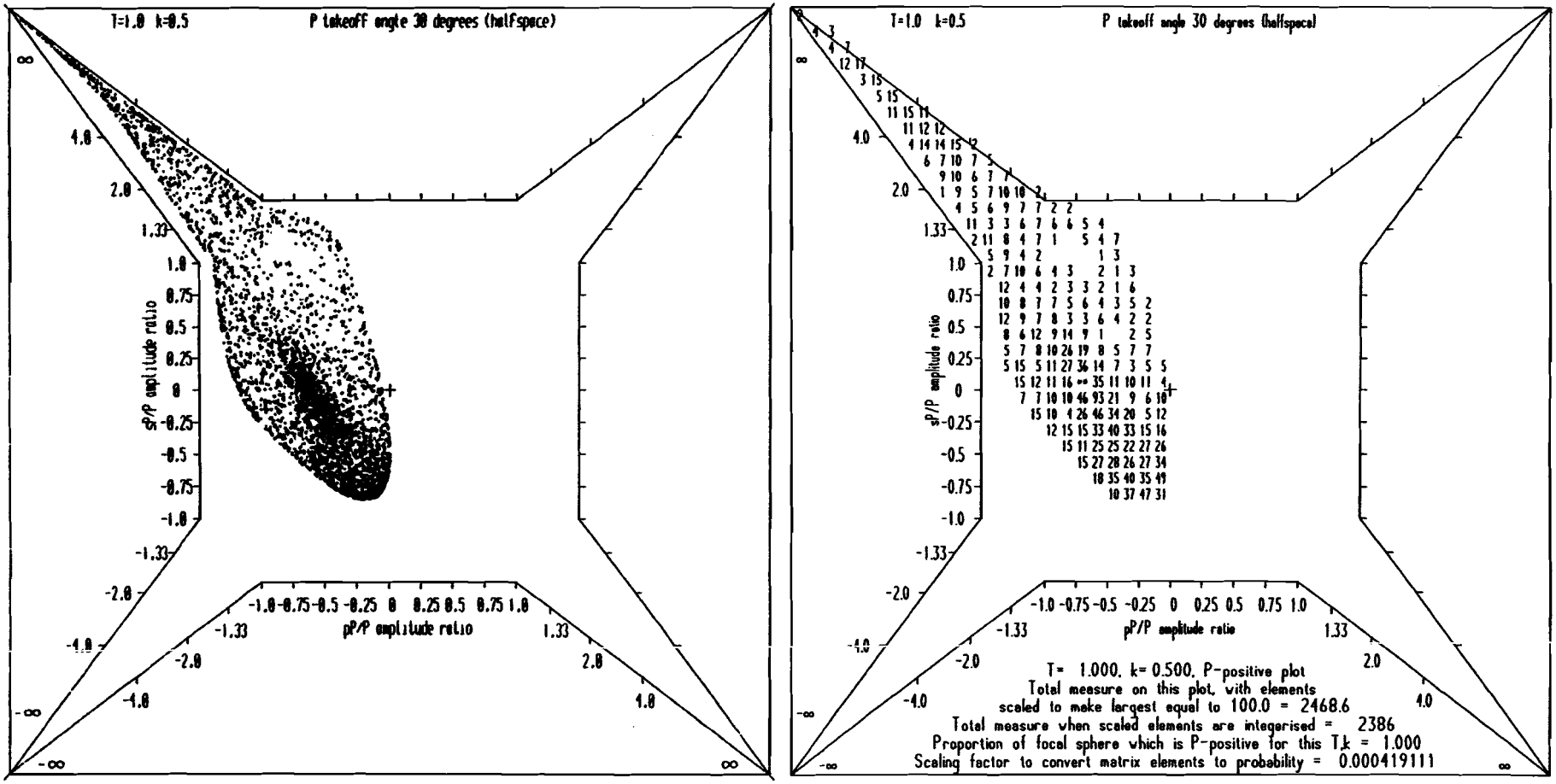
T=1.0 k=0.5
P takeoff angle 30 degrees (halfspace)
sP/P amplitude ratio
pP/P amplitude ratio
T= 1.000, k= 0.500, P-positive plot
Total measure on this plot, with elements
scaled to make largest equal to 100.0 = 2468.6
Total measure when scaled elements are integerised = 2386
Proportion of focal sphere which is P-positive for this T,k = 1.000
Scaling factor to convert matrix elements to probability = 0.000419111

Figure 29

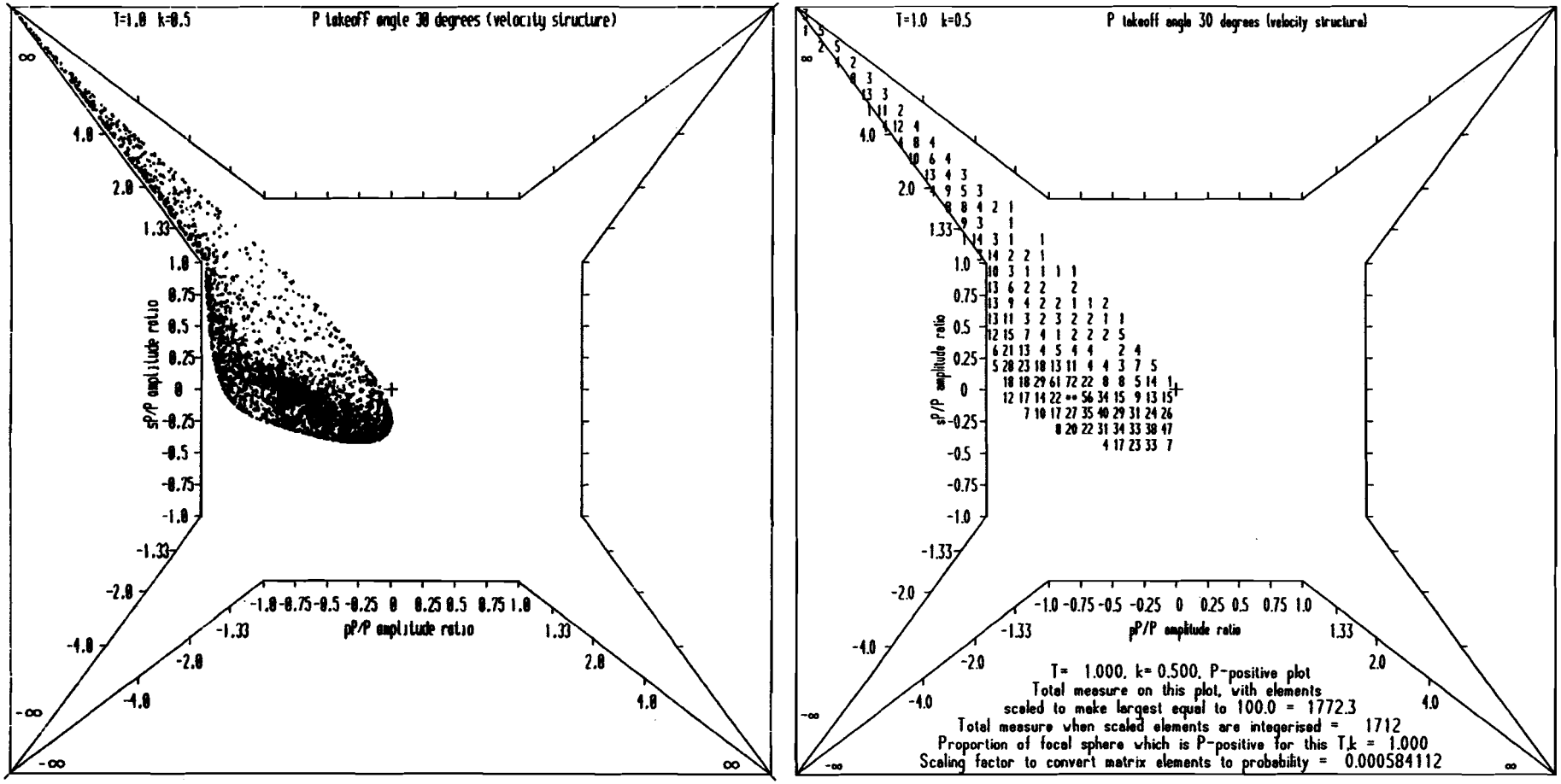
T=1.0 k=0.5
P takeoff angle 30 degrees (velocity structure)
sP/P amplitude ratio
pP/P amplitude ratio
T= 1.000, k= 0.500, P-positive plot
Total measure on this plot, with elements
scaled to make largest equal to 100.0 = 1772.3
Total measure when scaled elements are integerised = 1712
Proportion of focal sphere which is P-positive for this T,k = 1.000
Scaling factor to convert matrix elements to probability = 0.000584112

Figure 30

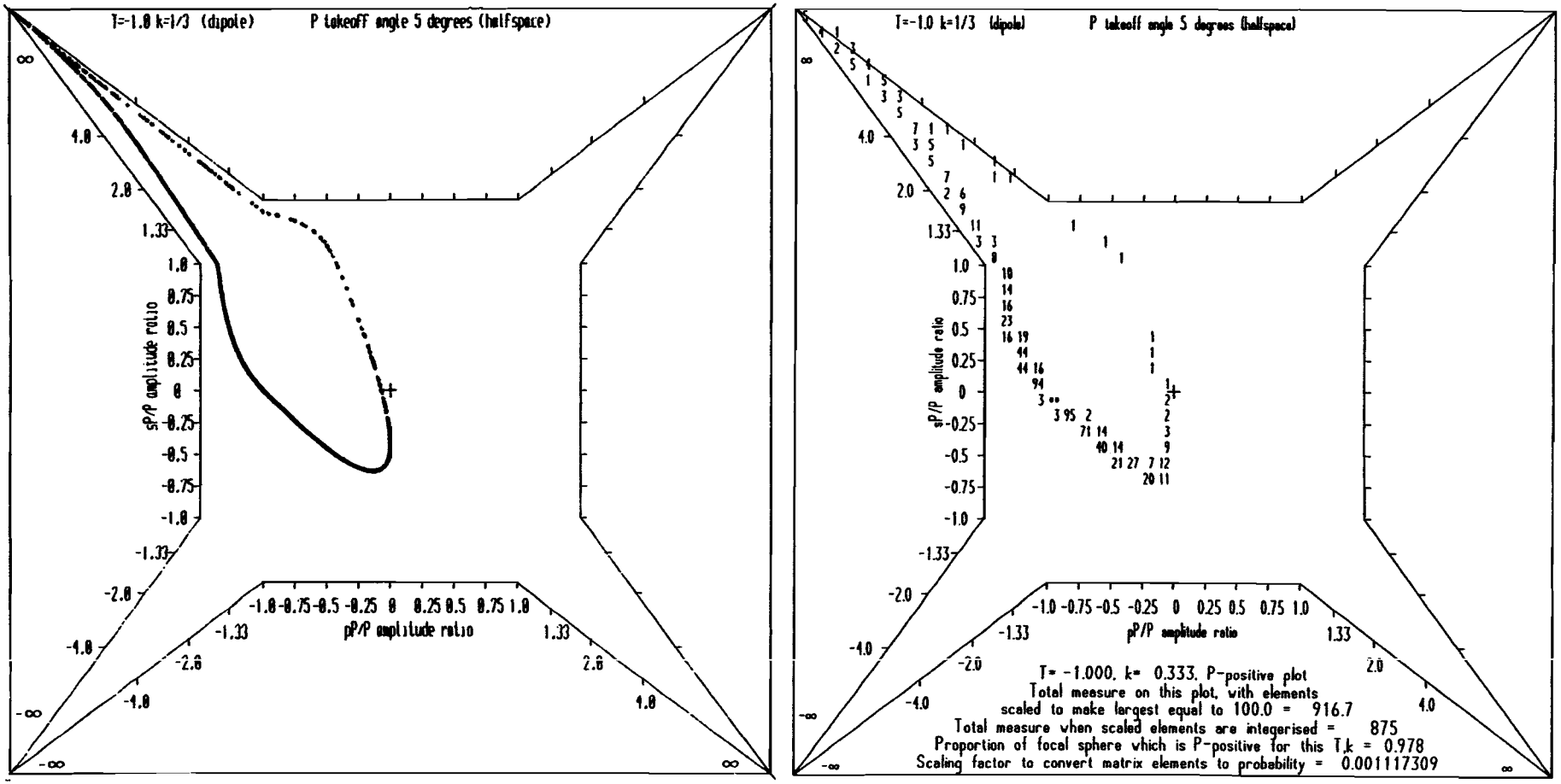
T=-1.0 k=1/3 (dipole) P takeoff angle 5 degrees (halfspace)
sP/P amplitude ratio
pP/P amplitude ratio
T=-1.0 k=1/3 (dipole) P takeoff angle 5 degrees (halfspace)
sP/P amplitude ratio
pP/P amplitude ratio
T= -1.000, k= 0.333, P-positive plot
Total measure on this plot, with elements
scaled to make largest equal to 100.0 = 916.7
Total measure when scaled elements are integerised = 875
Proportion of focal sphere which is P-positive for this T,k = 0.978
Scaling factor to convert matrix elements to probability = 0.001117309

Figure 31

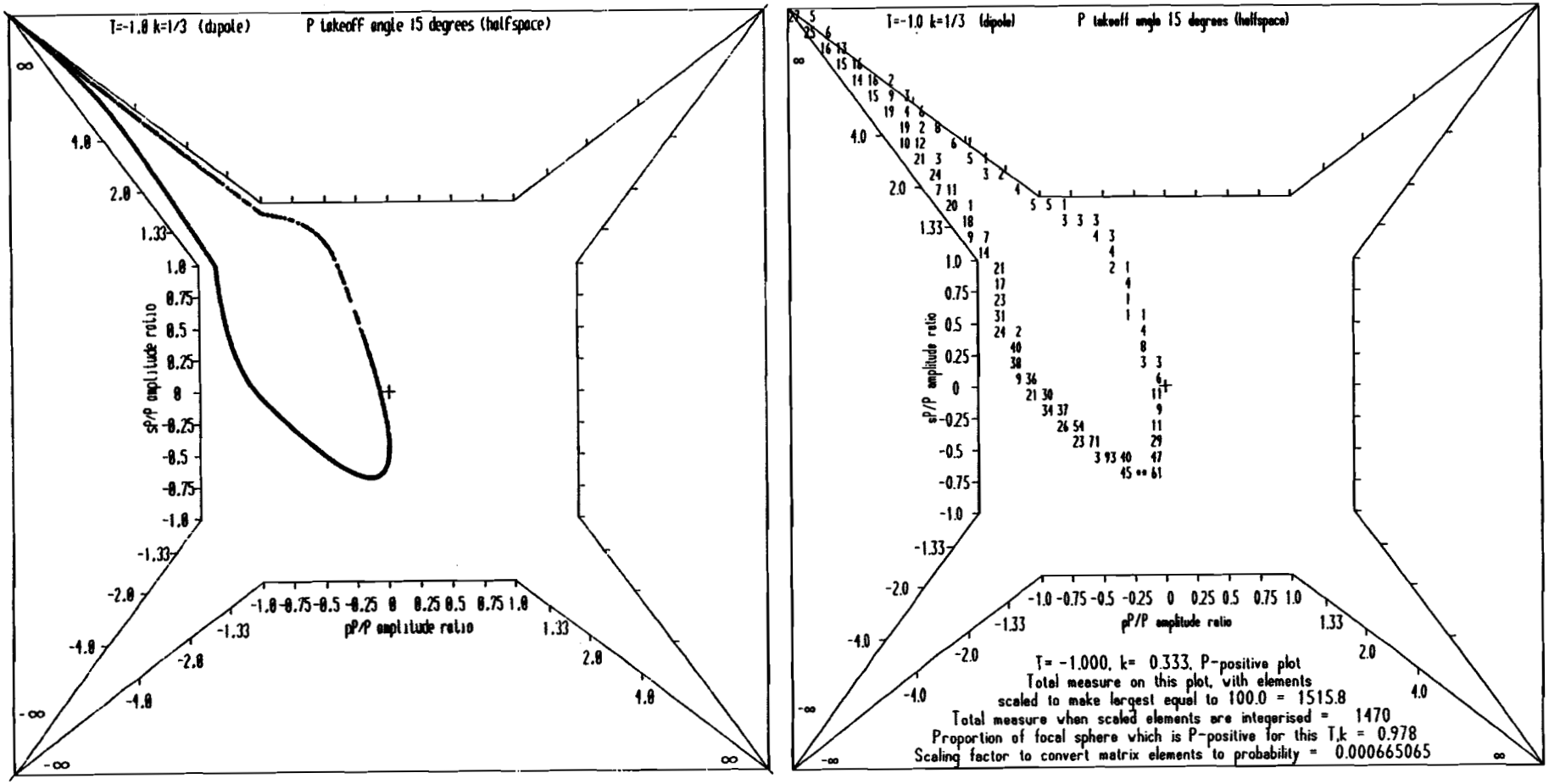
T=-1.0 k=1/3 (dipole) P takeoff angle 15 degrees (halfspace)
sP/P amplitude ratio
pP/P amplitude ratio
T=-1.0 k=1/3 (dipole) P takeoff angle 15 degrees (halfspace)
sP/P amplitude ratio
pP/P amplitude ratio
T= -1.000, k= 0.333, P-positive plot
Total measure on this plot, with elements
scaled to make largest equal to 100.0 = 1515.8
Total measure when scaled elements are integerised = 1470
Proportion of focal sphere which is P-positive for this T,k = 0.978
Scaling factor to convert matrix elements to probability = 0.000665065

Figure 32

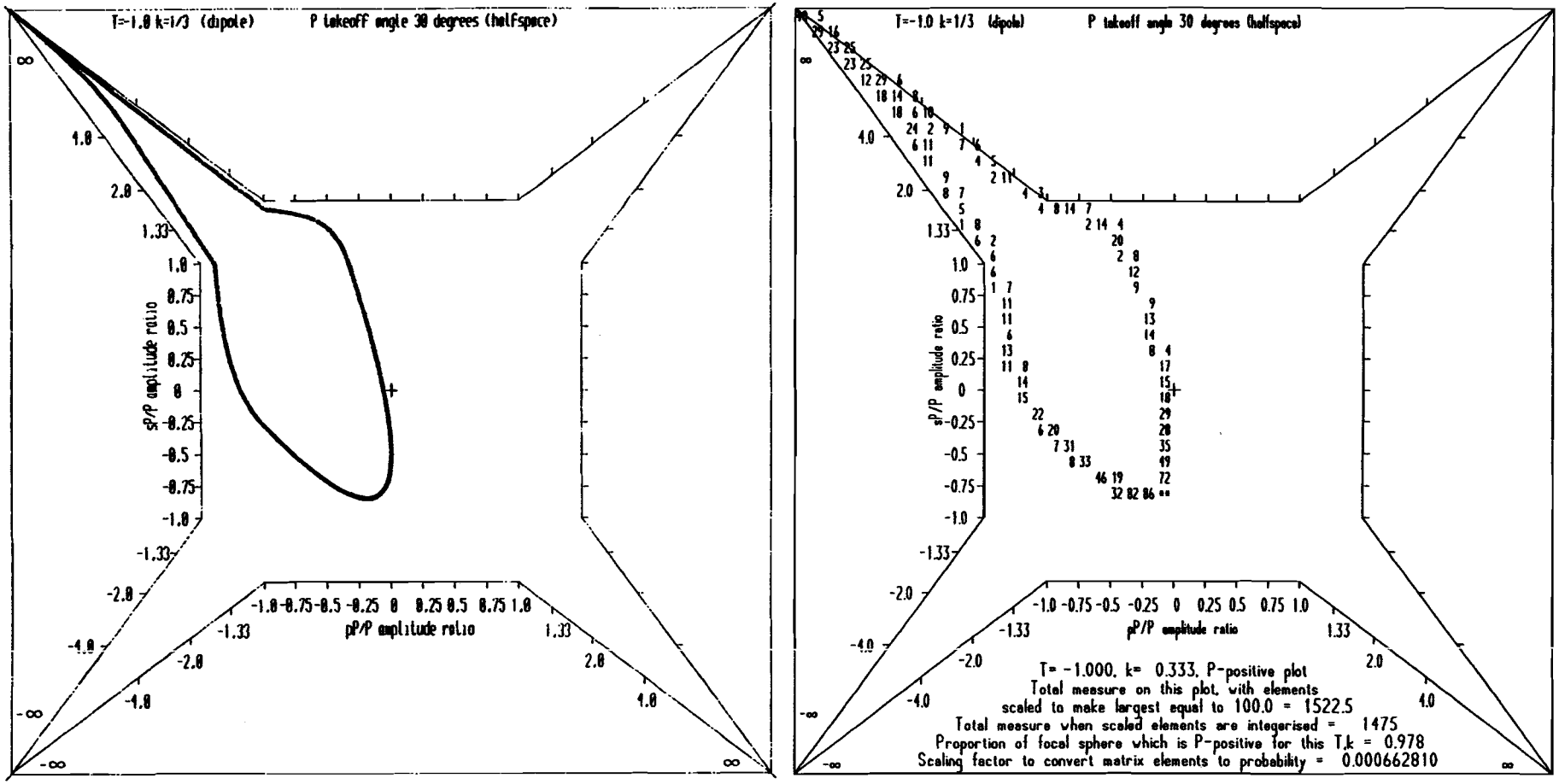
T=-1.0 k=1/3 (dipole) P takeoff angle 30 degrees (halfspace)
sP/P amplitude ratio
pP/P amplitude ratio
T= -1.000, k= 0.333, P-positive plot
Total measure on this plot, with elements
scaled to make largest equal to 100.0 = 1522.5
Total measure when scaled elements are integerised = 1475
Proportion of focal sphere which is P-positive for this T,k = 0.978
Scaling factor to convert matrix elements to probability = 0.000662810

Figure 33

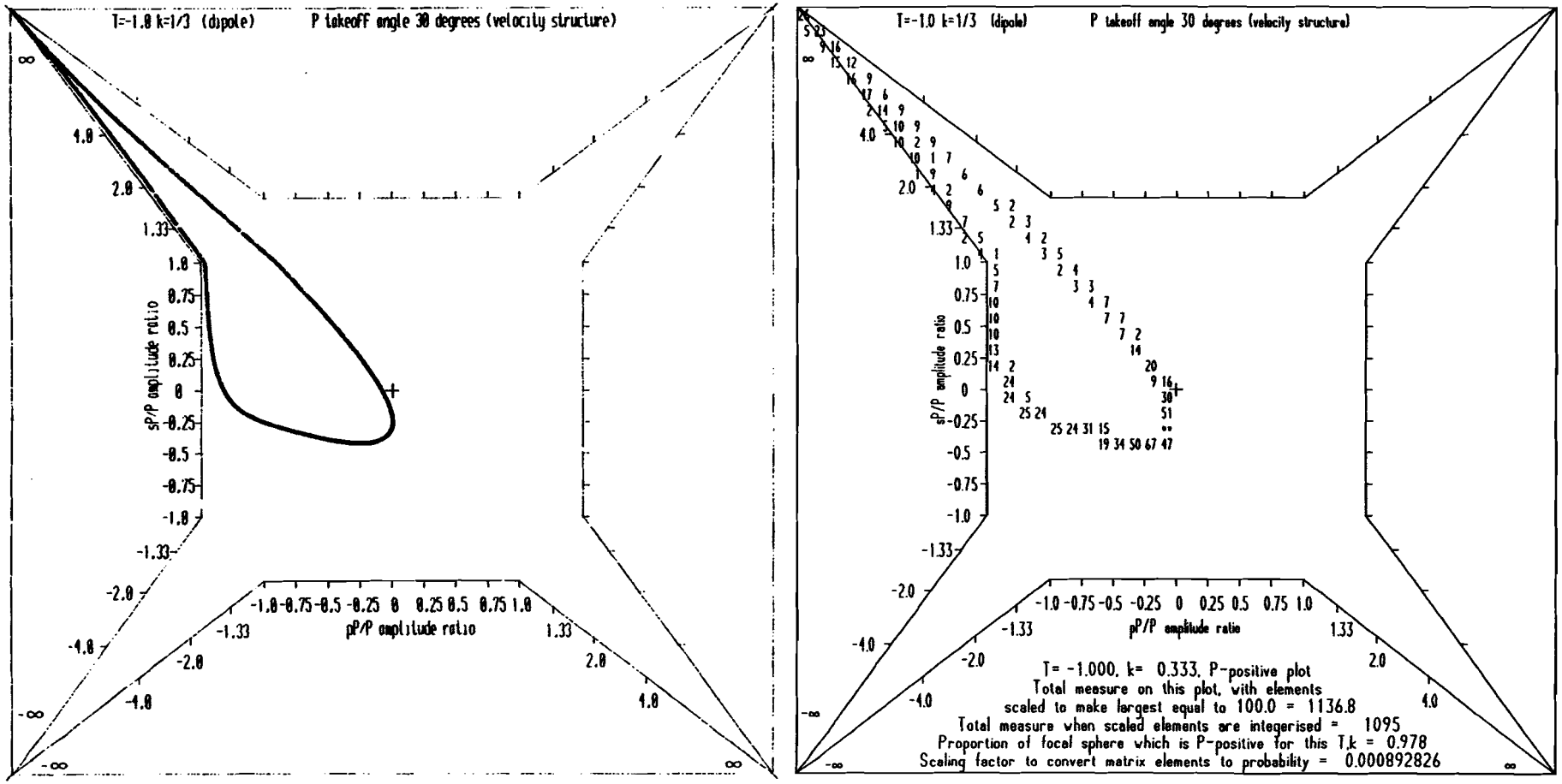
T=-1.0 k=1/3 (dipole)
P takeoff angle 30 degrees (velocity structure)
sP/P amplitude ratio
pP/P amplitude ratio
T=-1.0 k=1/3 (dipole)
P takeoff angle 30 degrees (velocity structure)
sP/P amplitude ratio
pP/P amplitude ratio
T= -1.000, k= 0.333, P-positive plot
Total measure on this plot, with elements
scaled to make largest equal to 100.0 = 1136.8
Total measure when scaled elements are integerised = 1095
Proportion of focal sphere which is P-positive for this T,k = 0.978
Scaling factor to convert matrix elements to probability = 0.000892826

Figure 34

This page intentionally left blank

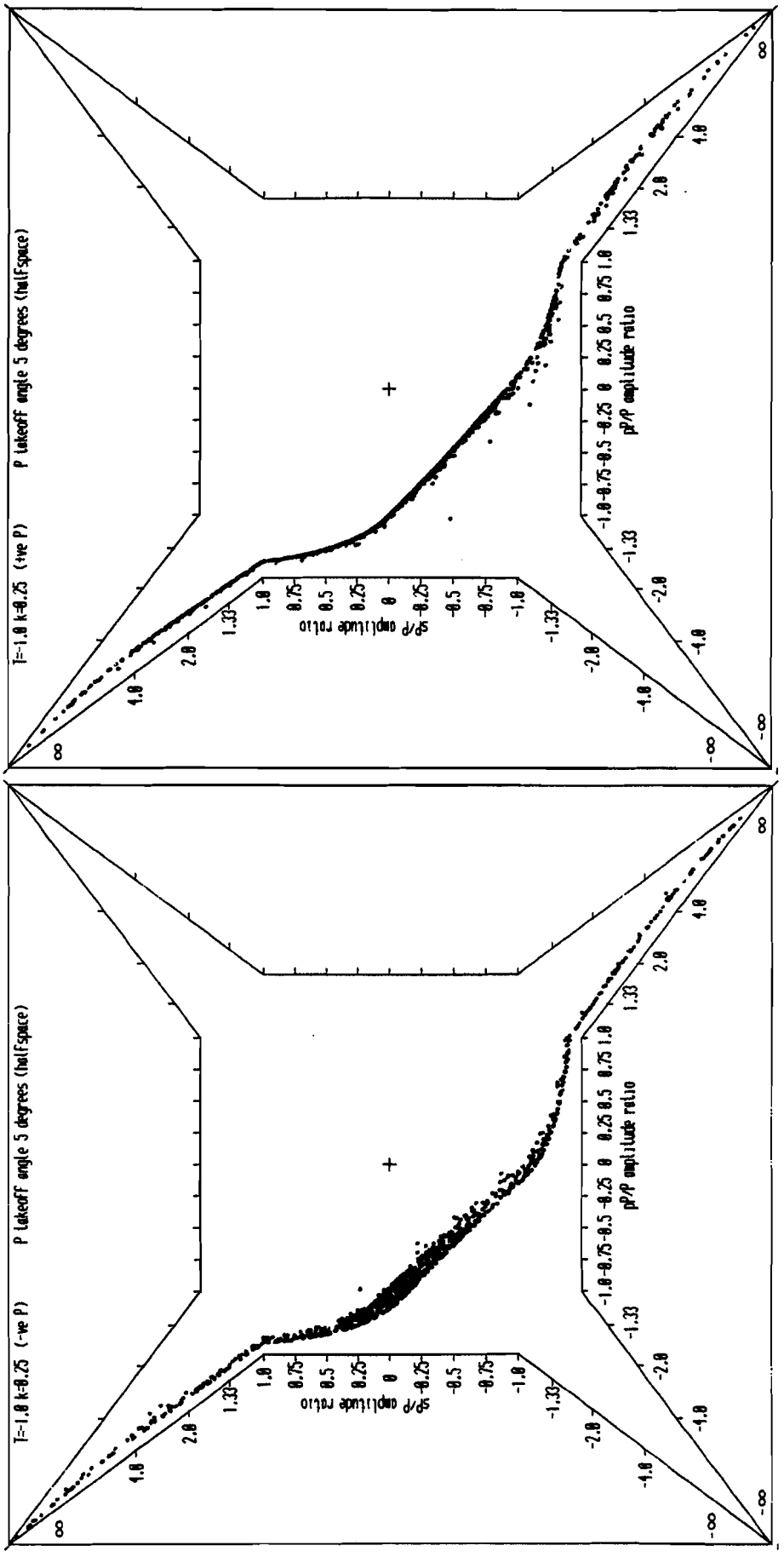
T=-1.0 k=0.25 (+ve P)
P takeoff angle 5 degrees (halfspace)
sP/P amplitude ratio
pP/P amplitude ratio
T=-1.0 k=0.25 (-ve P)
P takeoff angle 5 degrees (halfspace)
sP/P amplitude ratio
pP/P amplitude ratio

Figure 35

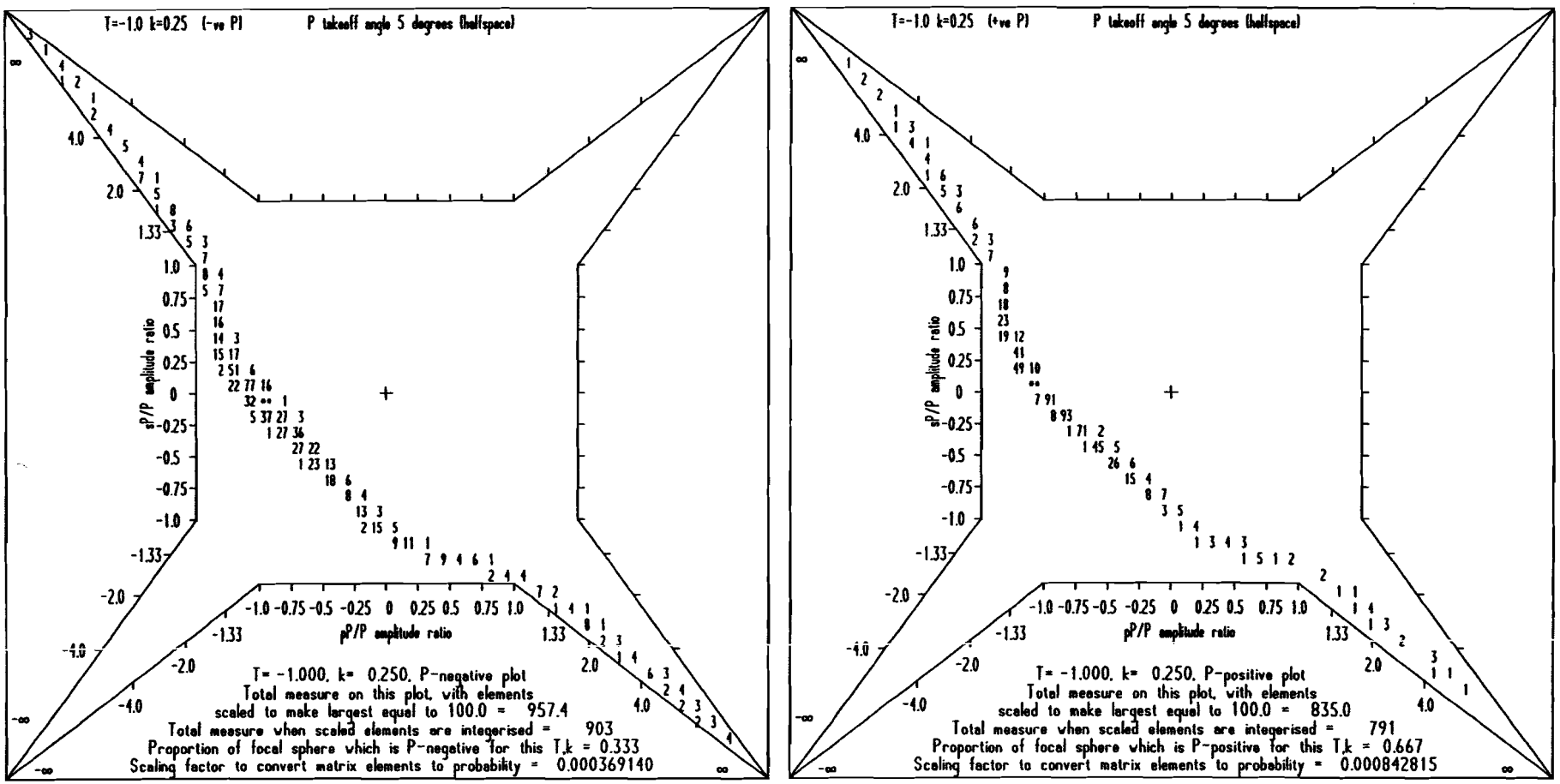

Figure 35 (continued)

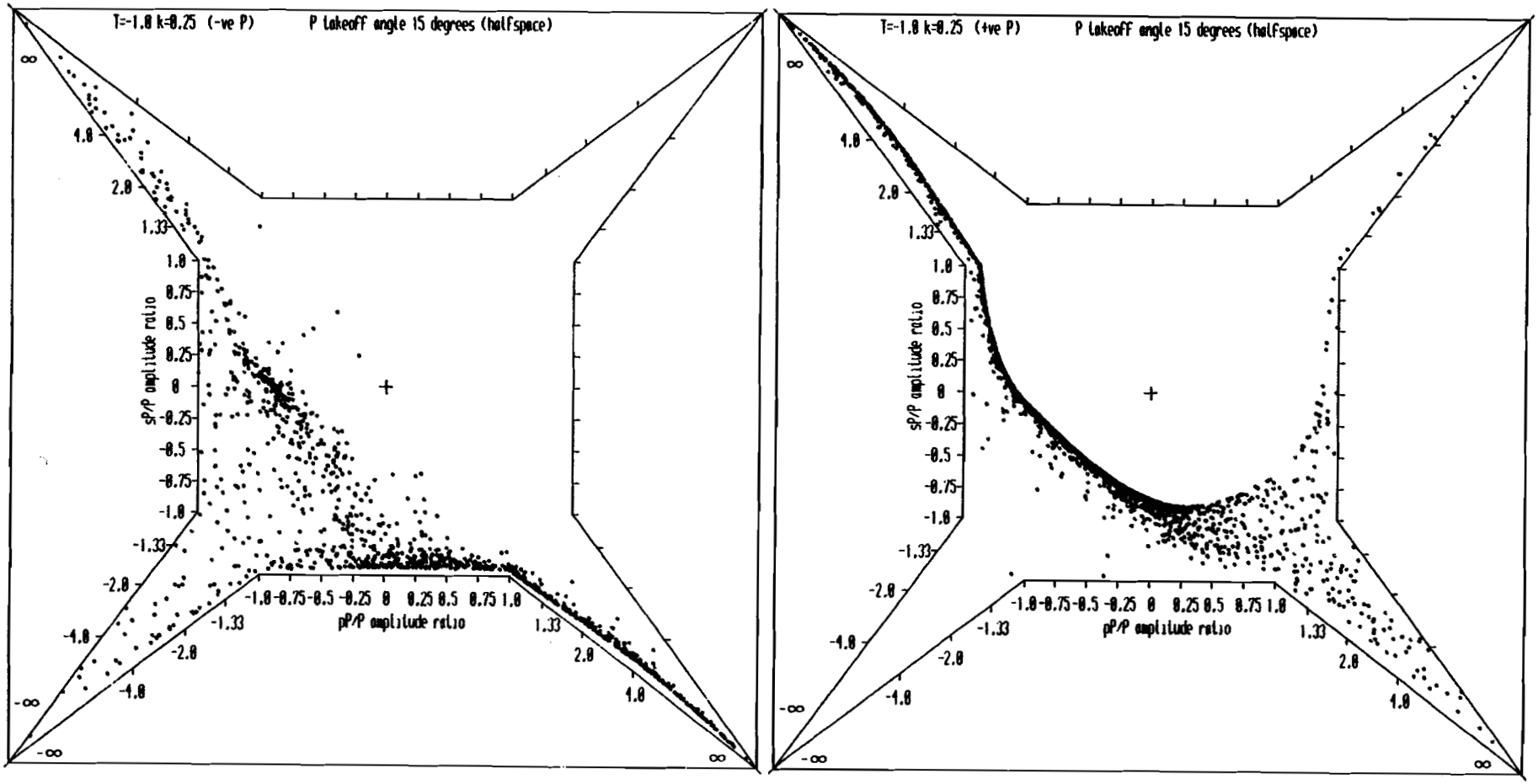
T=-1.0 k=0.25 (-ve P)
P takeoff angle 15 degrees (halfspace)
sP/P amplitude ratio
pP/P amplitude ratio
T=-1.0 k=0.25 (+ve P)
P takeoff angle 15 degrees (halfspace)
sP/P amplitude ratio
pP/P amplitude ratio

Figure 36

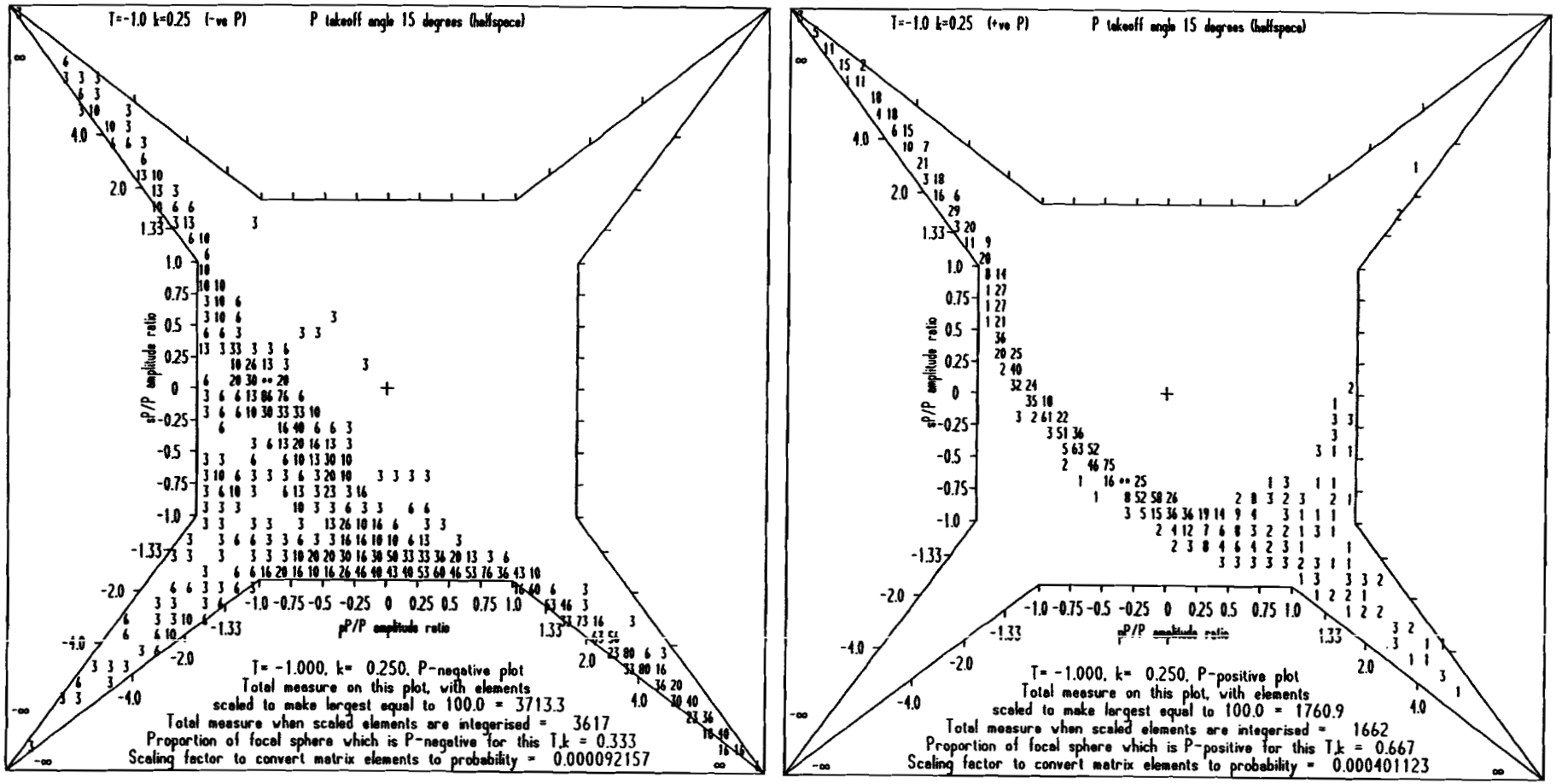

Figure 36 (continued)

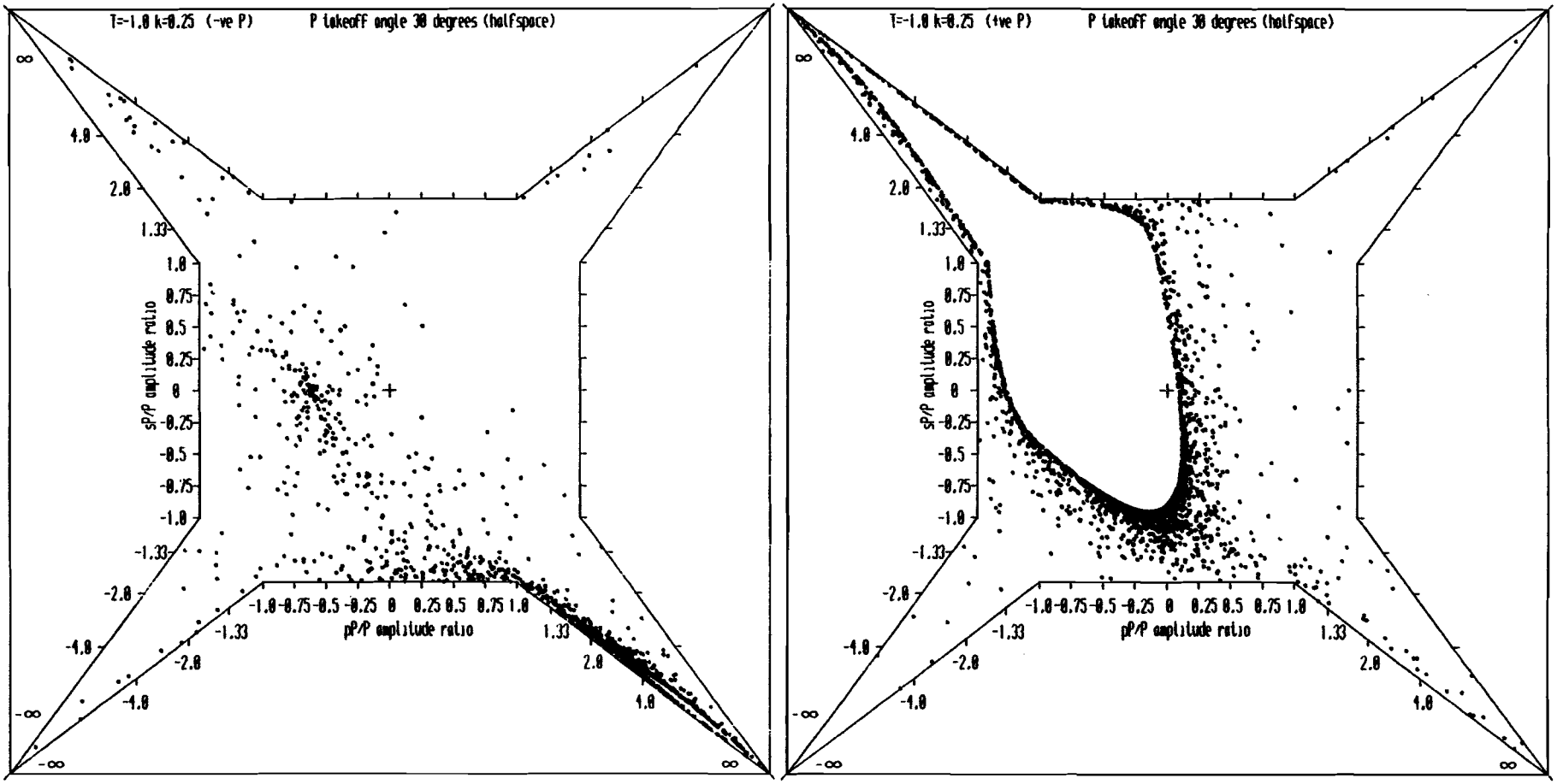
T=-1.0 k=0.25 (-ve P)
P takeoff angle 38 degrees (halfspace)
sP/P amplitude ratio
pP/P amplitude ratio
T=-1.0 k=0.25 (+ve P)
P takeoff angle 38 degrees (halfspace)
sP/P amplitude ratio
pP/P amplitude ratio

Figure 37

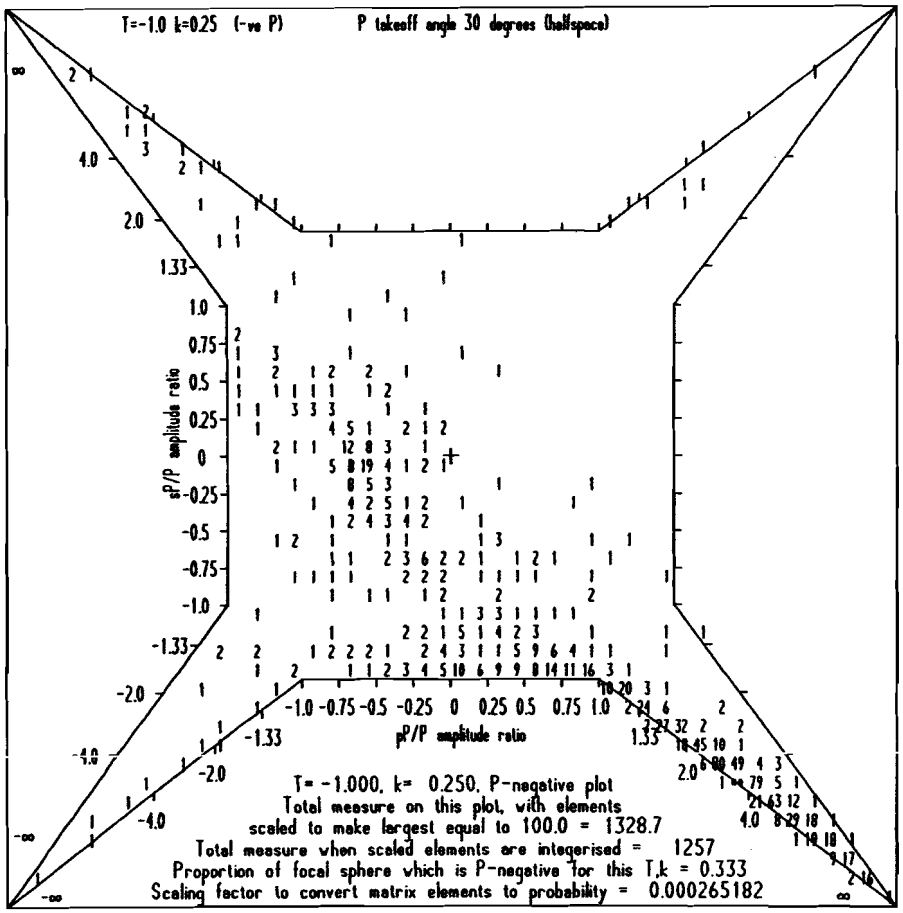

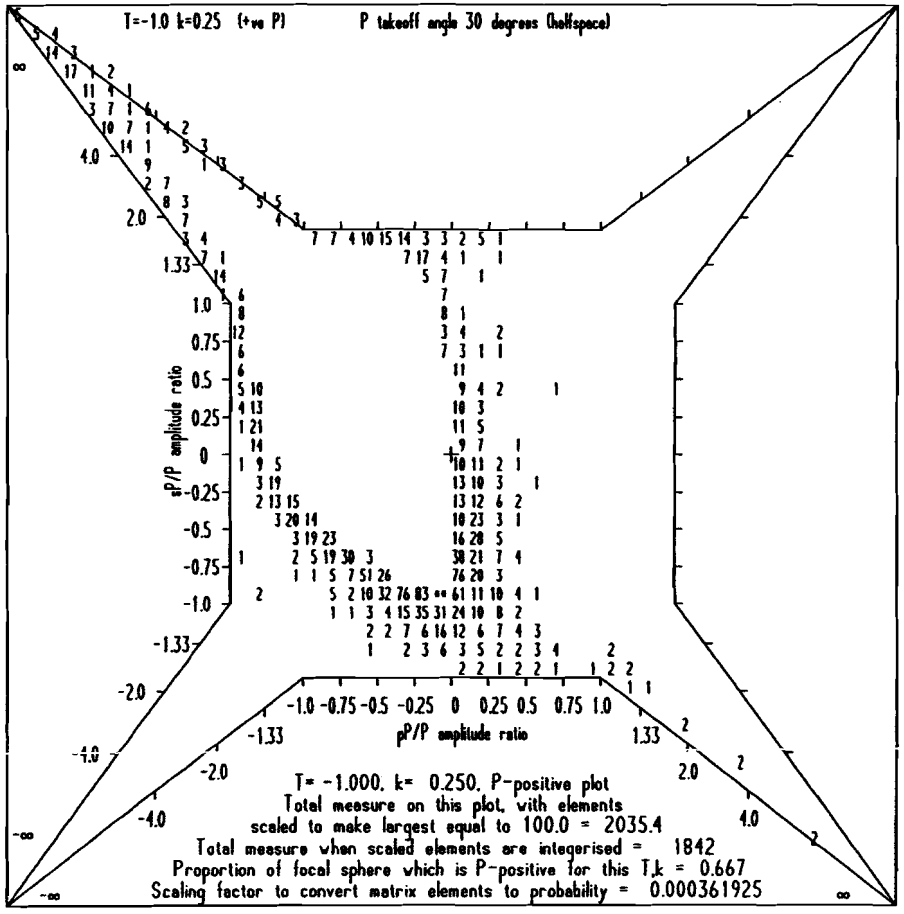

Figure 37 (continued)

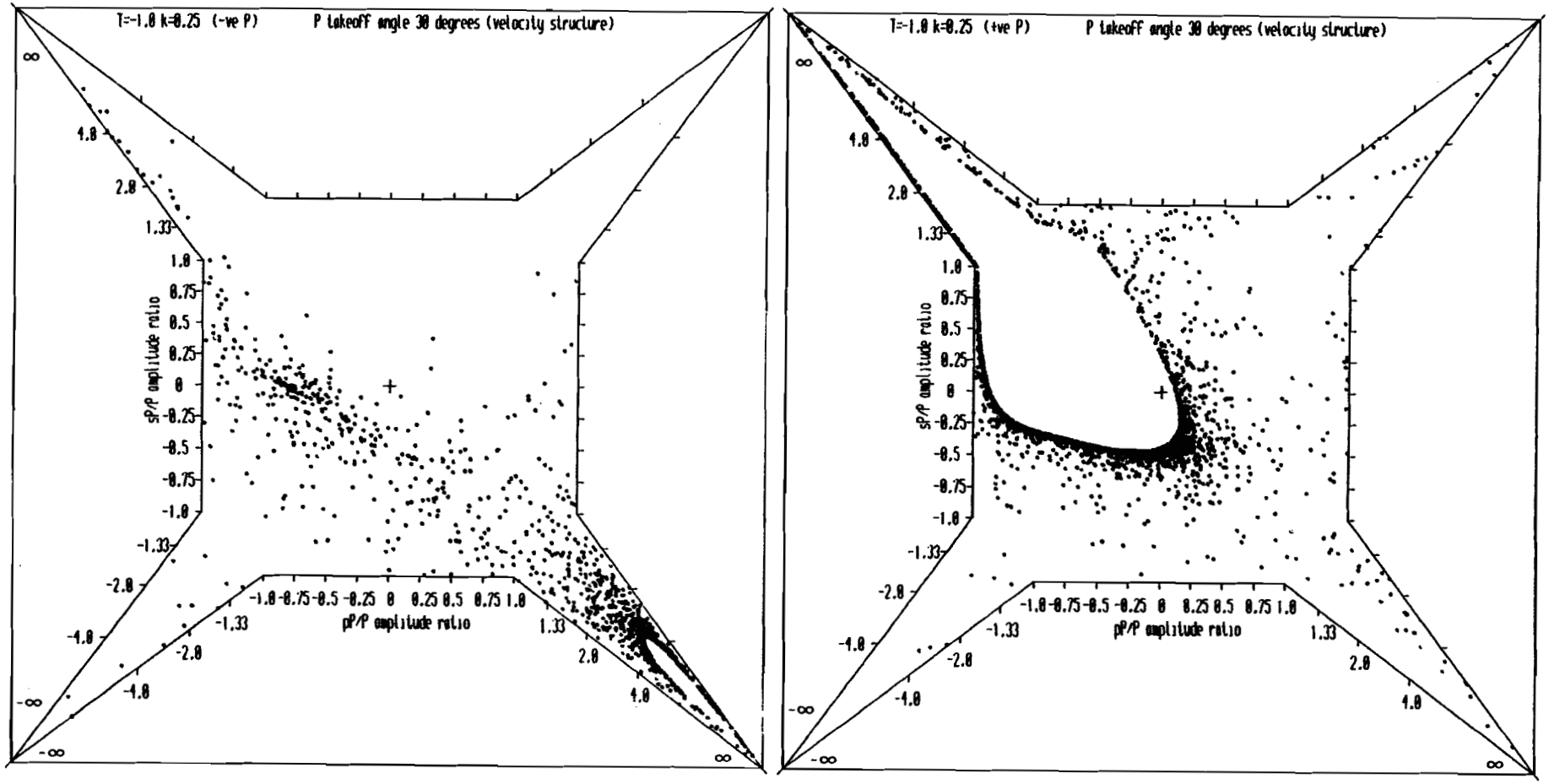
T=-1.0 k=0.25 (-ve P)
P takeoff angle 30 degrees (velocity structure)
sP/P amplitude ratio
pP/P amplitude ratio
T=-1.0 k=0.25 (+ve P)
P takeoff angle 30 degrees (velocity structure)
sP/P amplitude ratio
pP/P amplitude ratio

Figure 38

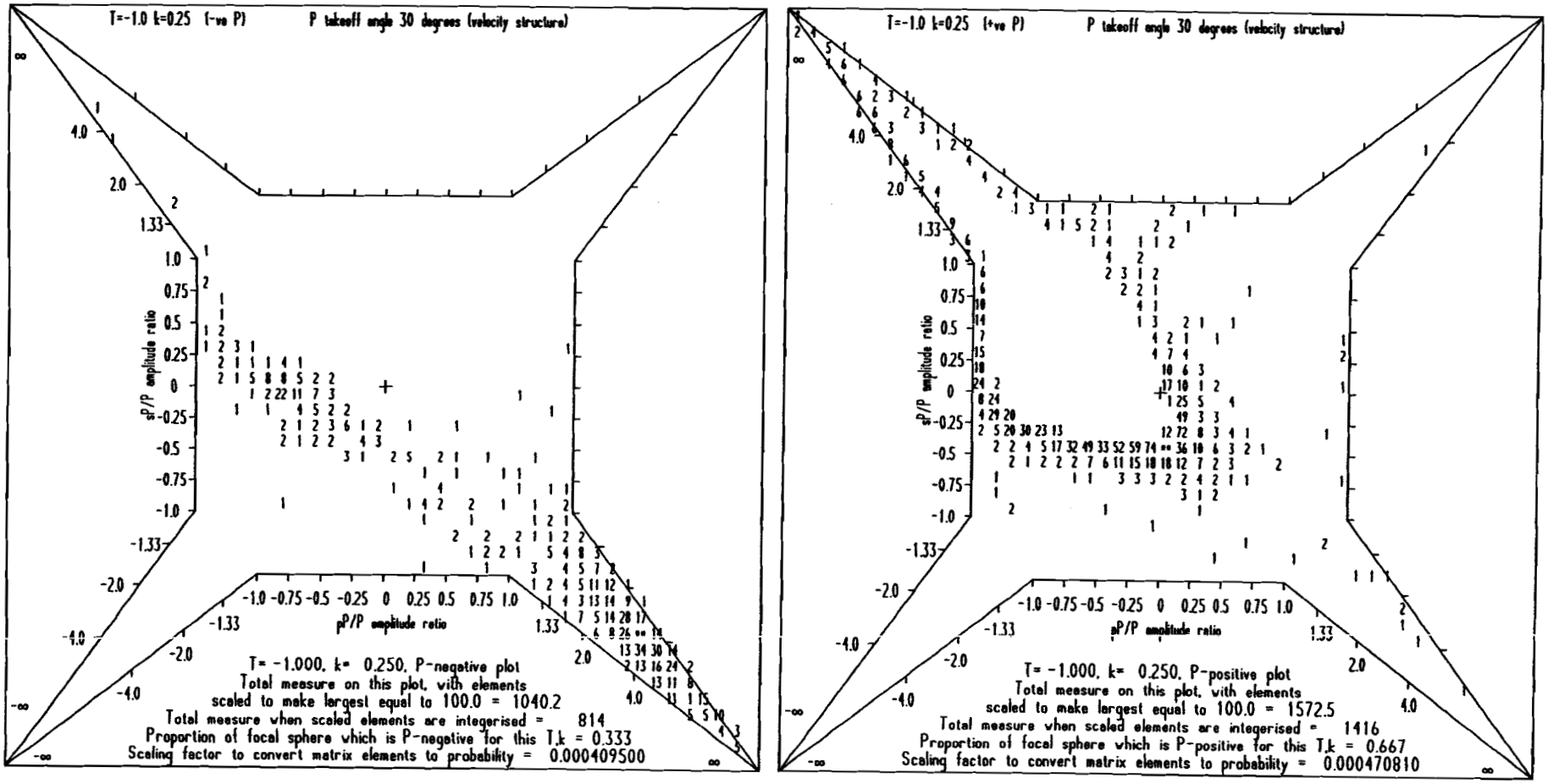

Figure 38 (continued)

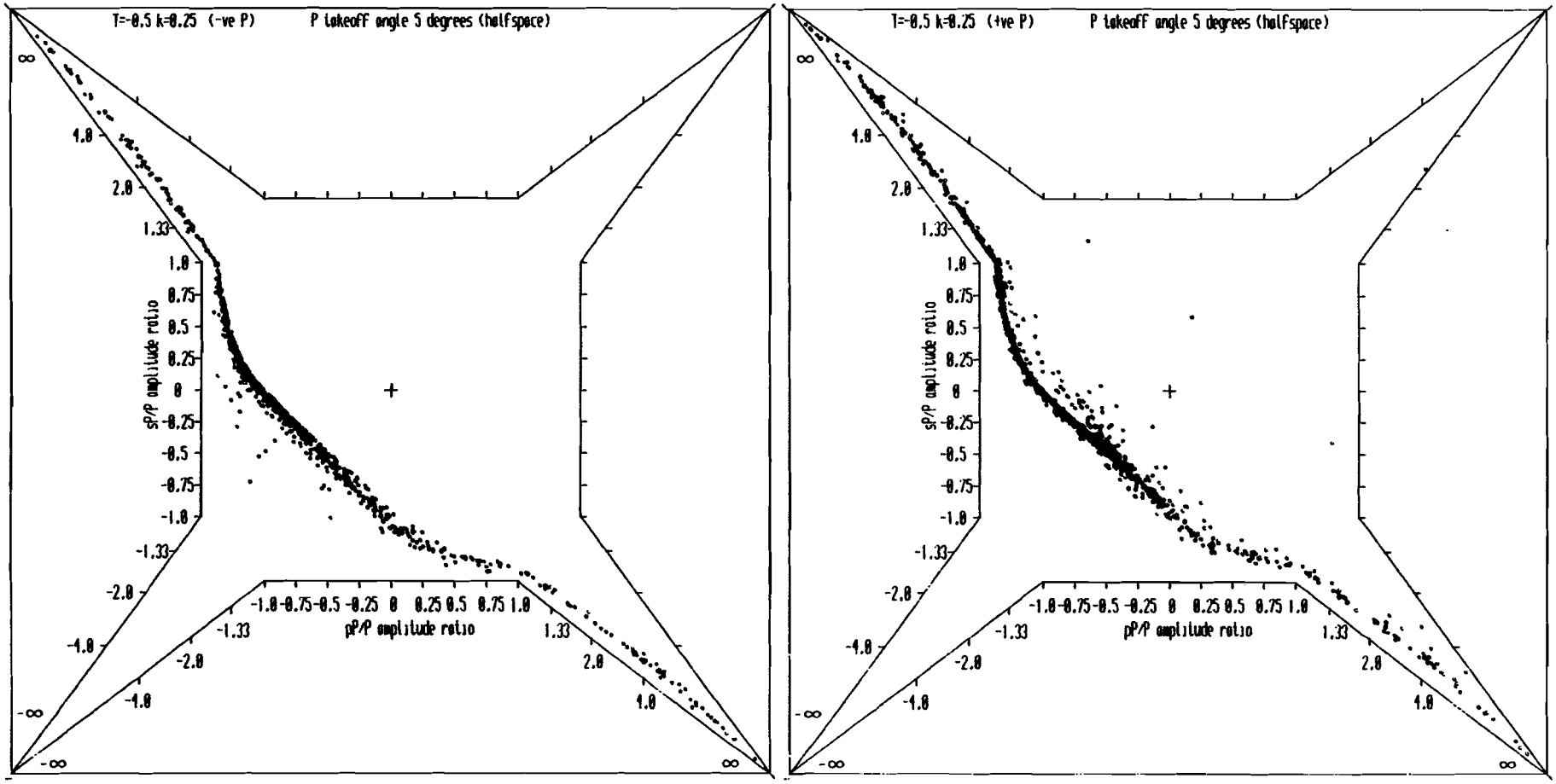
T=-0.5 k=0.25 (-ve P)
P takeoff angle 5 degrees (halfspace)
sP/P amplitude ratio
pP/P amplitude ratio
T=-0.5 k=0.25 (+ve P)
P takeoff angle 5 degrees (halfspace)
sP/P amplitude ratio
pP/P amplitude ratio

Figure 39

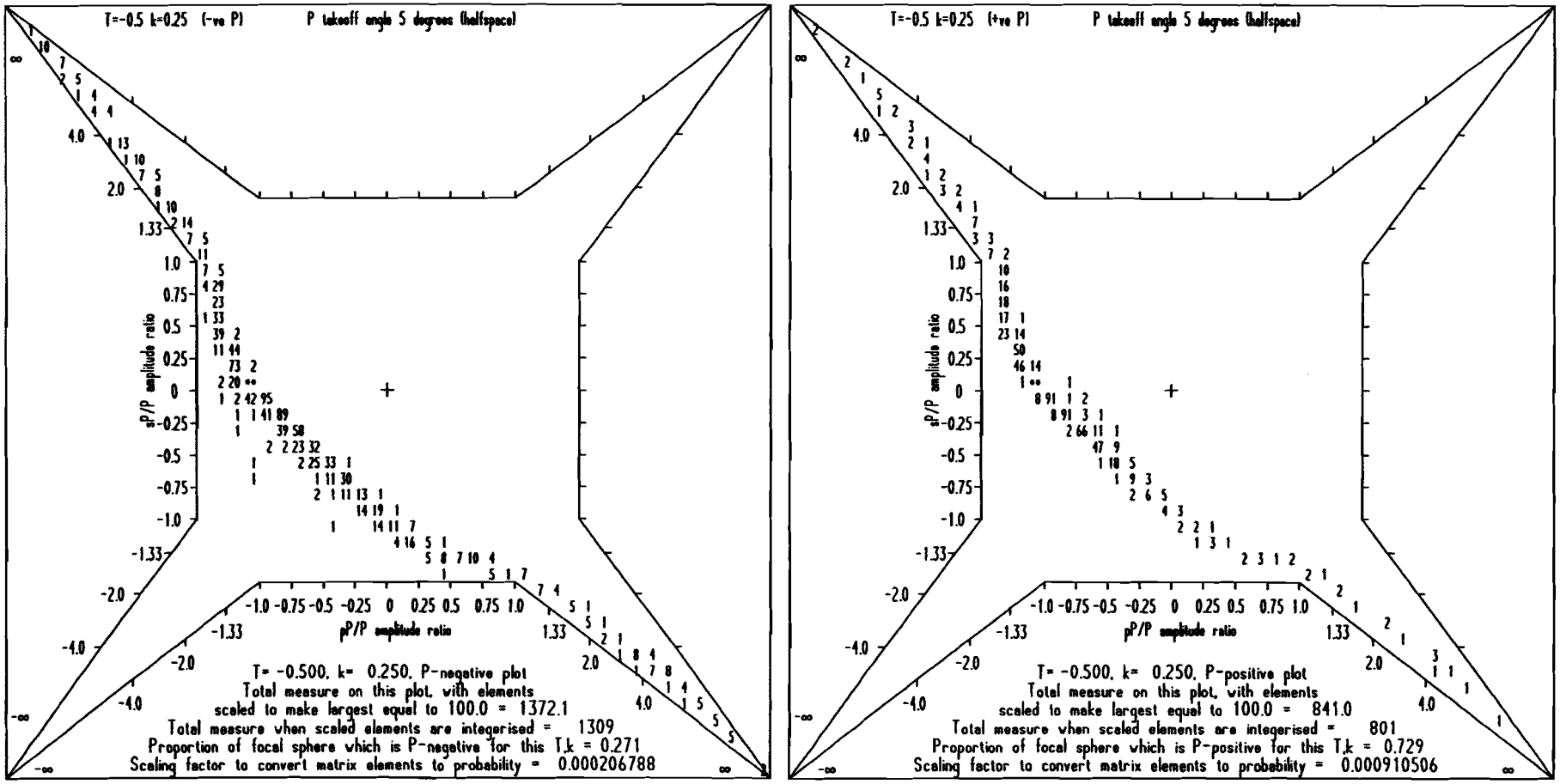

Figure 39 (continued)

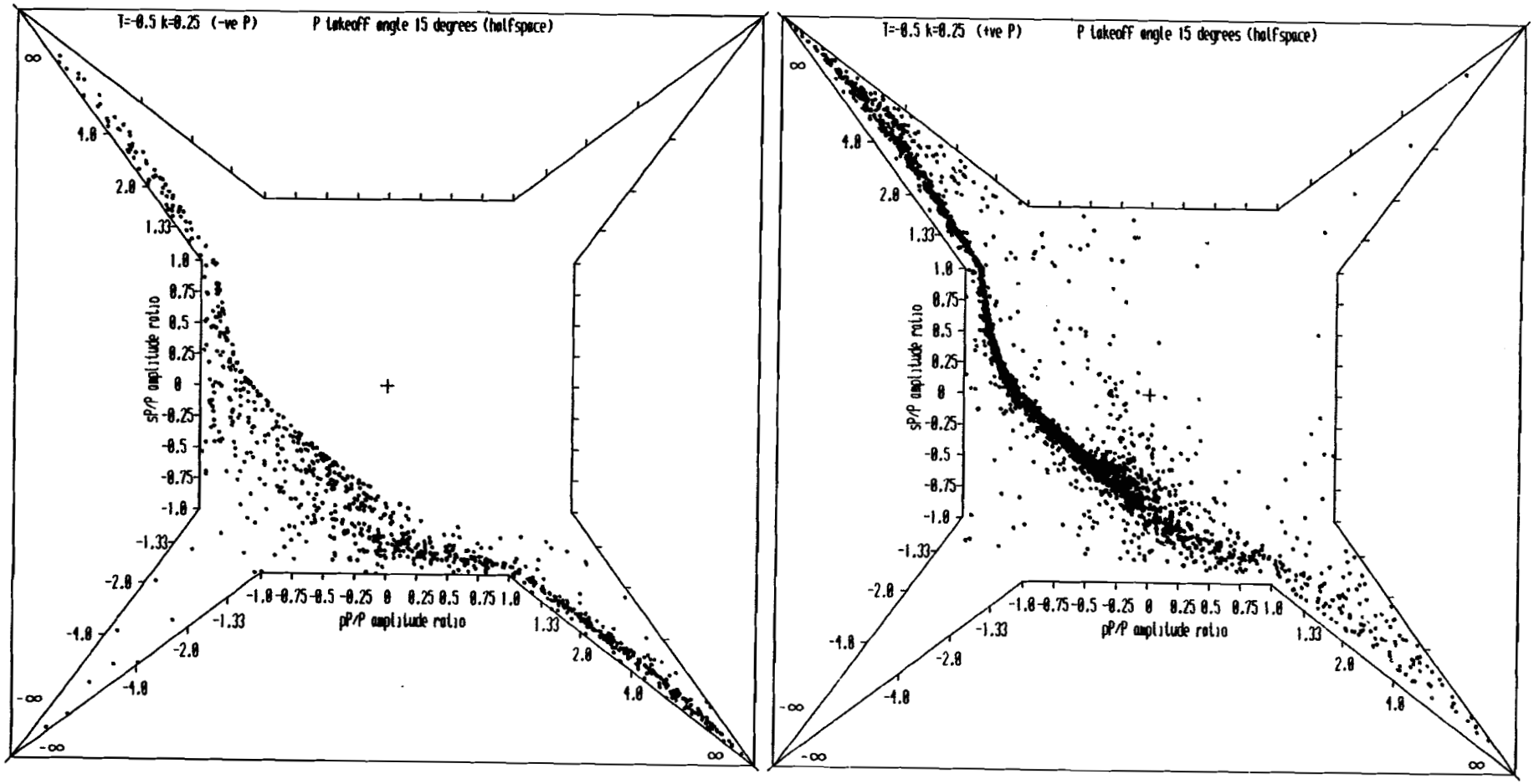
T=-0.5 k=0.25 (-ve P)
P takeoff angle 15 degrees (halfspace)
sP/P amplitude ratio
pP/P amplitude ratio
T=-0.5 k=0.25 (+ve P)
P takeoff angle 15 degrees (halfspace)
sP/P amplitude ratio
pP/P amplitude ratio

Figure 40

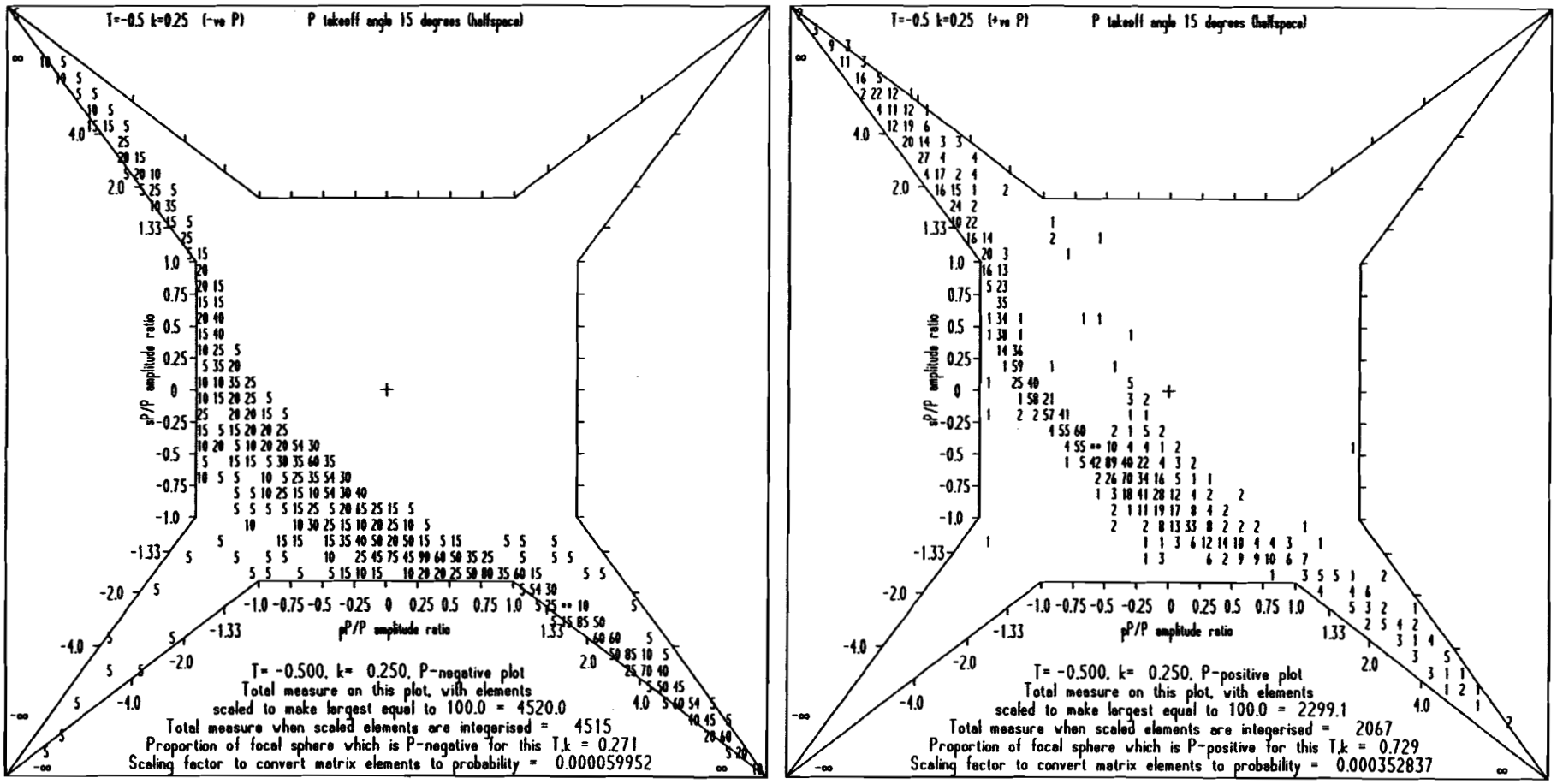

Figure 40 (continued)

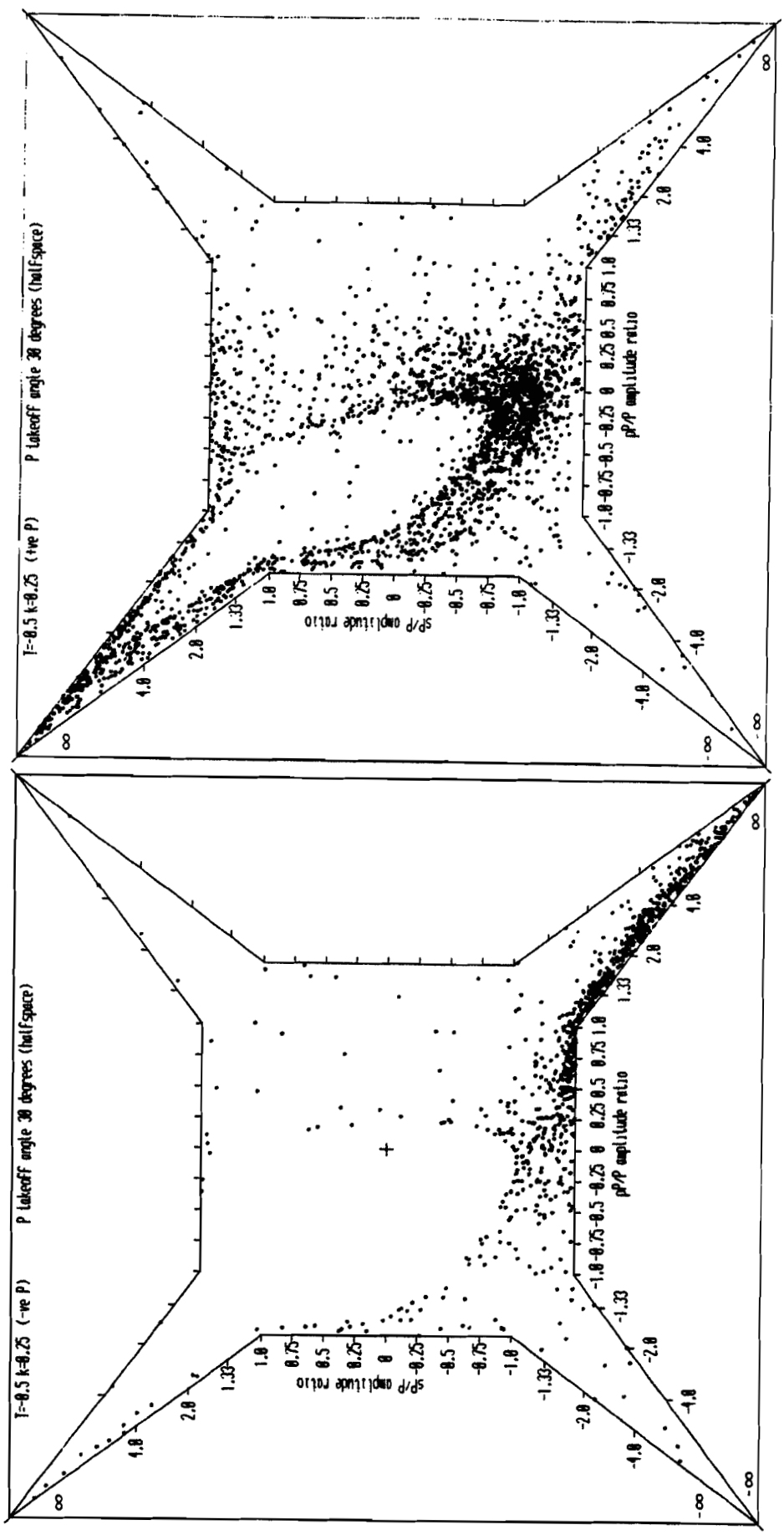
T=-0.5 k=0.25 (+ve P)
P takeoff angle 30 degrees (halfspace)
sP/P amplitude ratio
pP/P amplitude ratio
T=-0.5 k=0.25 (-ve P)
P takeoff angle 30 degrees (halfspace)
sP/P amplitude ratio
pP/P amplitude ratio

Figure 41

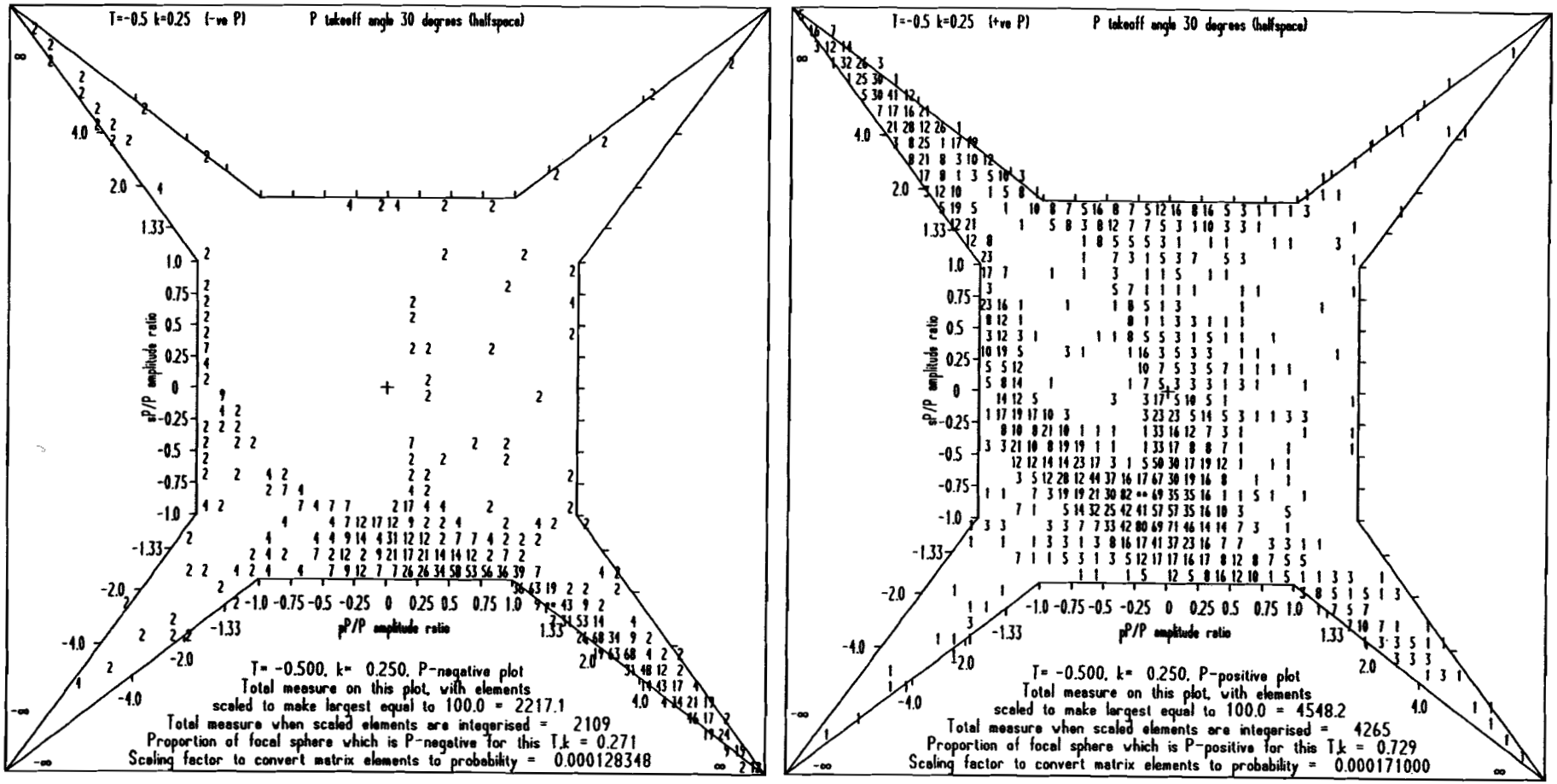

Figure 41 (continued)

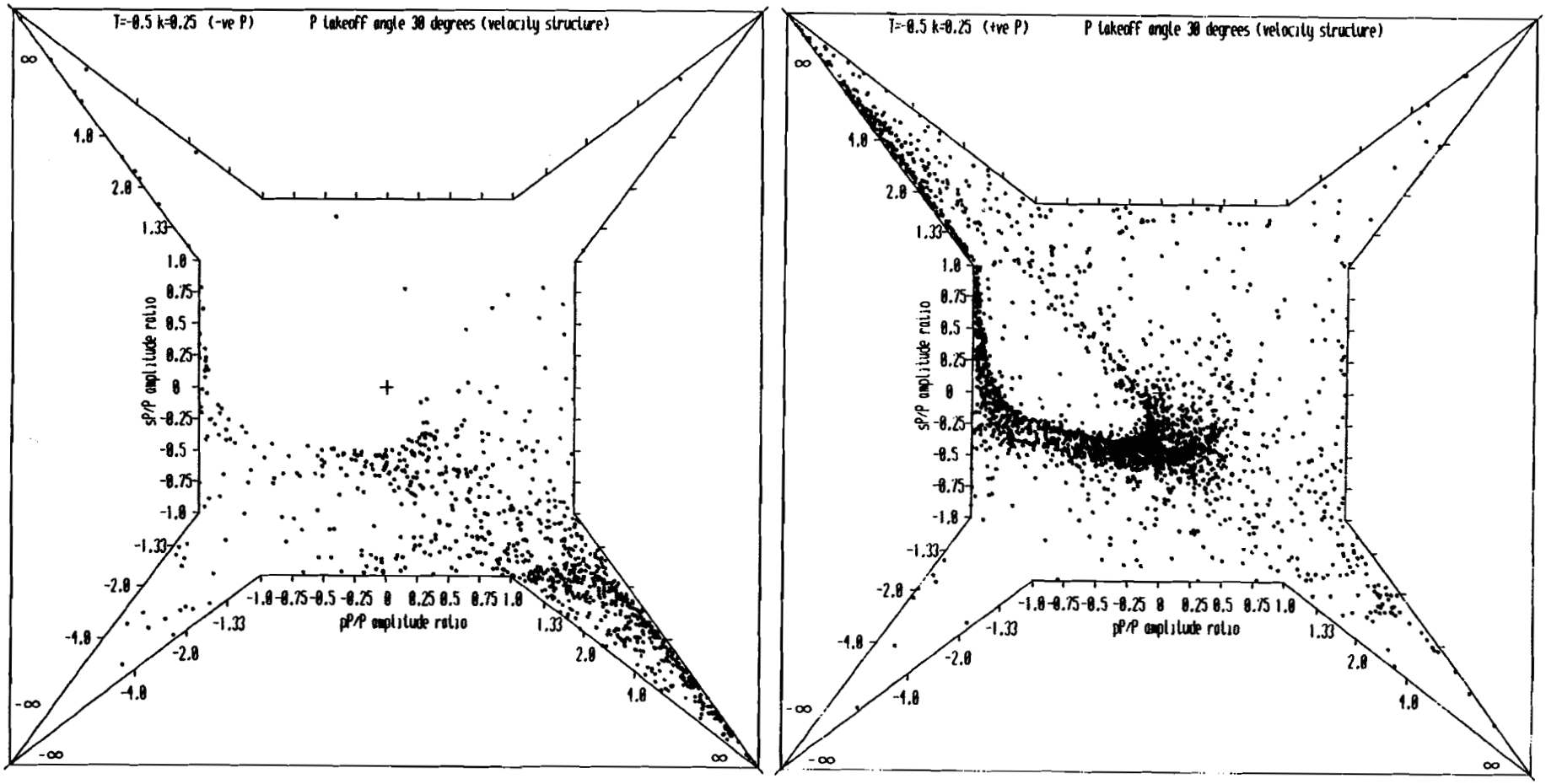
T=-0.5 k=0.25 (-ve P)
P takeoff angle 30 degrees (velocity structure)
sP/P amplitude ratio
pP/P amplitude ratio
T=-0.5 k=0.25 (+ve P)
P takeoff angle 30 degrees (velocity structure)
sP/P amplitude ratio
pP/P amplitude ratio

Figure 42

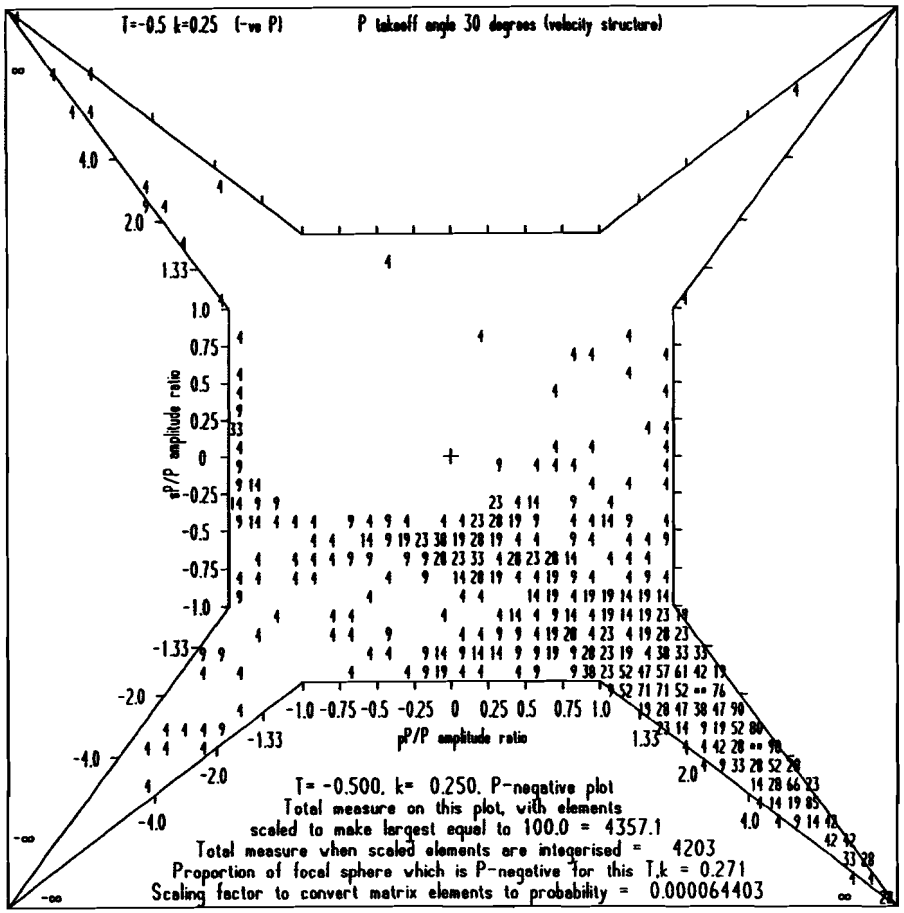

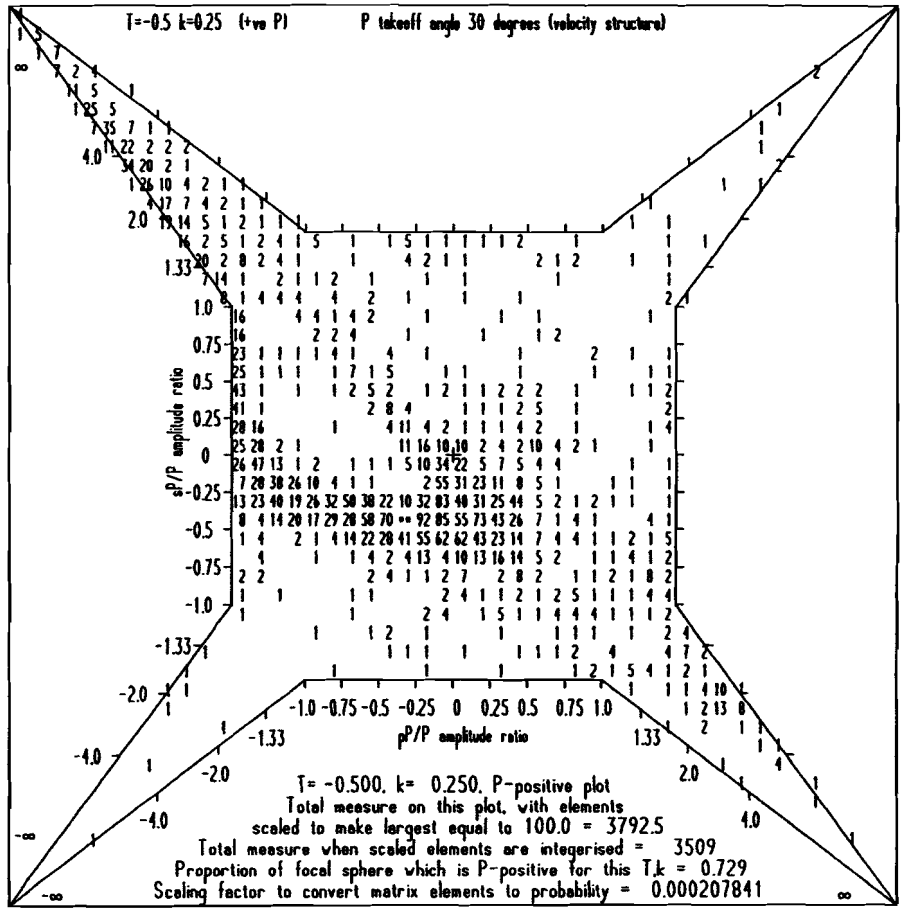

Figure 42 (continued)

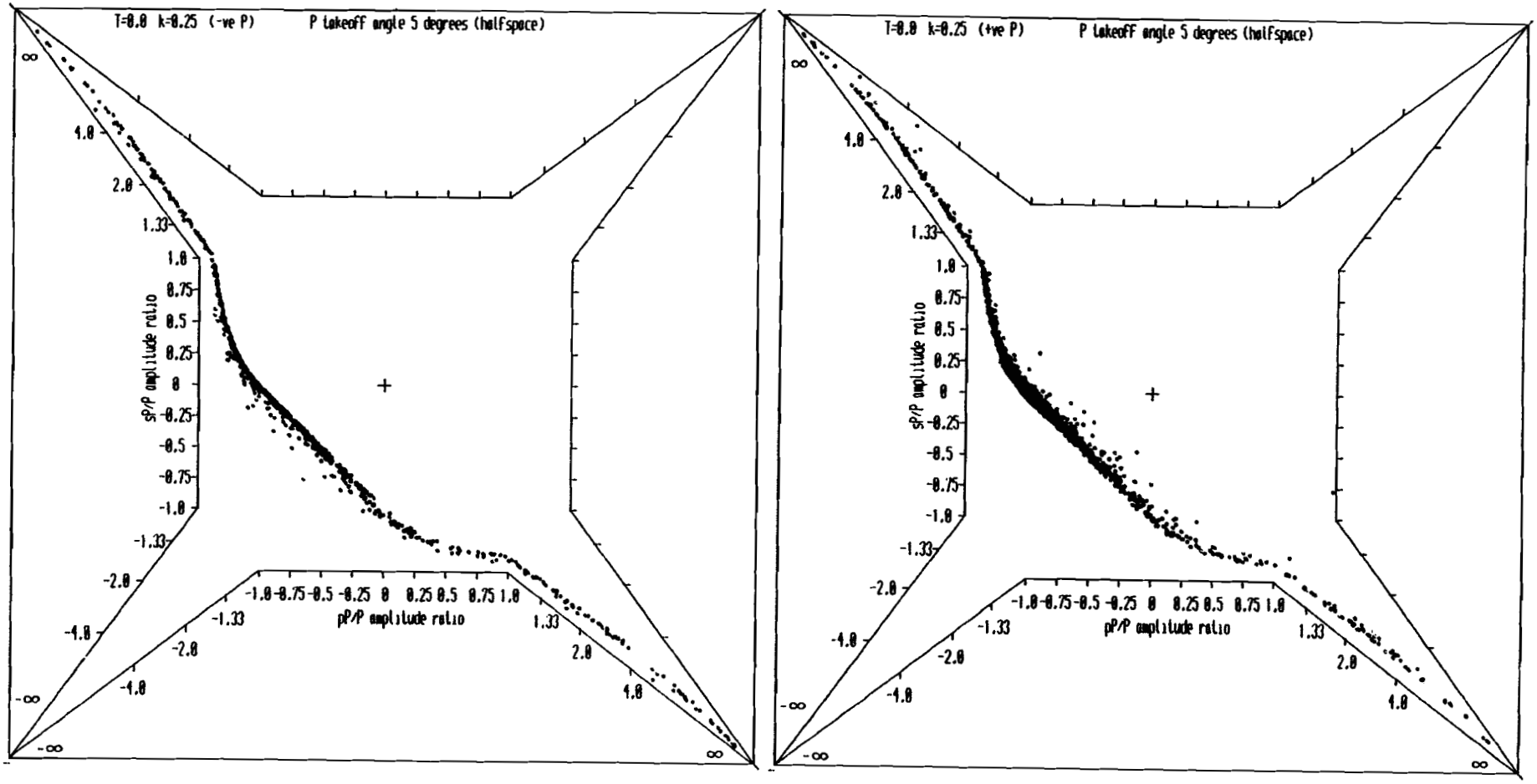
T=0.0 k=0.25 (-ve P)
P takeoff angle 5 degrees (halfspace)
sP/P amplitude ratio
pP/P amplitude ratio
T=0.0 k=0.25 (+ve P)
P takeoff angle 5 degrees (halfspace)
sP/P amplitude ratio
pP/P amplitude ratio

Figure 43

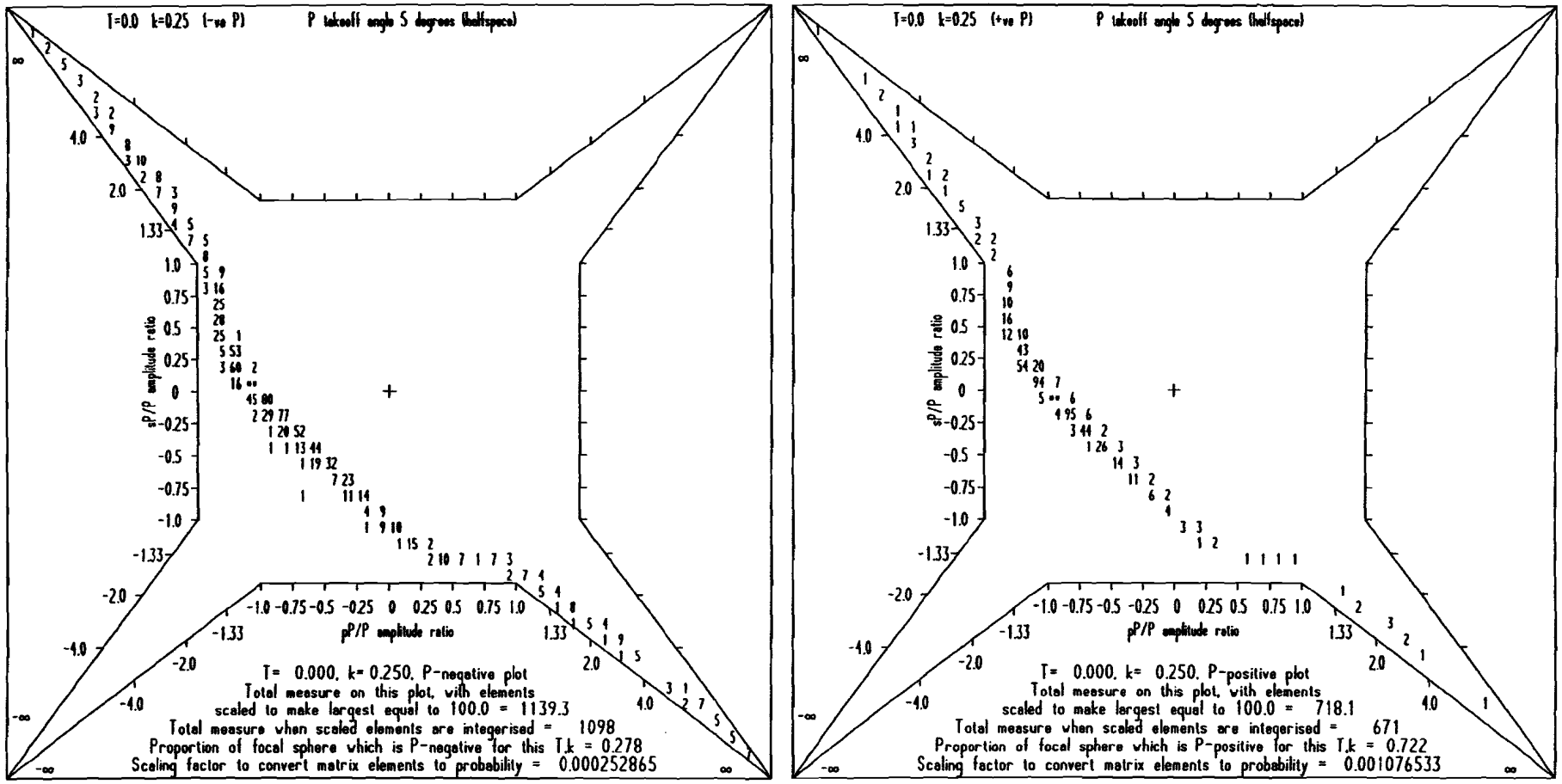

Figure 43 (continued)

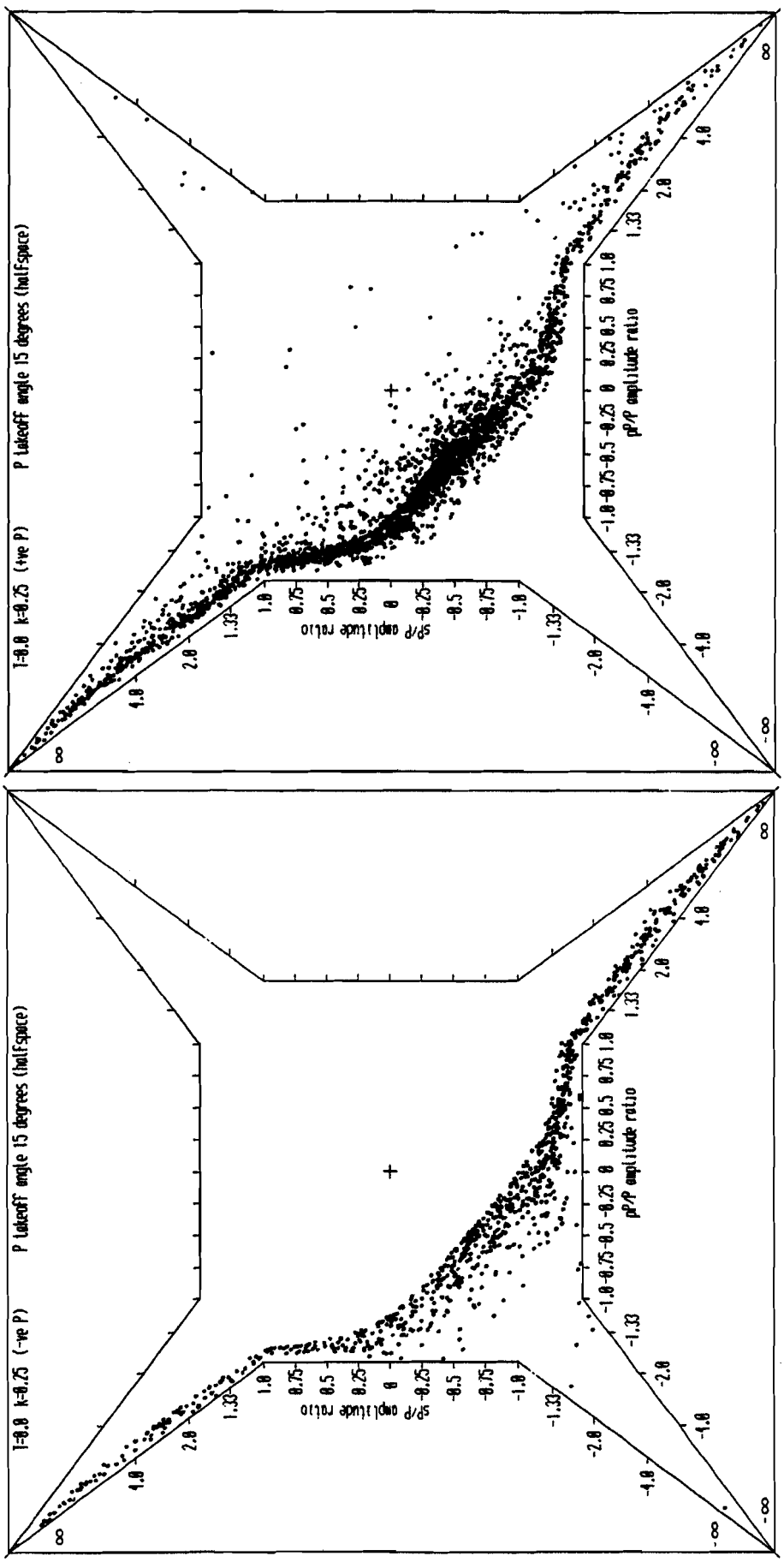
T=0.0 k=0.25 (-ve P)
P takeoff angle 15 degrees (halfspace)
T=0.0 k=0.25 (+ve P)
P takeoff angle 15 degrees (halfspace)
sP/P amplitude ratio
pP/P amplitude ratio
8
4.0
2.0
1.33
1.0
0.75
0.5
0.25
0
-0.25
-0.5
-0.75
-1.0
-1.33
-2.0
-4.0
-8

Figure 44

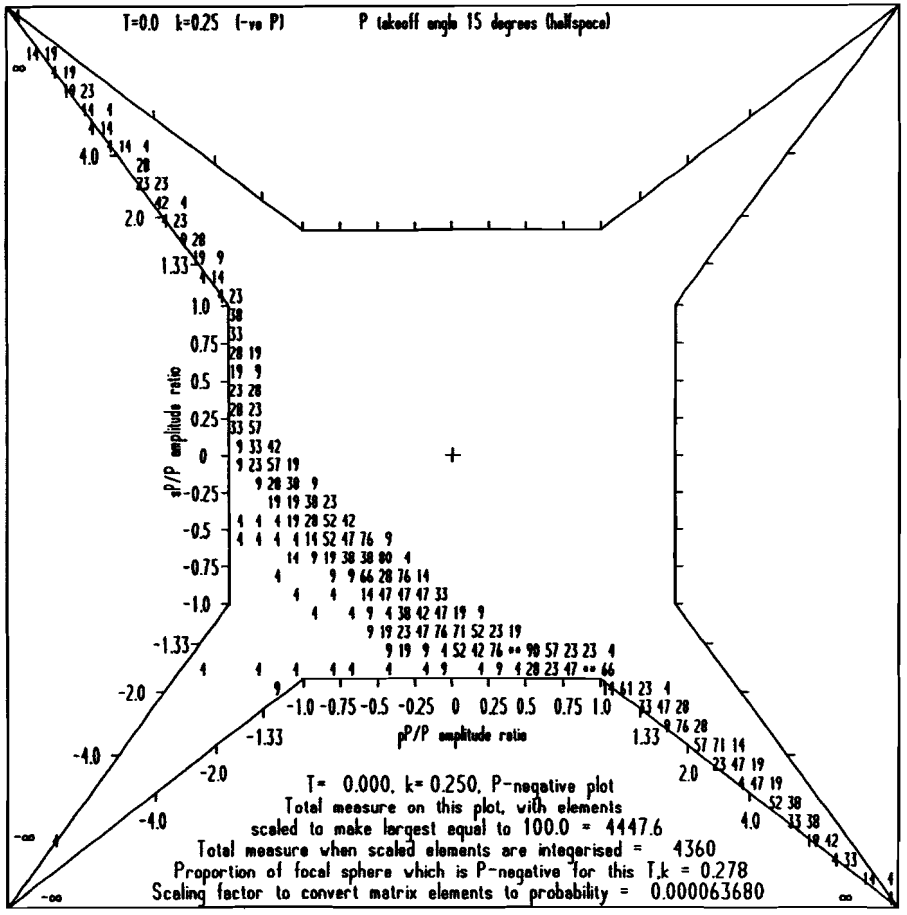

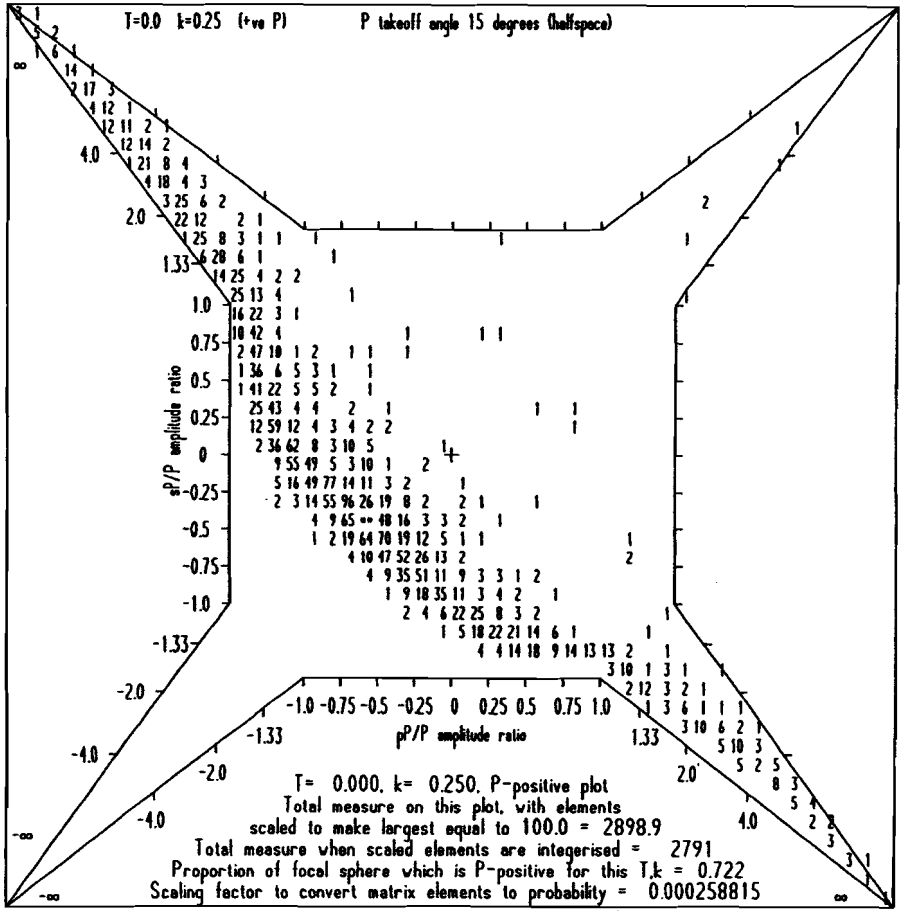

Figure 44 (continued)

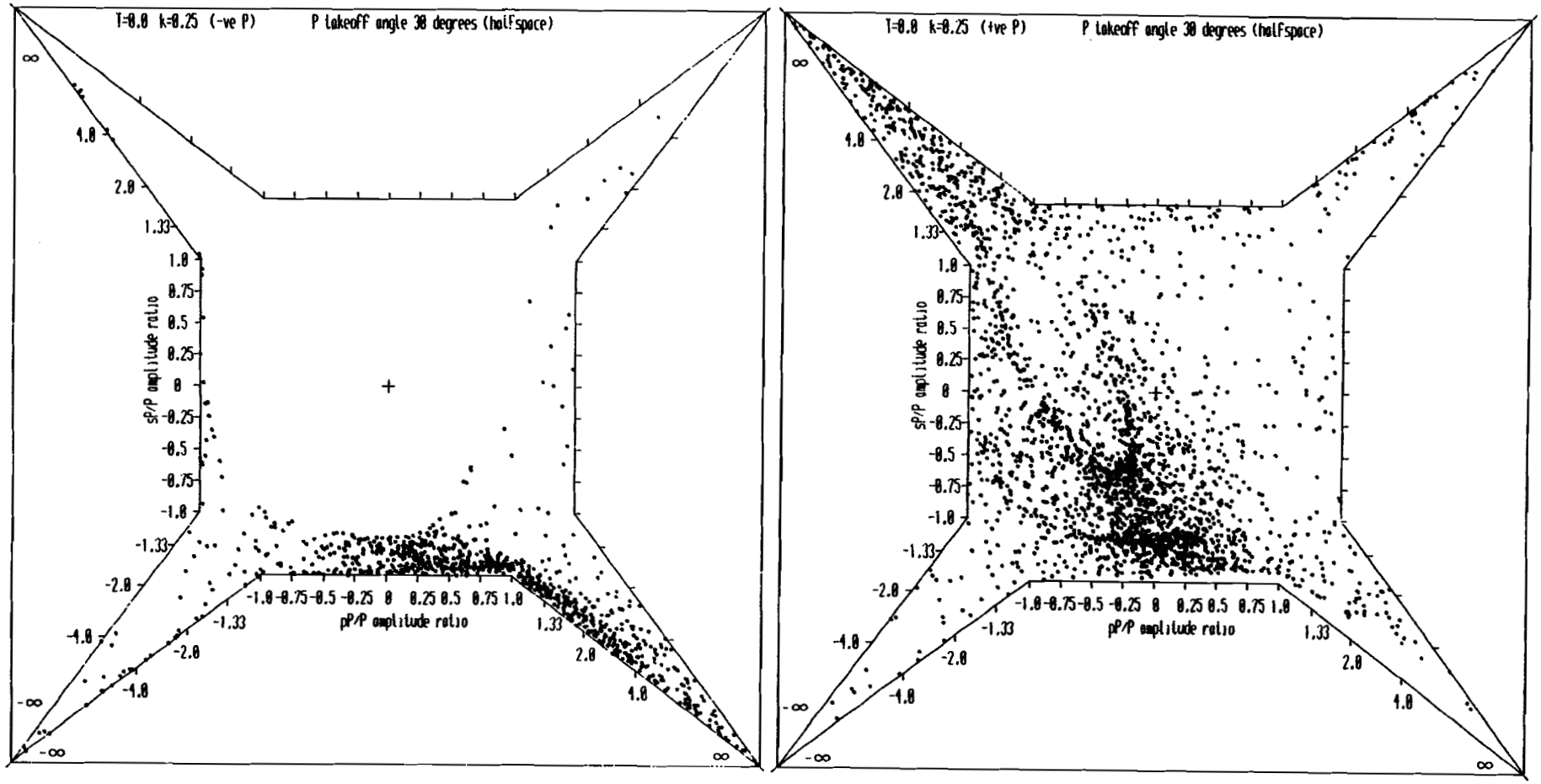
T=0.0 k=0.25 (-ve P)
P takeoff angle 30 degrees (halfspace)
sP/P amplitude ratio
pP/P amplitude ratio
T=0.0 k=0.25 (+ve P)
P takeoff angle 30 degrees (halfspace)
sP/P amplitude ratio
pP/P amplitude ratio

Figure 45

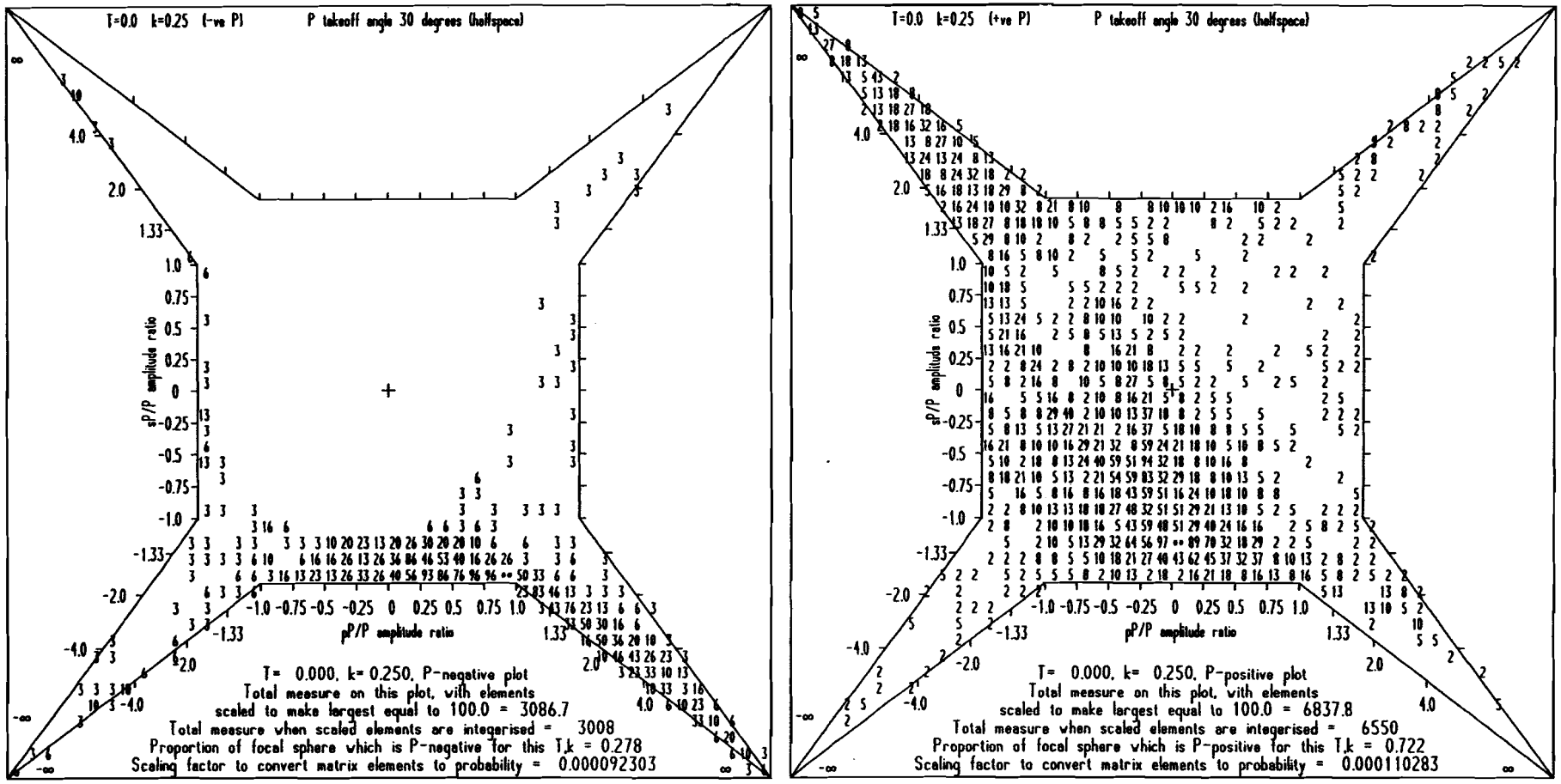

Figure 45 (continued)

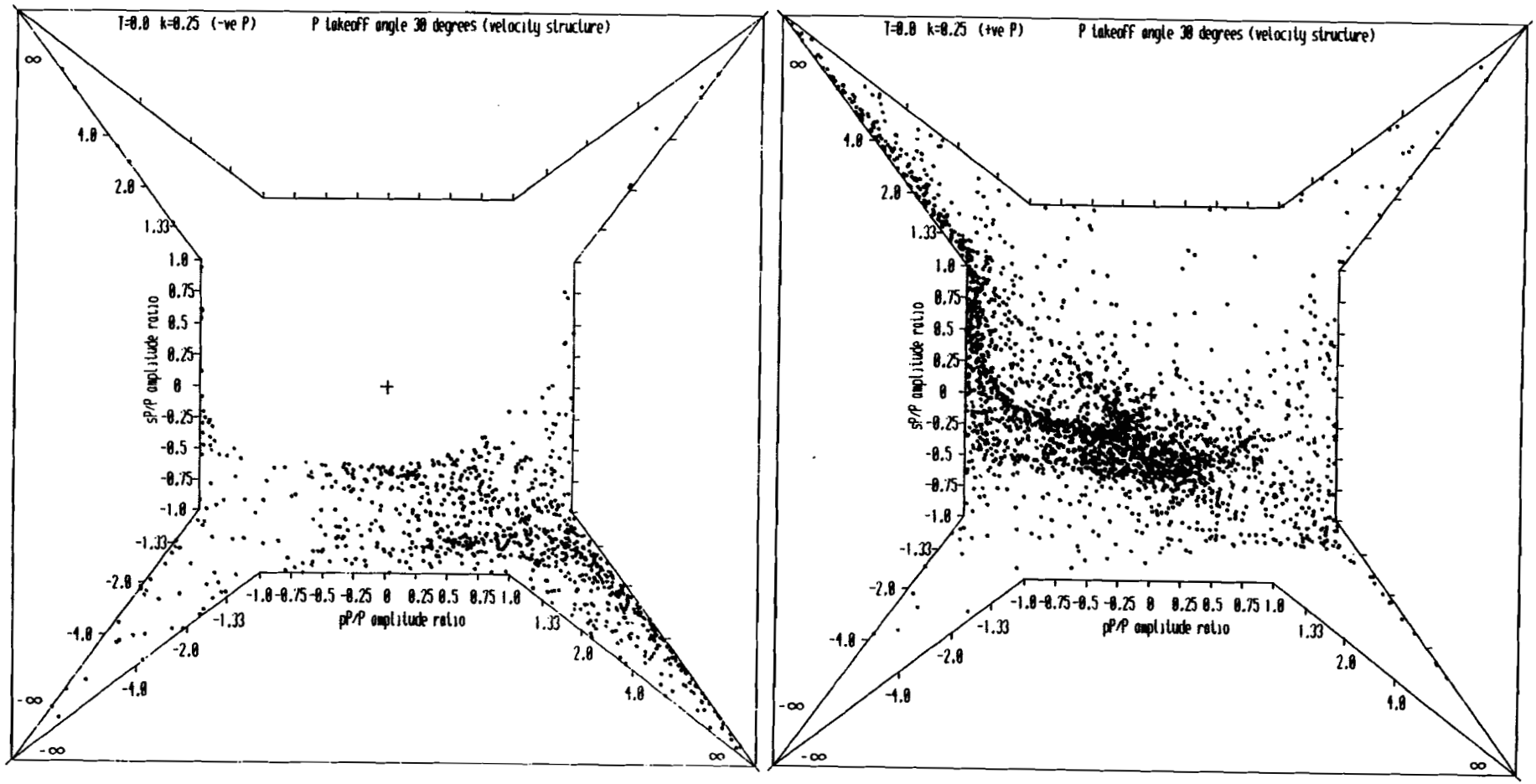
T=0.0 k=0.25 (-ve P)
P takeoff angle 30 degrees (velocity structure)
sP/P amplitude ratio
pP/P amplitude ratio
T=0.0 k=0.25 (+ve P)
P takeoff angle 30 degrees (velocity structure)
sP/P amplitude ratio
pP/P amplitude ratio

Figure 46

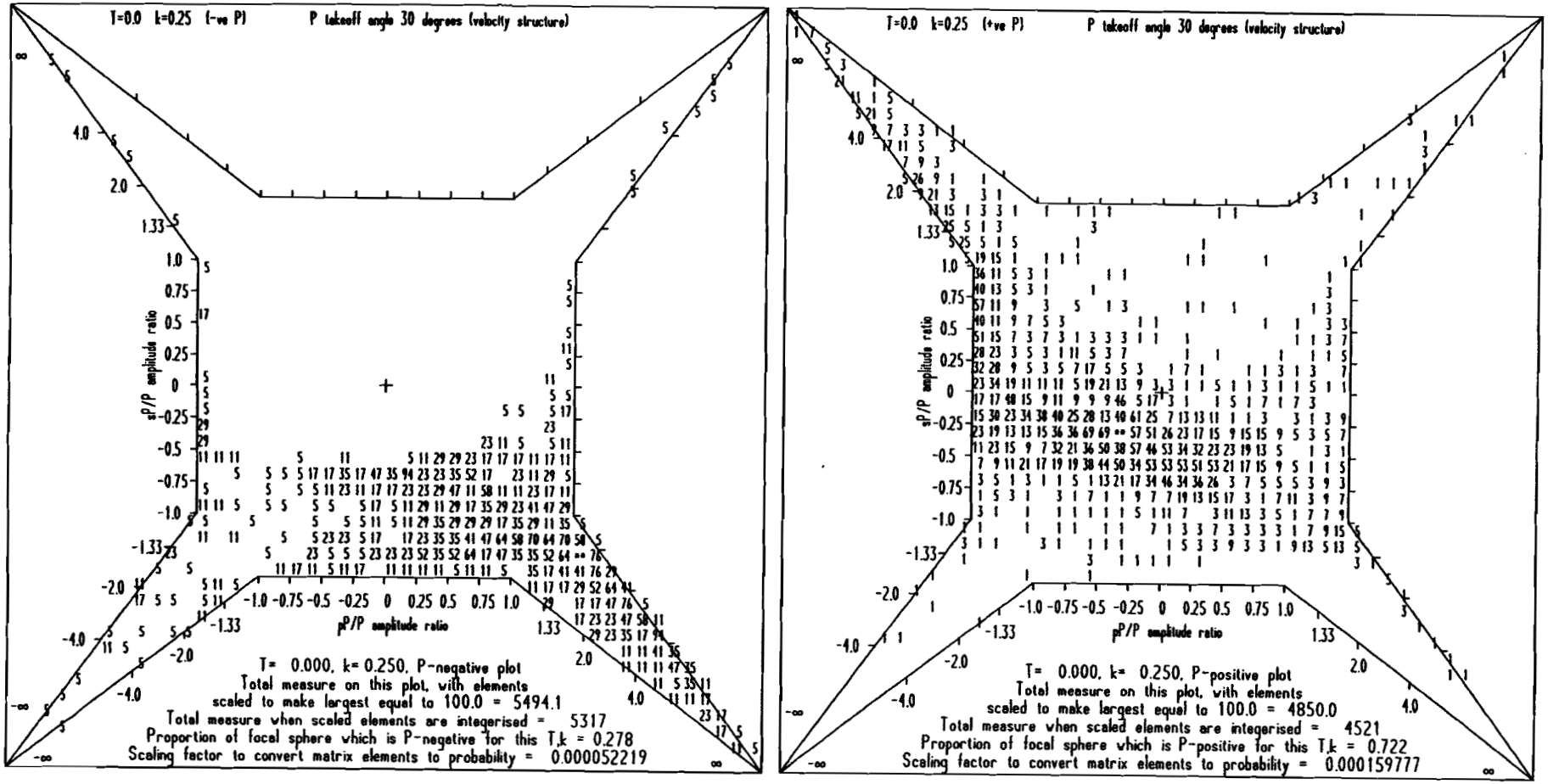

Figure 46 (continued)

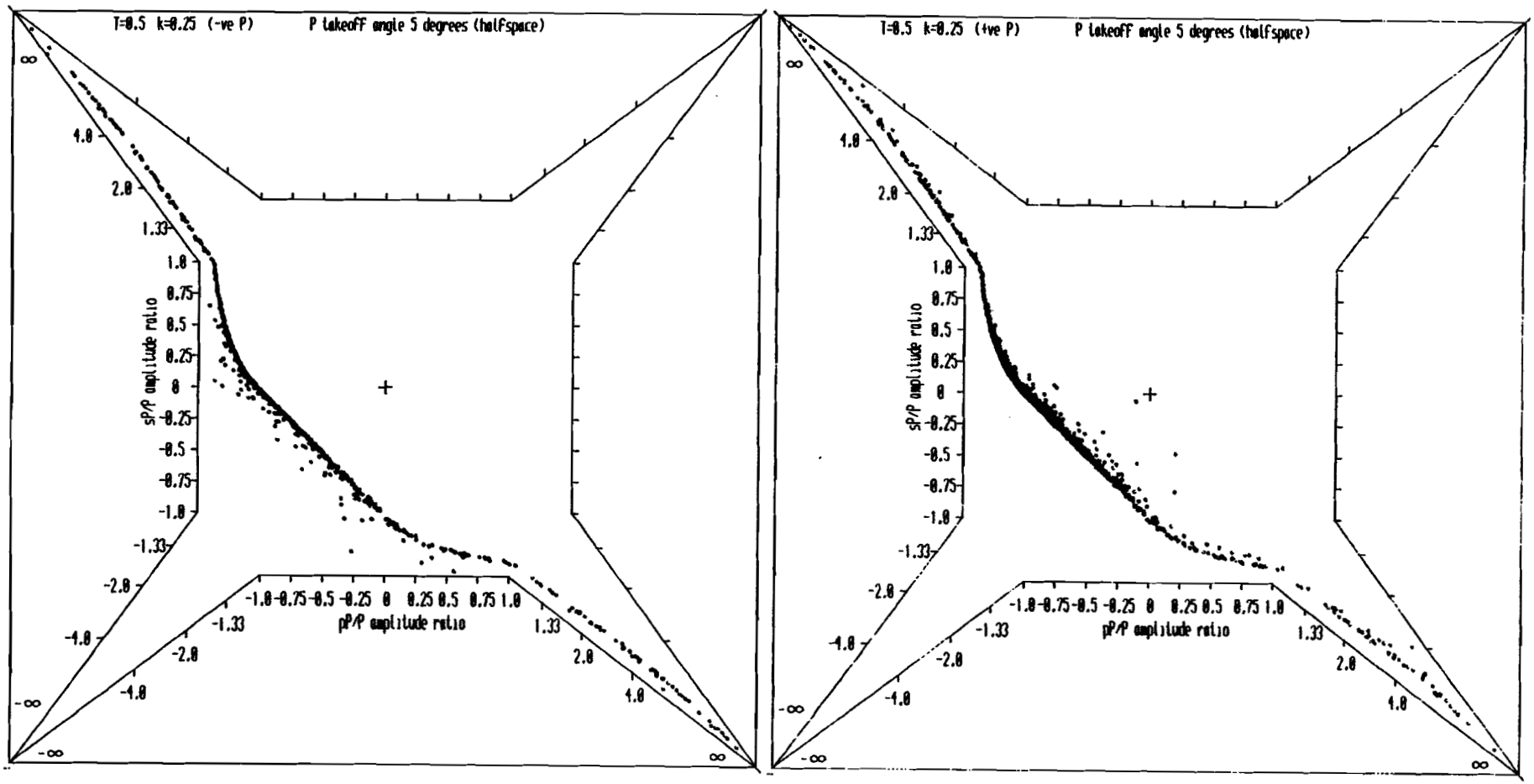
T=0.5 k=0.25 (-ve P)
P takeoff angle 5 degrees (halfspace)
sP/P amplitude ratio
pP/P amplitude ratio
T=0.5 k=0.25 (+ve P)
P takeoff angle 5 degrees (halfspace)
sP/P amplitude ratio
pP/P amplitude ratio

Figure 47

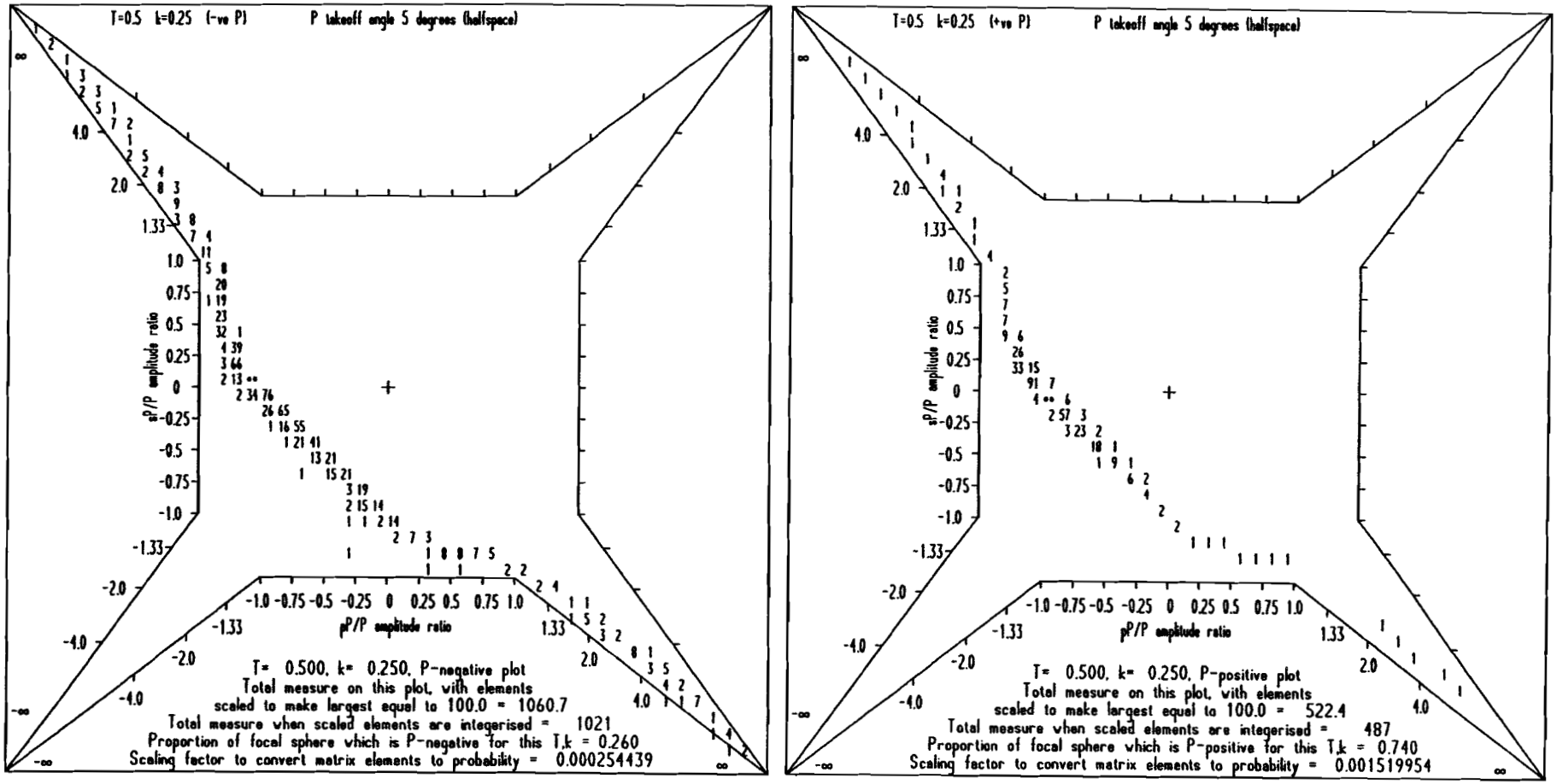

Figure 47 (continued)

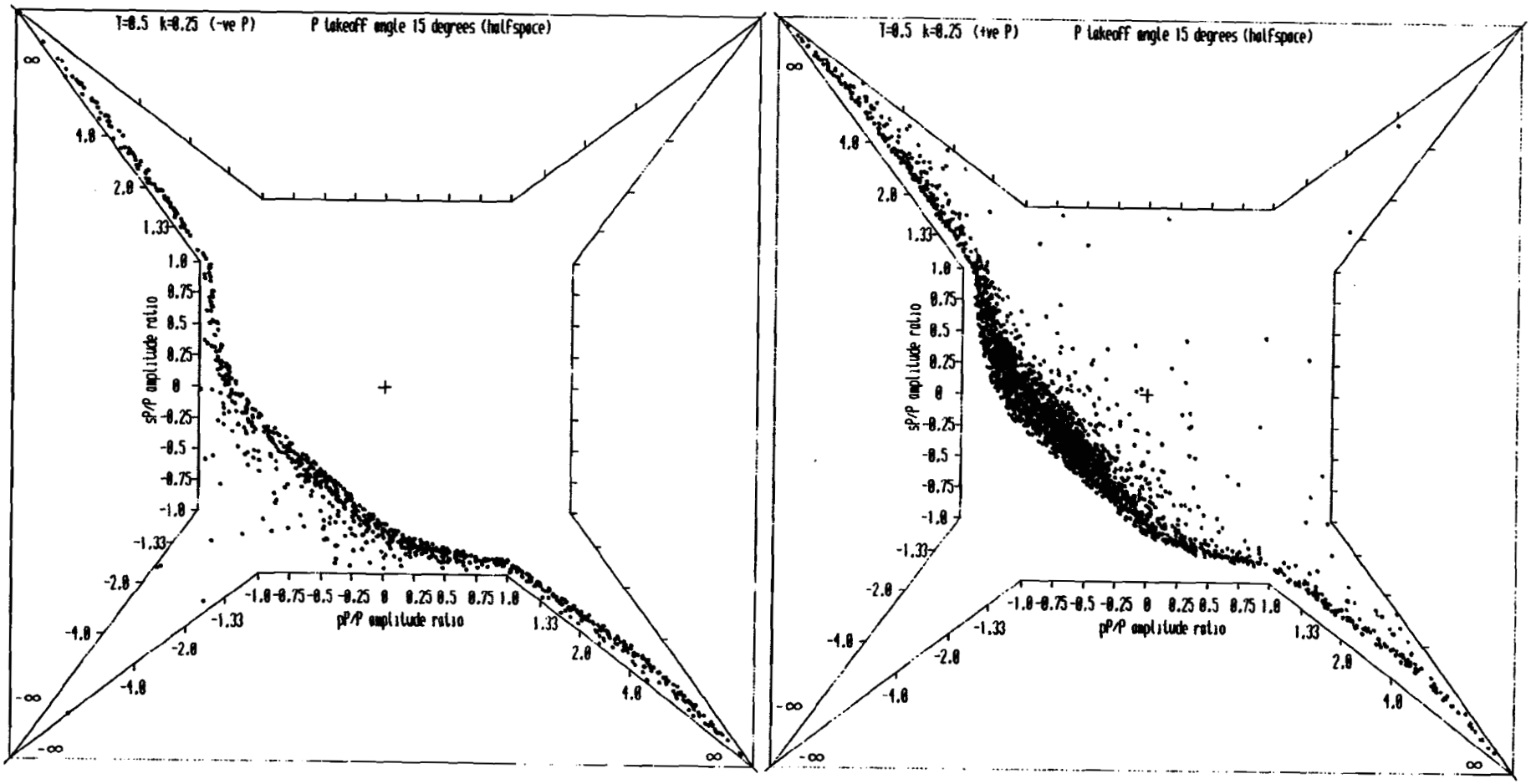
T=0.5 k=0.25 (-ve P)
P takeoff angle 15 degrees (halfspace)
sP/P amplitude ratio
pP/P amplitude ratio
T=0.5 k=0.25 (+ve P)
P takeoff angle 15 degrees (halfspace)
sP/P amplitude ratio
pP/P amplitude ratio

Figure 48

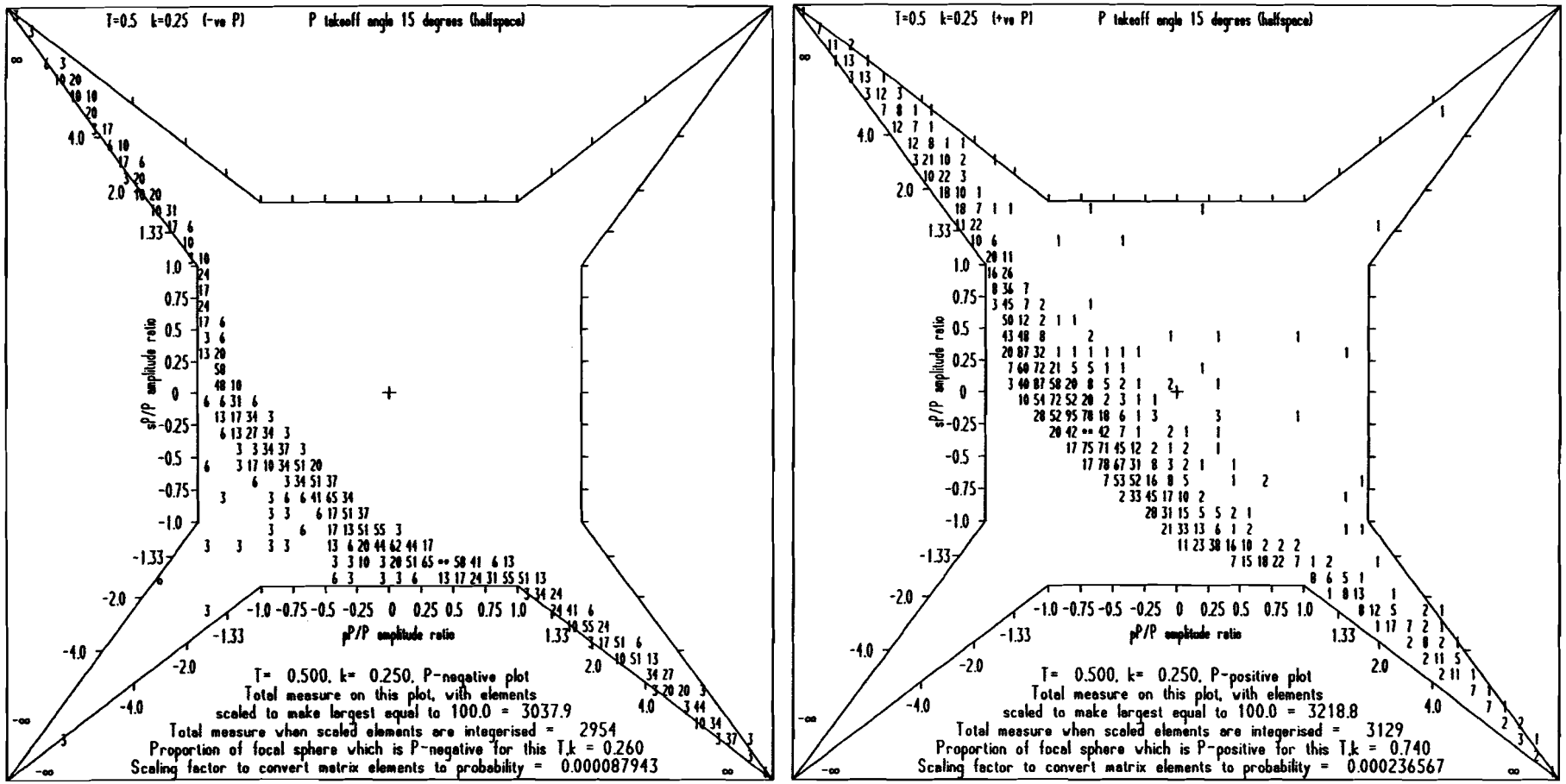

Figure 48 (continued)

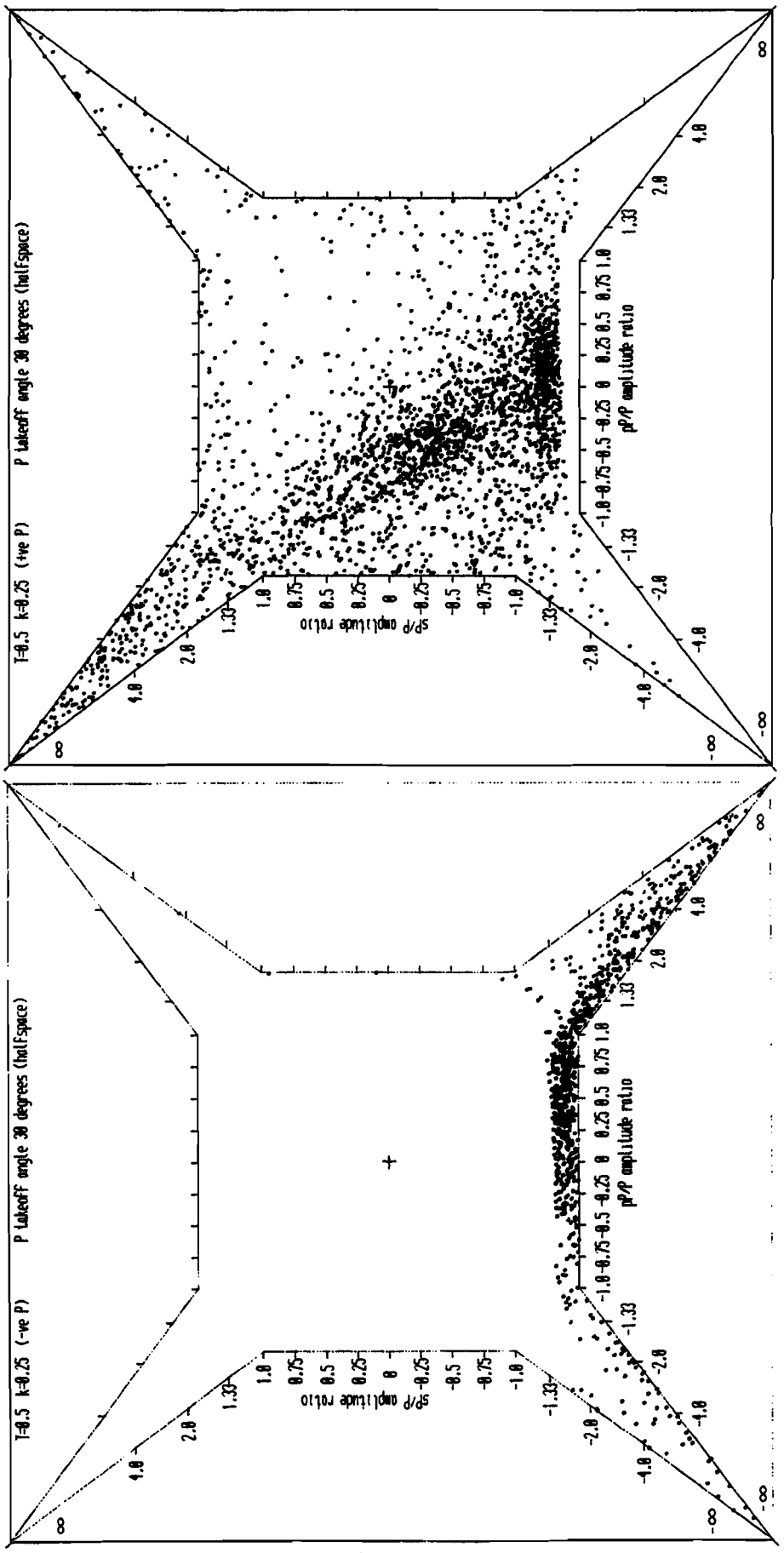
T=0.5 k=0.25 (+ve P)
P takeoff angle 30 degrees (halfspace)
T=0.5 k=0.25 (-ve P)
P takeoff angle 30 degrees (halfspace)
SP/P amplitude ratio
pP/P amplitude ratio

Figure 49

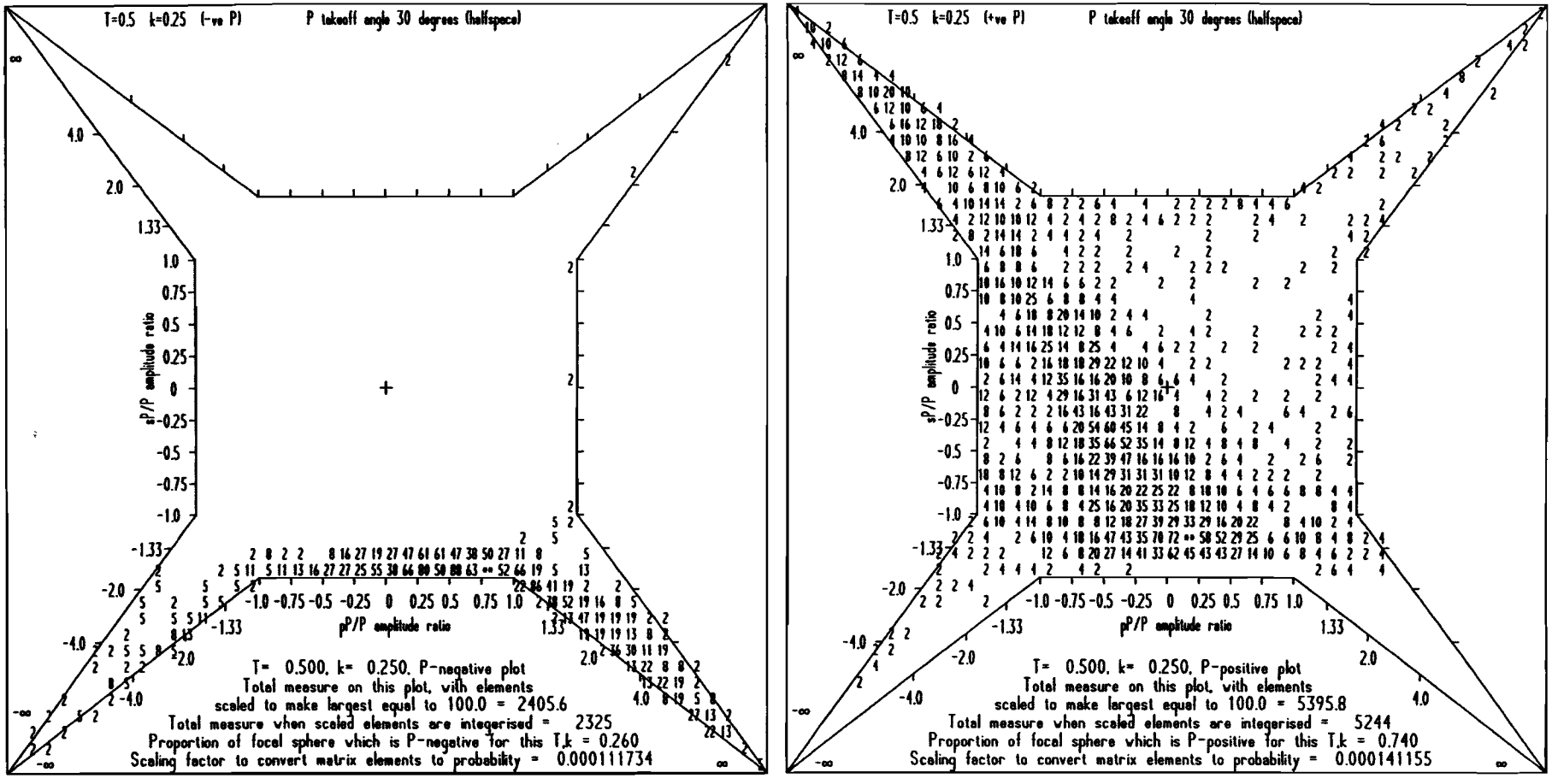

Figure 49 (continued)

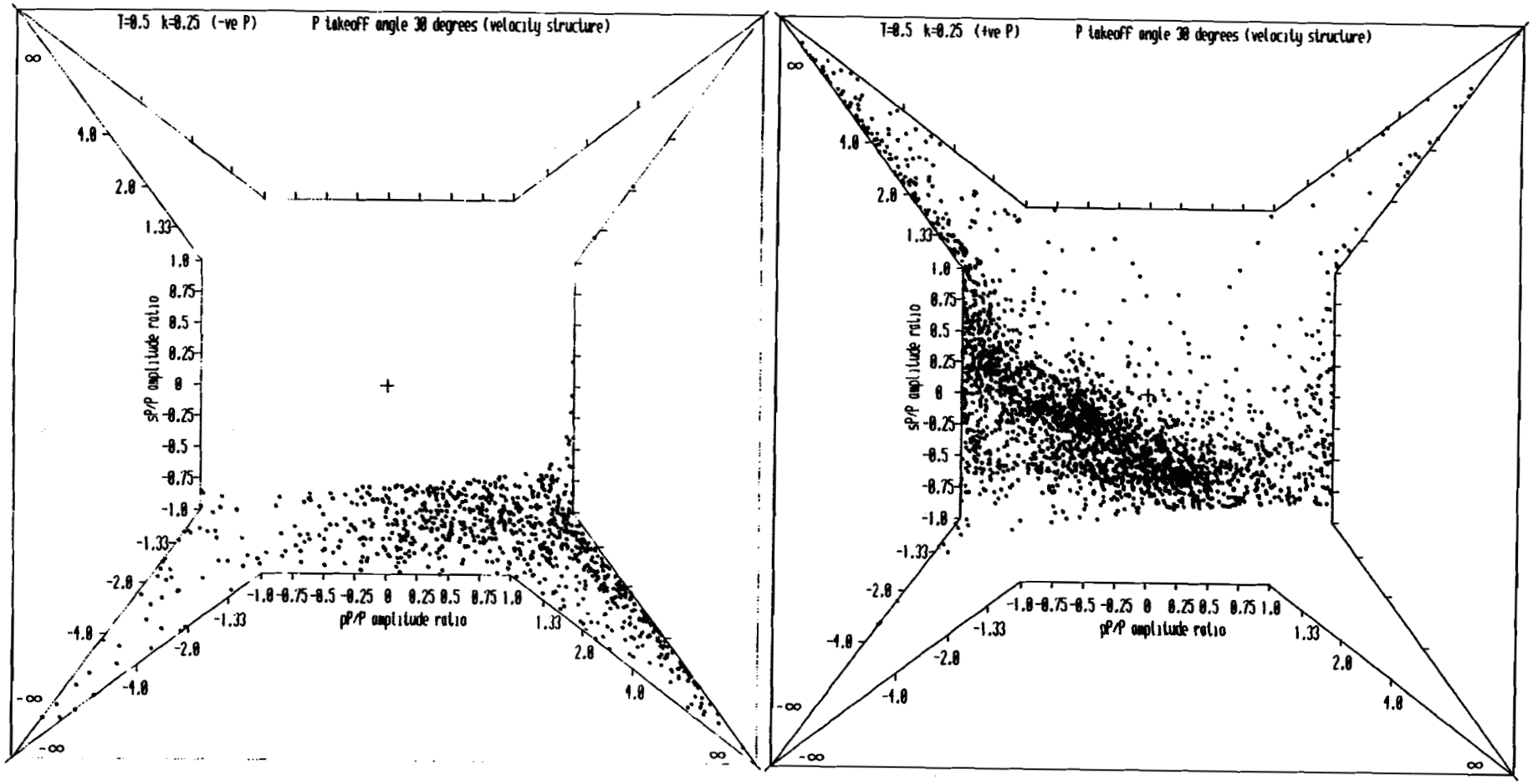
T=0.5 k=0.25 (-ve P)
P takeoff angle 30 degrees (velocity structure)
sP/P amplitude ratio
pP/P amplitude ratio
T=0.5 k=0.25 (+ve P)
P takeoff angle 30 degrees (velocity structure)
sP/P amplitude ratio
pP/P amplitude ratio

Figure 50

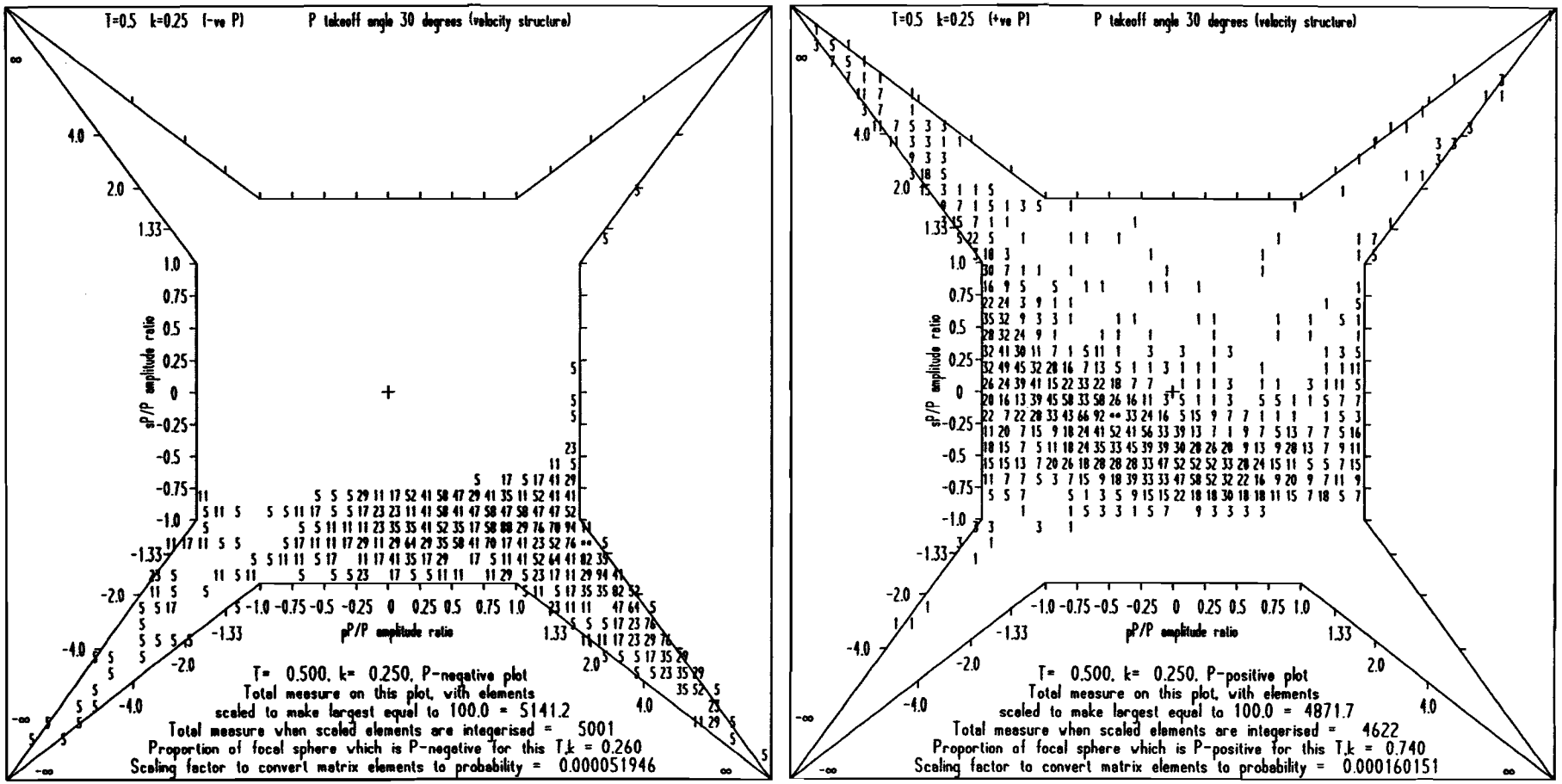

Figure 50 (continued)

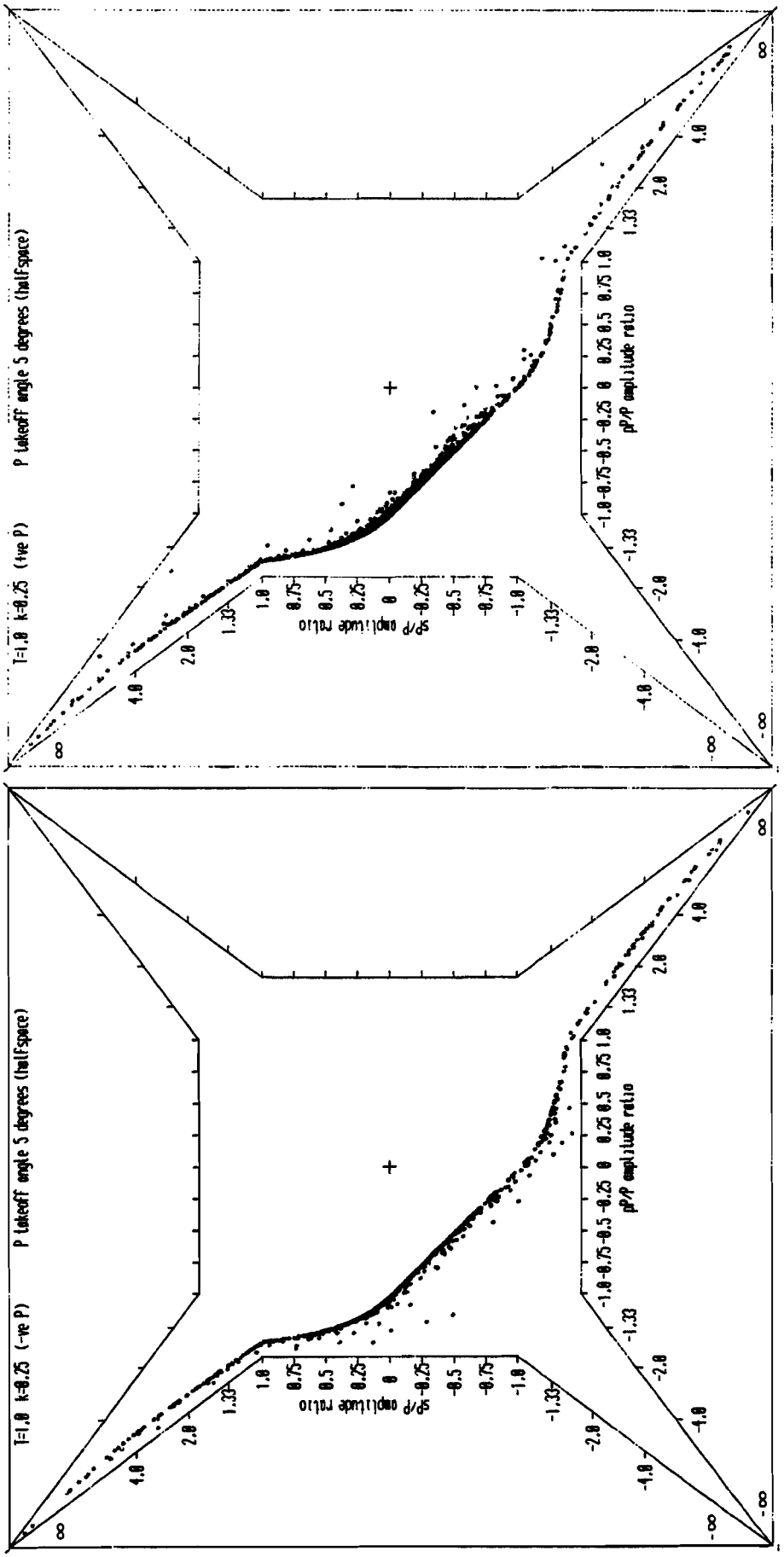
T=1.0 k=0.25 (+ve P)
P takeoff angle 5 degrees (halfspace)
sP/P amplitude ratio
pP/P amplitude ratio
T=1.0 k=0.25 (-ve P)
P takeoff angle 5 degrees (halfspace)
sP/P amplitude ratio
pP/P amplitude ratio

Figure 51

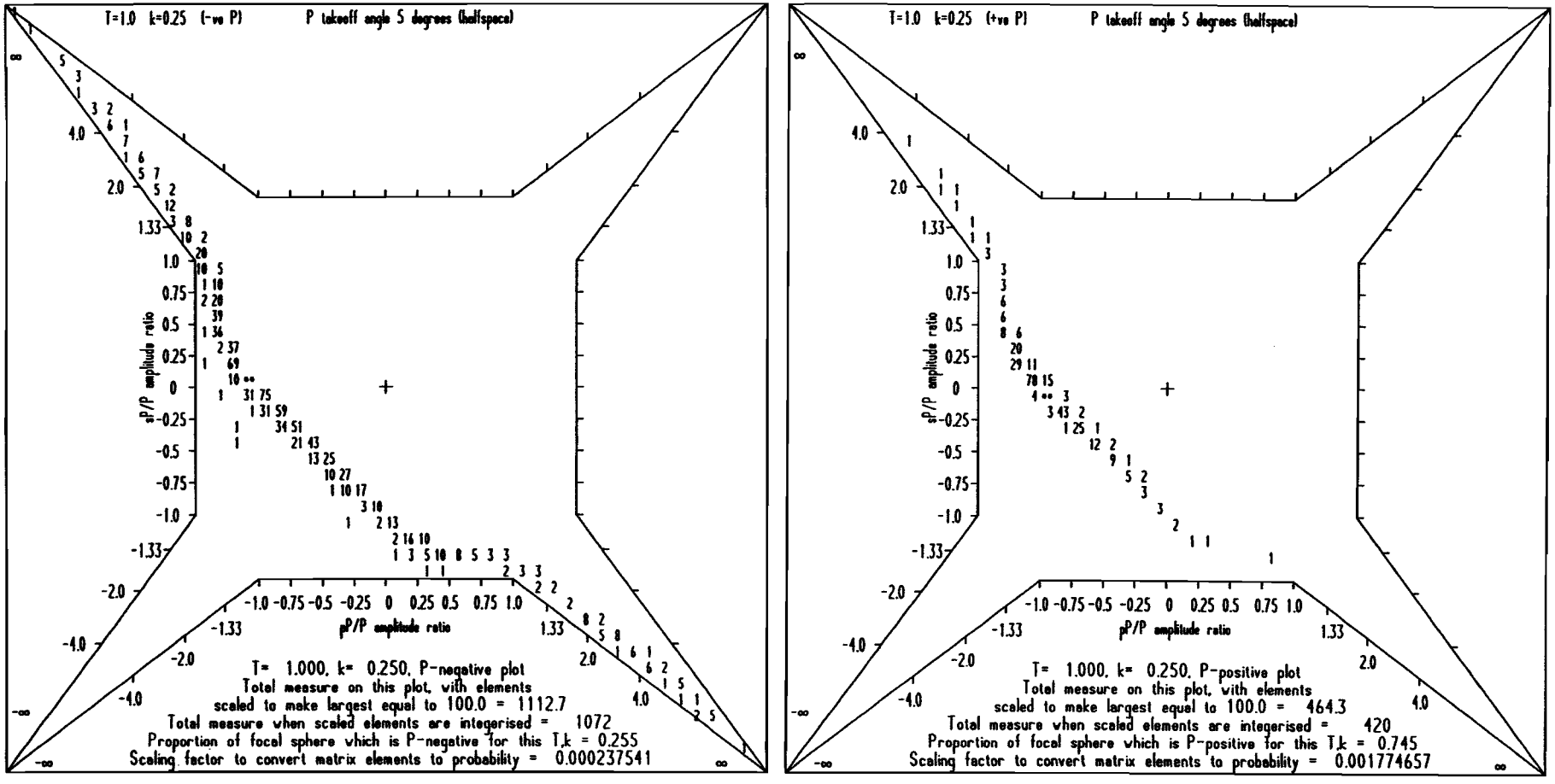

Figure 51 (continued)

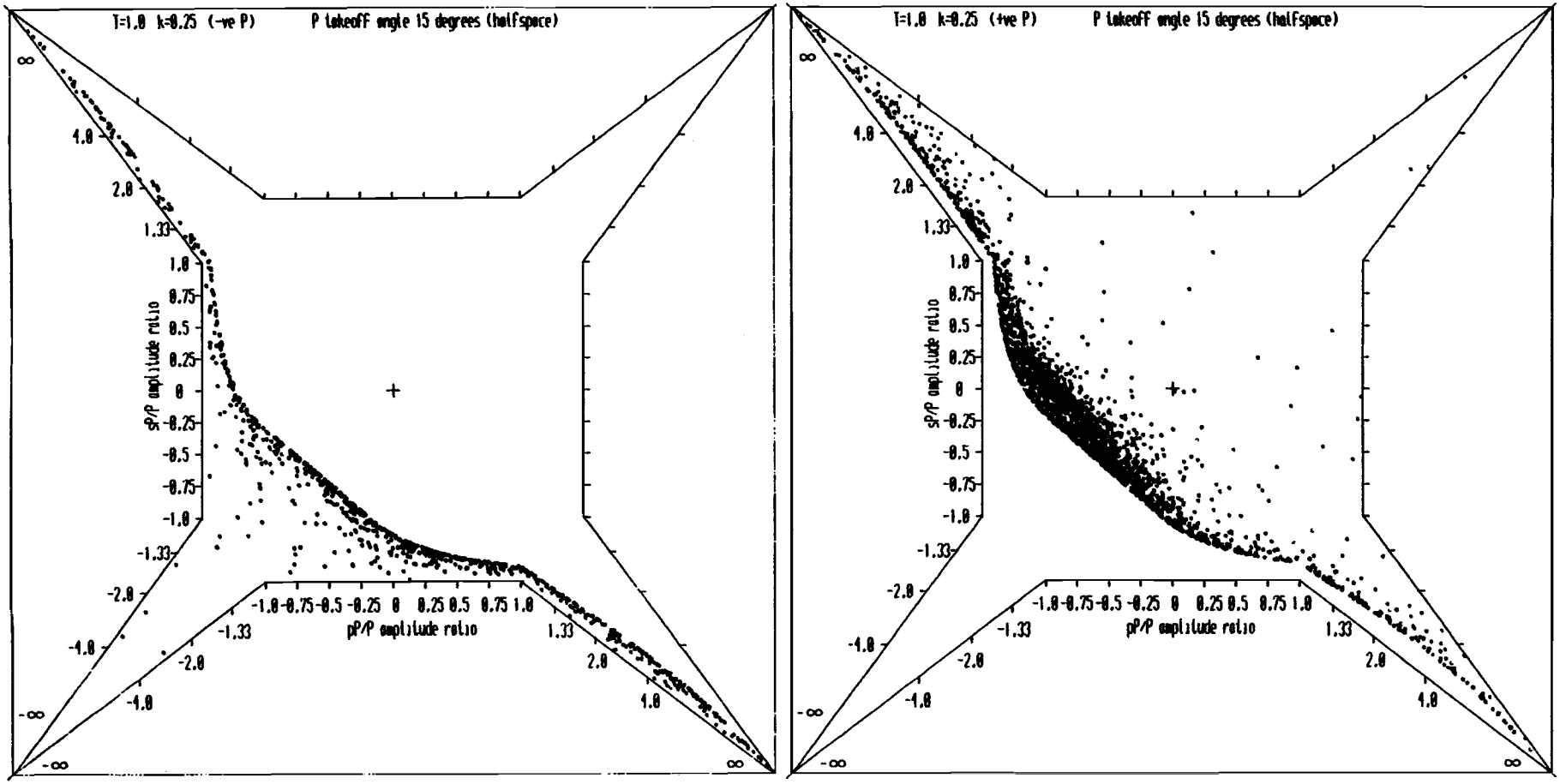
T=1.0 k=0.25 (-ve P)
P takeoff angle 15 degrees (halfspace)
sP/P amplitude ratio
pP/P amplitude ratio
T=1.0 k=0.25 (+ve P)
P takeoff angle 15 degrees (halfspace)
sP/P amplitude ratio
pP/P amplitude ratio

Figure 52

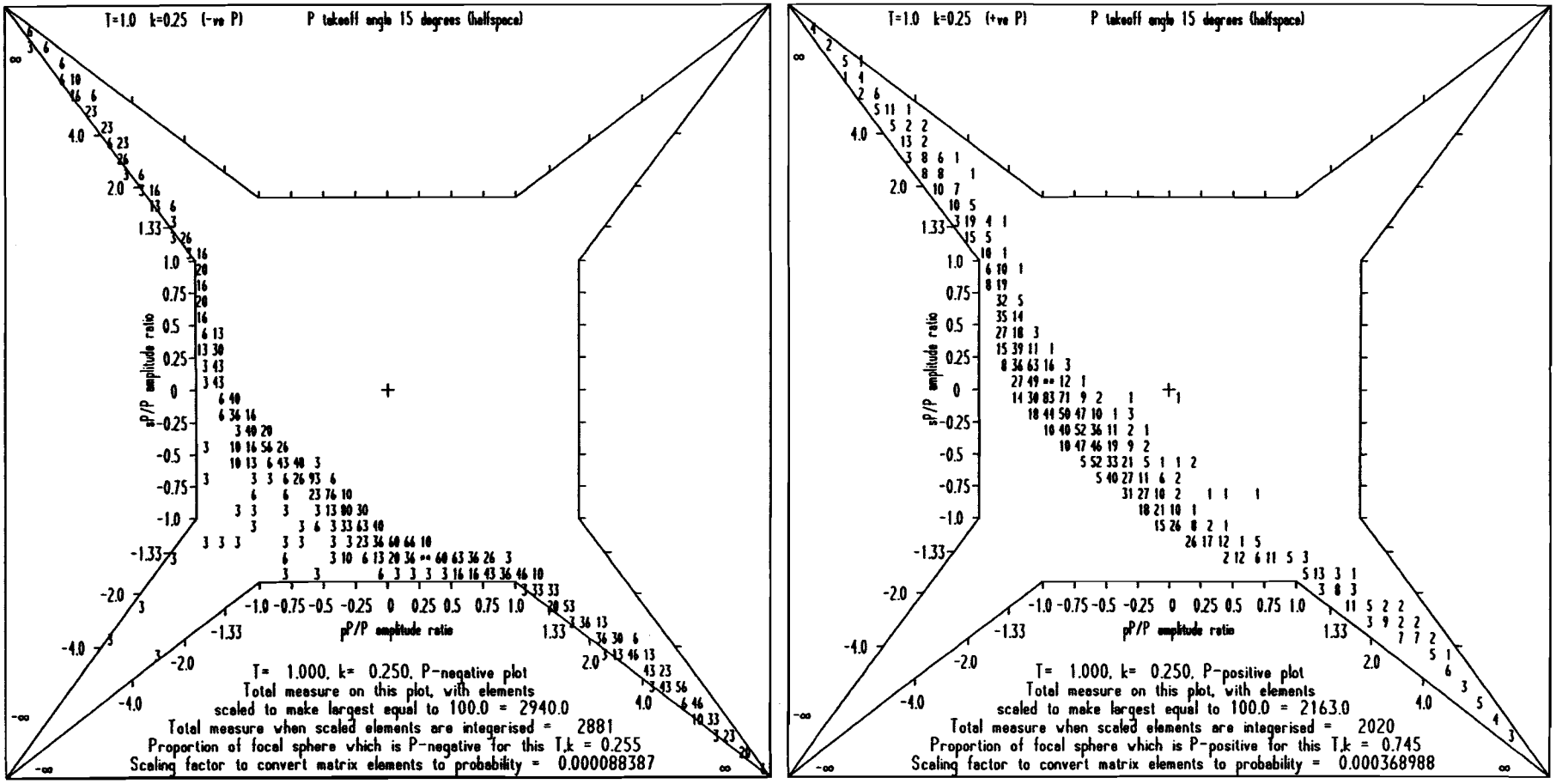

Figure 52 (continued)

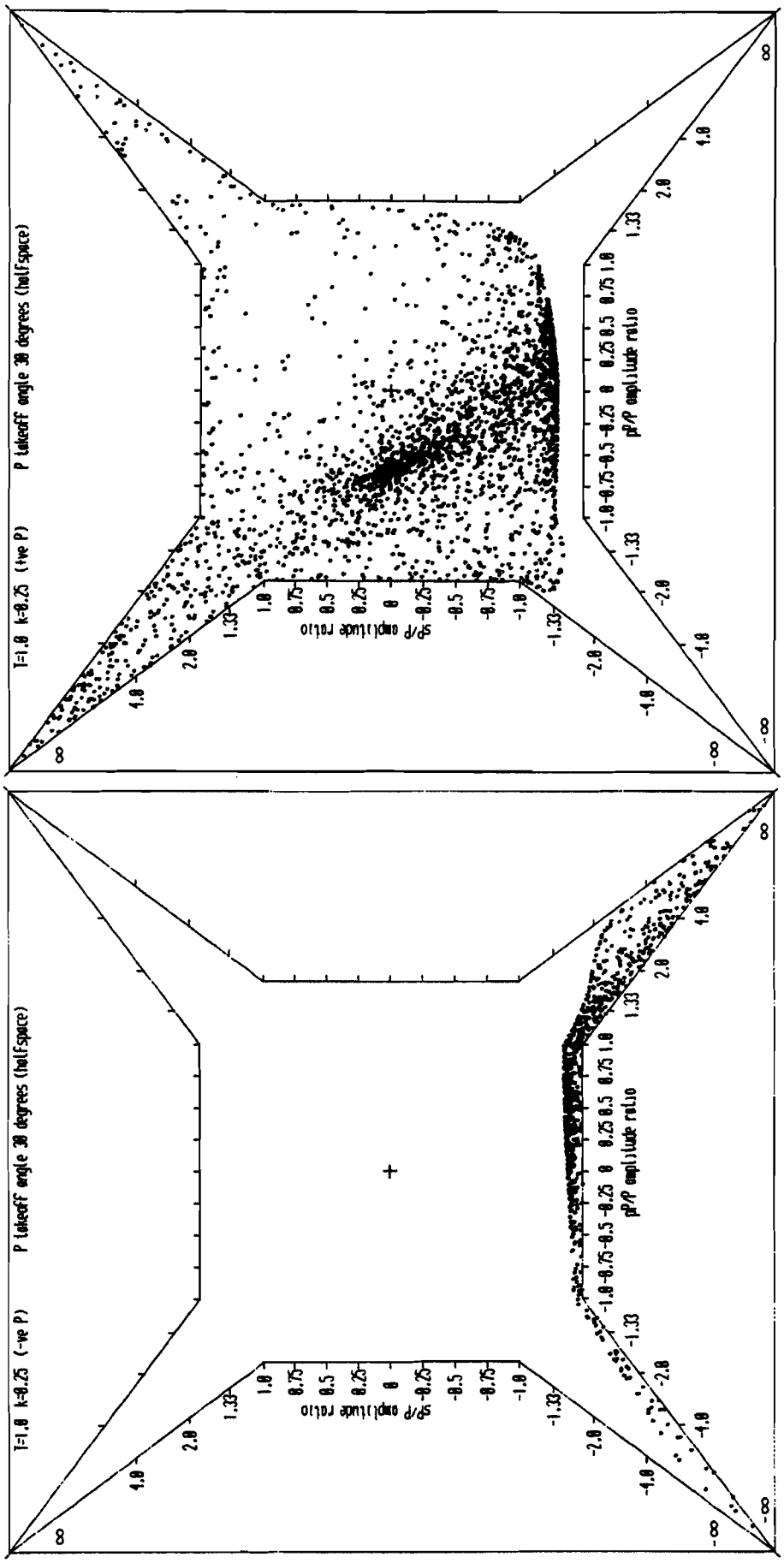
T=1.0 k=0.25 (+ve P)
P takeoff angle 30 degrees (halfspace)
SP/P amplitude ratio
P/P amplitude ratio
T=1.0 k=0.25 (-ve P)
P takeoff angle 30 degrees (halfspace)
SP/P amplitude ratio
P/P amplitude ratio

Figure 53

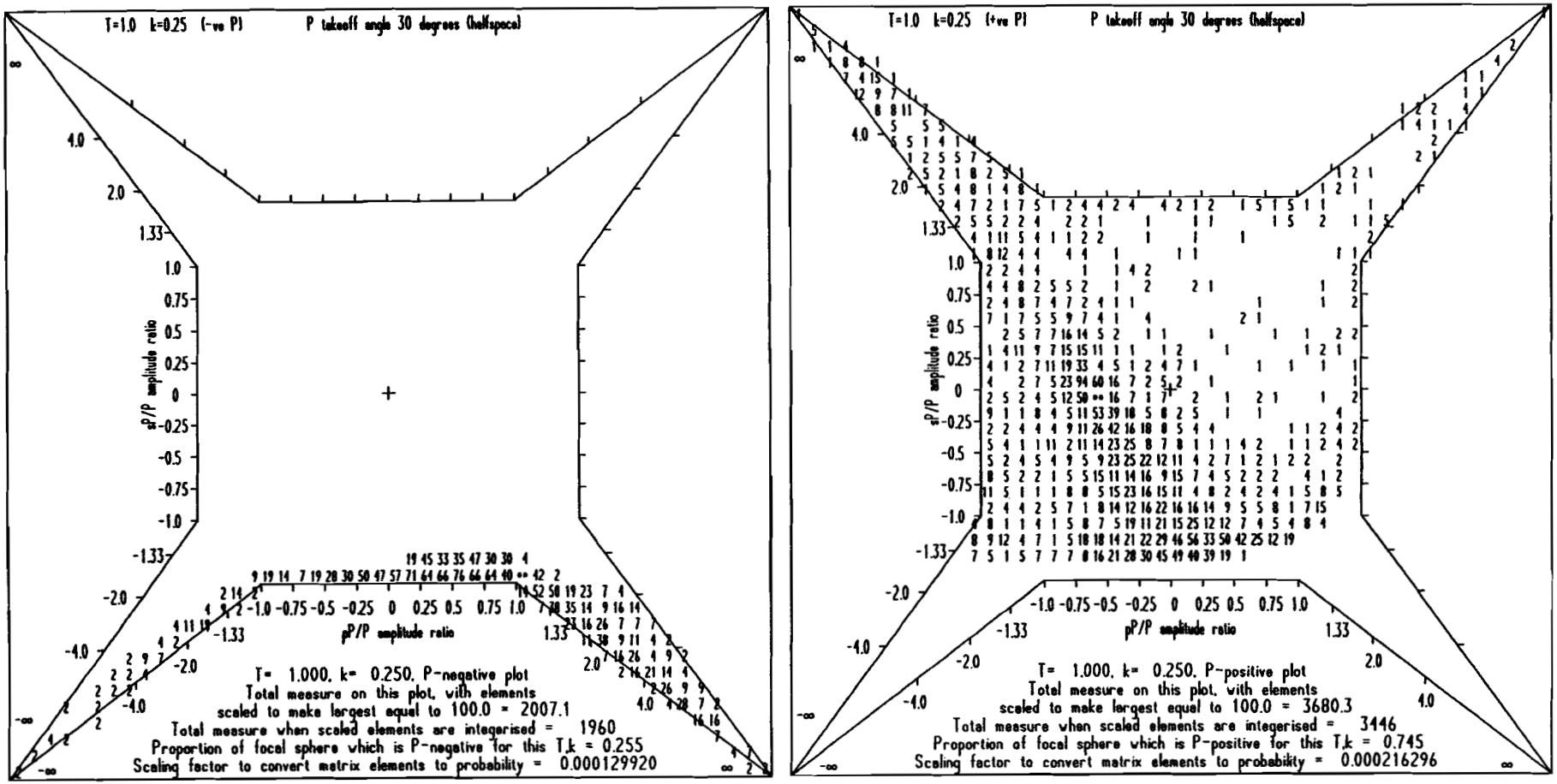

Figure 53 (continued)

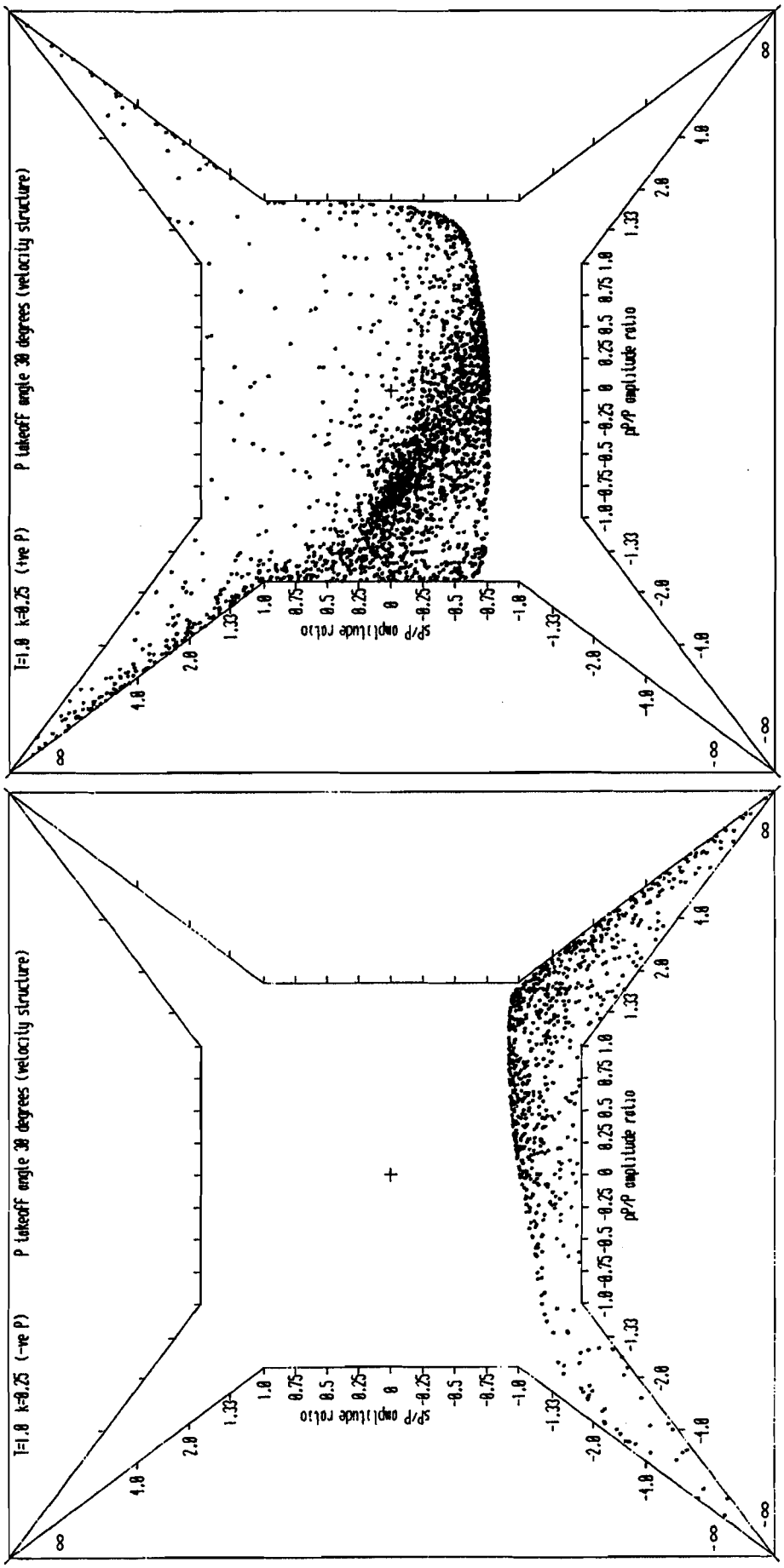
I=1.0 k=0.25 (+ve P)
P takeoff angle 30 degrees (velocity structure)
I=1.0 k=0.25 (-ve P)
P takeoff angle 30 degrees (velocity structure)
pP/P amplitude ratio
sP/P amplitude ratio

Figure 54

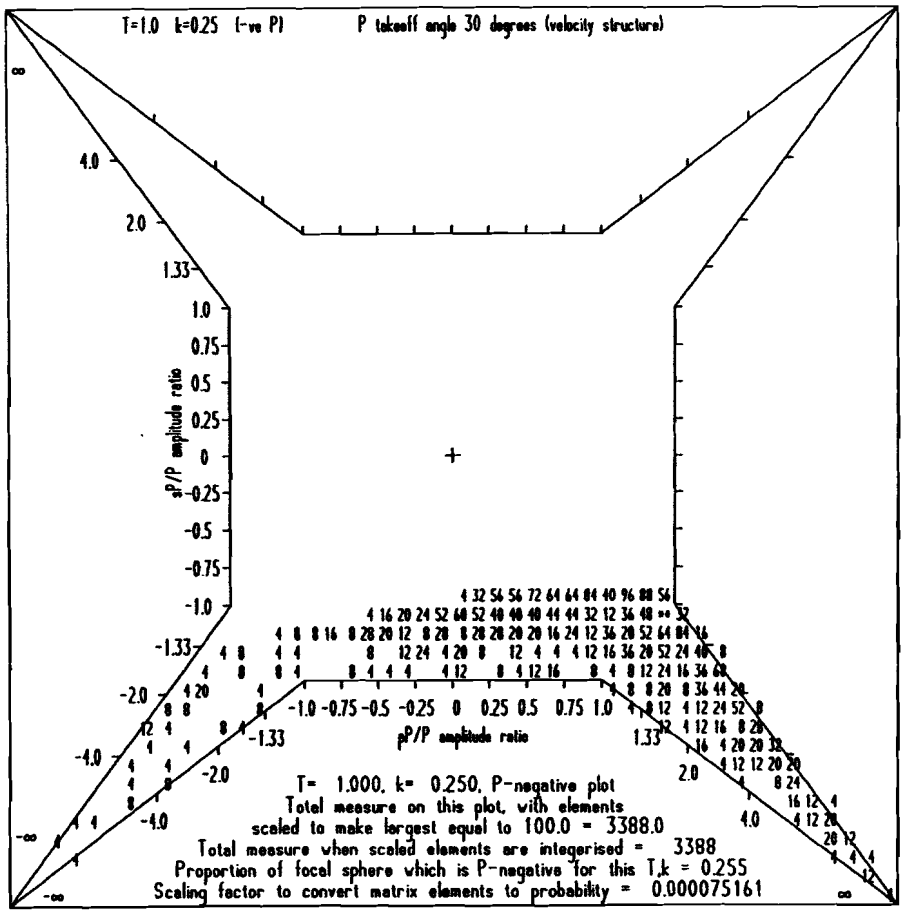

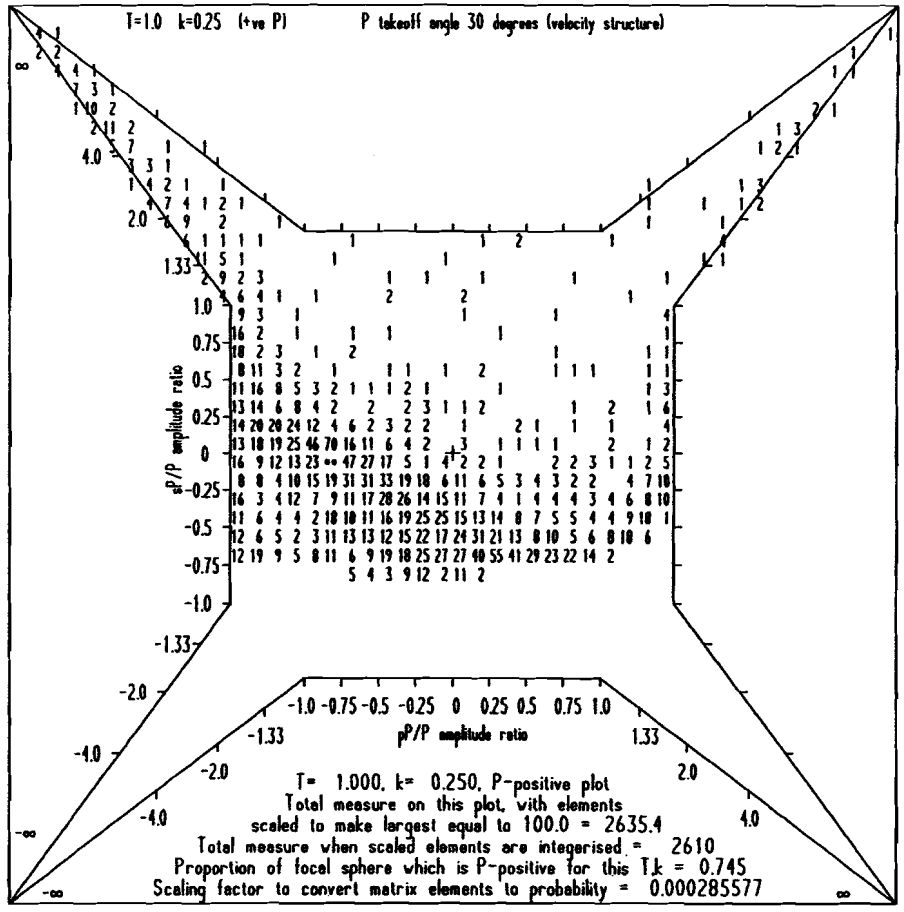

Figure 54 (continued)

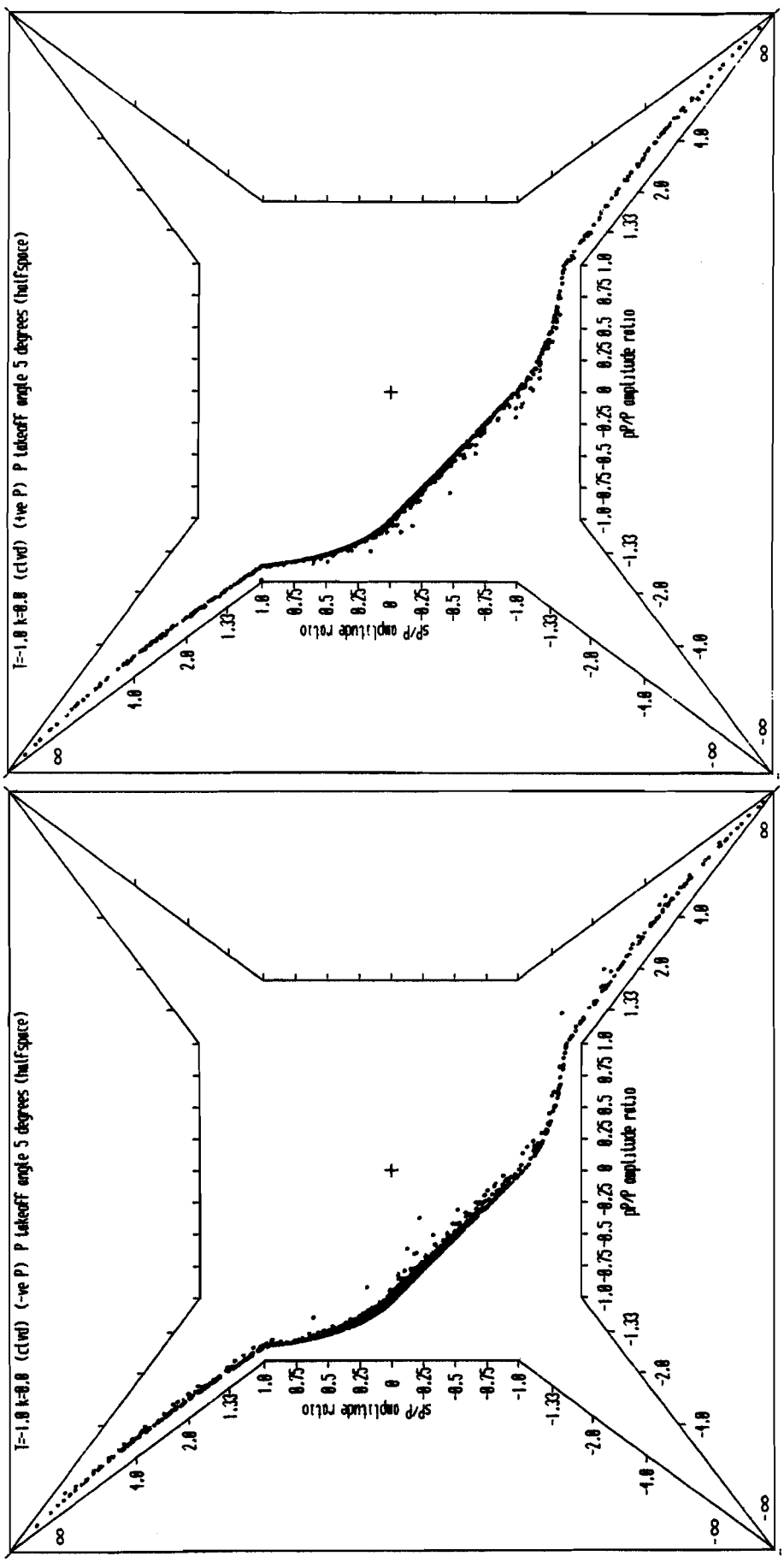
T=-1.0 k=0.0 (clvd) (+ve P) P takeoff angle 5 degrees (halfspace)
T=-1.0 k=0.0 (clvd) (-ve P) P takeoff angle 5 degrees (halfspace)
pP/P amplitude ratio
sP/P amplitude ratio

Figure 55

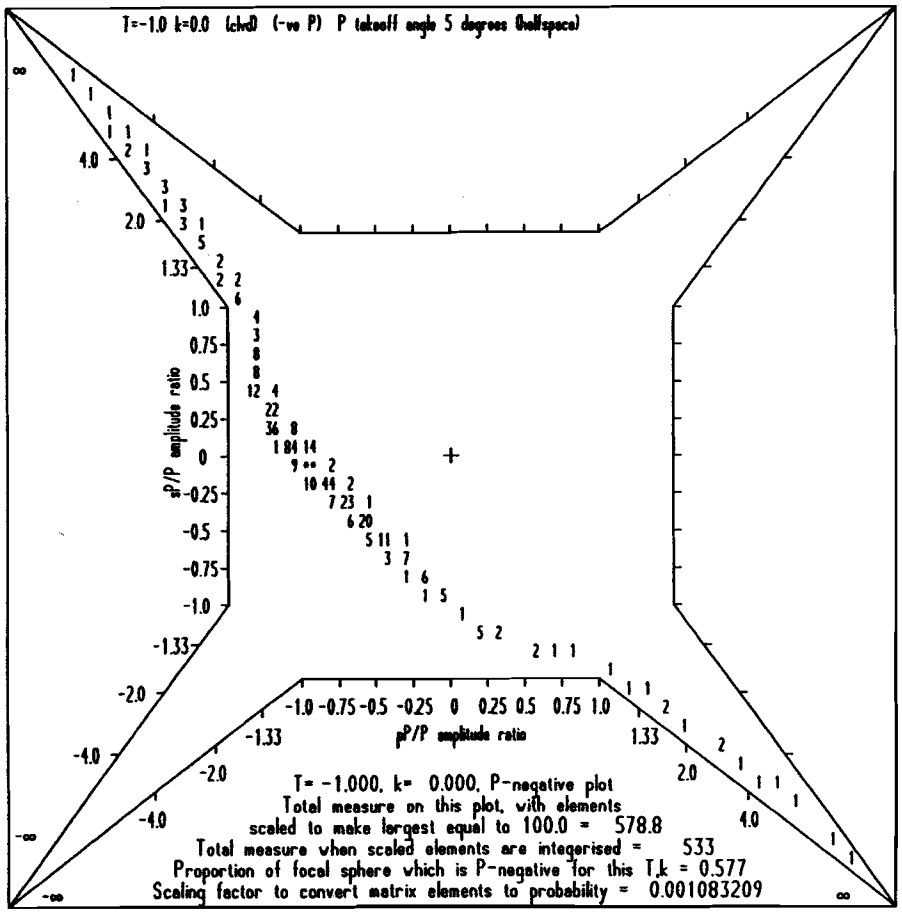

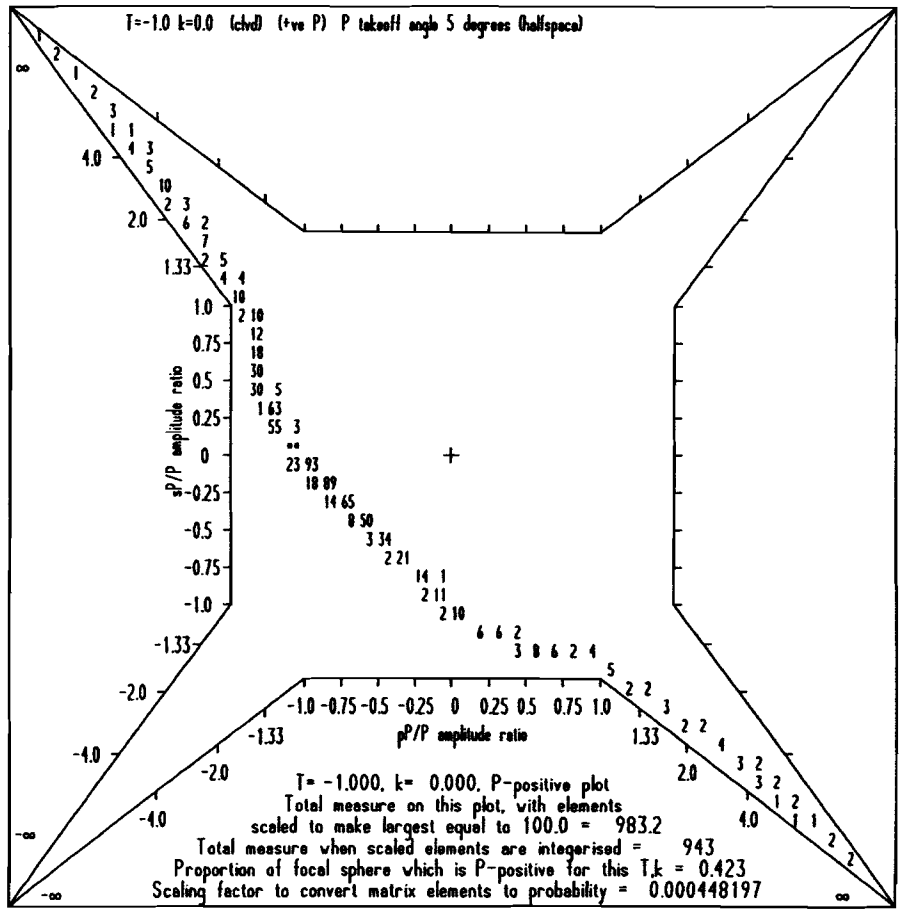

Figure 55 (continued)

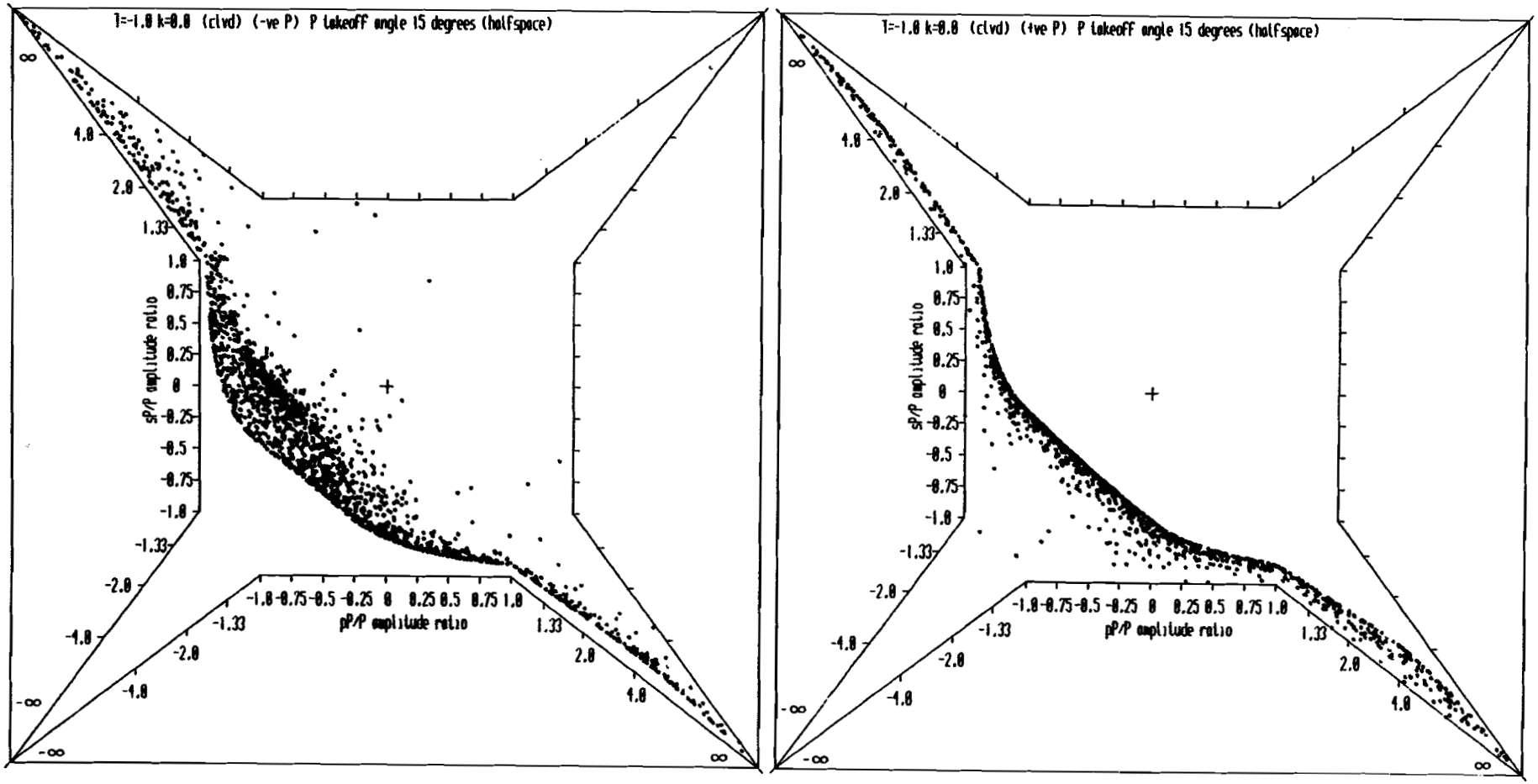
l=-1.0 k=0.0 (clvd) (-ve P) P takeoff angle 15 degrees (halfspace)
sP/P amplitude ratio
pP/P amplitude ratio
l=-1.0 k=0.0 (clvd) (+ve P) P takeoff angle 15 degrees (halfspace)
sP/P amplitude ratio
pP/P amplitude ratio

Figure 56

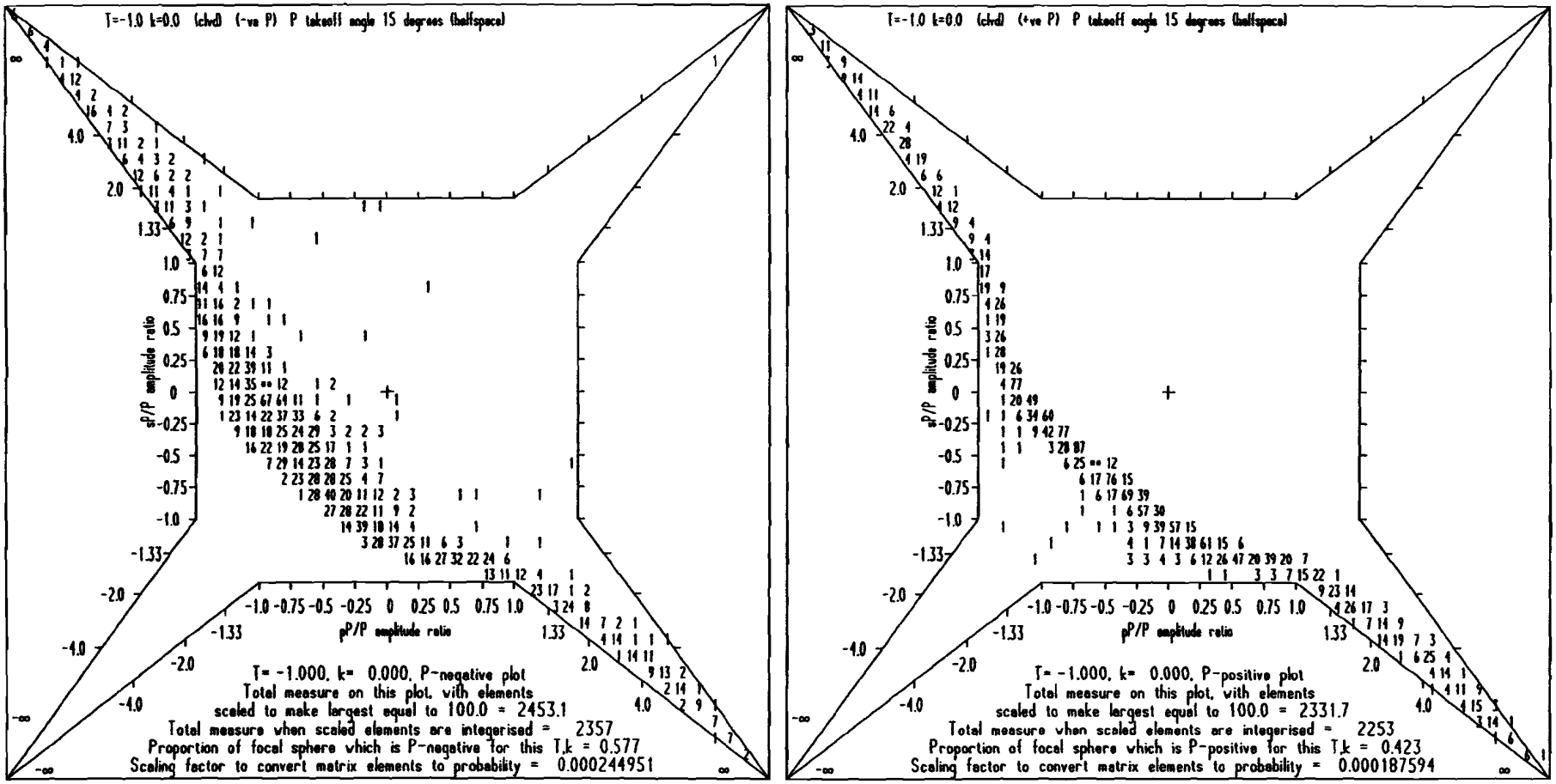

Figure 56 (continued)

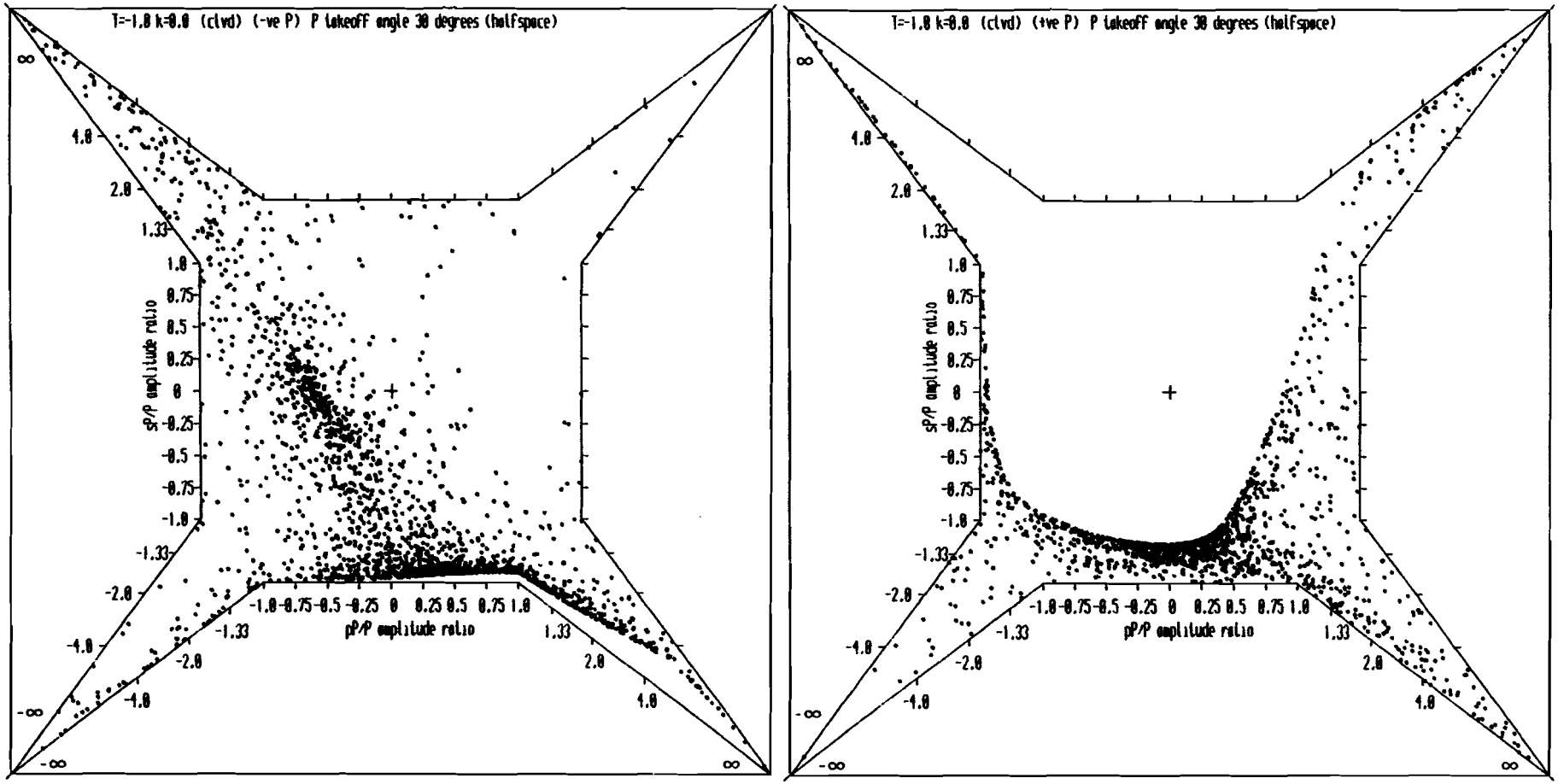
T=-1.0 k=0.0 (clvd) (-ve P) P takeoff angle 30 degrees (halfspace)
T=-1.0 k=0.0 (clvd) (+ve P) P takeoff angle 30 degrees (halfspace)
sP/P amplitude ratio
pP/P amplitude ratio
∞
4.0
2.0
1.33
1.0
0.75
0.5
0.25
0
-0.25
-0.5
-0.75
-1.0
-1.33
-2.0
-4.0
-∞

Figure 57

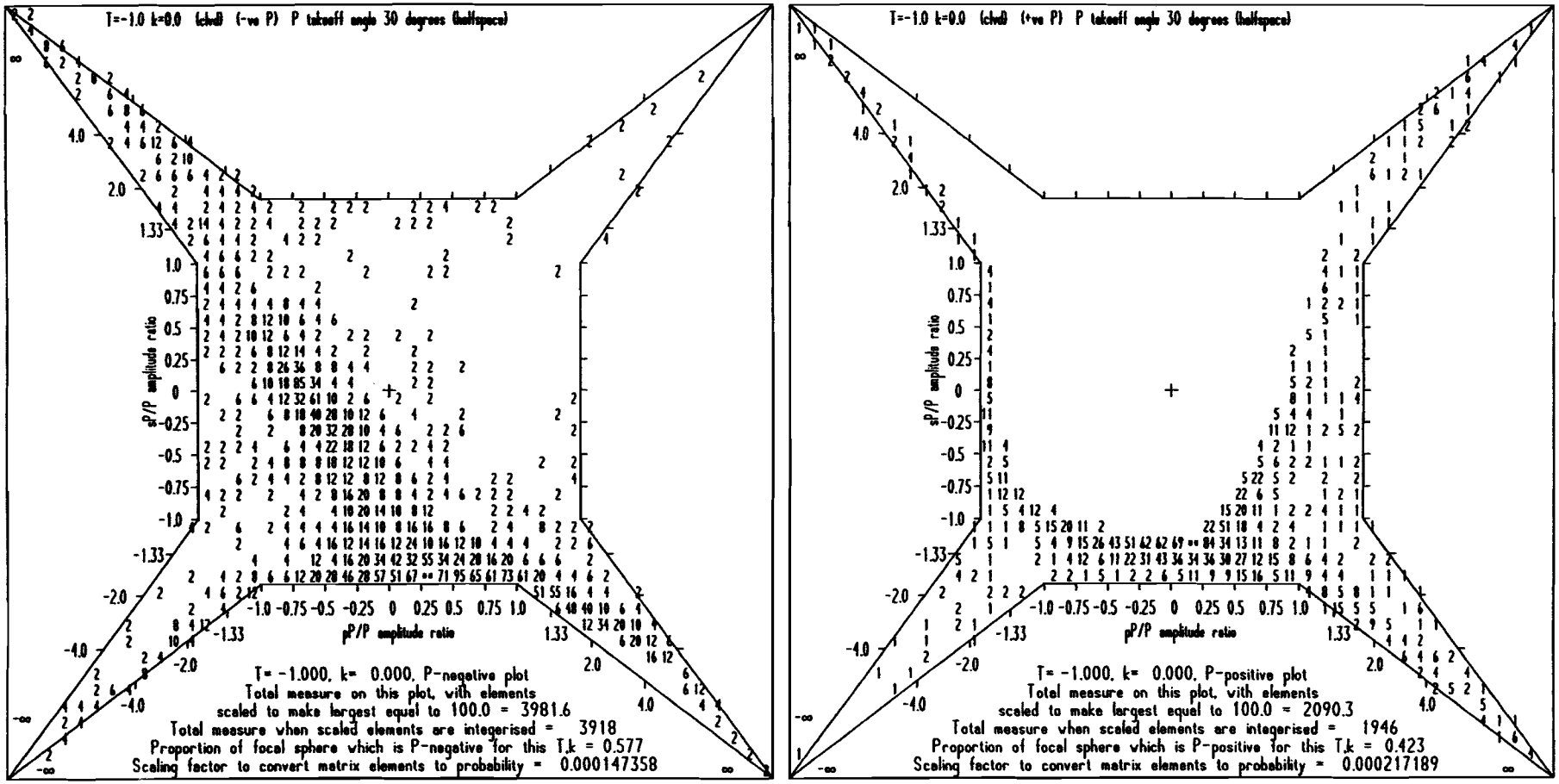

Figure 57 (continued)

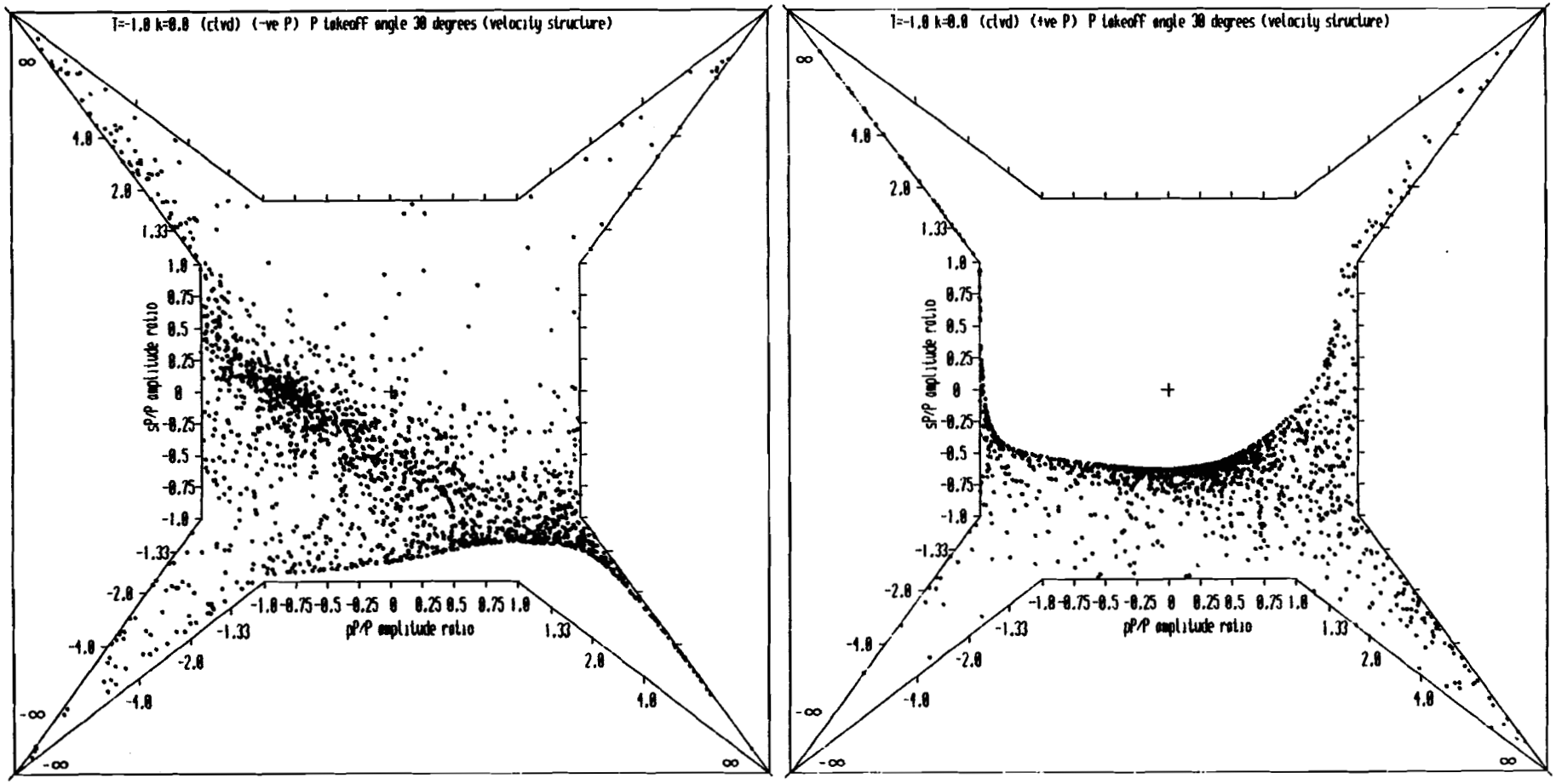
T=-1.0 k=0.0 (clvd) (-ve P) P takeoff angle 30 degrees (velocity structure)
T=-1.0 k=0.0 (clvd) (+ve P) P takeoff angle 30 degrees (velocity structure)
sP/P amplitude ratio
pP/P amplitude ratio
∞
4.0
2.0
1.33
1.0
0.75
0.5
0.25
0
-0.25
-0.5
-0.75
-1.0
-1.33
-2.0
-4.0
-∞
-1.0 -0.75 -0.5 -0.25 0 0.25 0.5 0.75 1.0

Figure 58

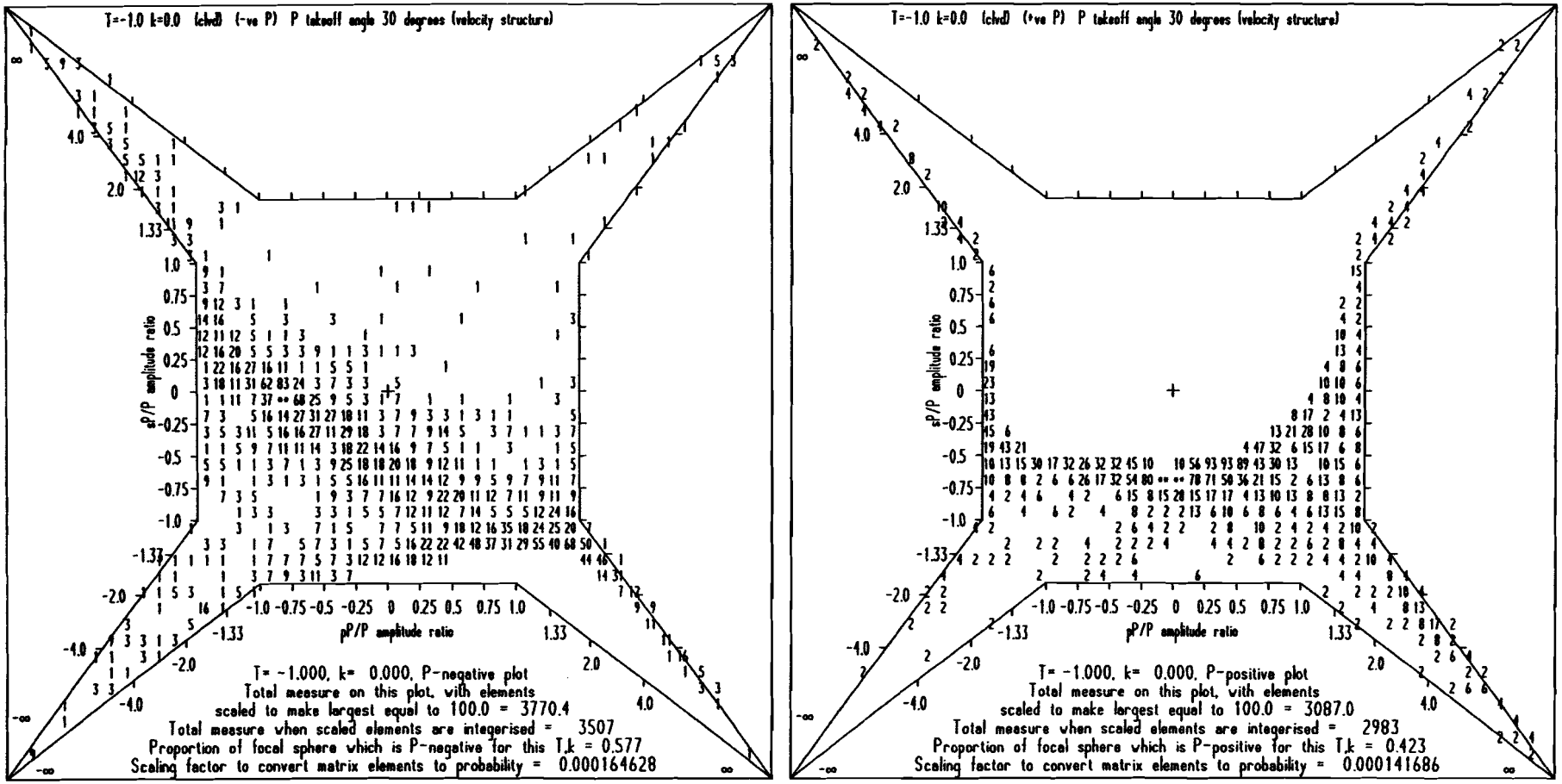

Figure 58 (continued)

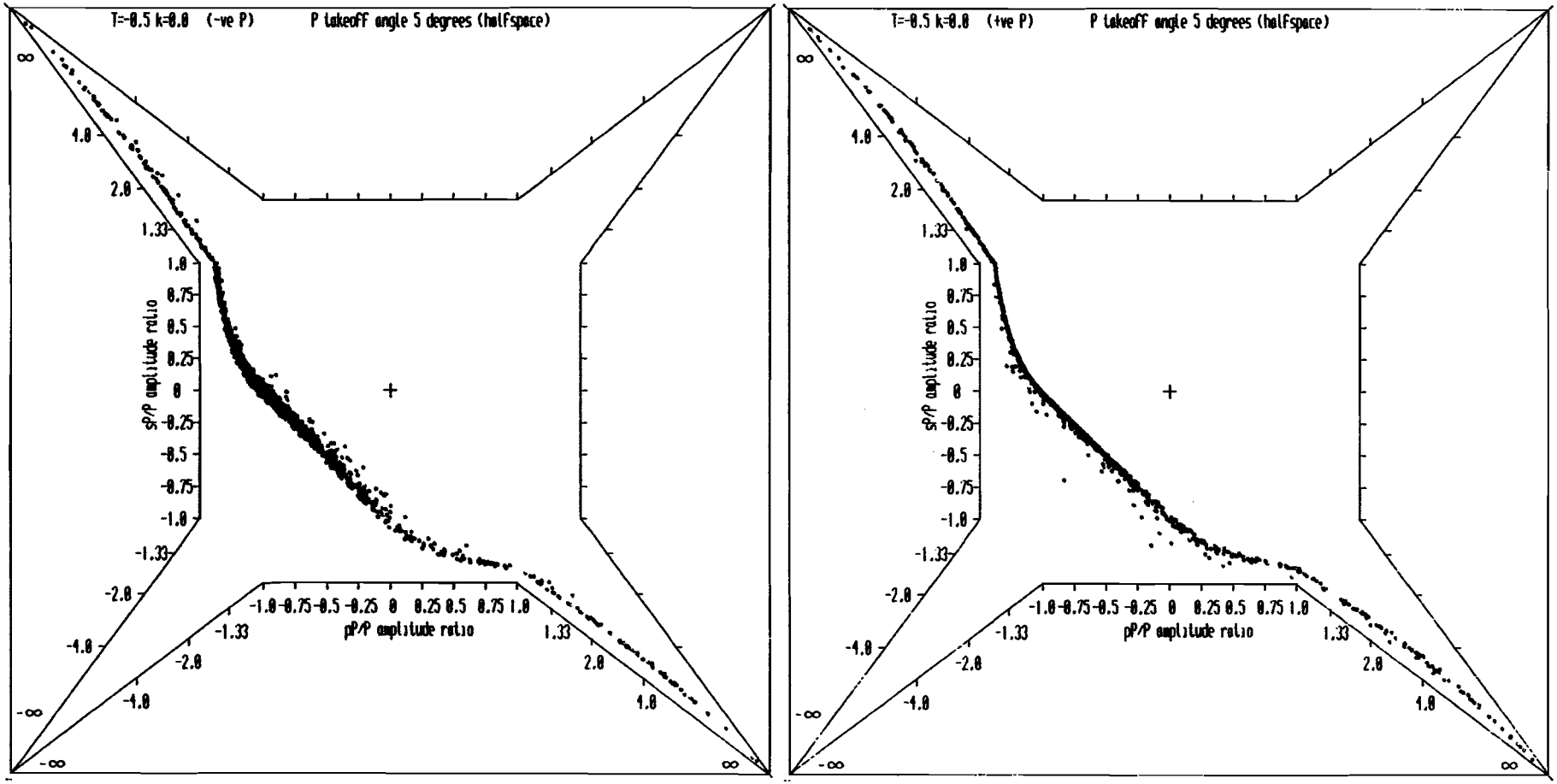
T=-0.5 k=0.0 (-ve P)
P takeoff angle 5 degrees (halfspace)
sP/P amplitude ratio
pP/P amplitude ratio
T=-0.5 k=0.0 (+ve P)
P takeoff angle 5 degrees (halfspace)
sP/P amplitude ratio
pP/P amplitude ratio

Figure 59

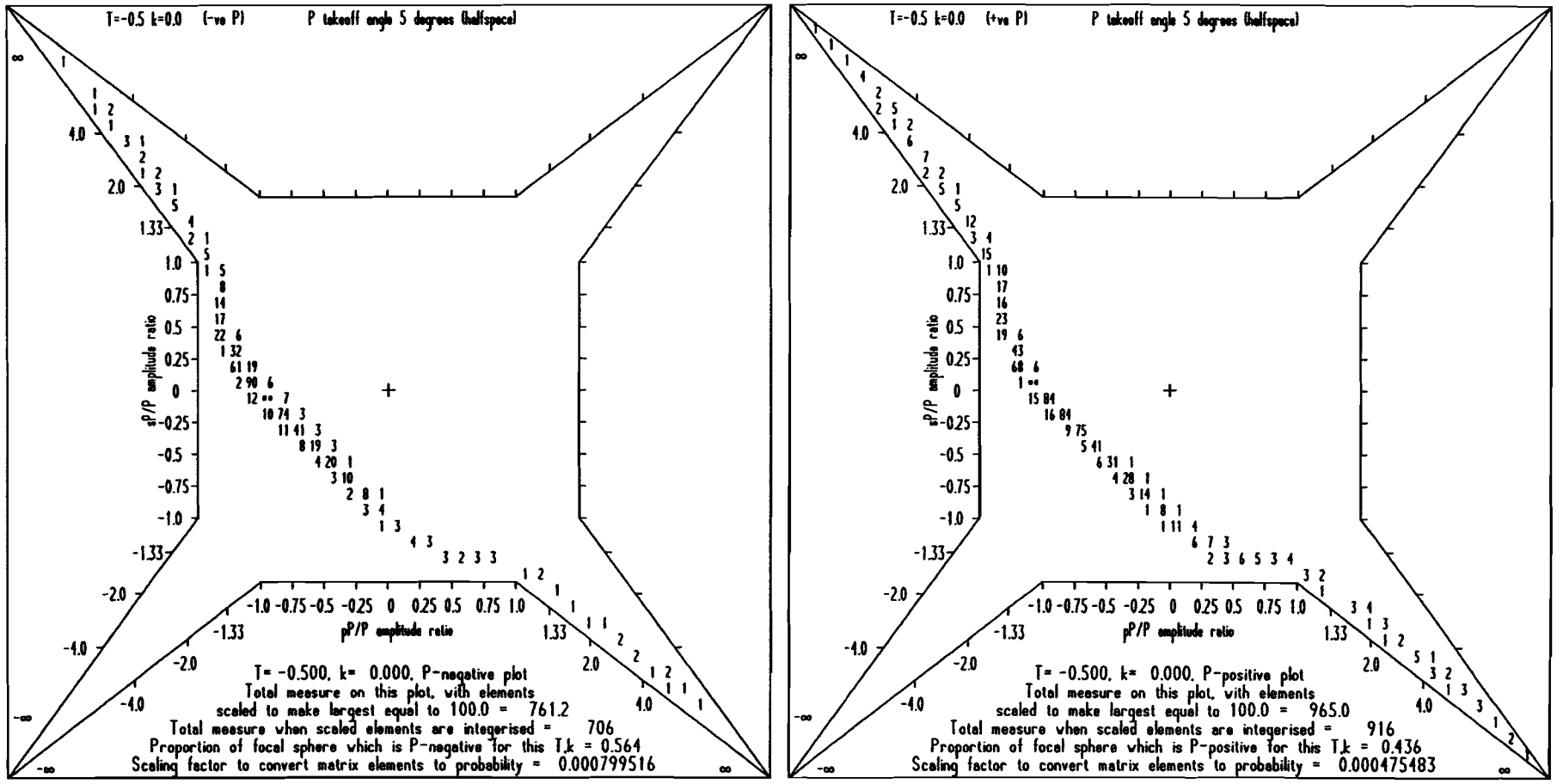

Figure 59 (continued)

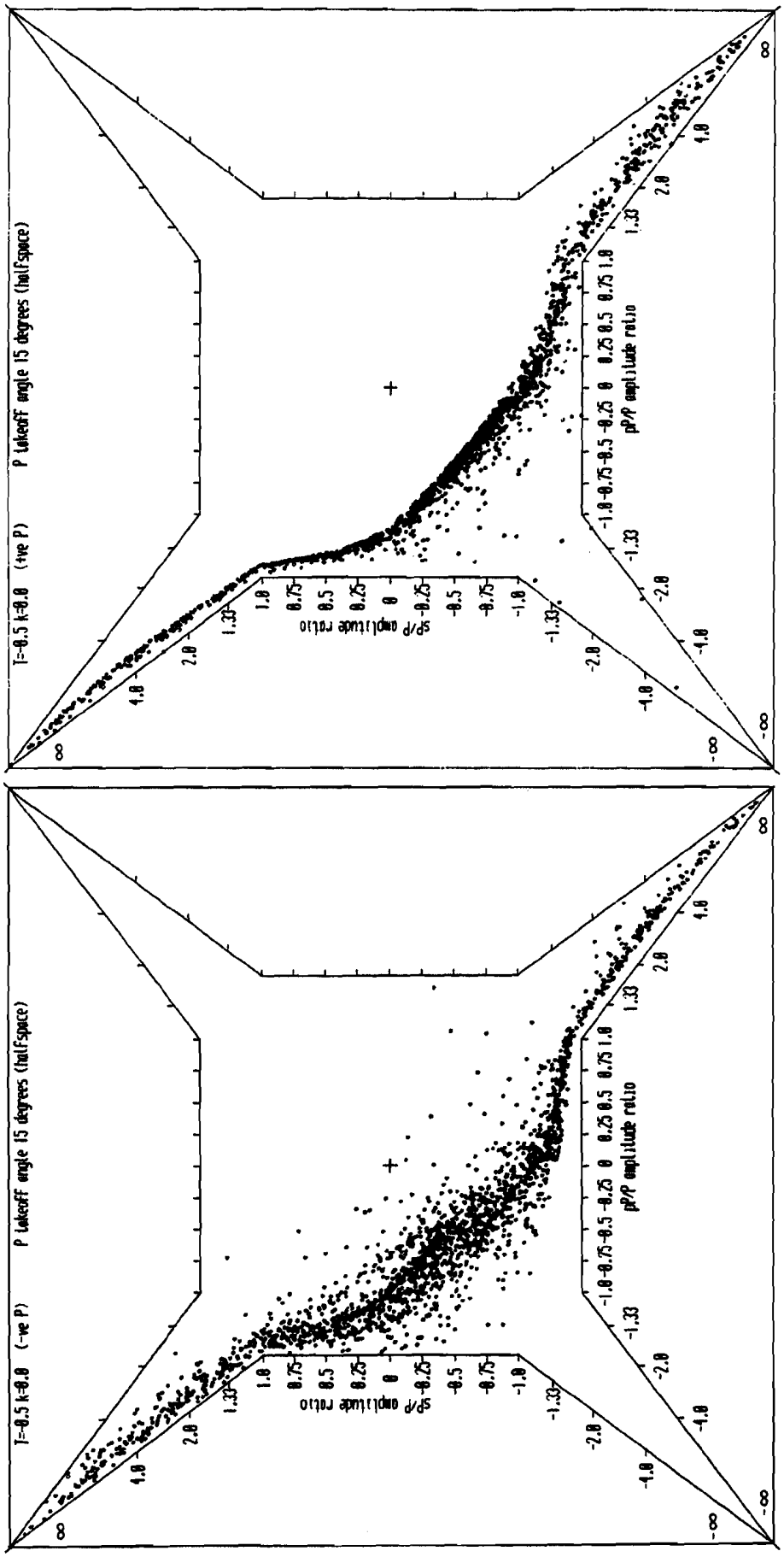
T=-0.5 k=0.0 (-ve P)
P takeoff angle 15 degrees (halfspace)
SP/P amplitude ratio
pP/P amplitude ratio
T=-0.5 k=0.0 (+ve P)
P takeoff angle 15 degrees (halfspace)
SP/P amplitude ratio
pP/P amplitude ratio

Figure 60

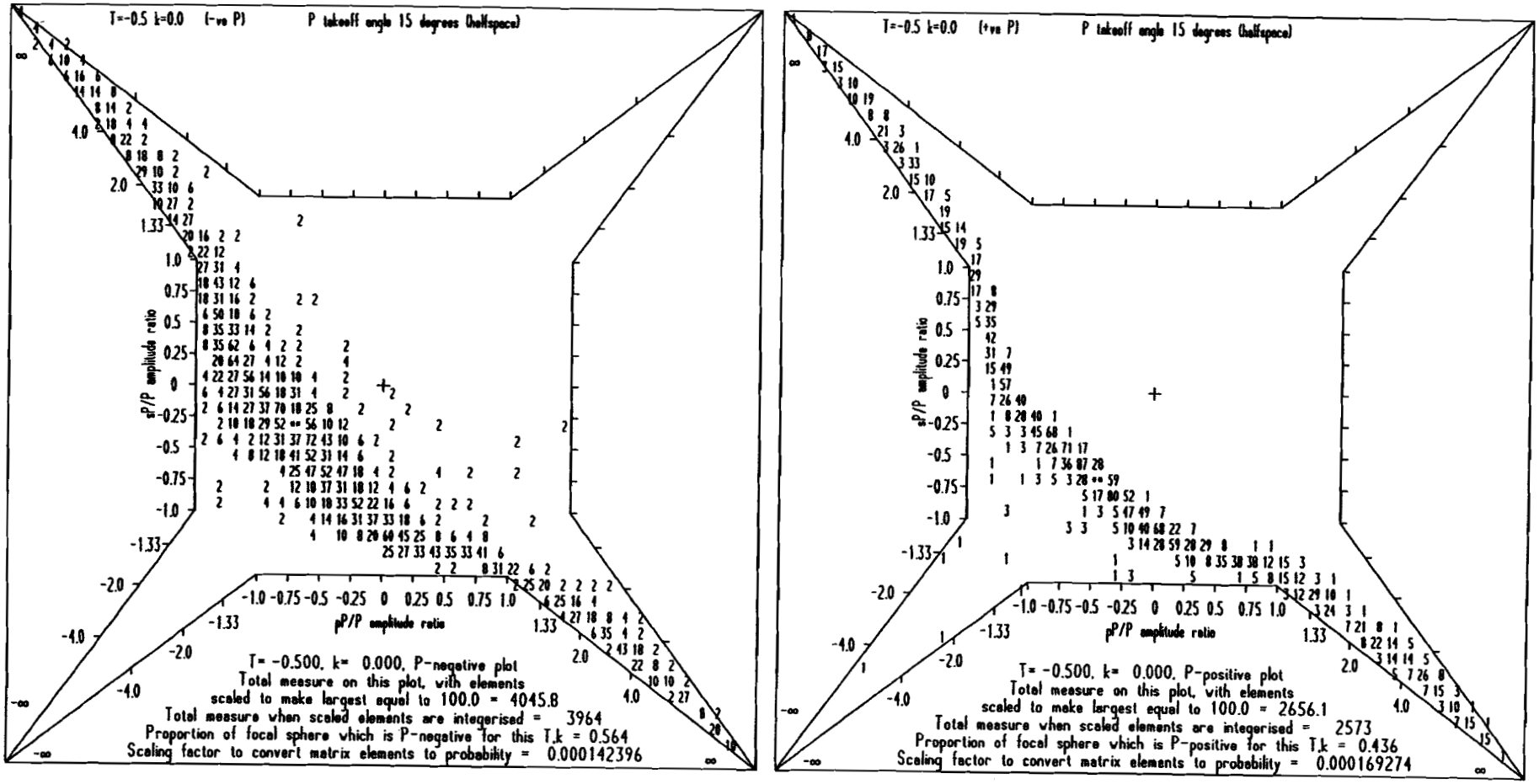

Figure 60 (continued)

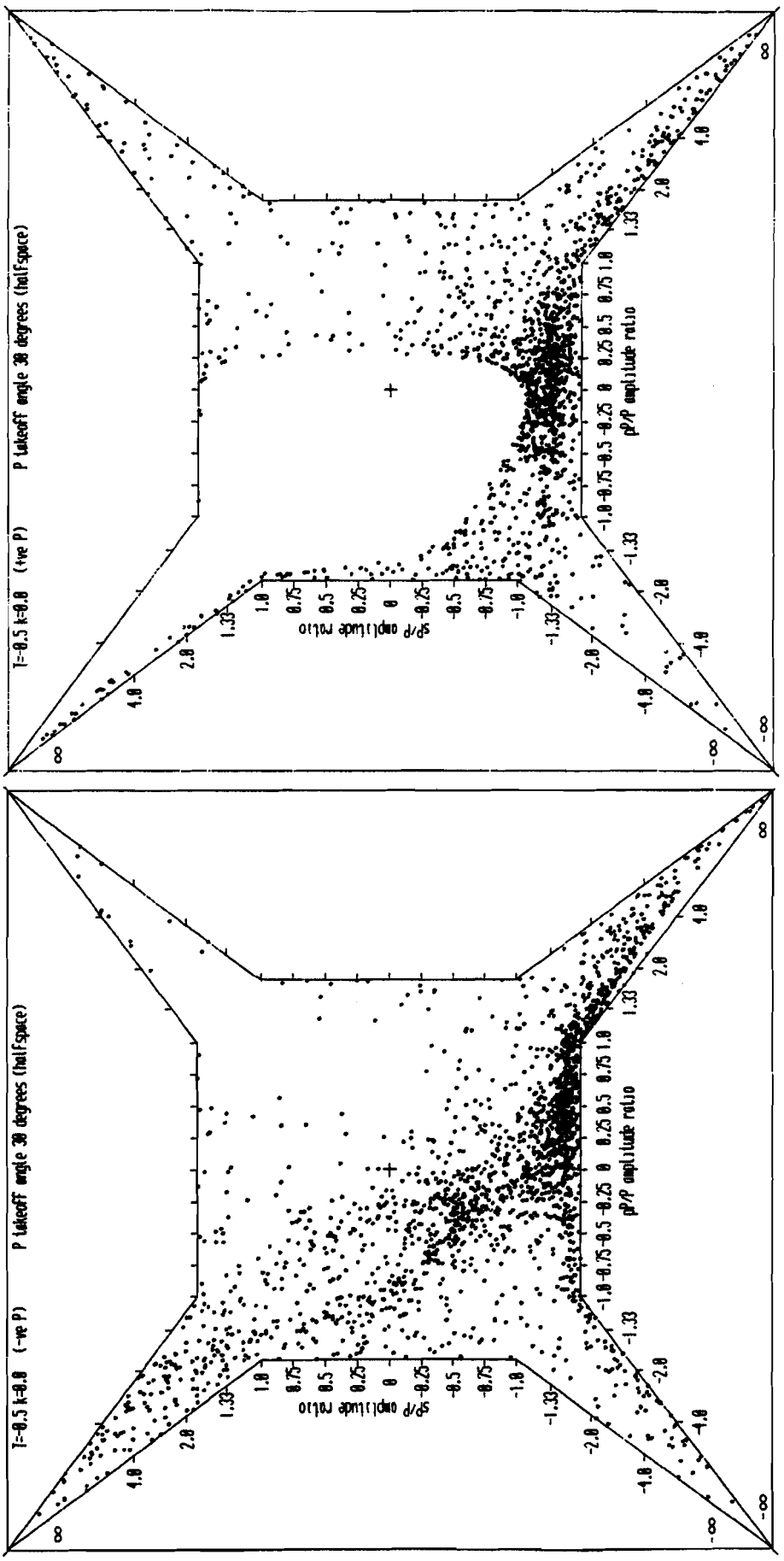
T=-0.5 k=0.0 (-ve P)
P takeoff angle 30 degrees (halfspace)
T=-0.5 k=0.0 (+ve P)
P takeoff angle 30 degrees (halfspace)
pP/P amplitude ratio
sP/P amplitude ratio

Figure 61

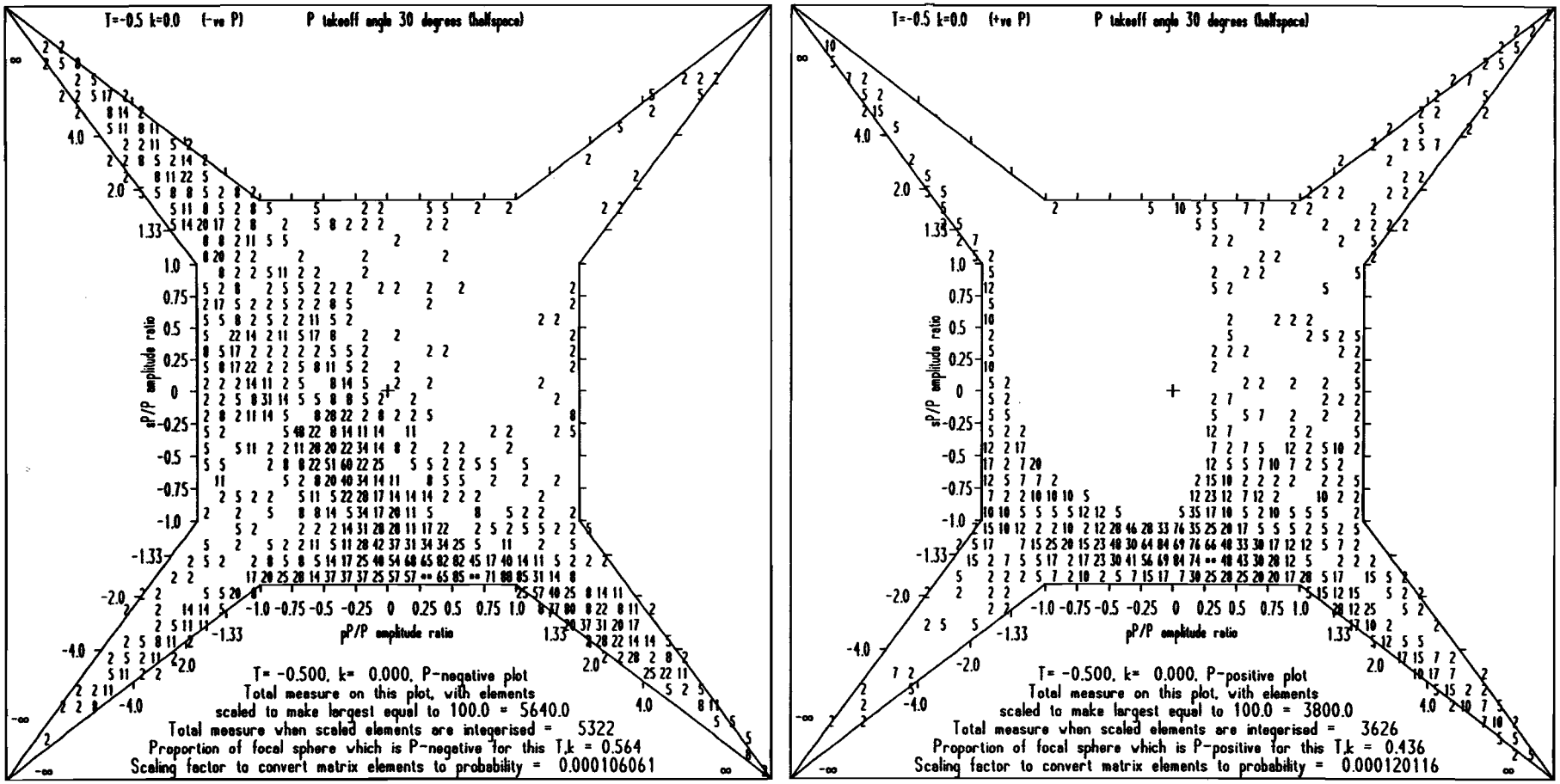

Figure 61 (continued)

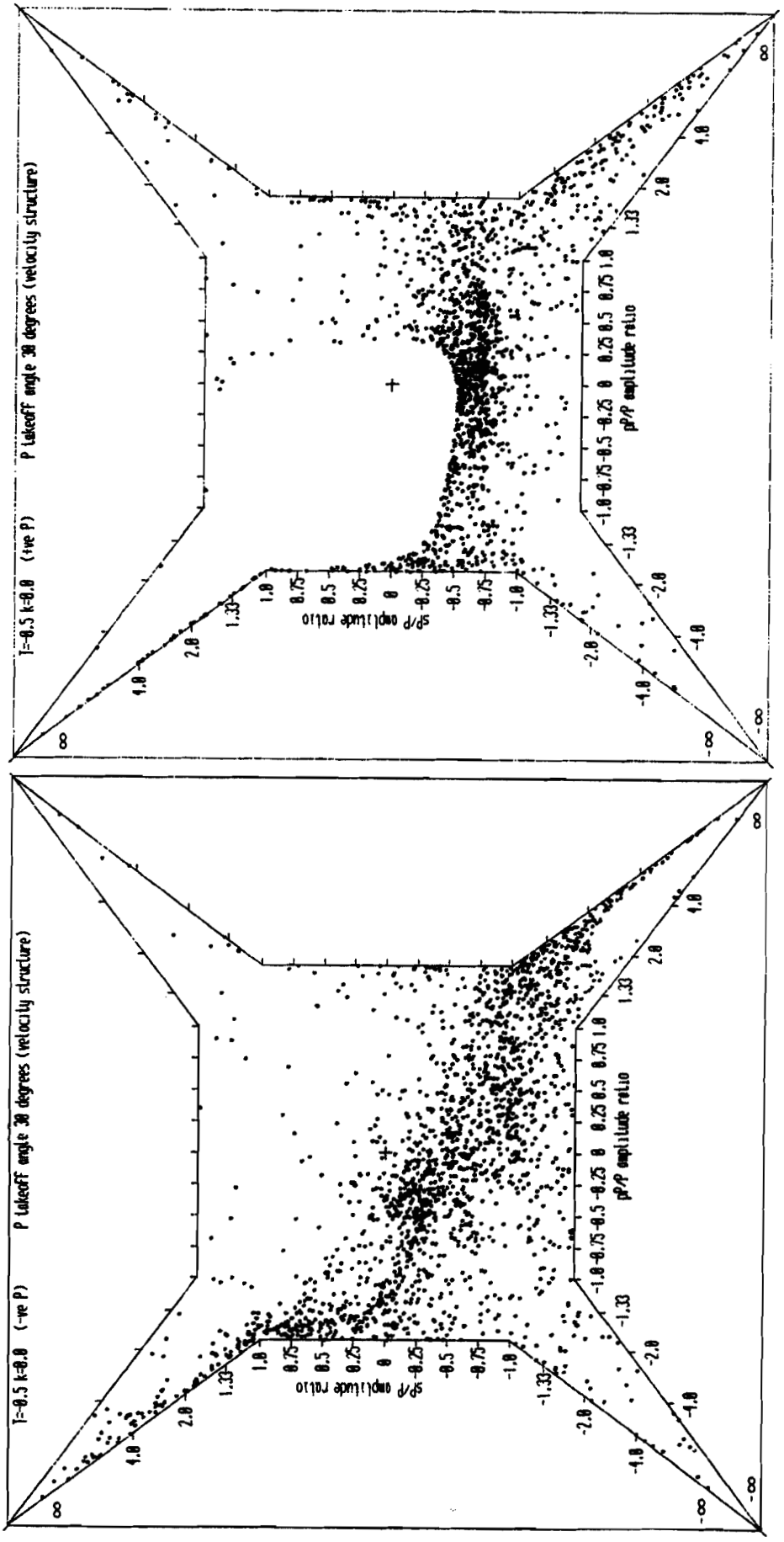
P takeoff angle 30 degrees (velocity structure)
λ=-0.5 k=0.0 (-ve P)
sP/P amplitude ratio
pP/P amplitude ratio
P takeoff angle 30 degrees (velocity structure)
λ=-0.5 k=0.0 (+ve P)
sP/P amplitude ratio
pP/P amplitude ratio

Figure 62

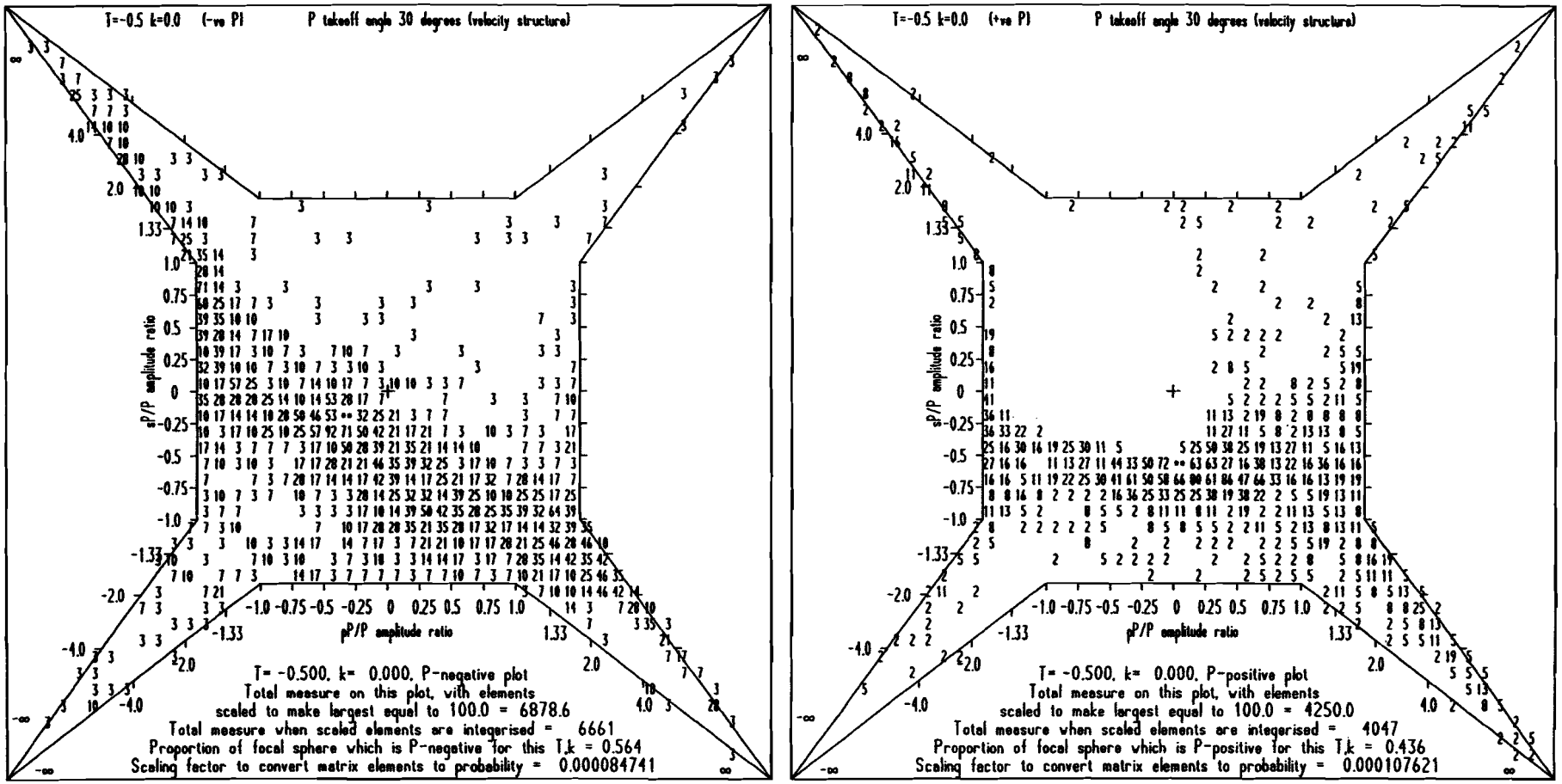

Figure 62 (continued)

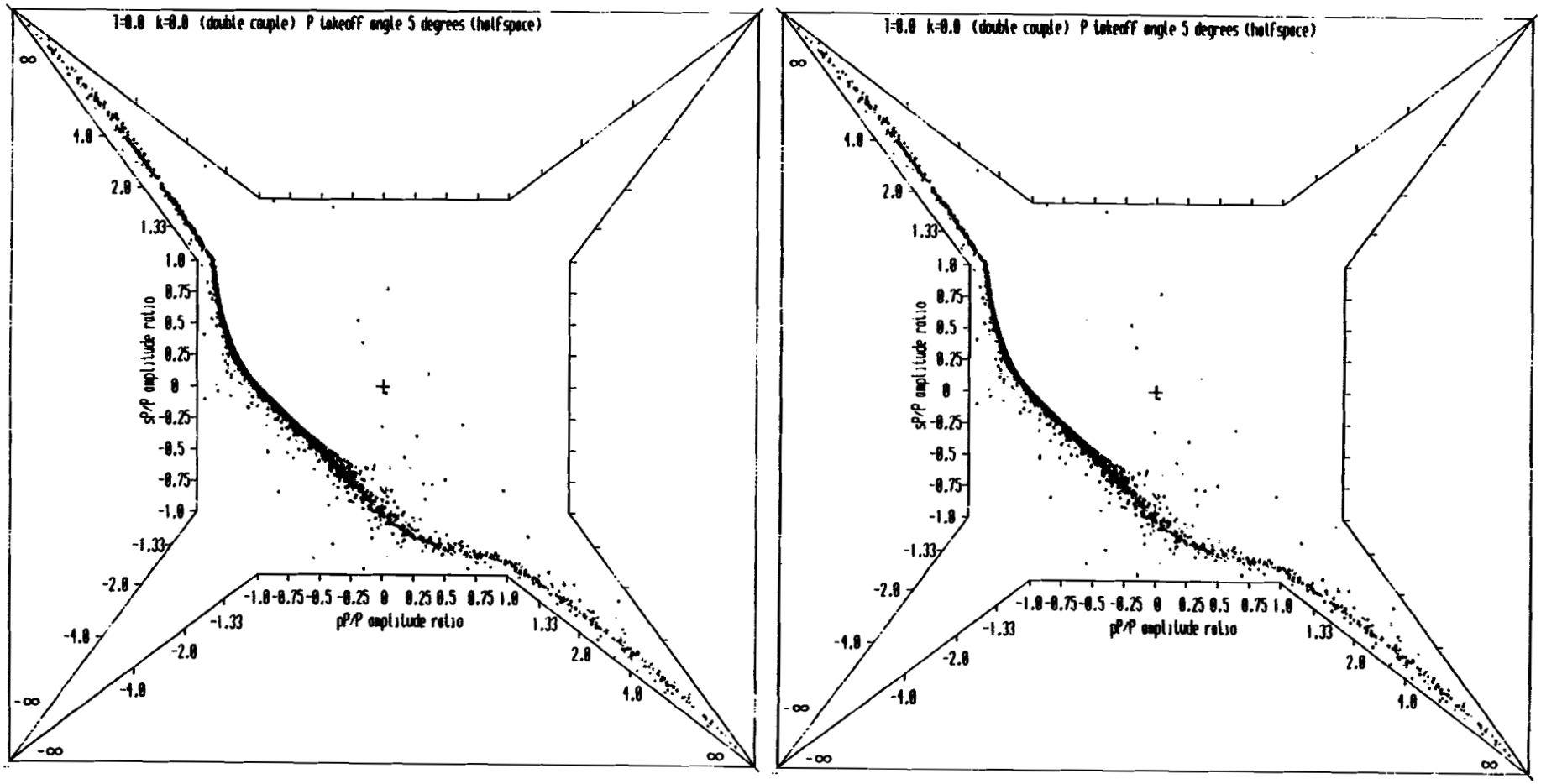
l=0.0 k=0.0 (double couple) P takeoff angle 5 degrees (halfspace)
sP/P amplitude ratio
pP/P amplitude ratio
l=0.0 k=0.0 (double couple) P takeoff angle 5 degrees (halfspace)
sP/P amplitude ratio
pP/P amplitude ratio

Figure 63

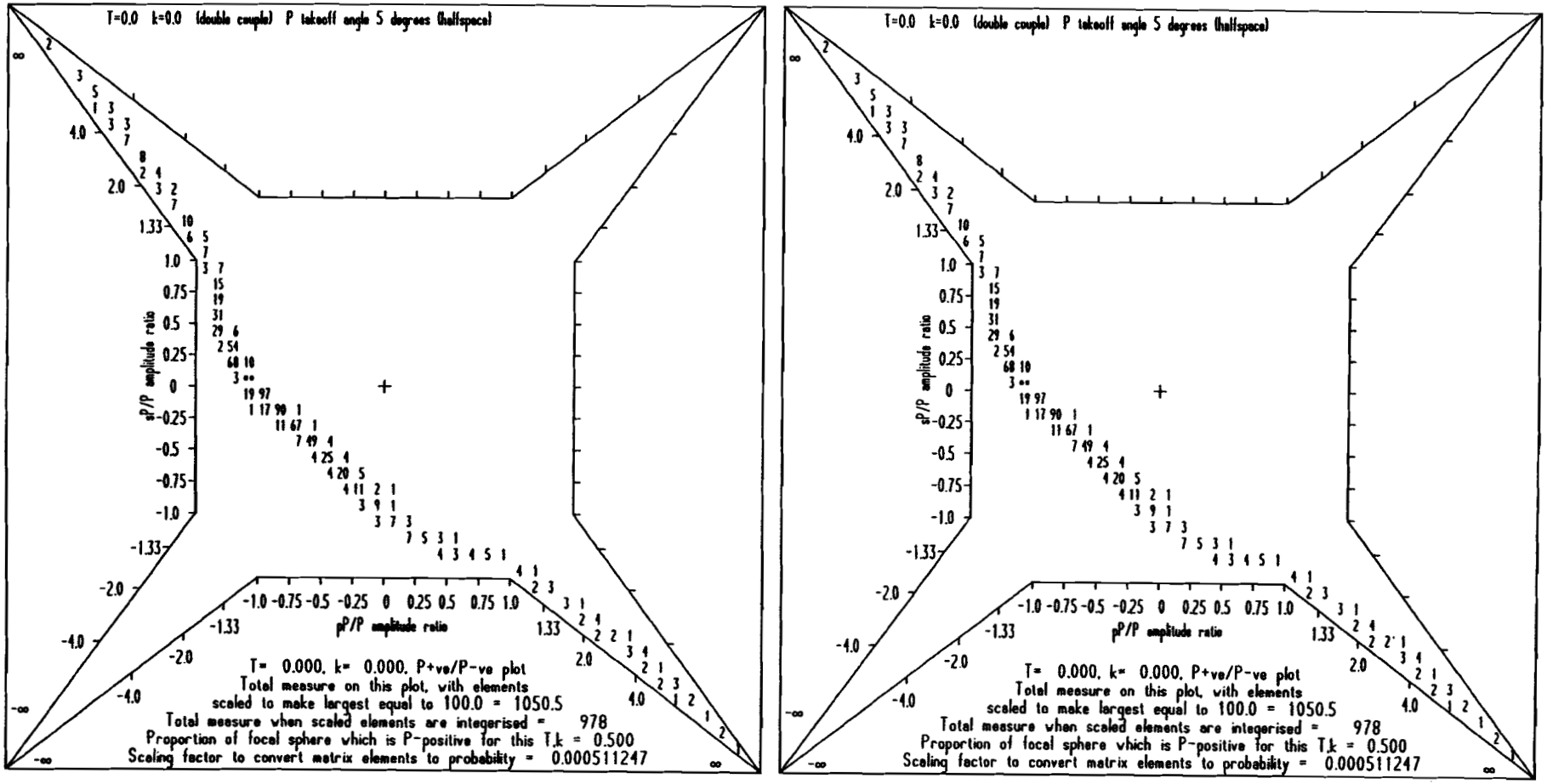

Figure 63 (continued)

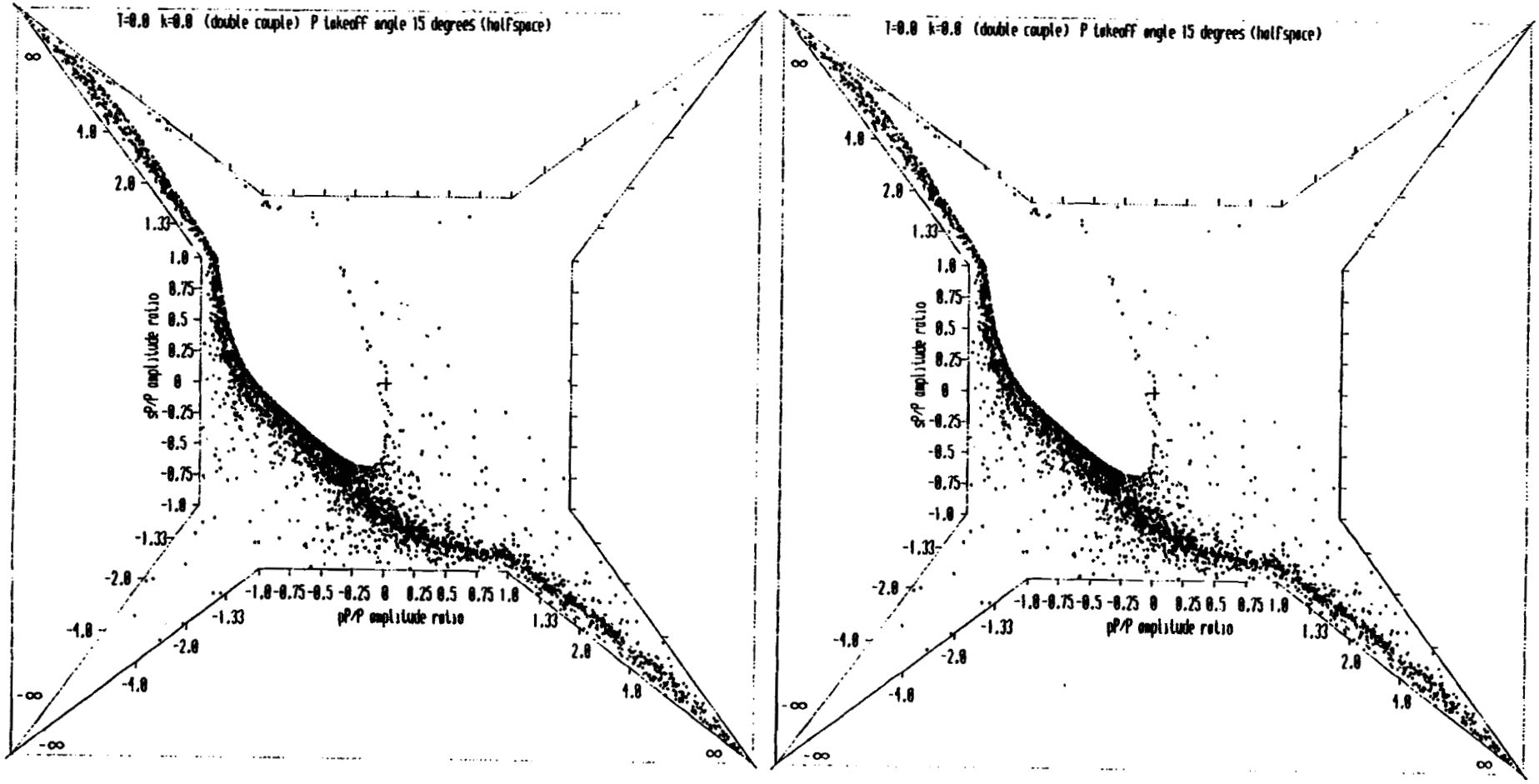
T=0.0 k=0.0 (double couple) P takeoff angle 15 degrees (halfspace)
sP/P amplitude ratio
pP/P amplitude ratio
T=0.0 k=0.0 (double couple) P takeoff angle 15 degrees (halfspace)
sP/P amplitude ratio
pP/P amplitude ratio

Figure 64

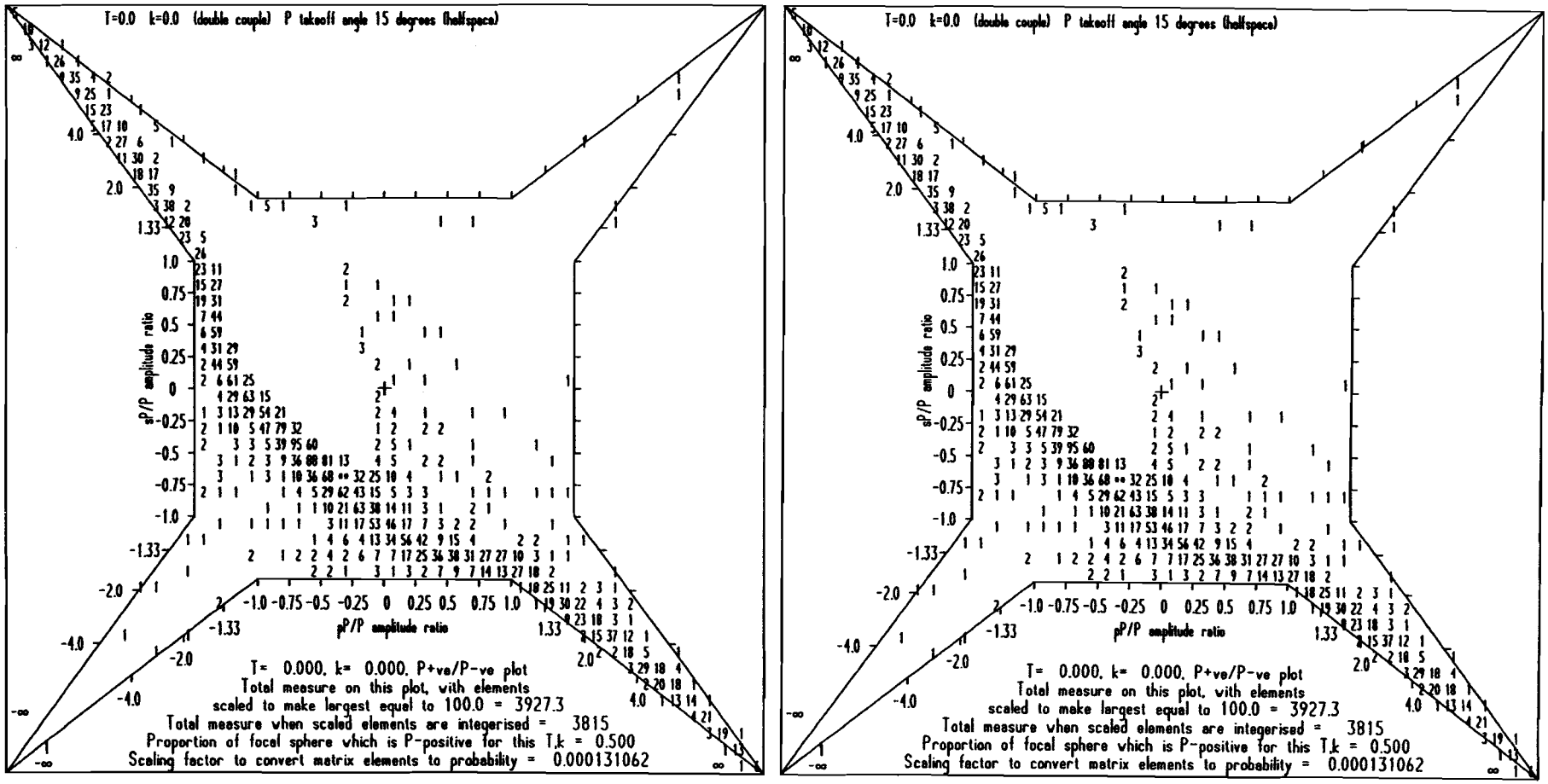

Figure 64 (continued)

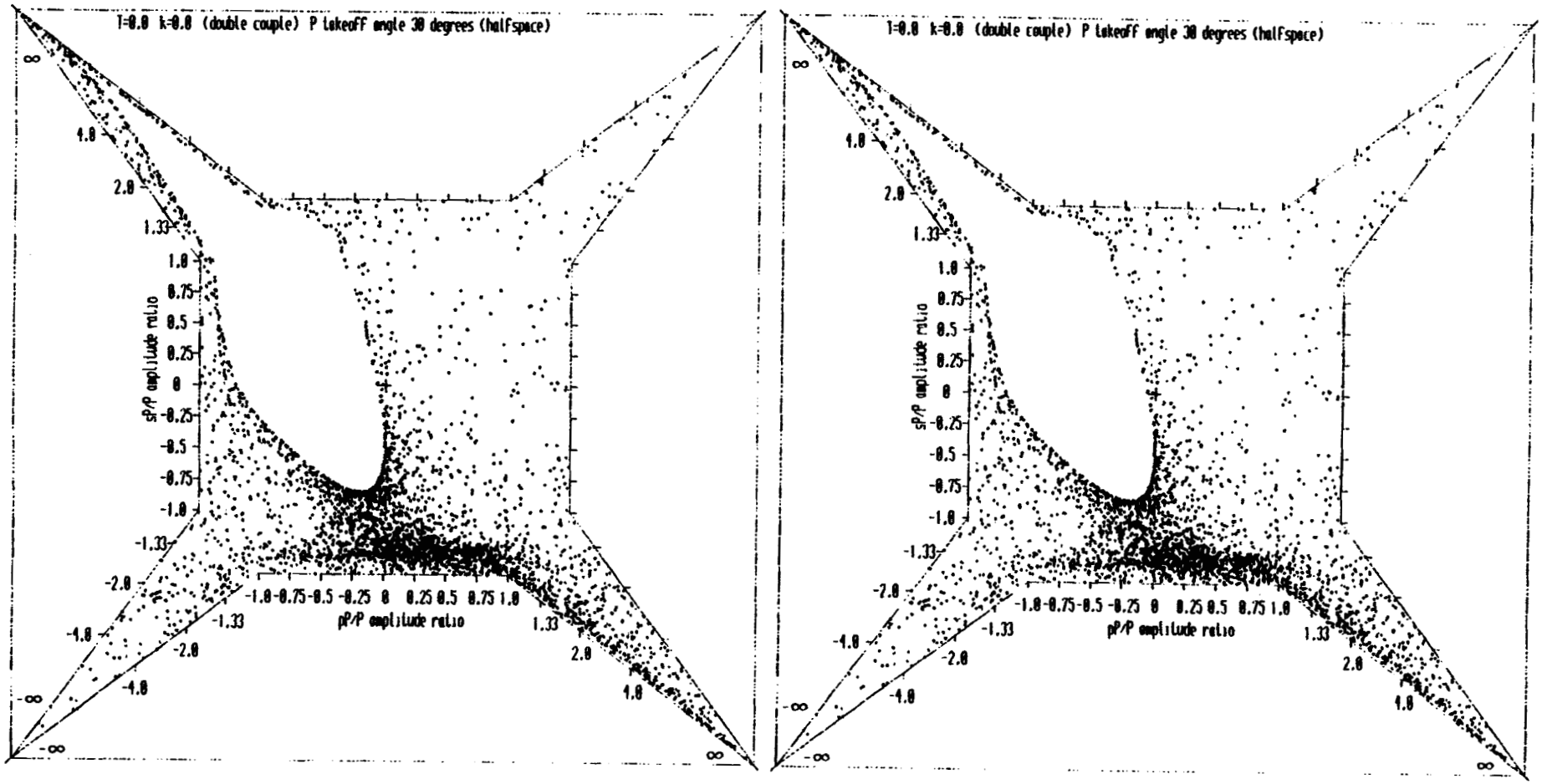
I=0.0 k=0.0 (double couple) P takeoff angle 30 degrees (halfspace)
sP/P amplitude ratio
pP/P amplitude ratio
I=0.0 k=0.0 (double couple) P takeoff angle 30 degrees (halfspace)
sP/P amplitude ratio
pP/P amplitude ratio

Figure 65

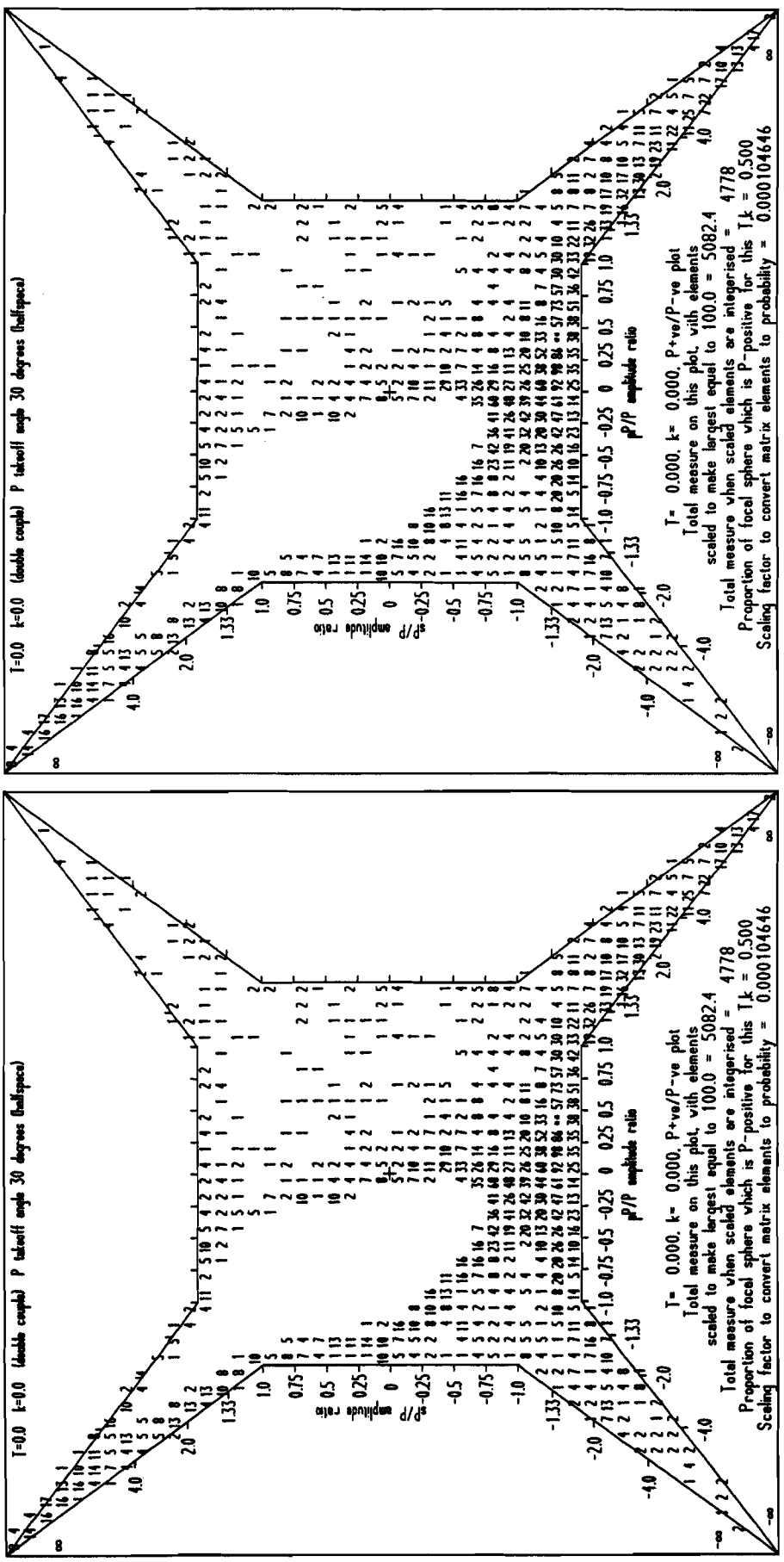

Figure 65 (continued)

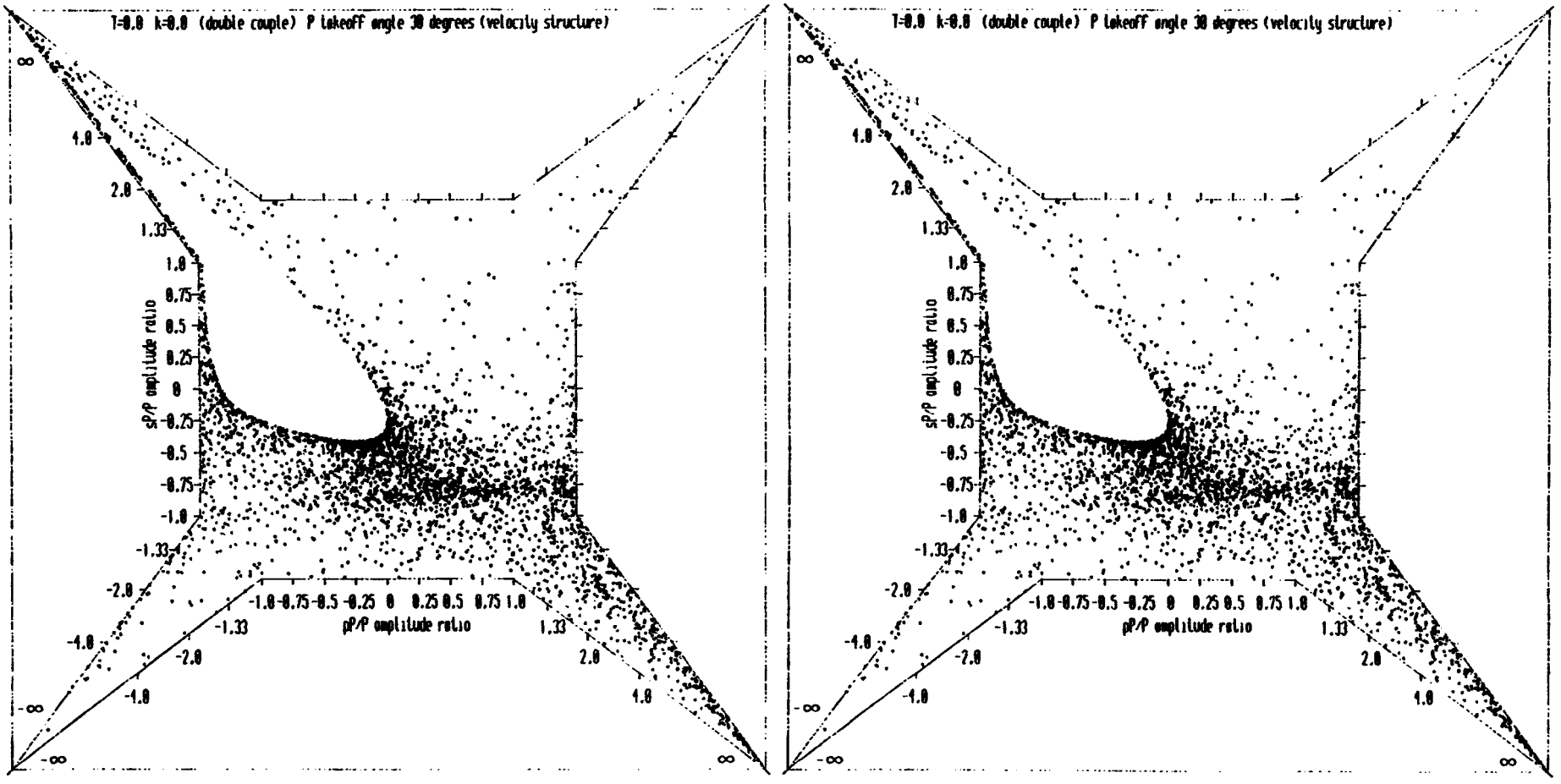
T=0.0 k=0.0 (double couple) P takeoff angle 30 degrees (velocity structure)
sP/P amplitude ratio
pP/P amplitude ratio
T=0.0 k=0.0 (double couple) P takeoff angle 30 degrees (velocity structure)
sP/P amplitude ratio
pP/P amplitude ratio

Figure 66

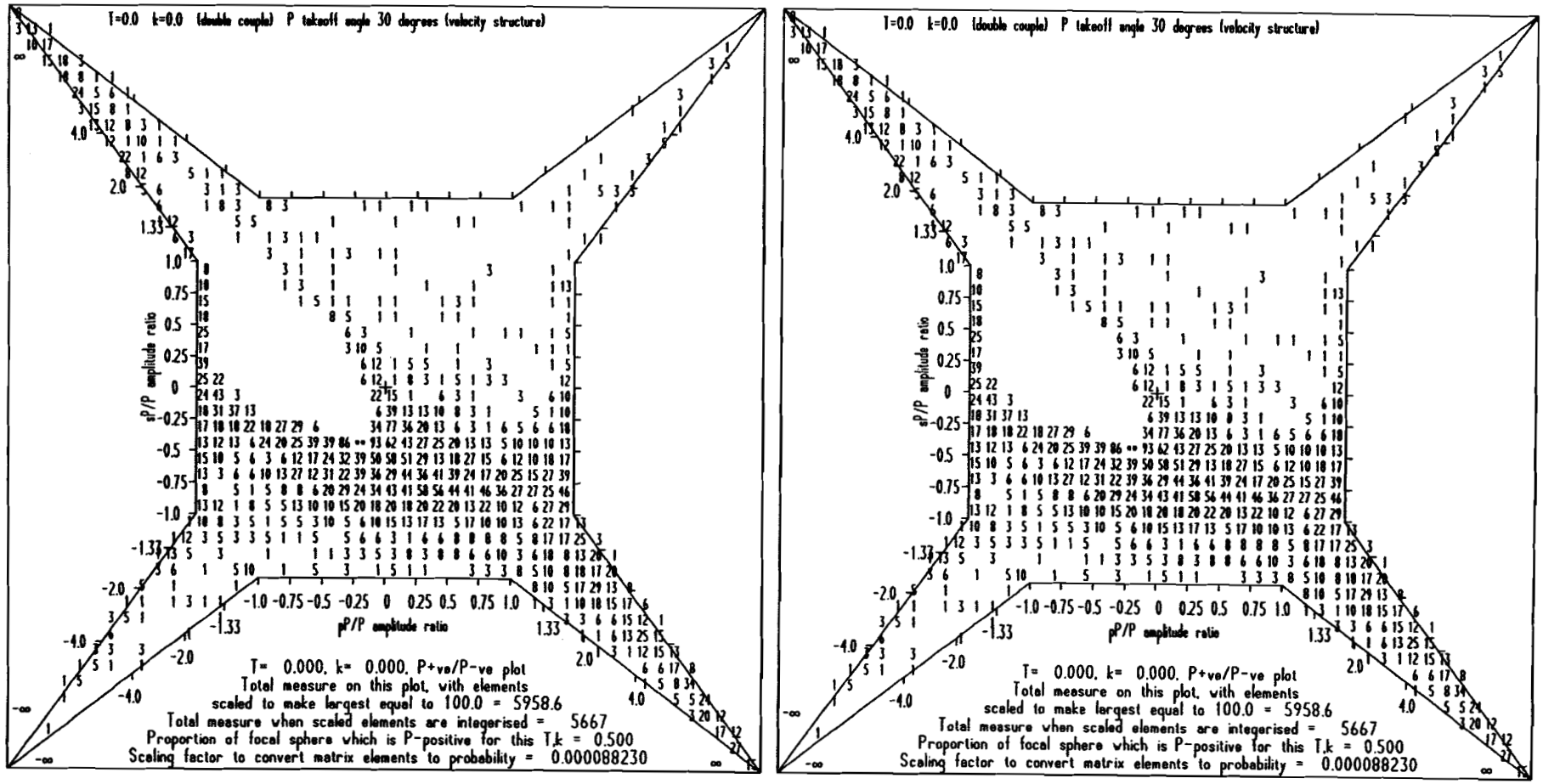

Figure 66 (continued)

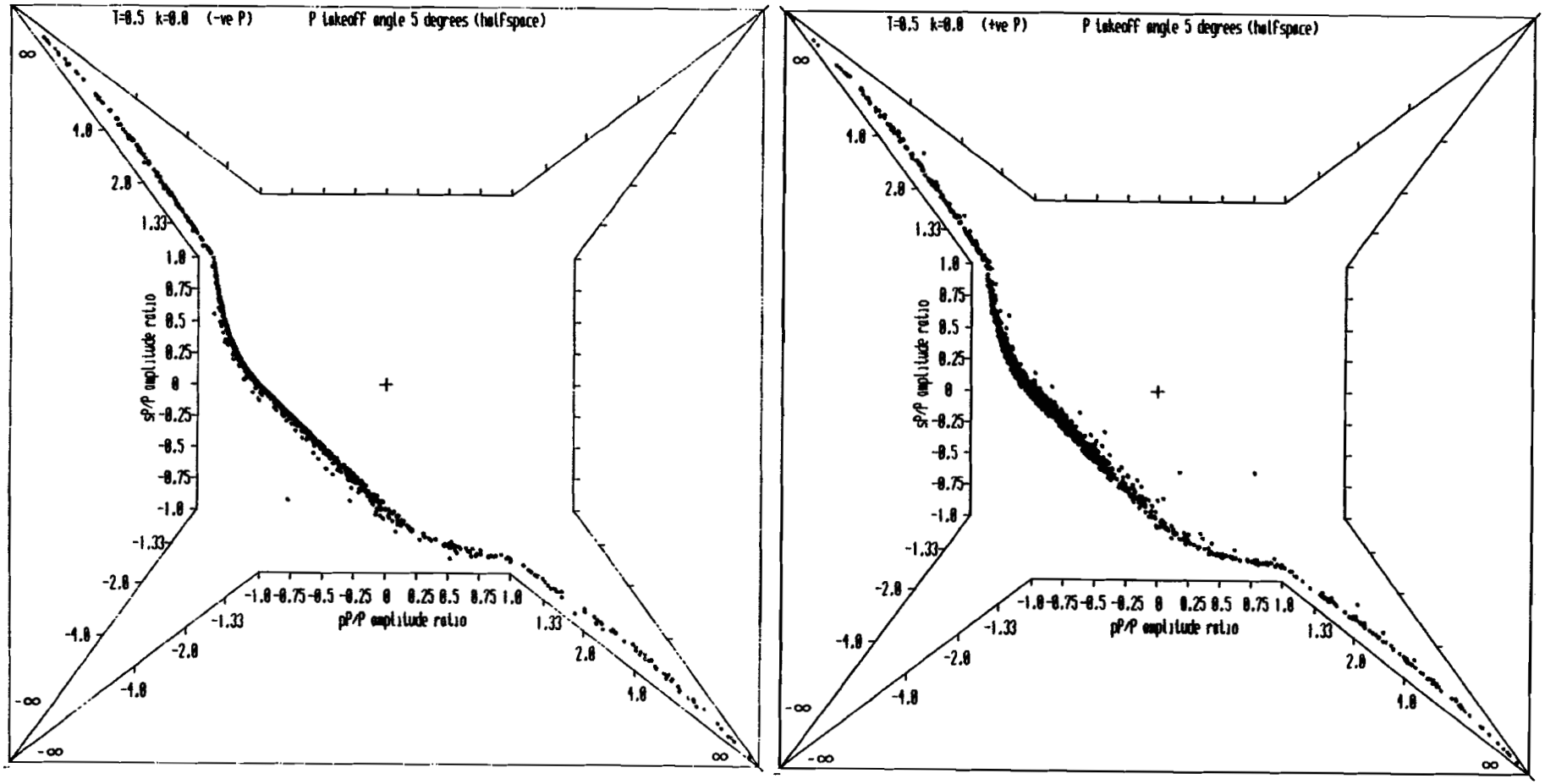
T=0.5 k=0.0 (-ve P)
P takeoff angle 5 degrees (halfspace)
sP/P amplitude ratio
pP/P amplitude ratio
T=0.5 k=0.0 (+ve P)
P takeoff angle 5 degrees (halfspace)
sP/P amplitude ratio
pP/P amplitude ratio

Figure 67

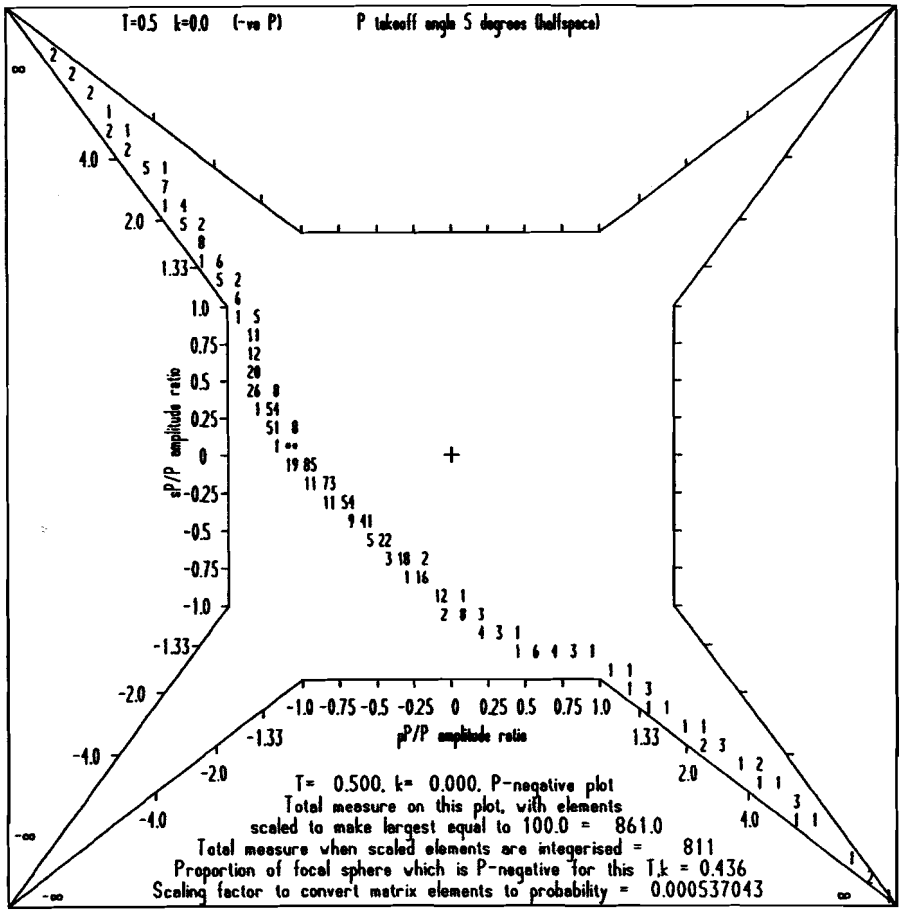

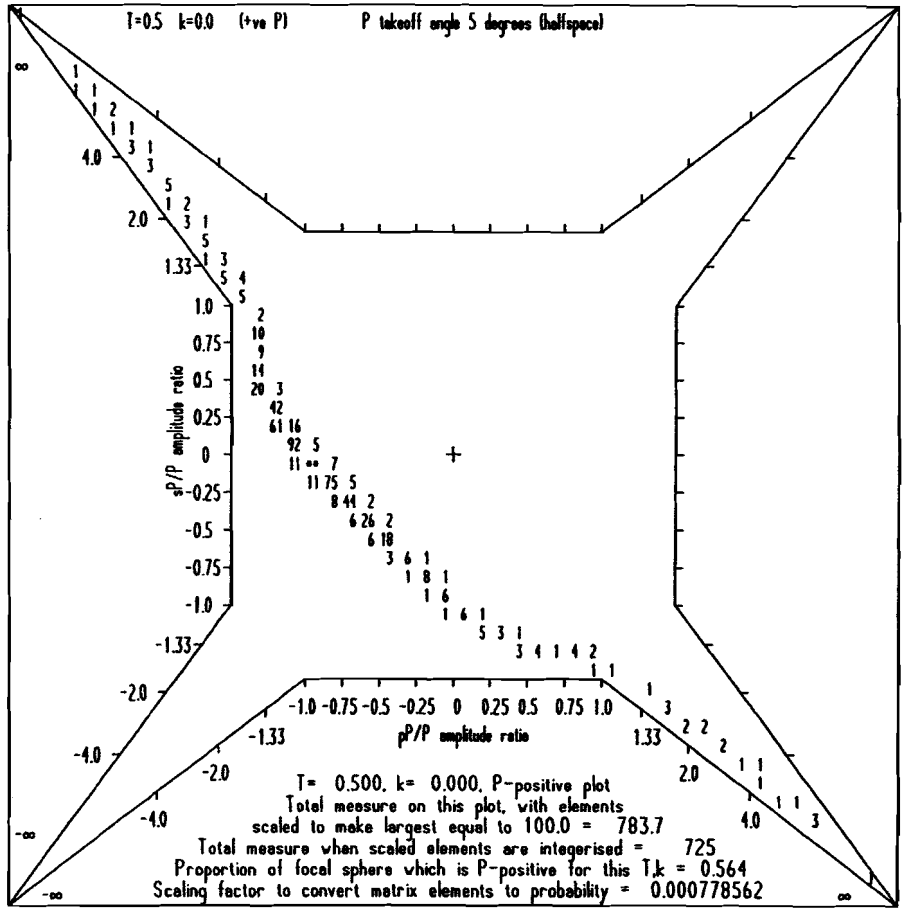

Figure 67 (continued)

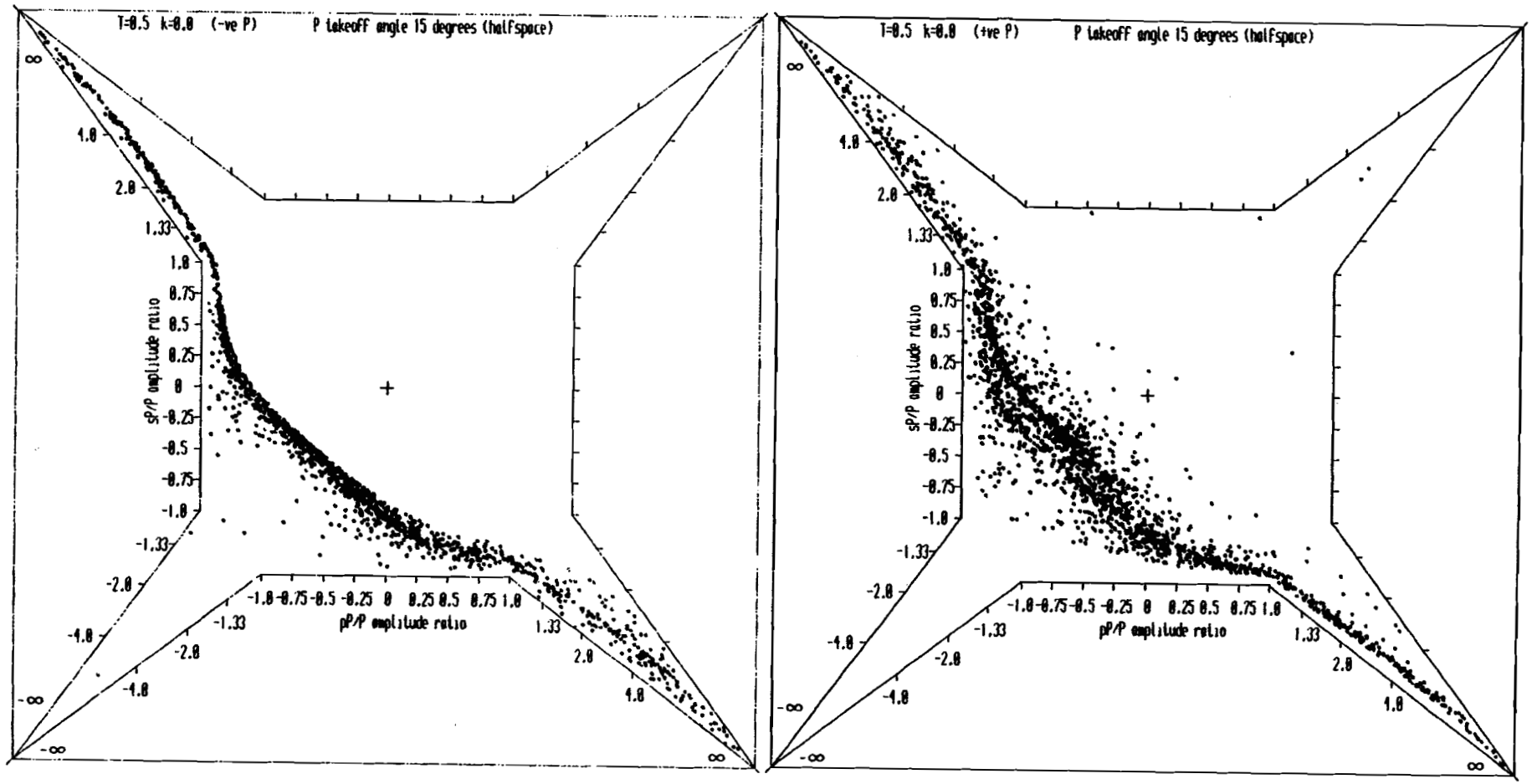
T=0.5 k=0.0 (-ve P)
P takeoff angle 15 degrees (halfspace)
sP/P amplitude ratio
pP/P amplitude ratio
T=0.5 k=0.0 (+ve P)
P takeoff angle 15 degrees (halfspace)
sP/P amplitude ratio
pP/P amplitude ratio

Figure 68

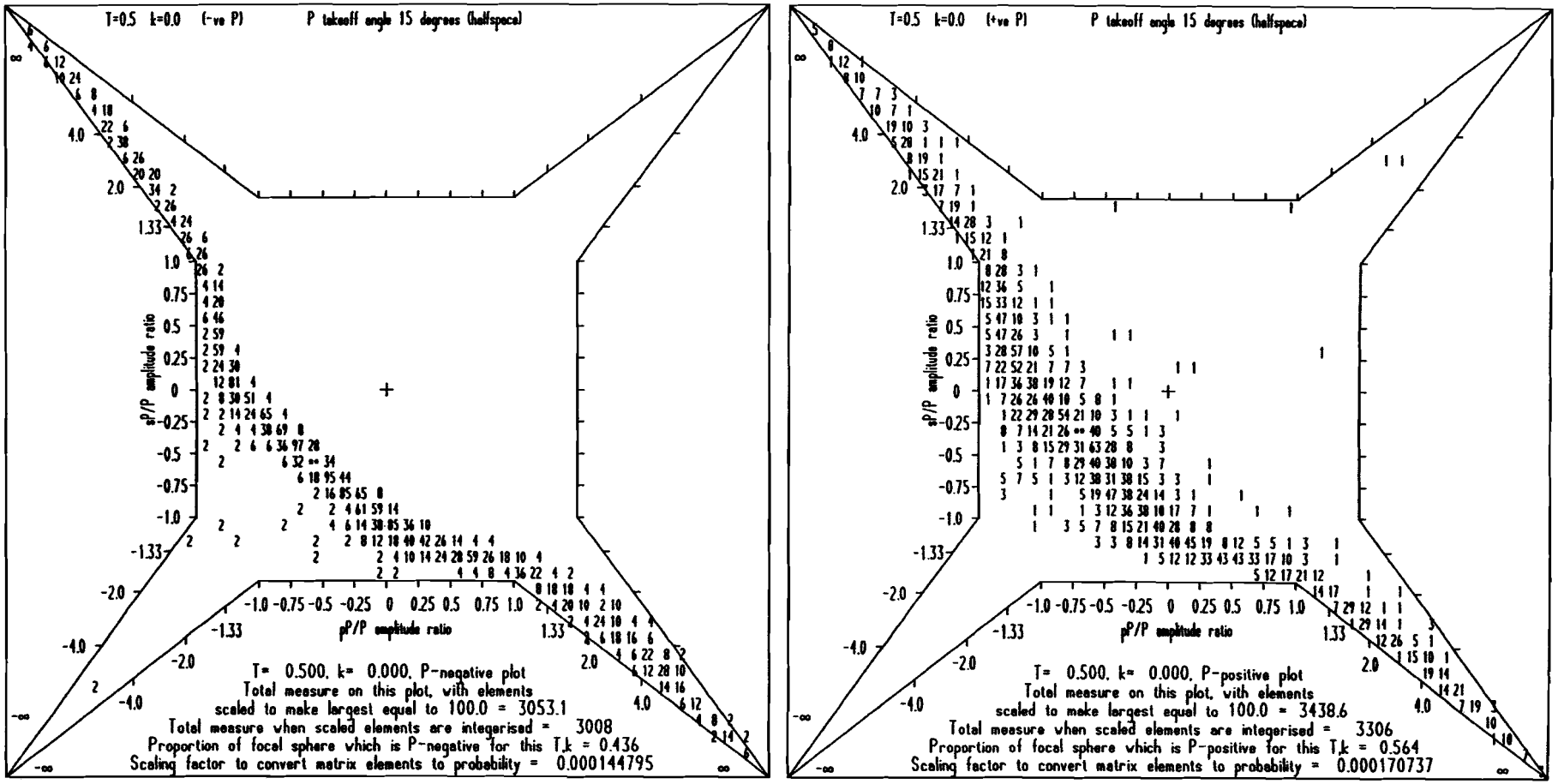

Figure 68 (continued)

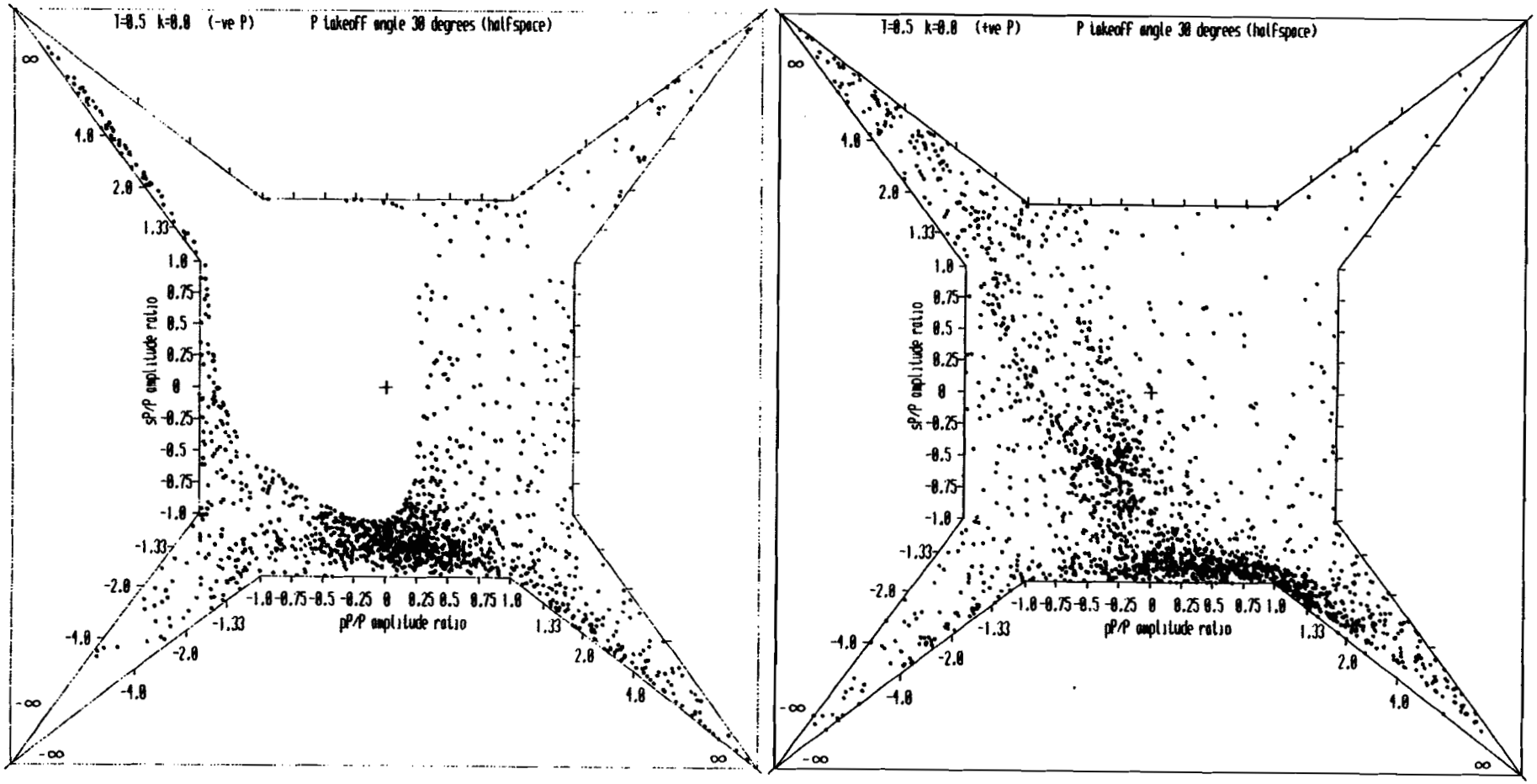
T=0.5 k=0.0 (-ve P)
P takeoff angle 30 degrees (halfspace)
sP/P amplitude ratio
pP/P amplitude ratio
T=0.5 k=0.0 (+ve P)
P takeoff angle 30 degrees (halfspace)
sP/P amplitude ratio
pP/P amplitude ratio

Figure 69

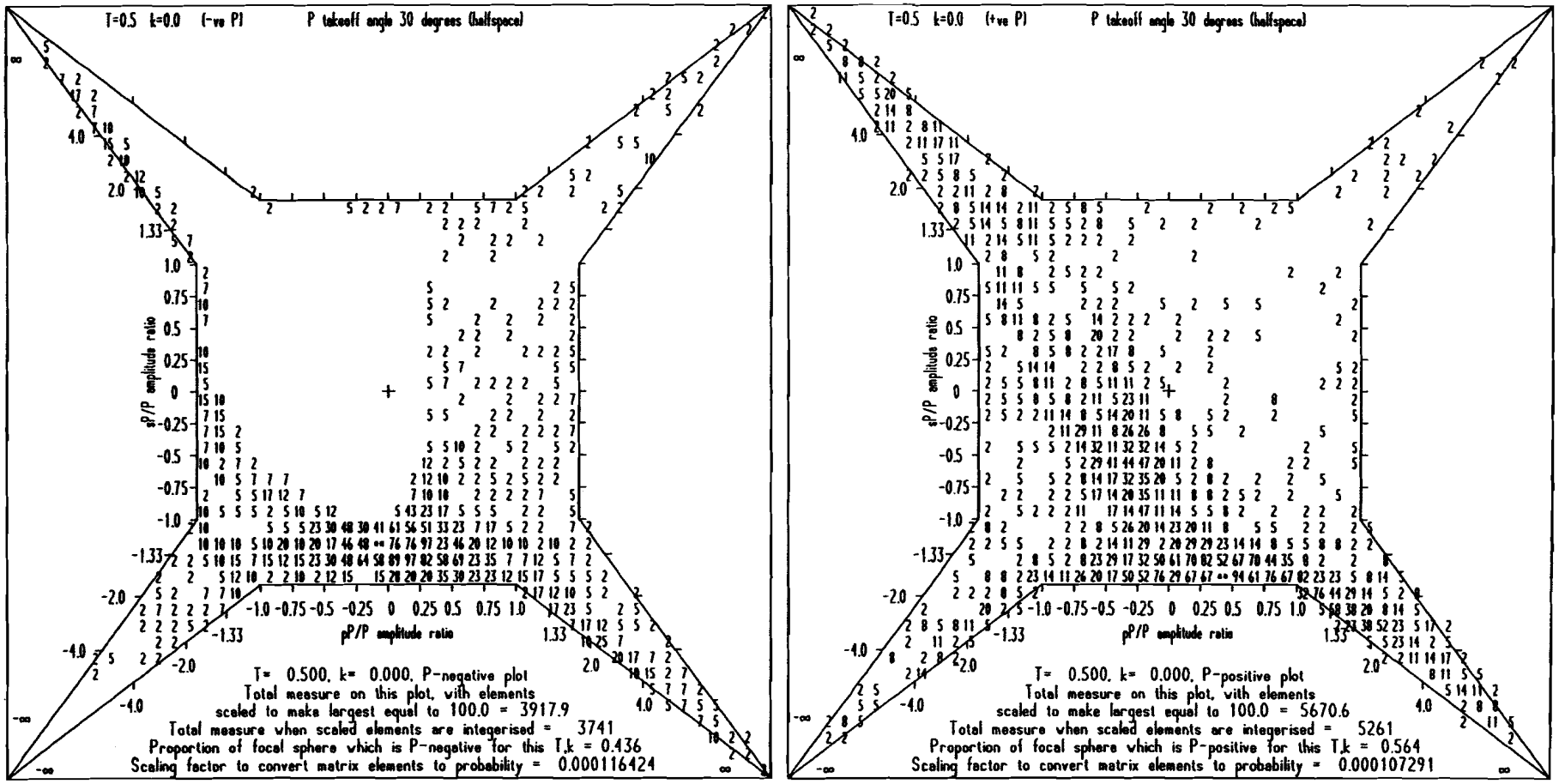

Figure 69 (continued)

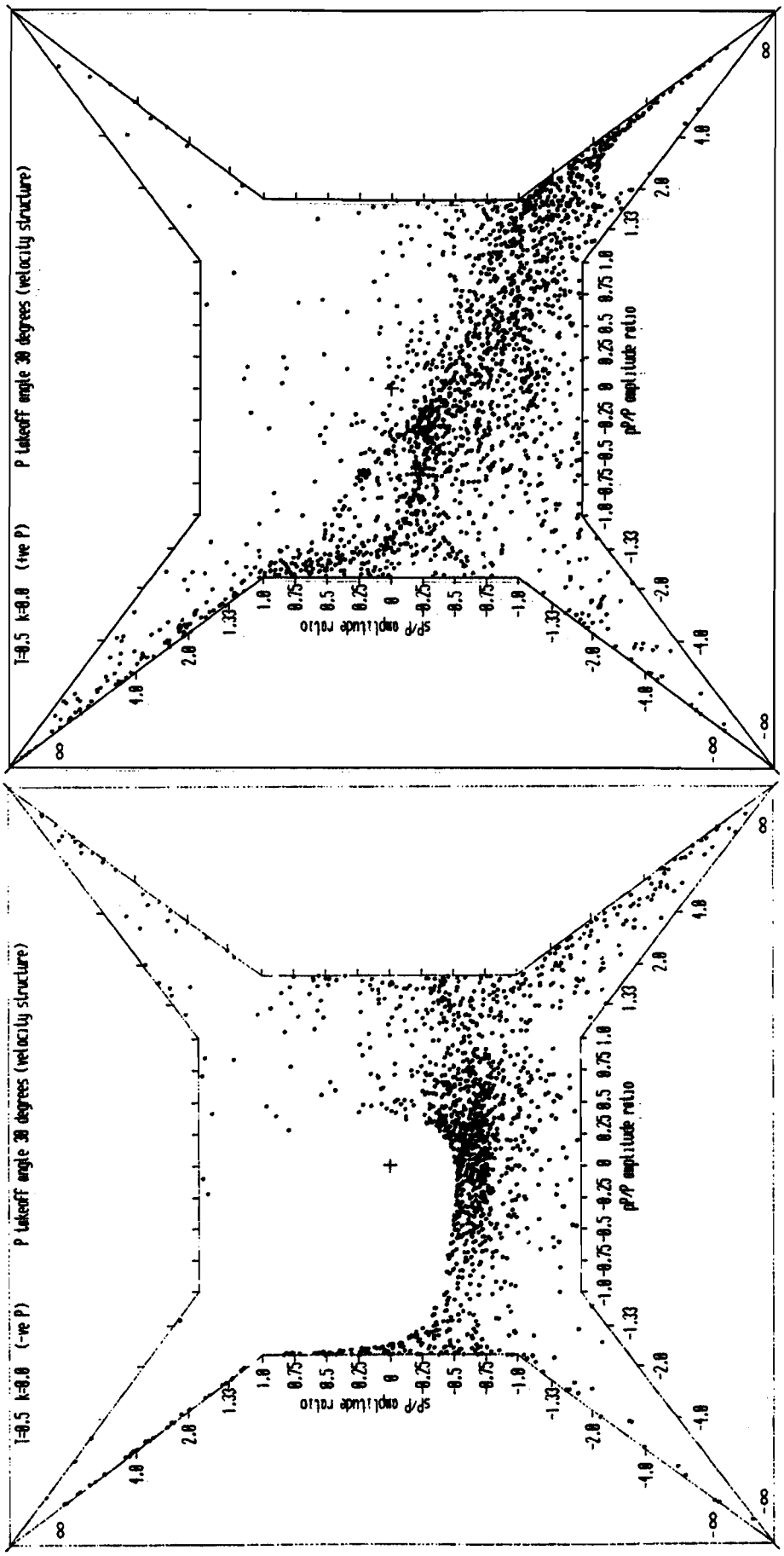
T=0.5 k=0.0 (+ve P)
P takeoff angle 30 degrees (velocity structure)
sP/P amplitude ratio
pP/P amplitude ratio
T=0.5 k=0.0 (-ve P)
P takeoff angle 30 degrees (velocity structure)
sP/P amplitude ratio
pP/P amplitude ratio

Figure 70

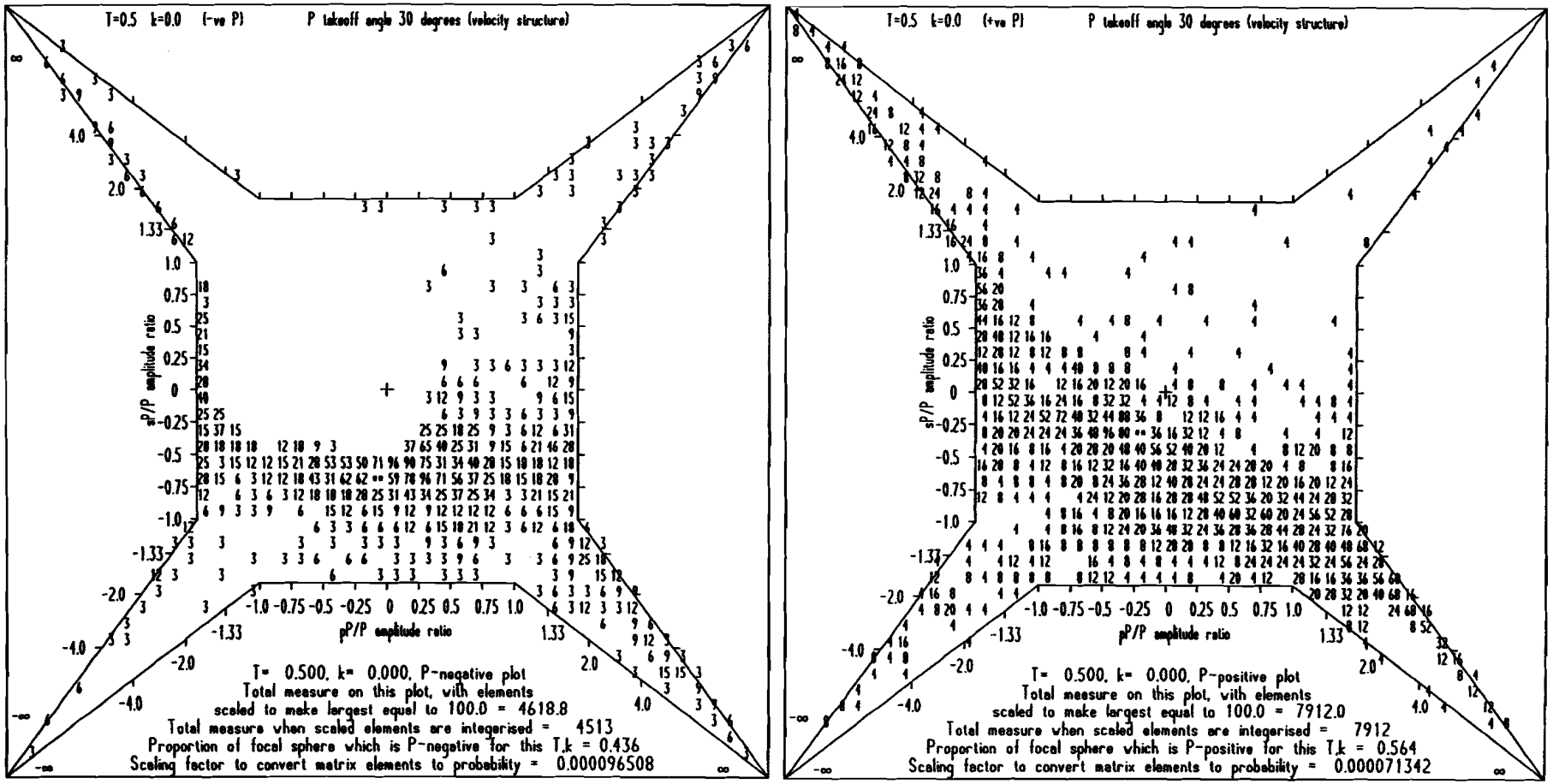

Figure 70 (continued)

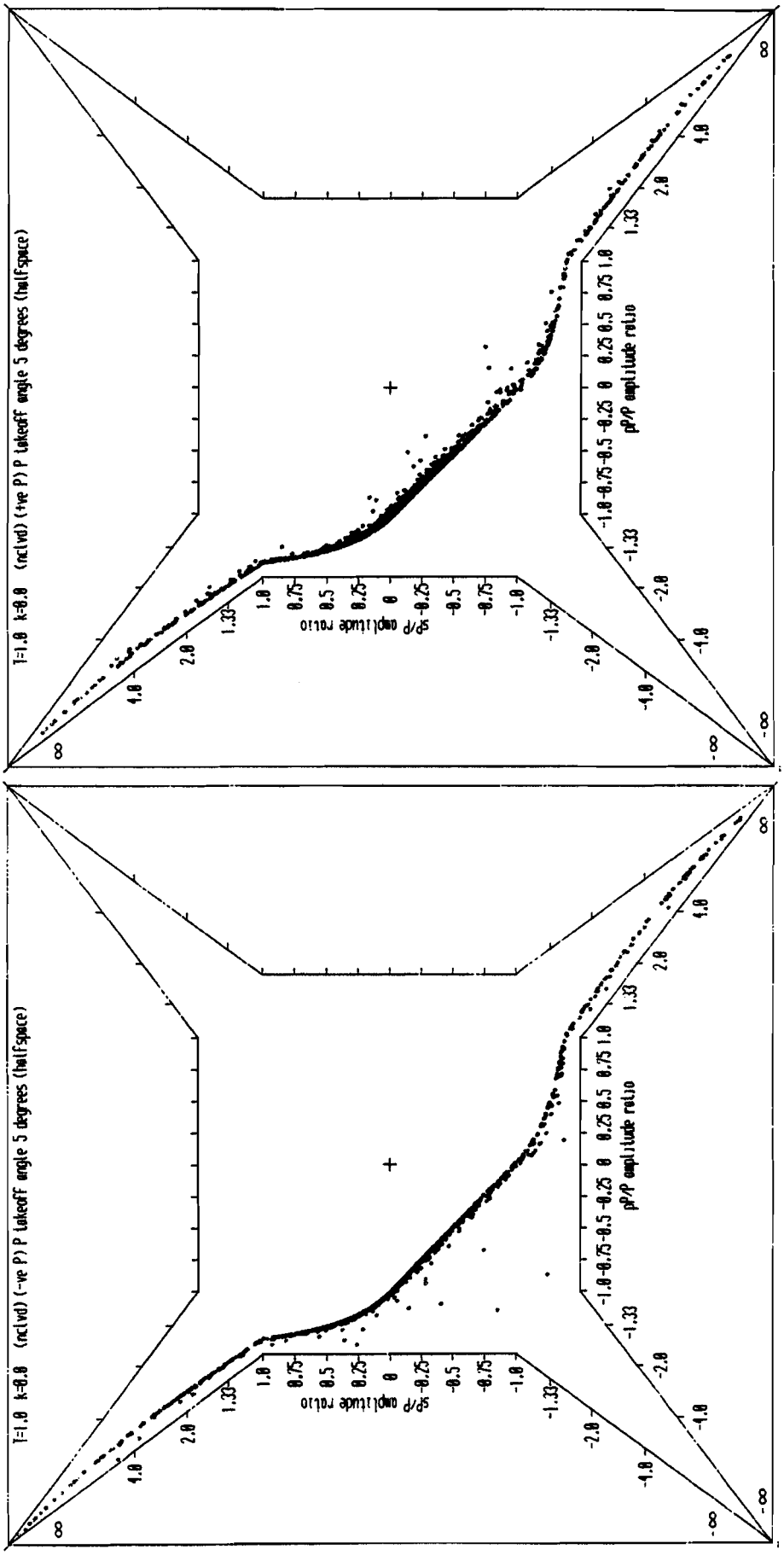
T=1.0 k=0.0 (nclvd) (-ve P) P takeoff angle 5 degrees (halfspace)
T=1.0 k=0.0 (nclvd) (+ve P) P takeoff angle 5 degrees (halfspace)
sP/P amplitude ratio
pP/P amplitude ratio
1.0
0.75
0.5
0.25
0
-0.25
-0.5
-0.75
-1.0
1.33
2.0
-1.33
-2.0
8
-8

Figure 71

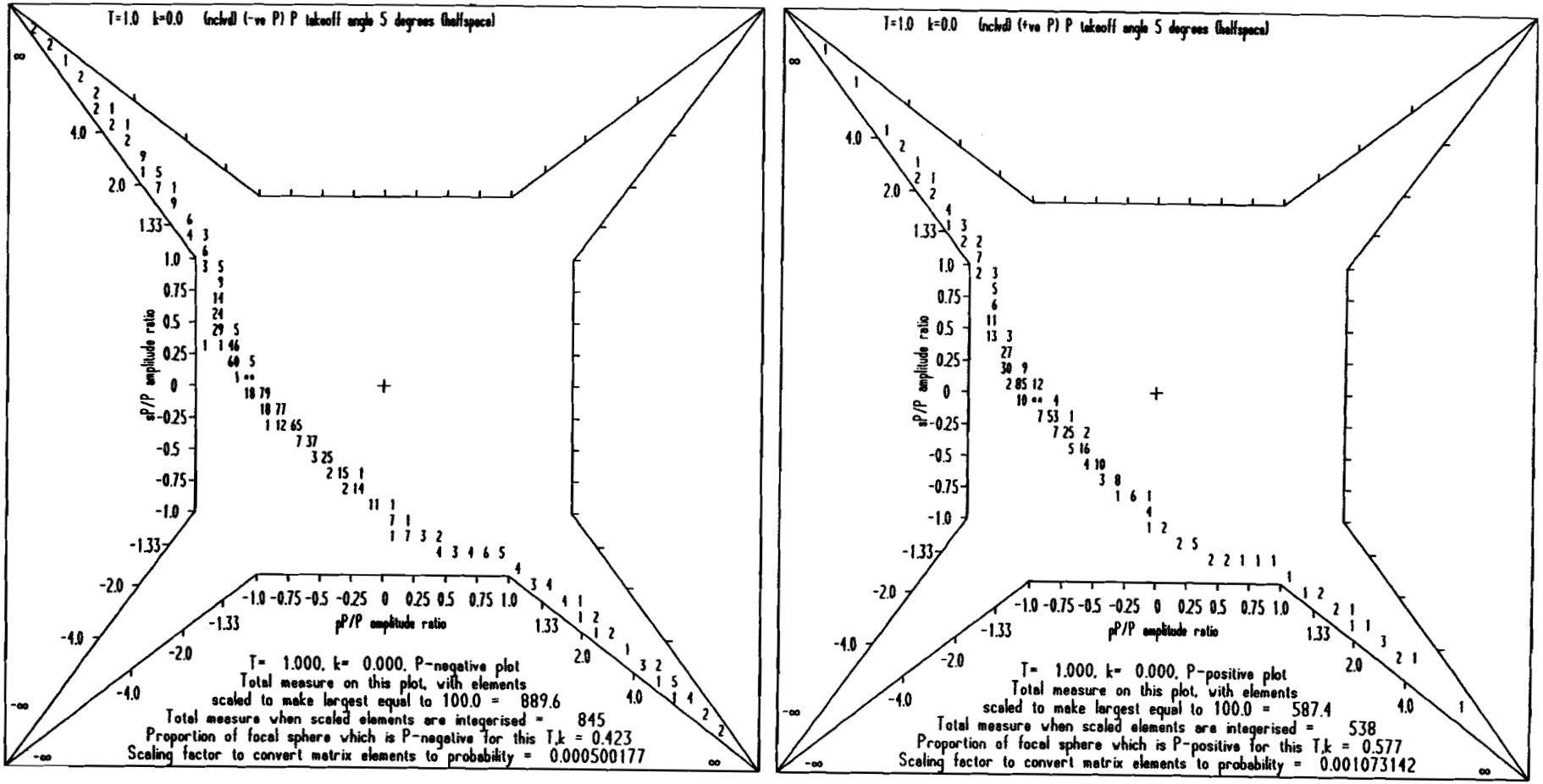

Figure 71 (continued)

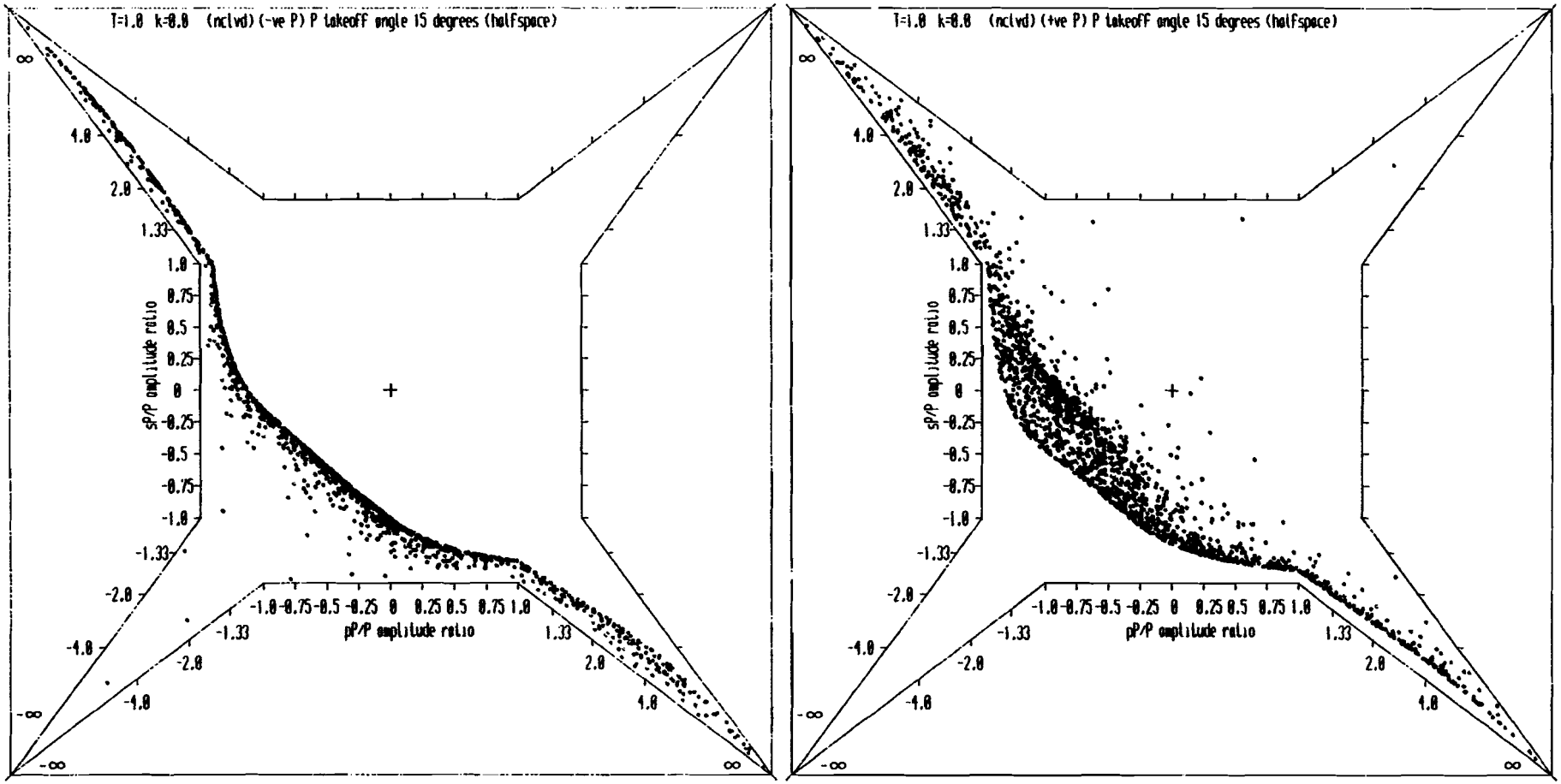
T=1.0 k=0.0 (nclvd) (-ve P) P takeoff angle 15 degrees (halfspace)
T=1.0 k=0.0 (nclvd) (+ve P) P takeoff angle 15 degrees (halfspace)
sP/P amplitude ratio
pP/P amplitude ratio
∞
4.0
2.0
1.33
1.0
0.75
0.5
0.25
0
-0.25
-0.5
-0.75
-1.0
-1.33
-2.0
-4.0
-∞

Figure 72

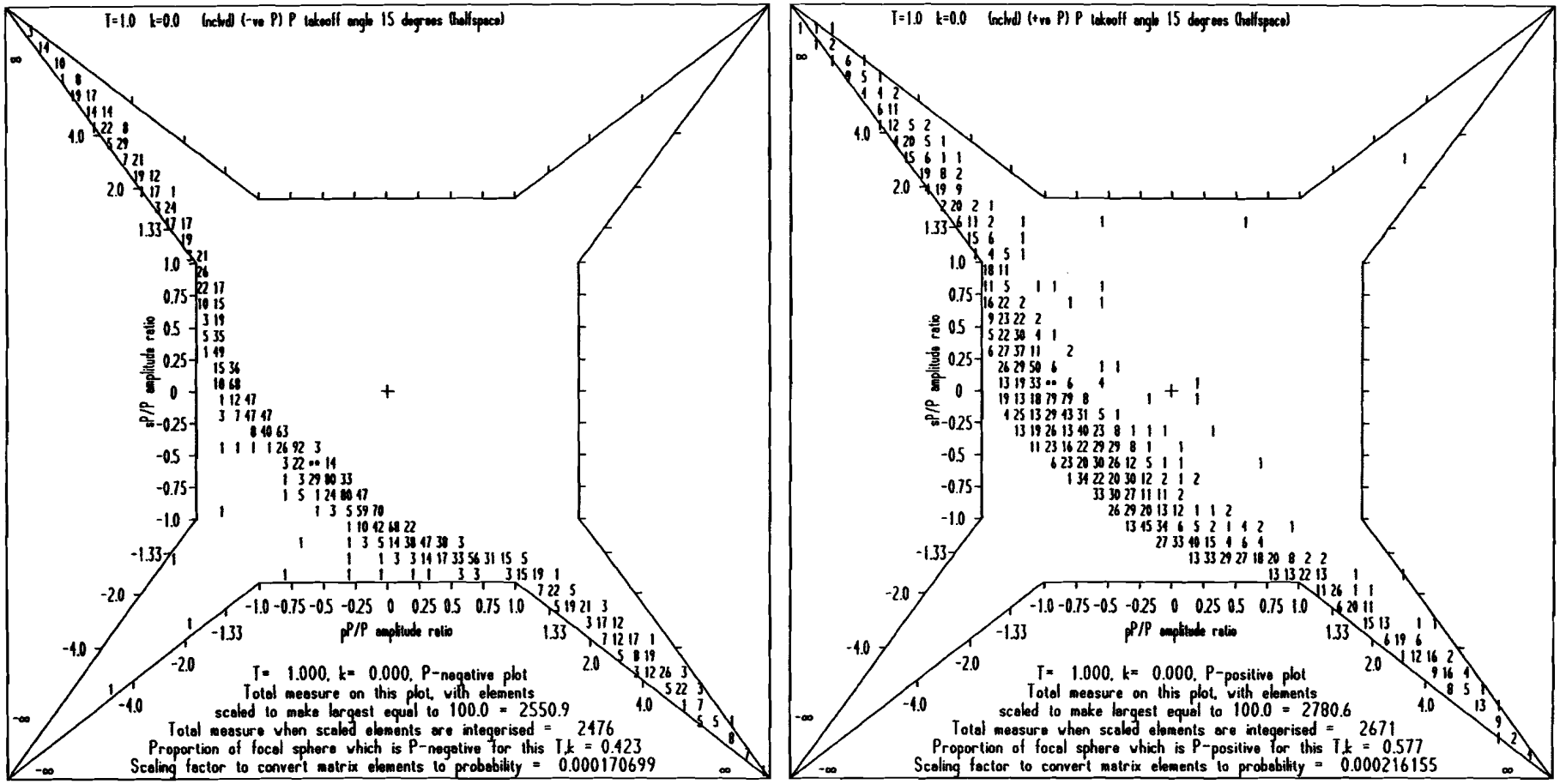

Figure 72 (continued)

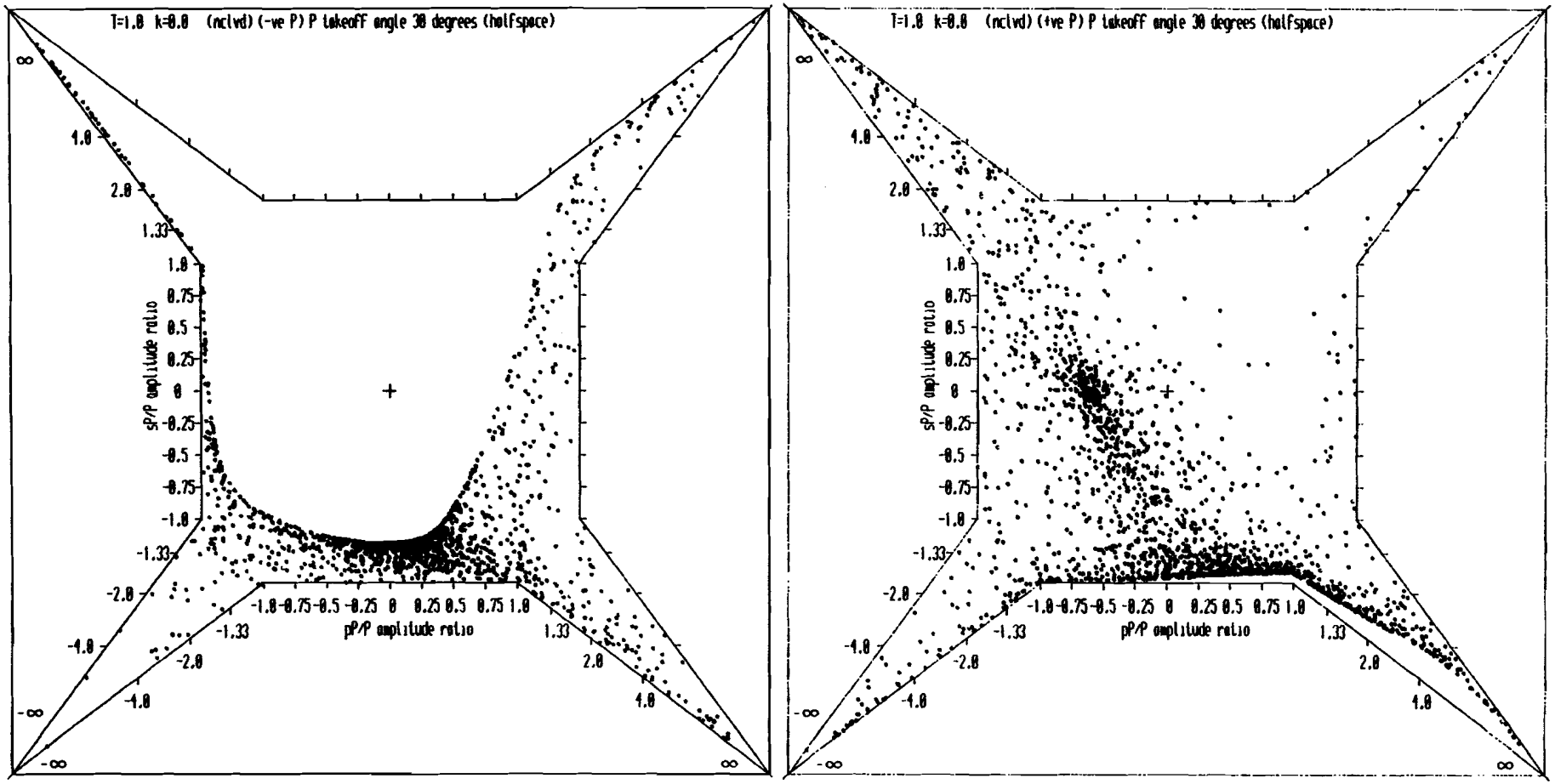
T=1.0 k=0.0 (nclvd) (-ve P) P takeoff angle 30 degrees (halfspace)
T=1.0 k=0.0 (nclvd) (+ve P) P takeoff angle 30 degrees (halfspace)
sP/P amplitude ratio
pP/P amplitude ratio
∞
1.0
2.0
1.33
0.75
0.5
0.25
0
-0.25
-0.5
-0.75
-1.0
-1.33
-2.0
-4.0
-1.0 -0.75 -0.5 -0.25 0 0.25 0.5 0.75 1.0

Figure 73

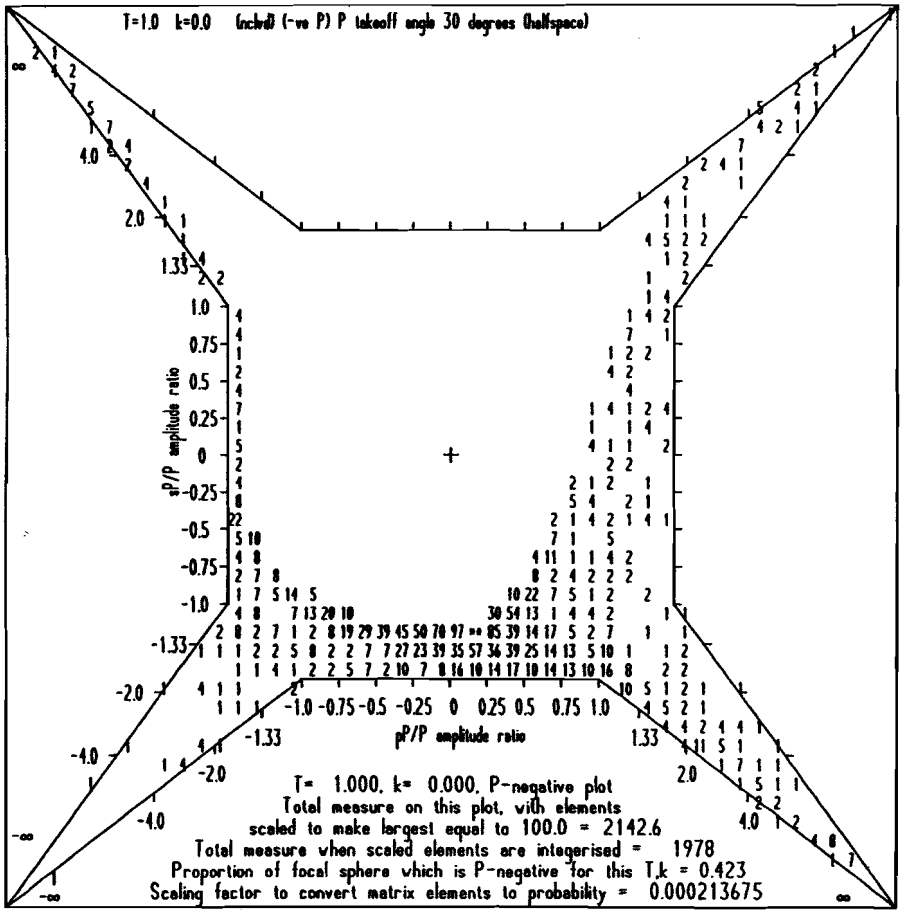

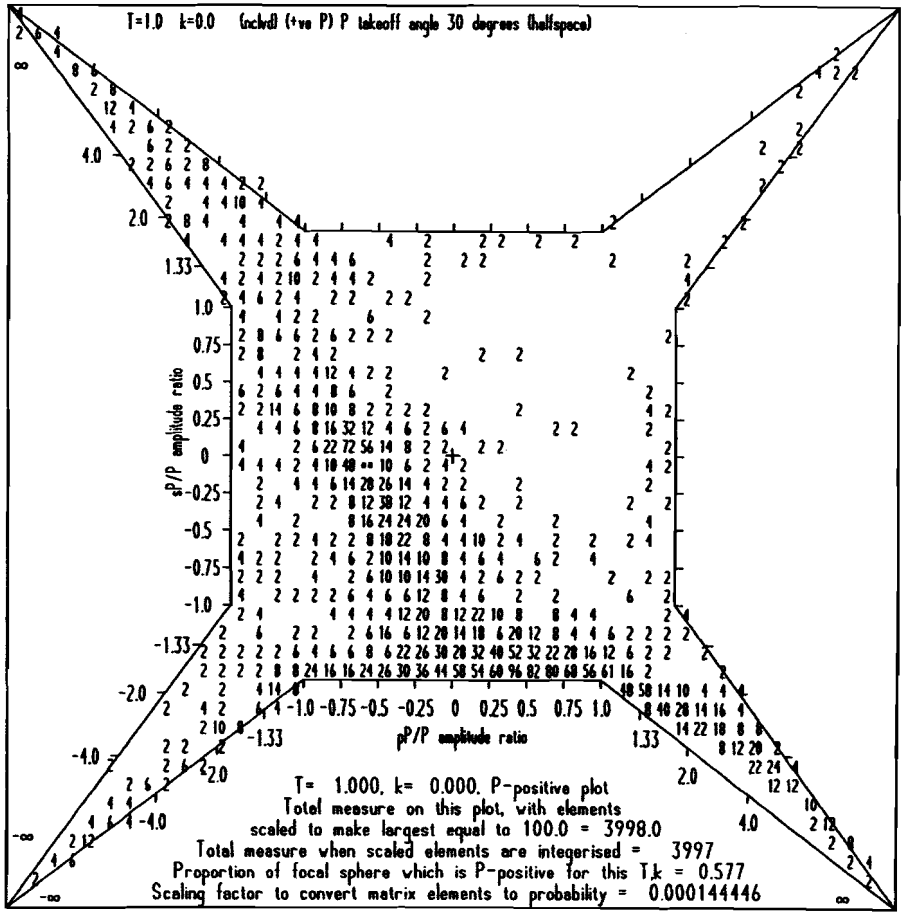

Figure 73 (continued)

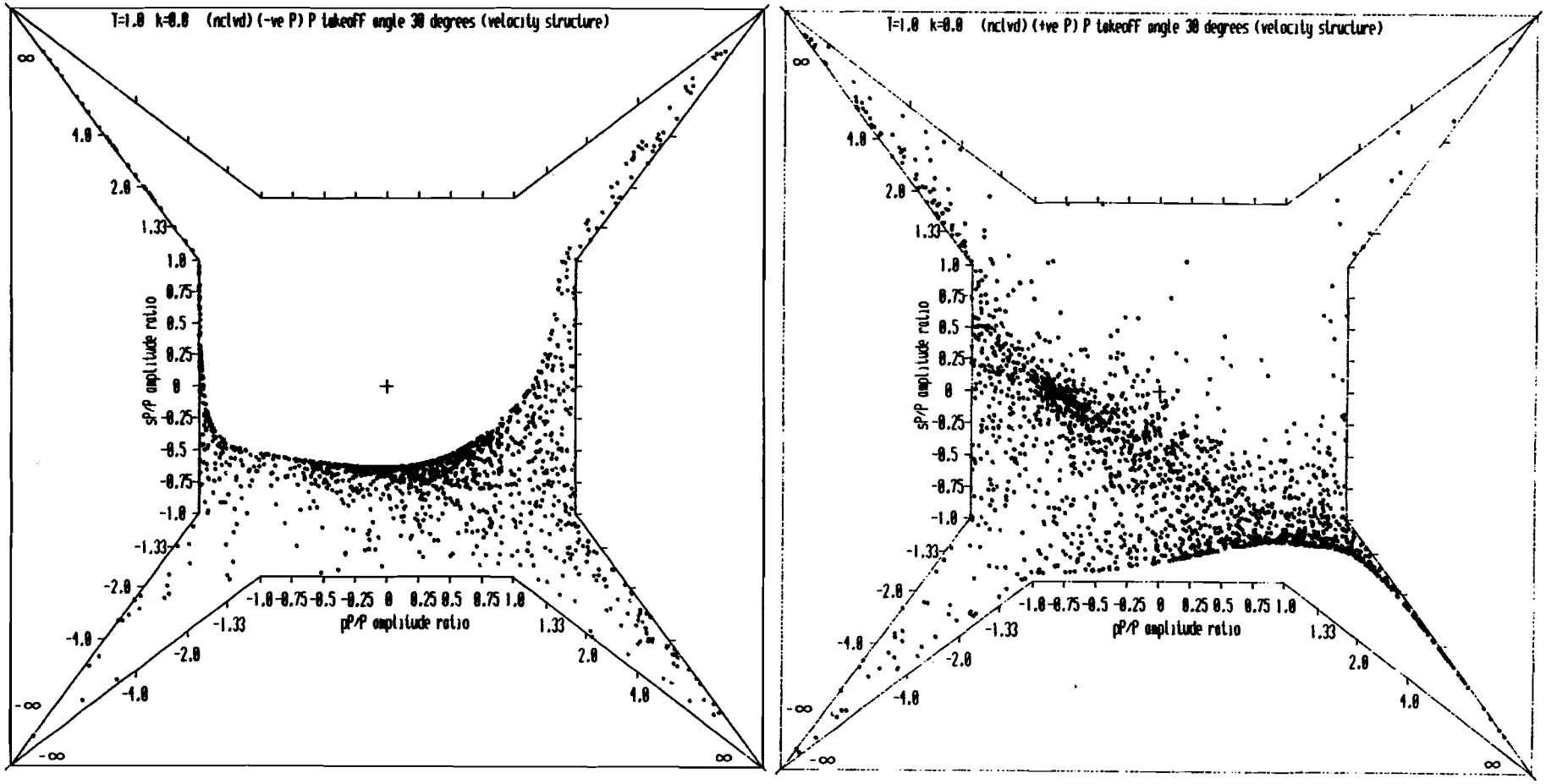
T=1.0 k=0.0 (nclvd) (-ve P) P takeoff angle 30 degrees (velocity structure)
T=1.0 k=0.0 (nclvd) (+ve P) P takeoff angle 30 degrees (velocity structure)
sP/P amplitude ratio
pP/P amplitude ratio
∞
4.0
2.0
1.33
1.0
0.75
0.5
0.25
0
-0.25
-0.5
-0.75
-1.0
-1.33
-2.0
-4.0
-∞
-1.0 -0.75 -0.5 -0.25 0 0.25 0.5 0.75 1.0

Figure 74

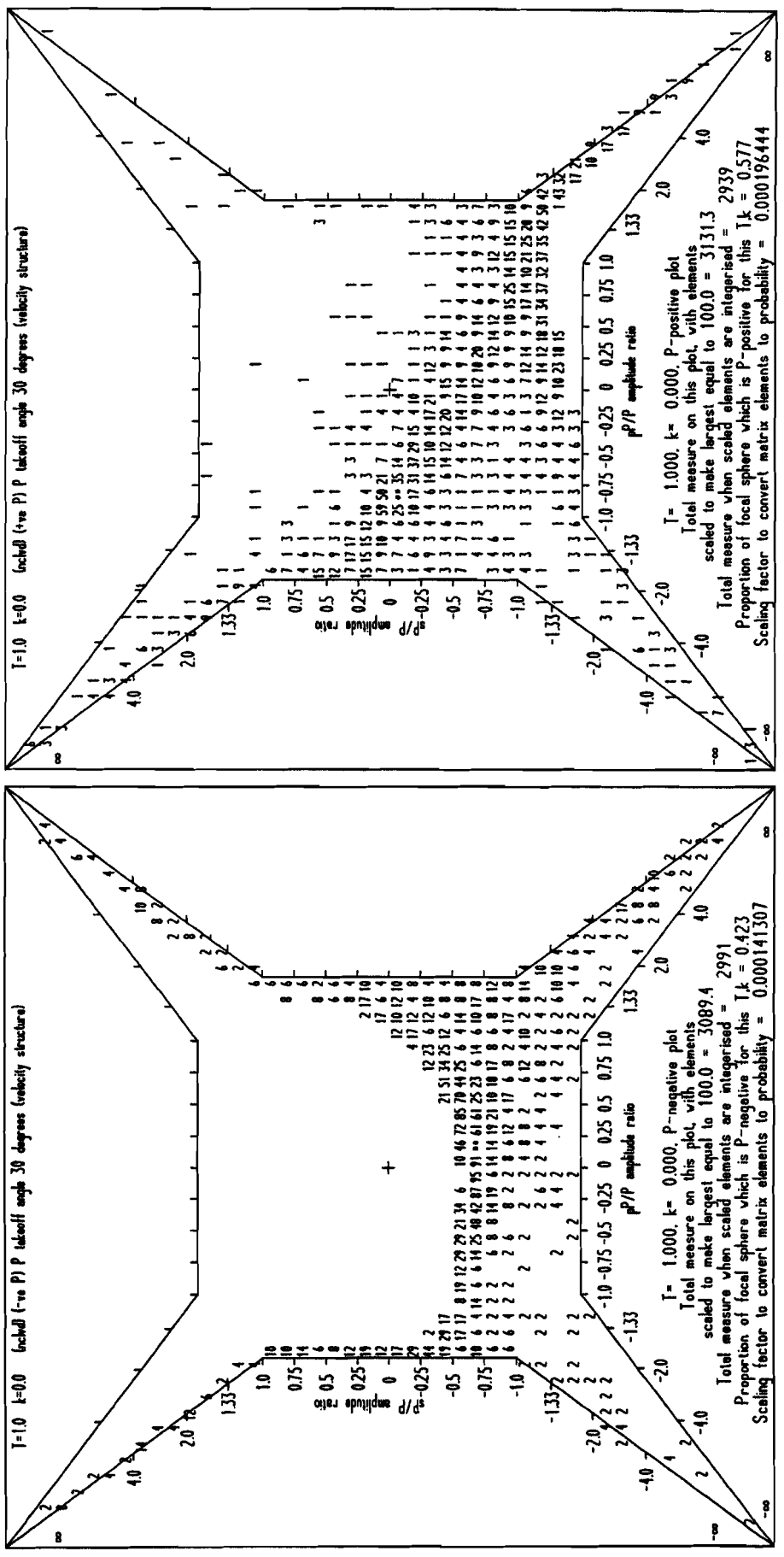

Figure 74 (continued)

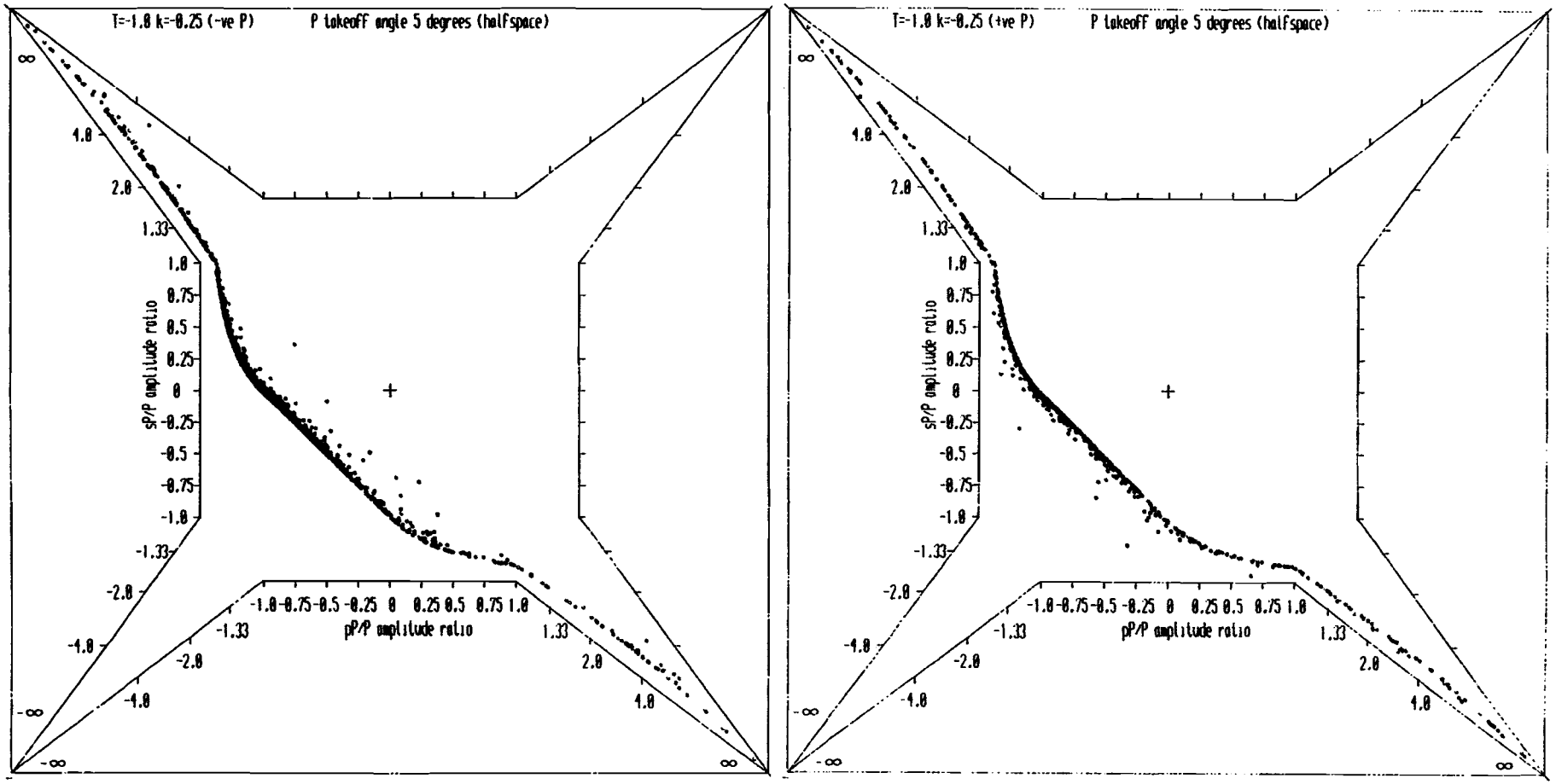
T=-1.0 k=-0.25 (-ve P)
P takeoff angle 5 degrees (halfspace)
sP/P amplitude ratio
pP/P amplitude ratio
T=-1.0 k=-0.25 (+ve P)
P takeoff angle 5 degrees (halfspace)
sP/P amplitude ratio
pP/P amplitude ratio

Figure 75

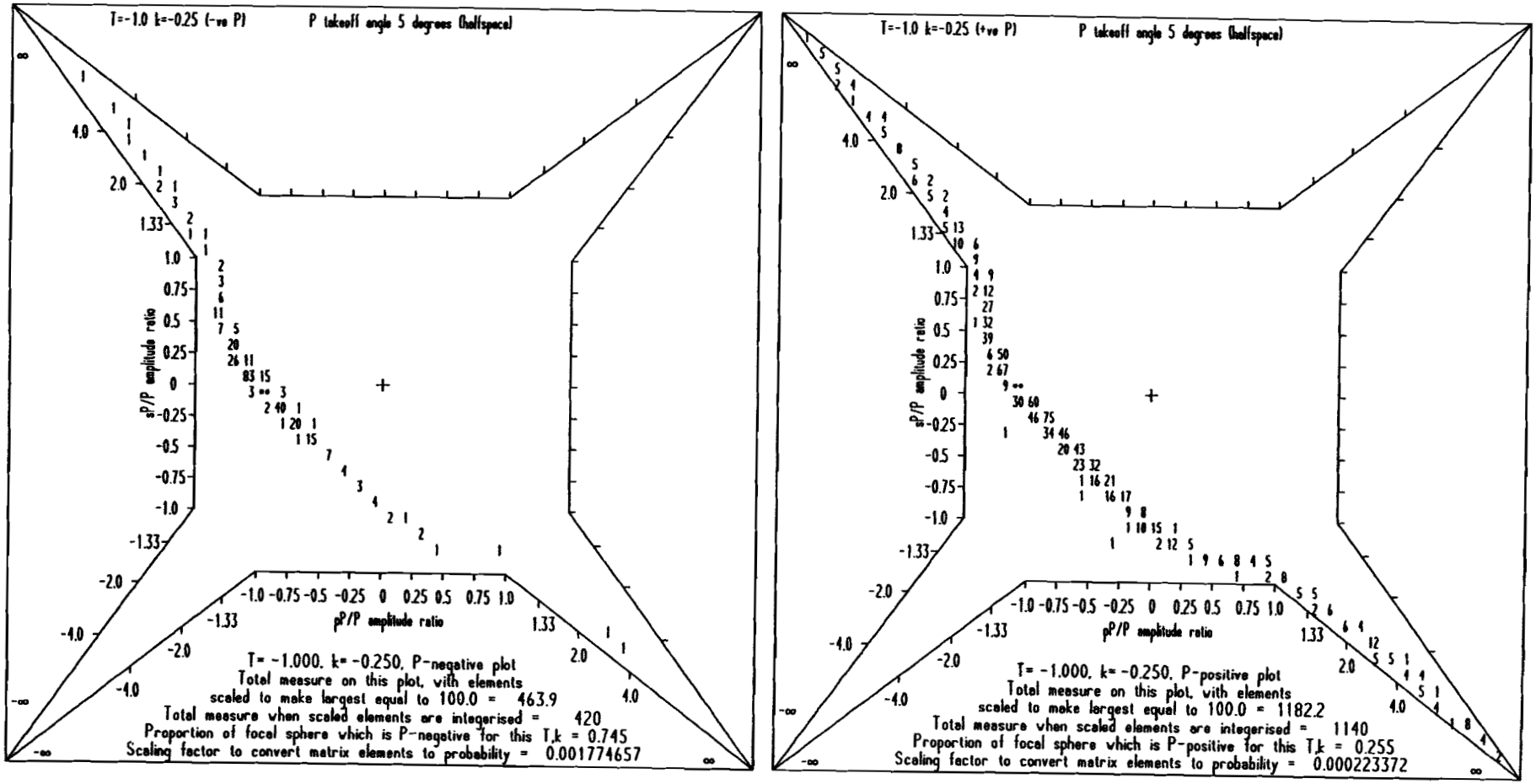

Figure 75 (continued)

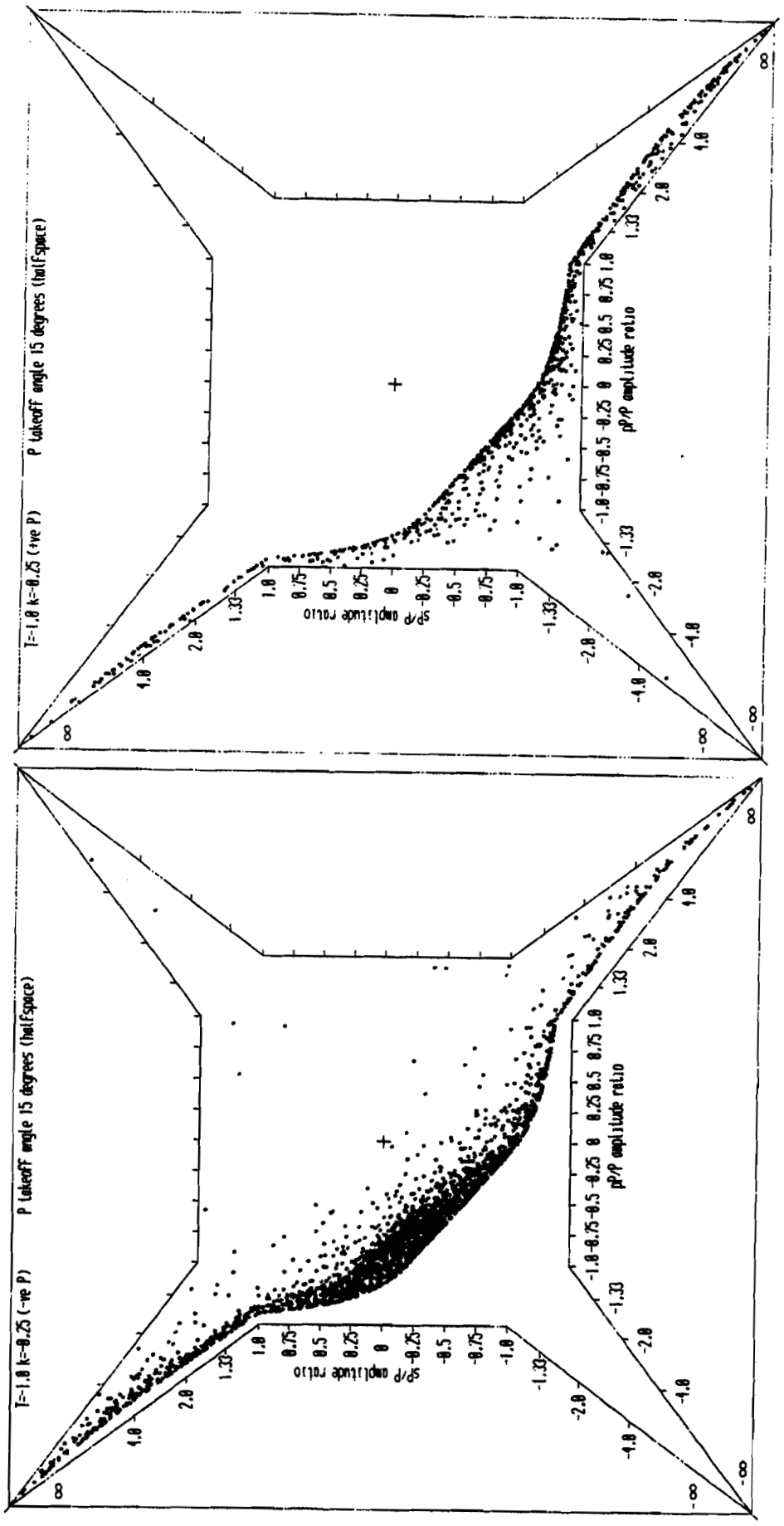
T=-1.0 k=-0.25 (-ve P)
P takeoff angle 15 degrees (halfspace)
sP/P amplitude ratio
pP/P amplitude ratio
T=-1.0 k=-0.25 (+ve P)
P takeoff angle 15 degrees (halfspace)
sP/P amplitude ratio
pP/P amplitude ratio

Figure 76

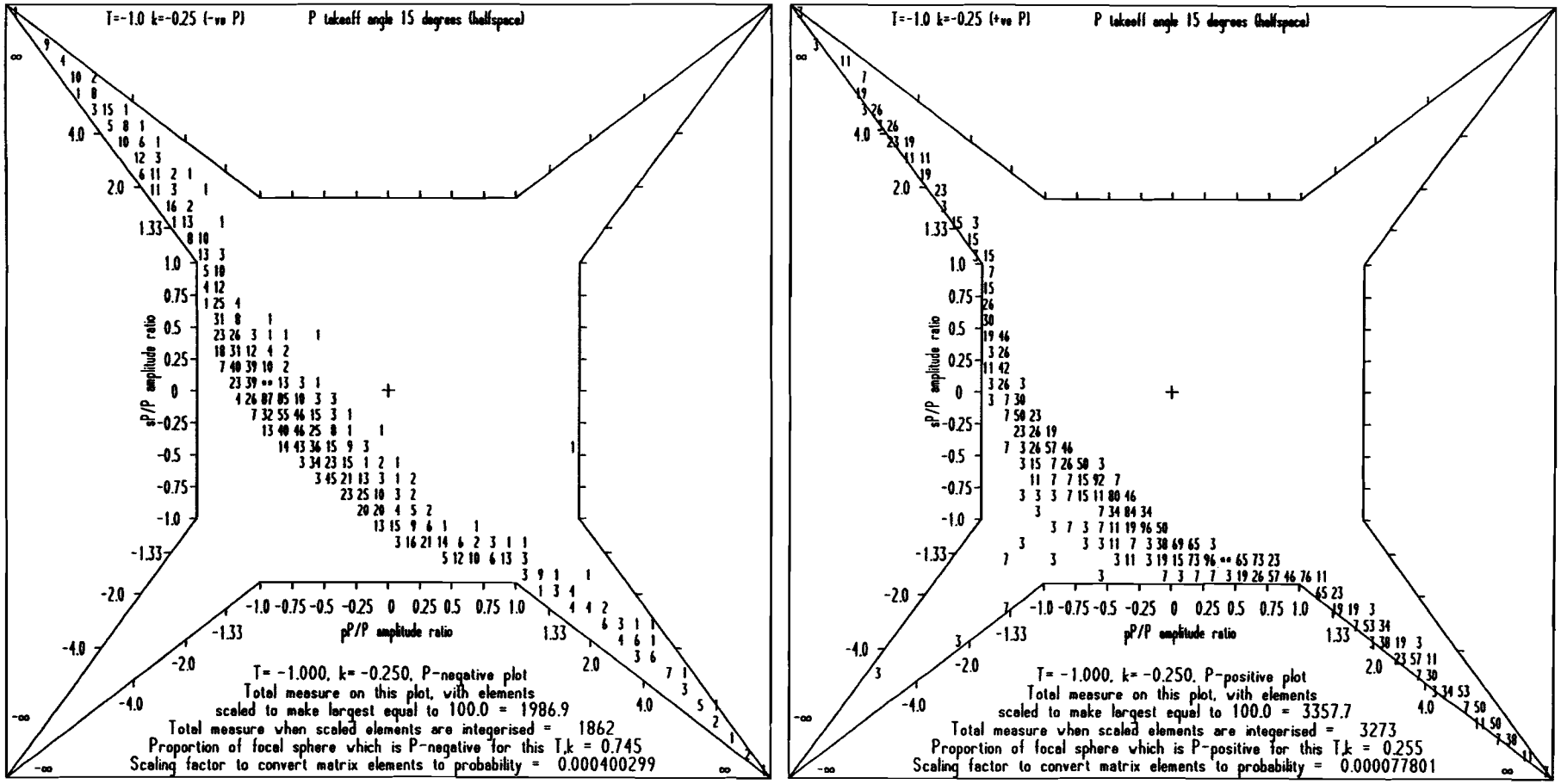

Figure 76 (continued)

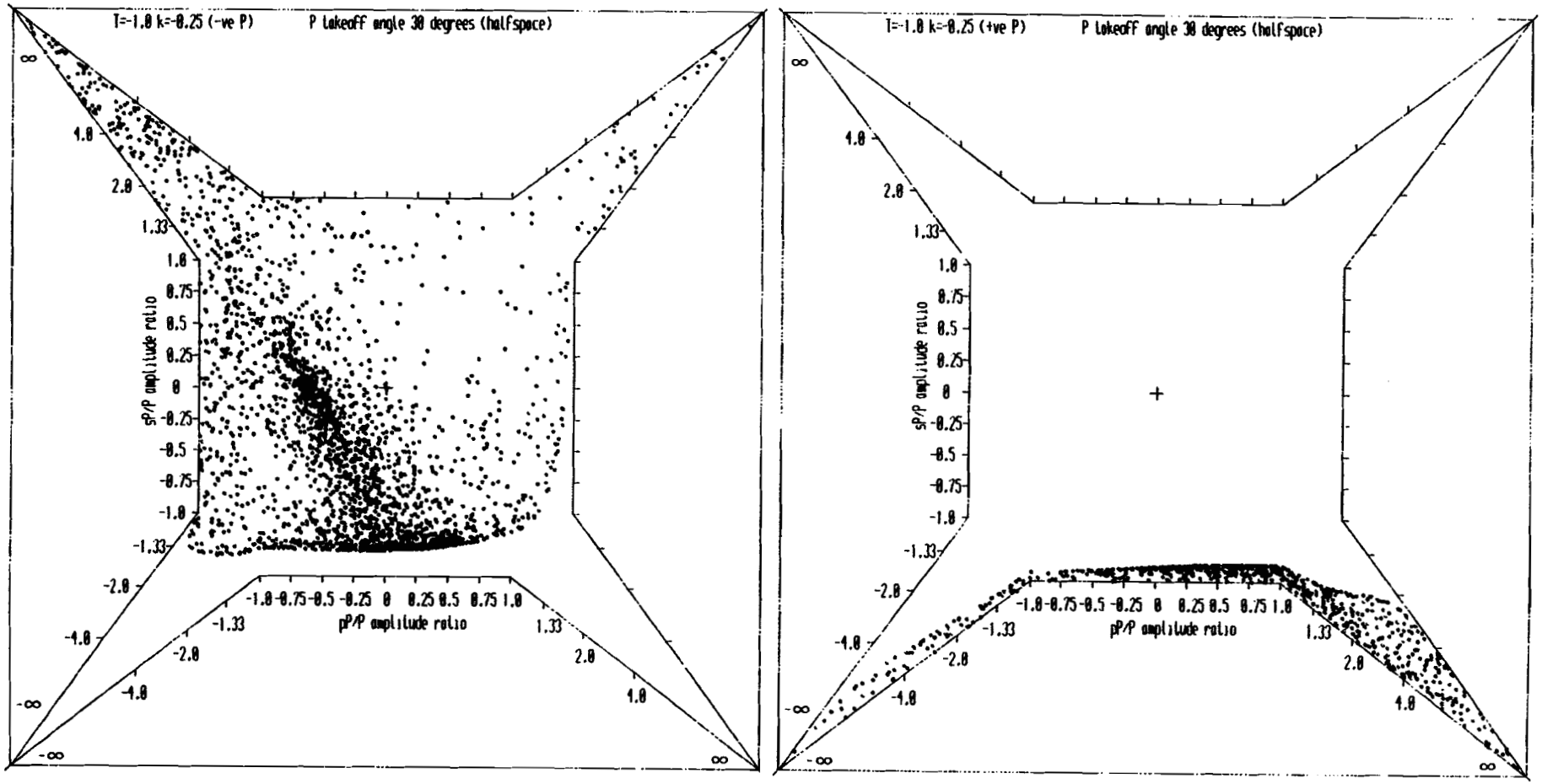
T=-1.0 k=-0.25 (-ve P)
P takeoff angle 30 degrees (halfspace)
sP/P amplitude ratio
pP/P amplitude ratio
T=-1.0 k=-0.25 (+ve P)
P takeoff angle 30 degrees (halfspace)
sP/P amplitude ratio
pP/P amplitude ratio

Figure 77

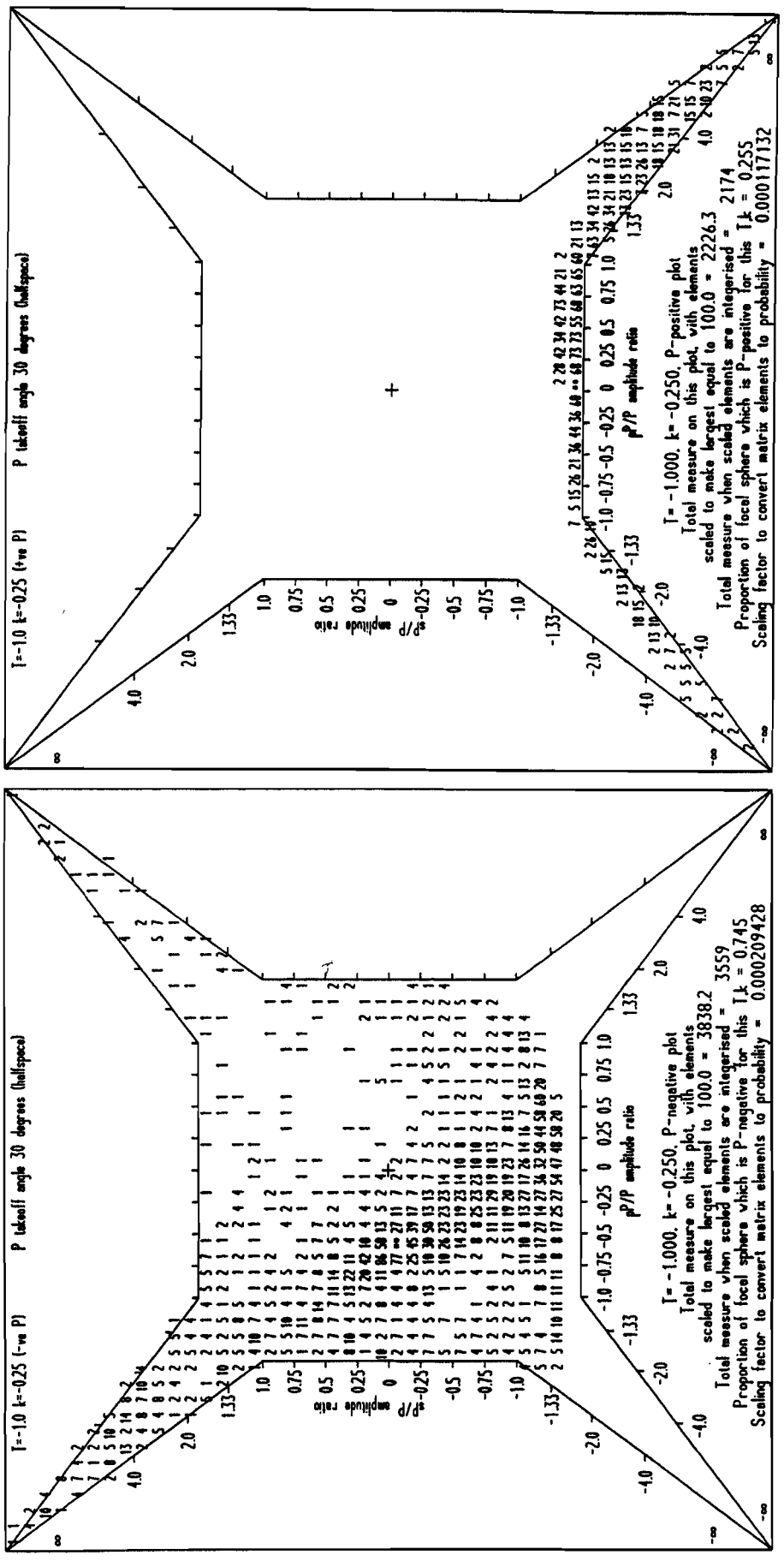

Figure 77 (continued)

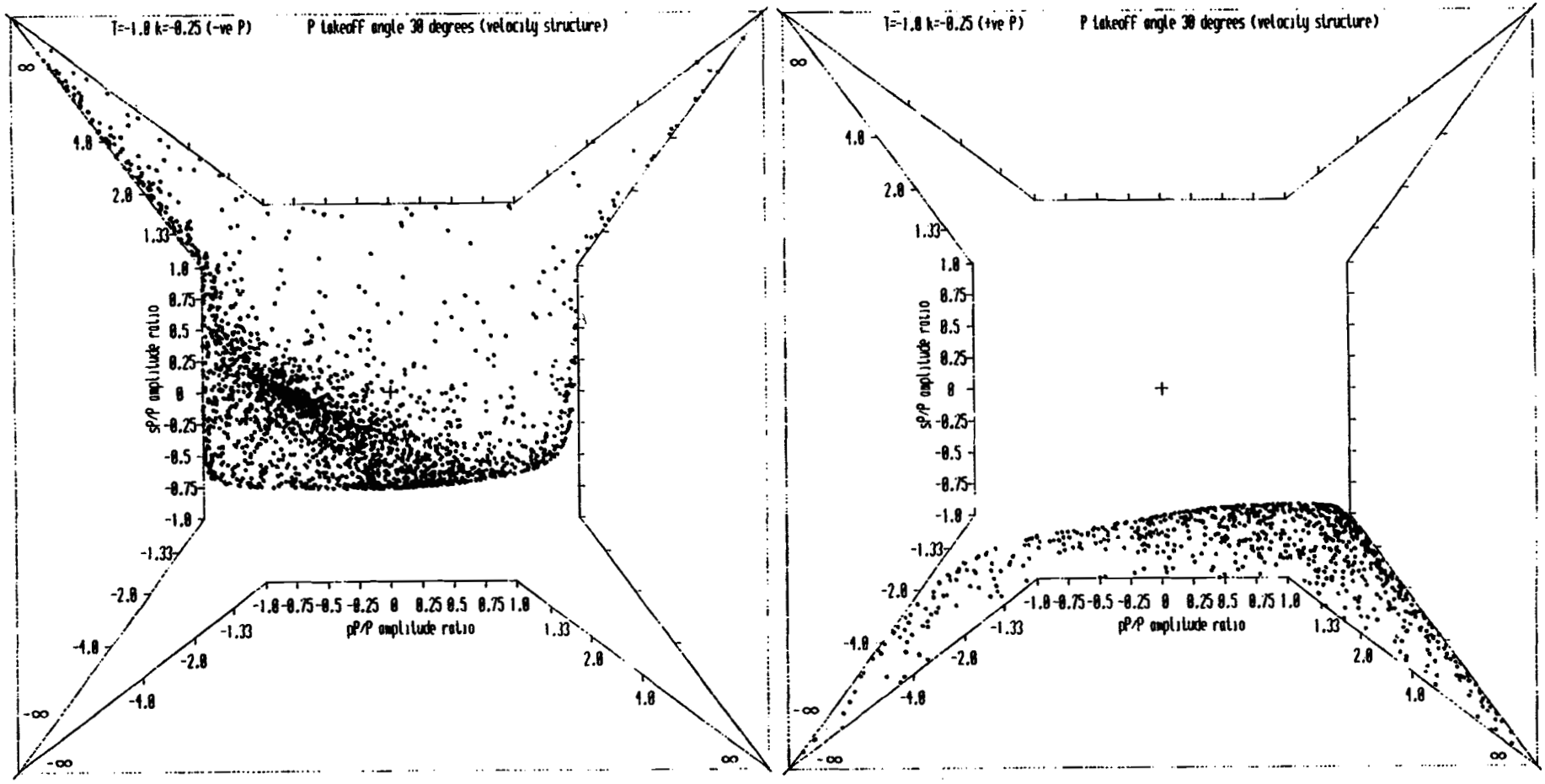
T=-1.0 k=-0.25 (-ve P)
P takeoff angle 30 degrees (velocity structure)
sP/P amplitude ratio
pP/P amplitude ratio
T=-1.0 k=-0.25 (+ve P)
P takeoff angle 30 degrees (velocity structure)
sP/P amplitude ratio
pP/P amplitude ratio

Figure 78

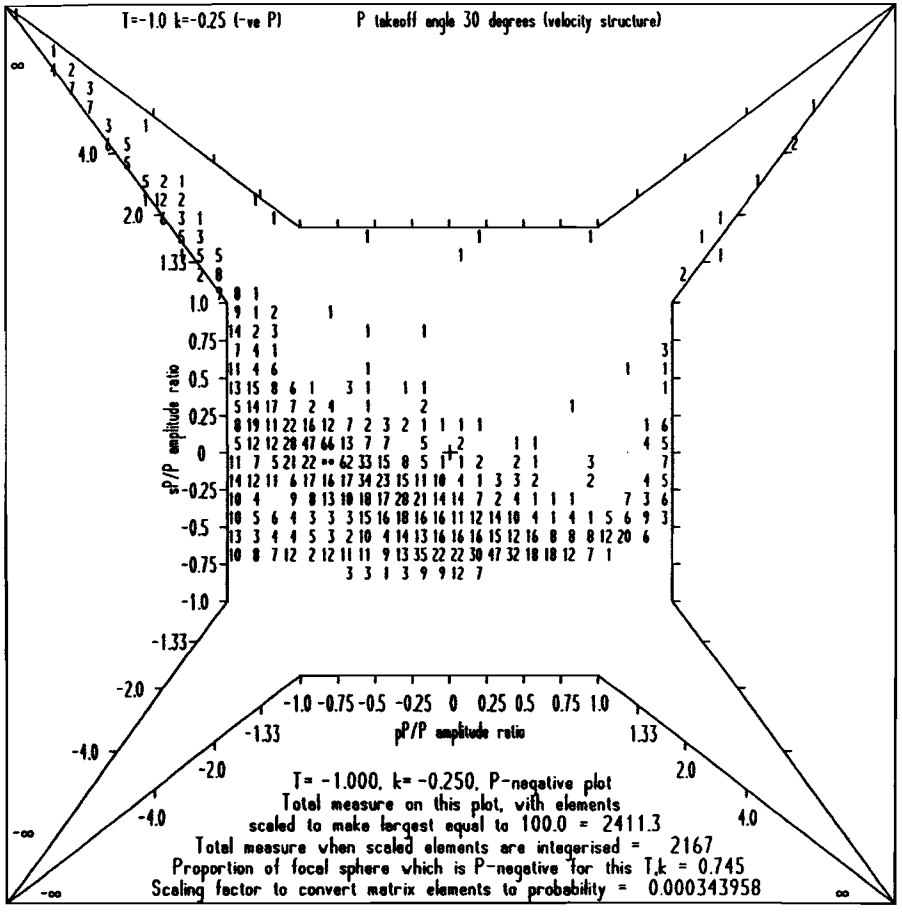

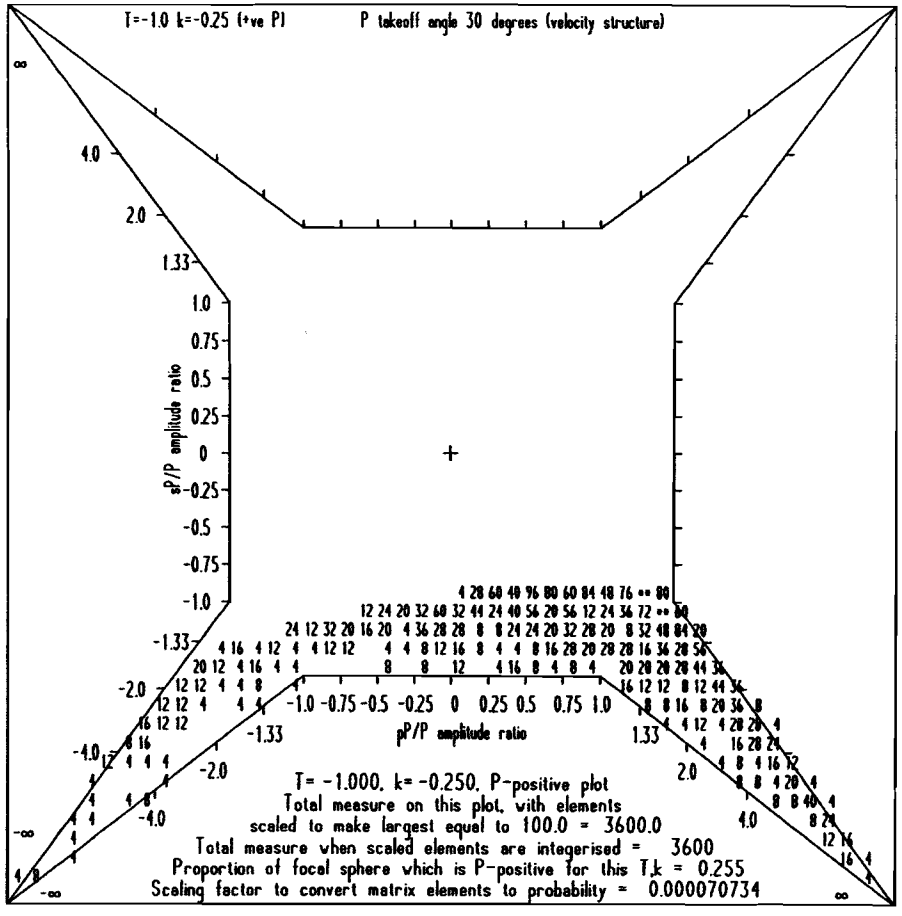

Figure 78 (continued)

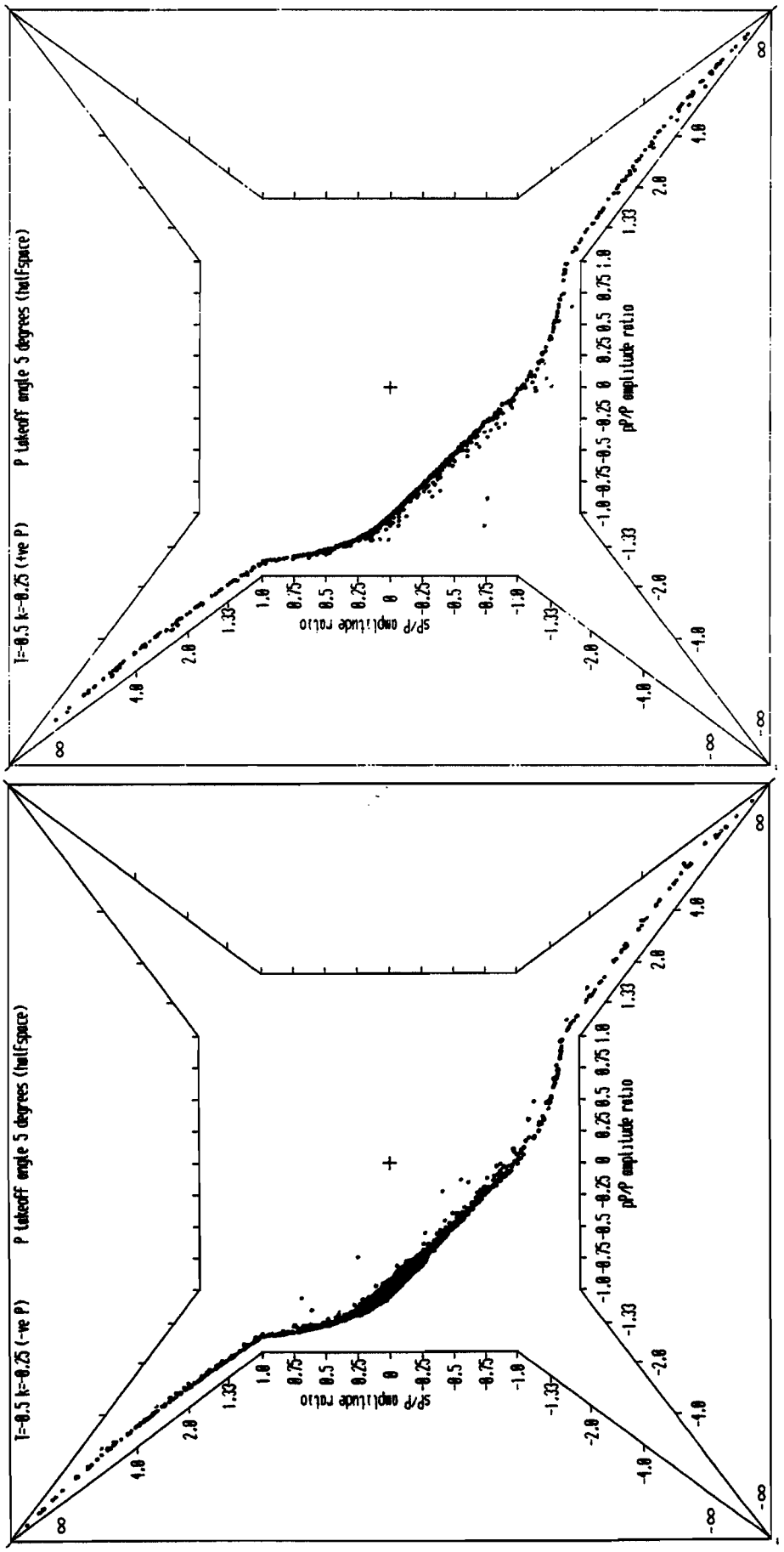
I=-0.5 k=-0.25 (+ve P)
P takeoff angle 5 degrees (halfspace)
I=-0.5 k=-0.25 (-ve P)
P takeoff angle 5 degrees (halfspace)
SP/P amplitude ratio
pP/P amplitude ratio

Figure 79

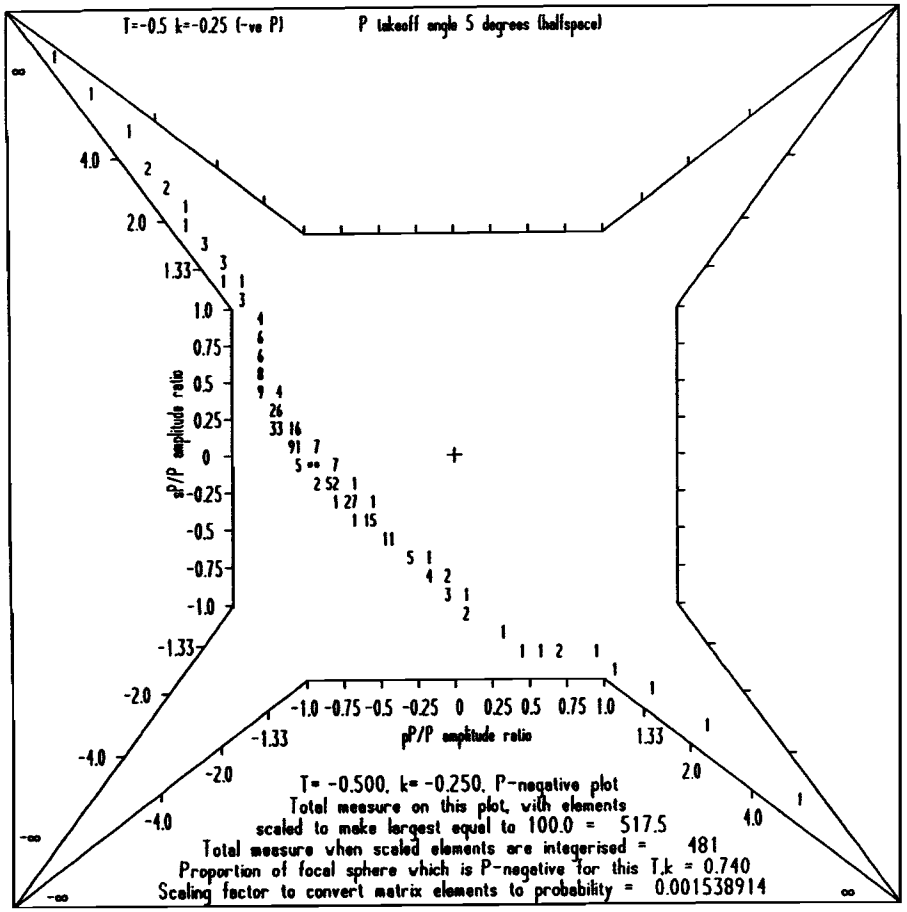

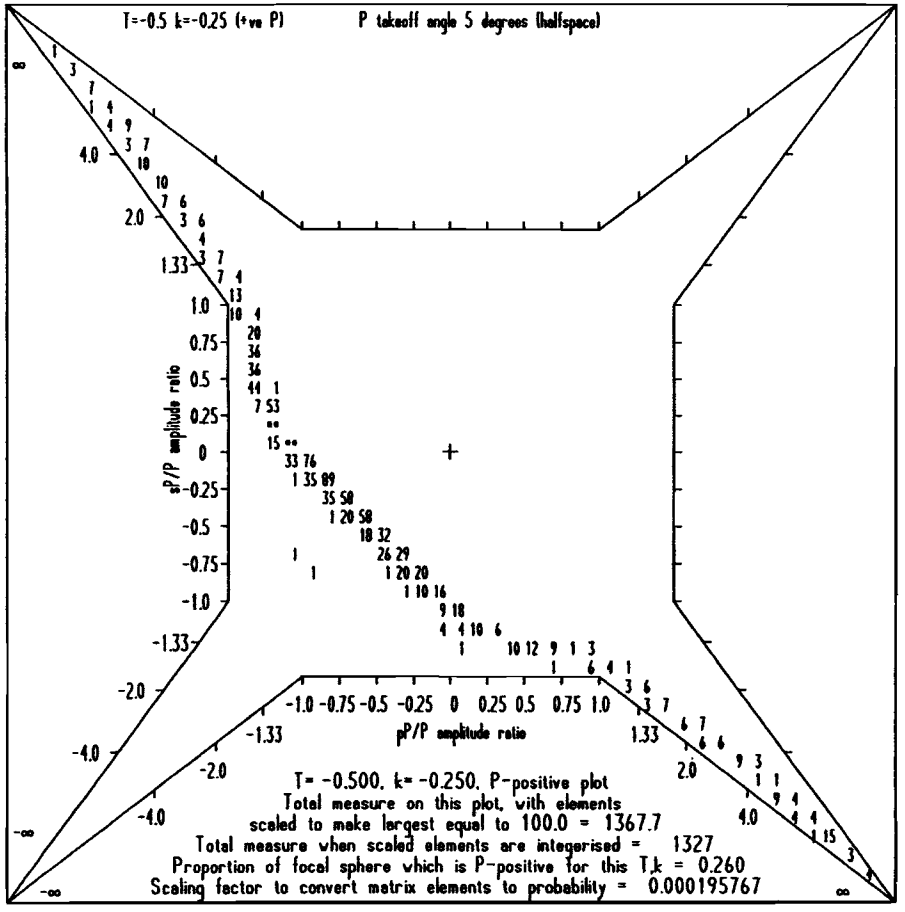

Figure 79 (continued)

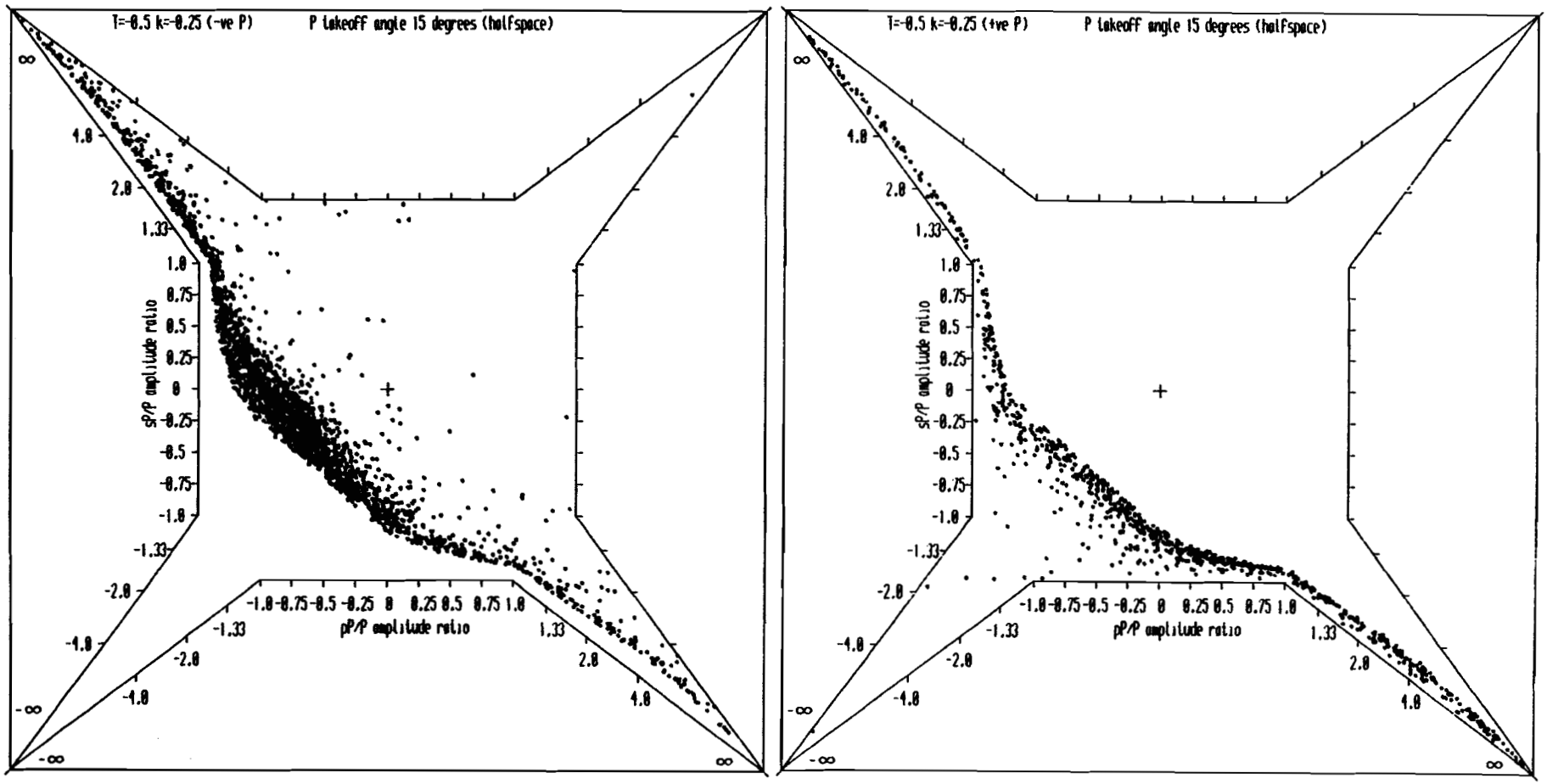
T=-0.5 k=-0.25 (-ve P)
P takeoff angle 15 degrees (halfspace)
sP/P amplitude ratio
pP/P amplitude ratio
T=-0.5 k=-0.25 (+ve P)
P takeoff angle 15 degrees (halfspace)
sP/P amplitude ratio
pP/P amplitude ratio

Figure 80

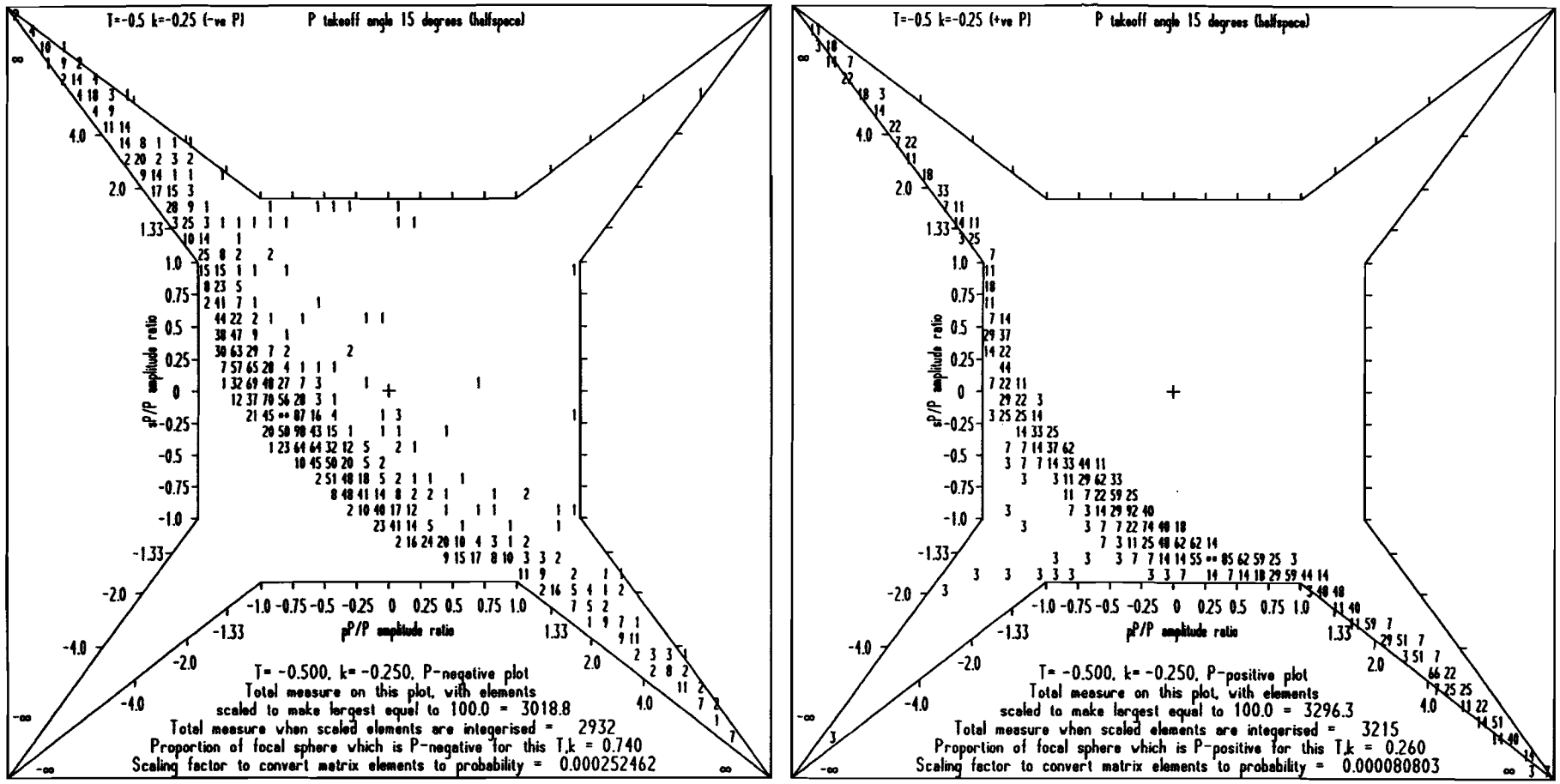

Figure 80 (continued)

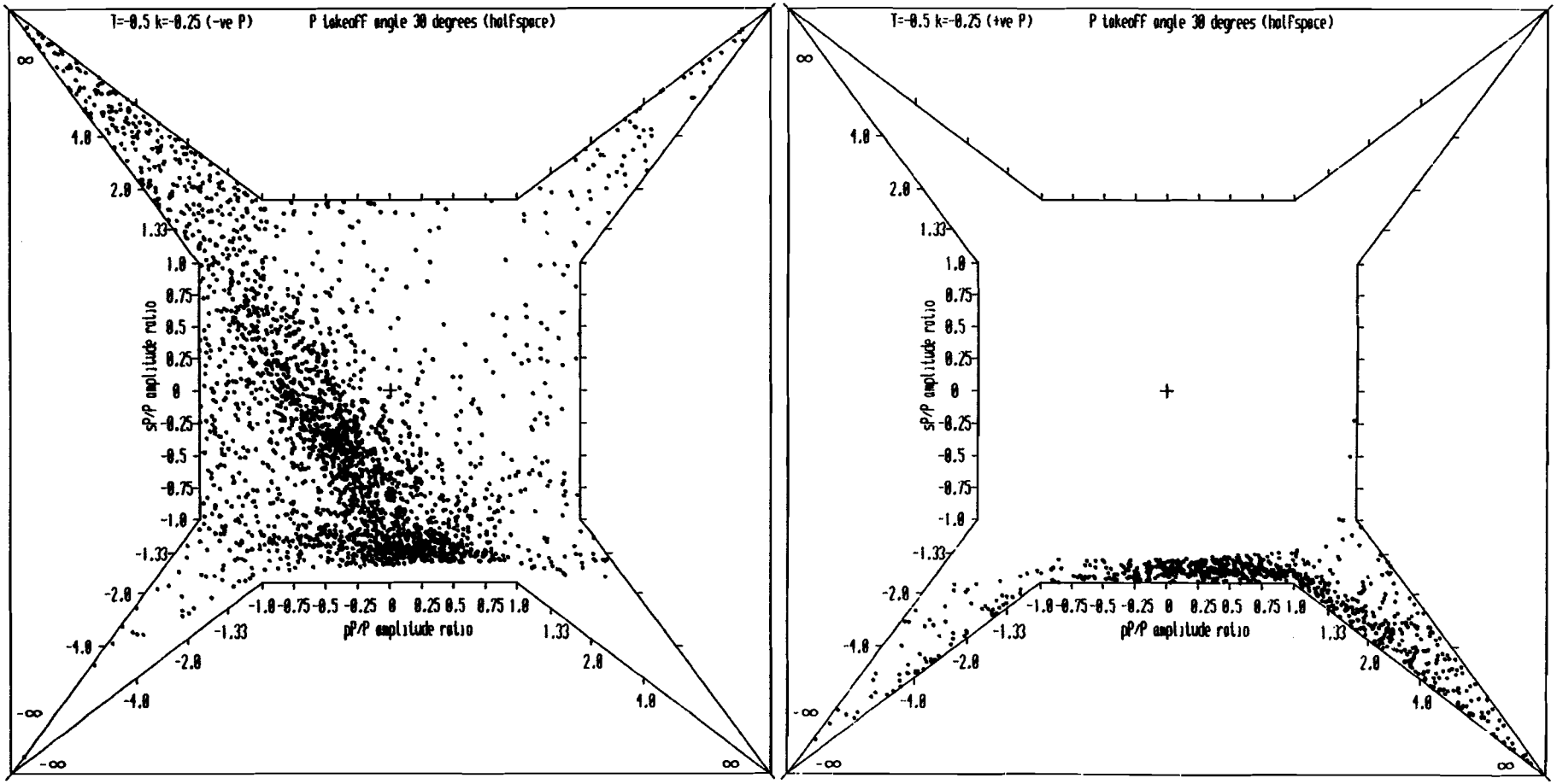
T=-0.5 k=-0.25 (-ve P)
P takeoff angle 30 degrees (halfspace)
sP/P amplitude ratio
pP/P amplitude ratio
T=-0.5 k=-0.25 (+ve P)
P takeoff angle 30 degrees (halfspace)
sP/P amplitude ratio
pP/P amplitude ratio

Figure 81

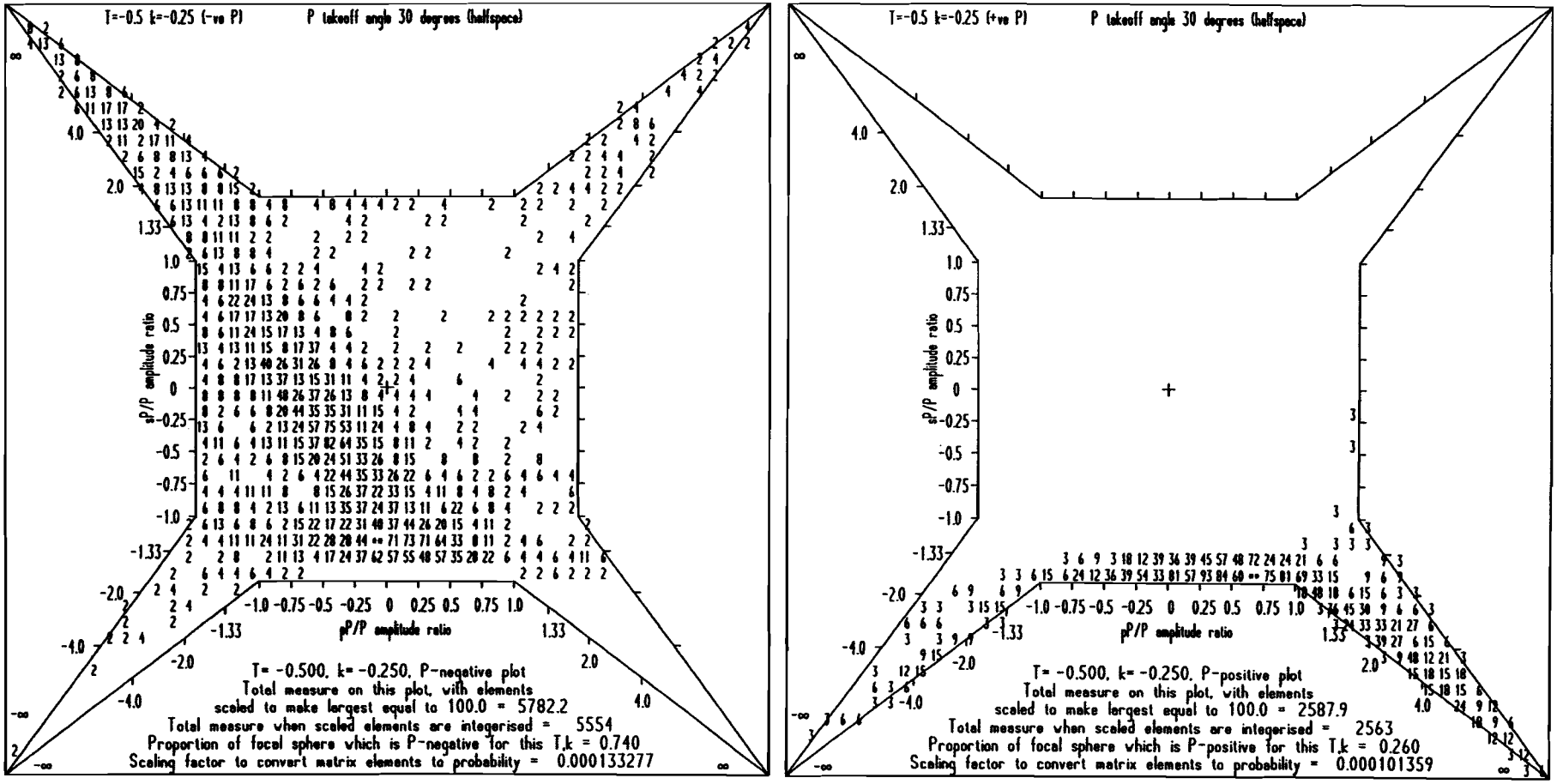

Figure 81 (continued)

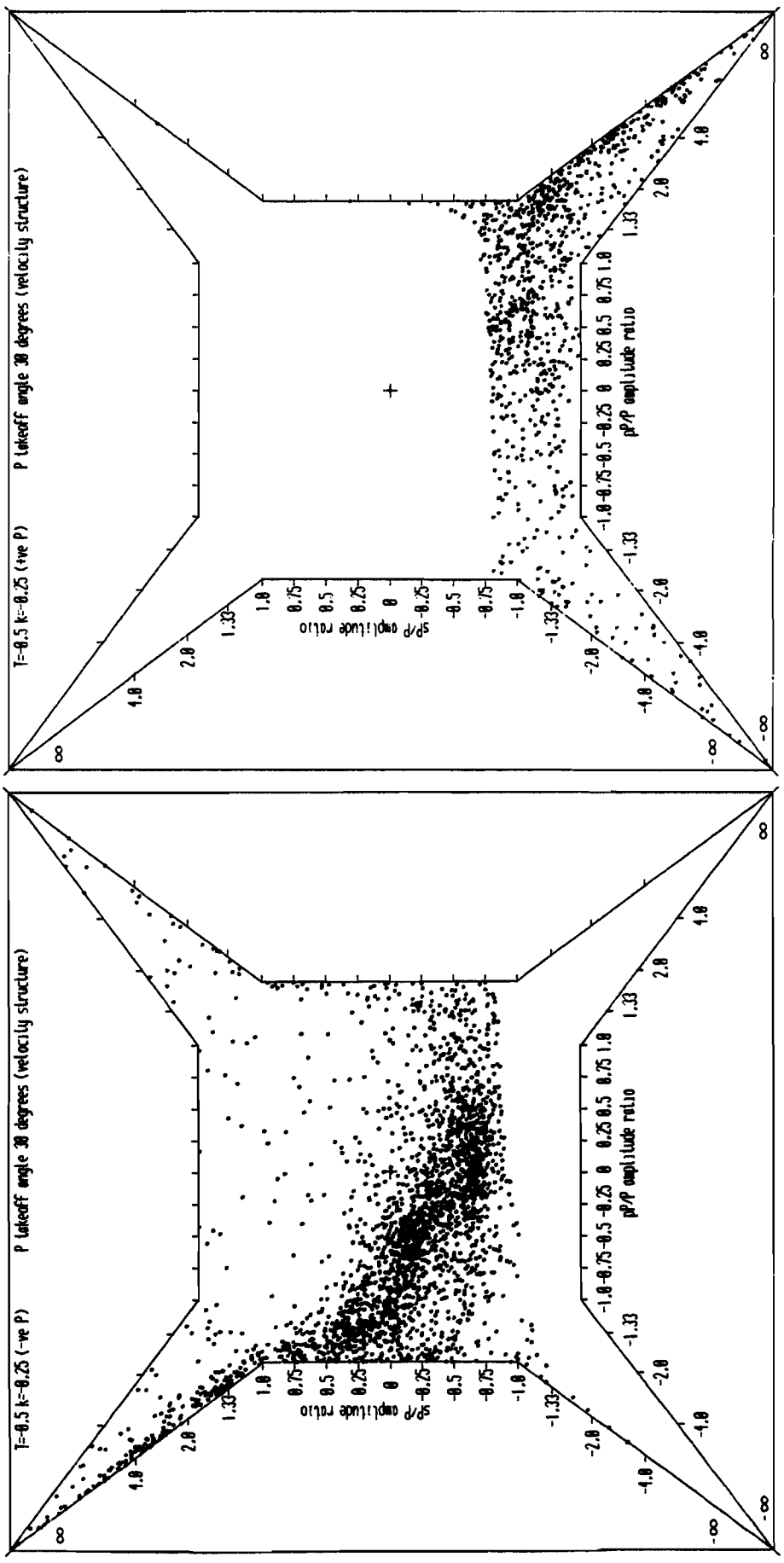
T=-0.5 k=-0.25 (-ve P)
P takeoff angle 30 degrees (velocity structure)
T=-0.5 k=-0.25 (+ve P)
P takeoff angle 30 degrees (velocity structure)
sP/P amplitude ratio
pP/P amplitude ratio

Figure 82

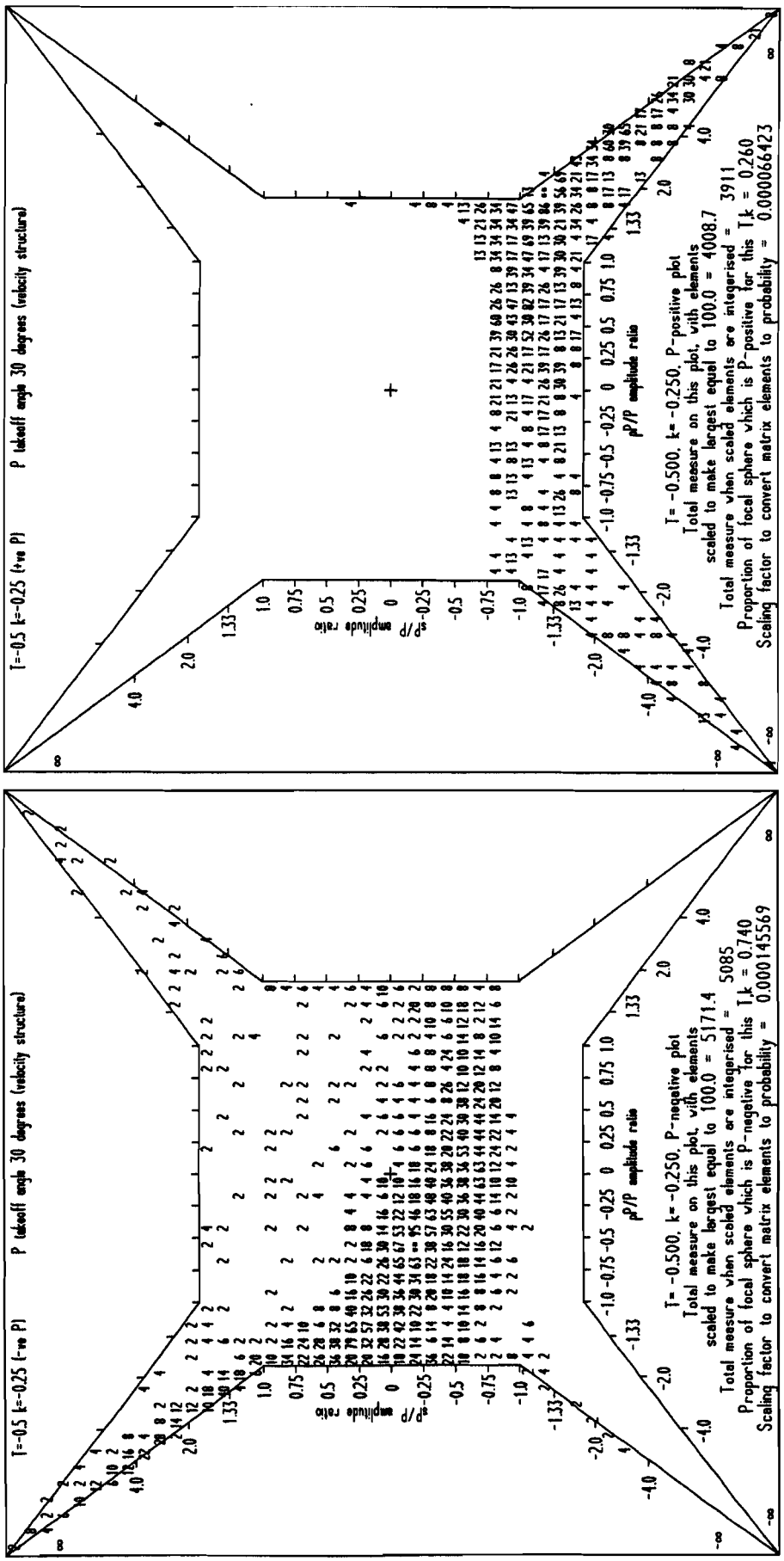

Figure 82 (continued)

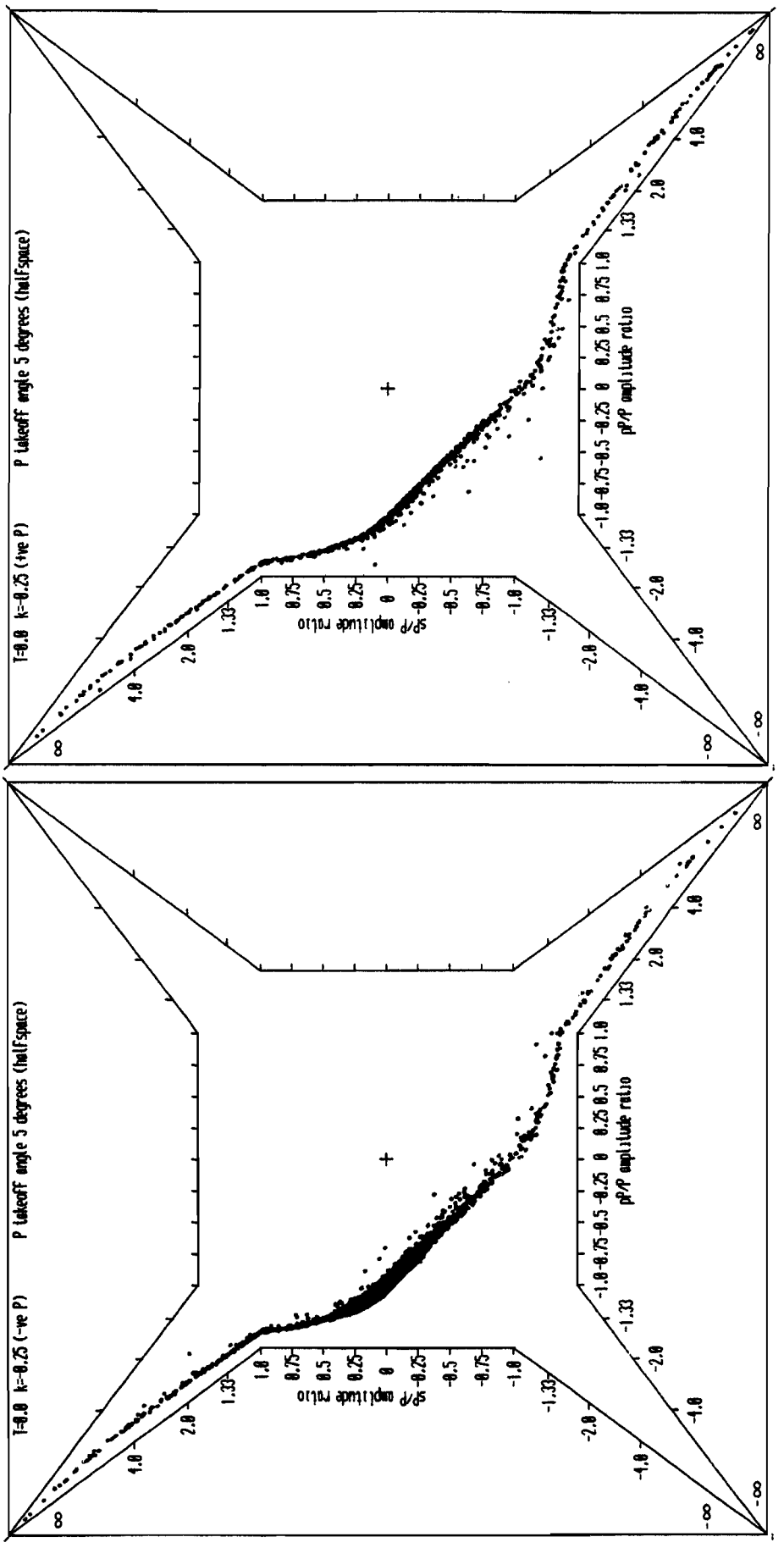
T=0.0 k=-0.25 (+ve P)
P takeoff angle 5 degrees (halfspace)
sP/P amplitude ratio
pP/P amplitude ratio
T=0.0 k=-0.25 (-ve P)
P takeoff angle 5 degrees (halfspace)
sP/P amplitude ratio
pP/P amplitude ratio

Figure 83

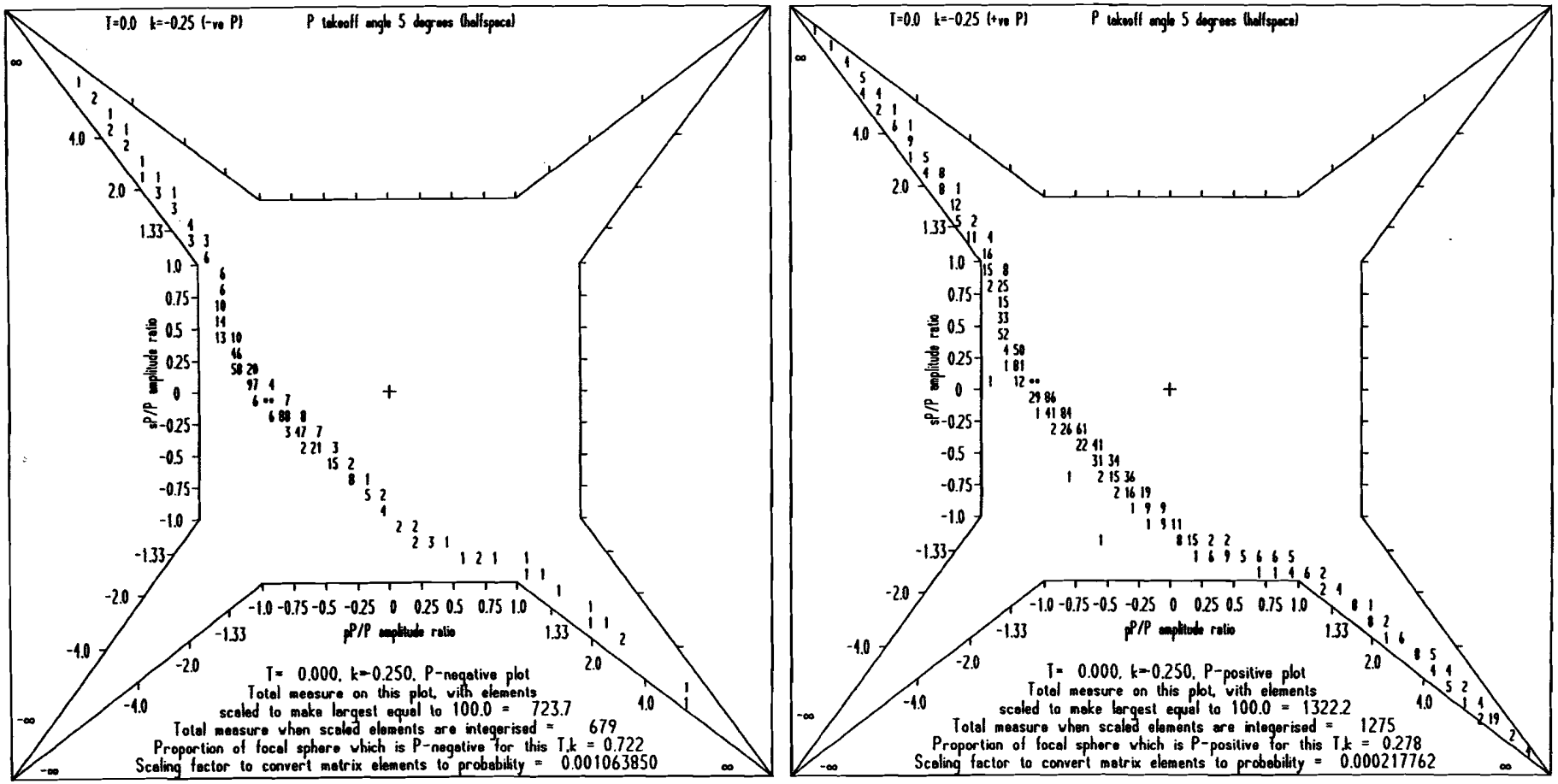

Figure 83 (continued)

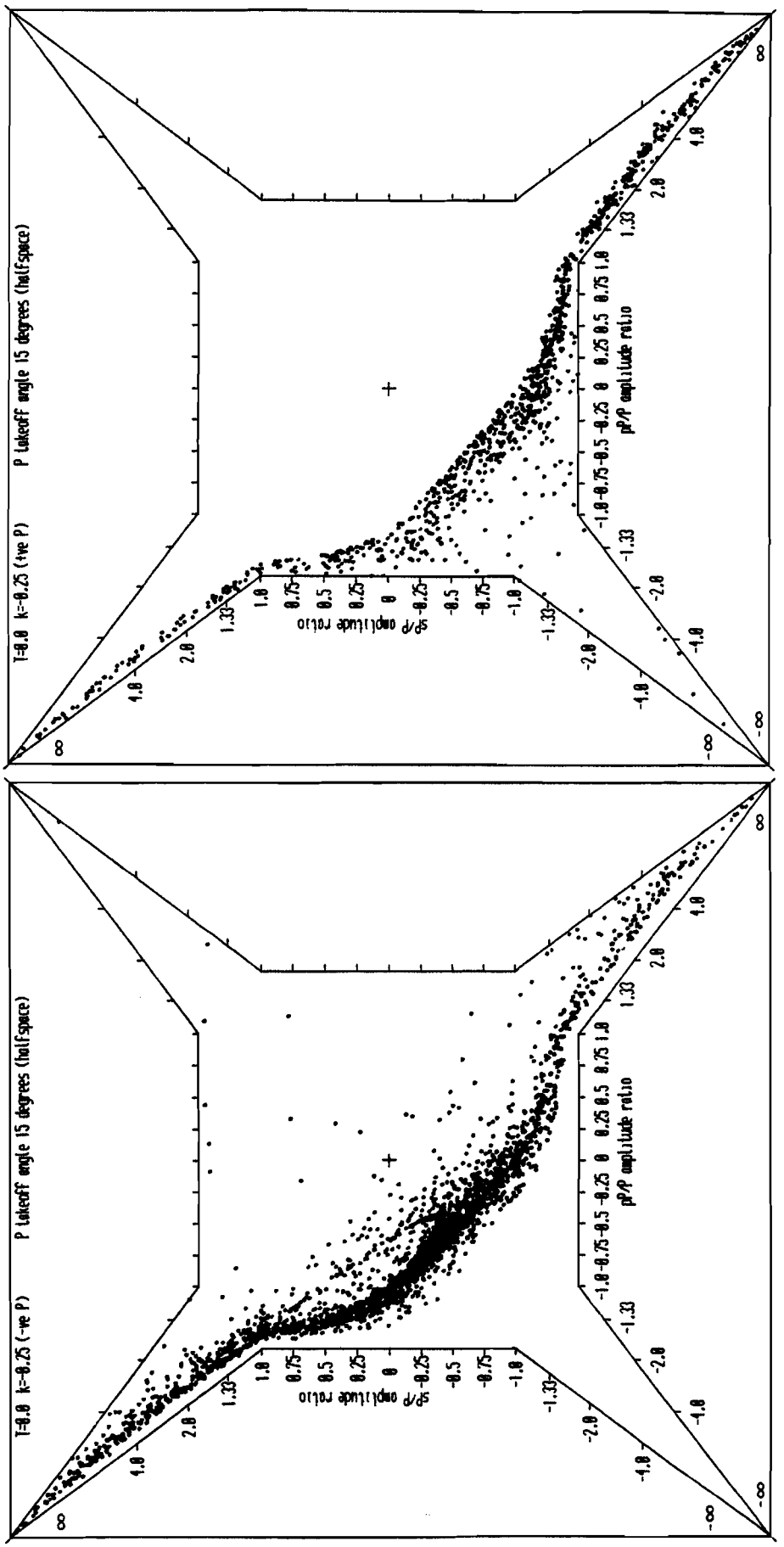
T=0.0 k=-0.25 (-we P)
P takeoff angle 15 degrees (halfspace)
T=0.0 k=-0.25 (+we P)
P takeoff angle 15 degrees (halfspace)
sP/P amplitude ratio
pP/P amplitude ratio
8
4.0
2.0
1.33
1.0
0.75
0.5
0.25
0
-0.25
-0.5
-0.75
-1.0
-1.33
-2.0
-4.0
-8

Figure 84

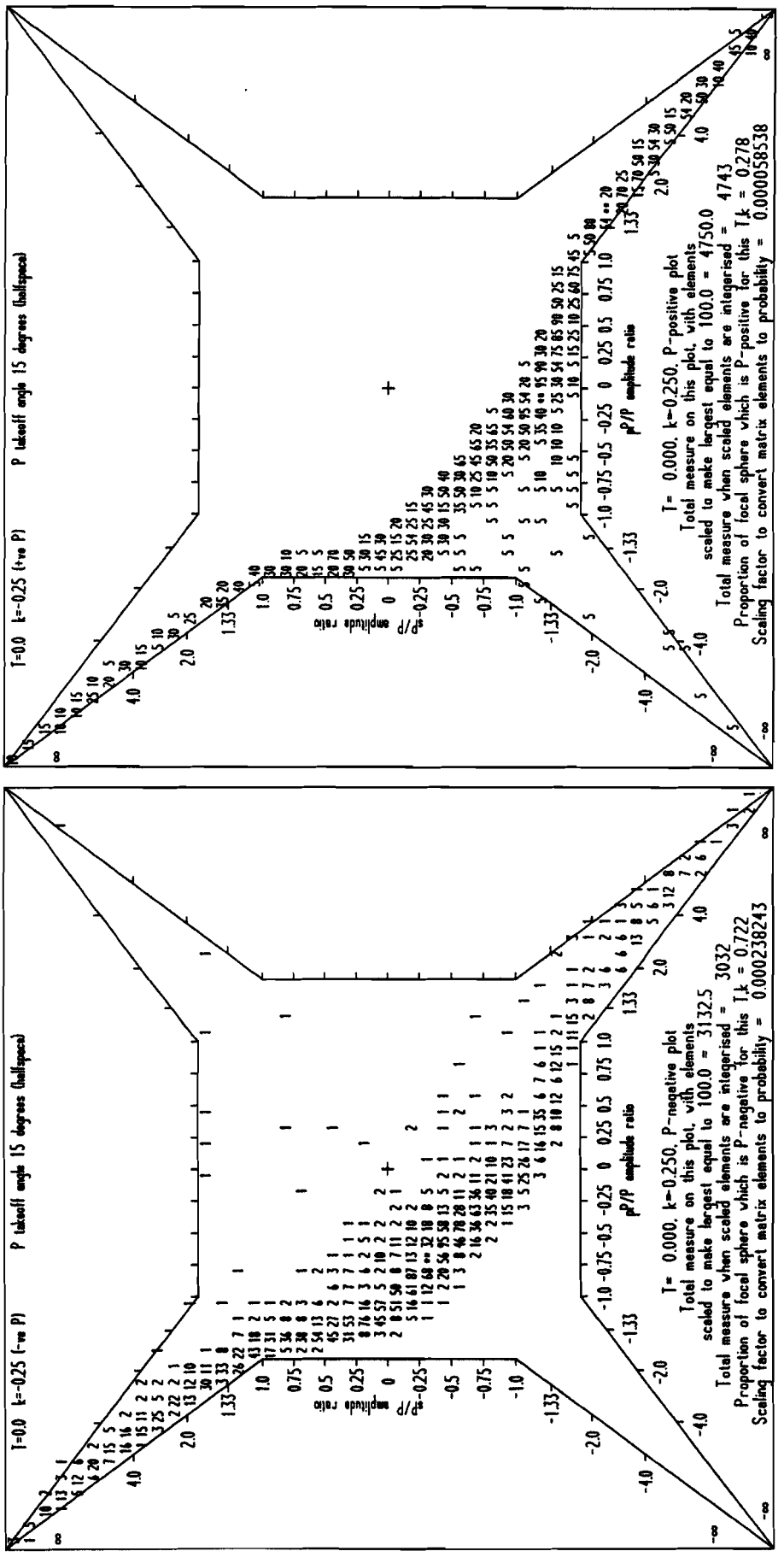

Figure 84 (continued)

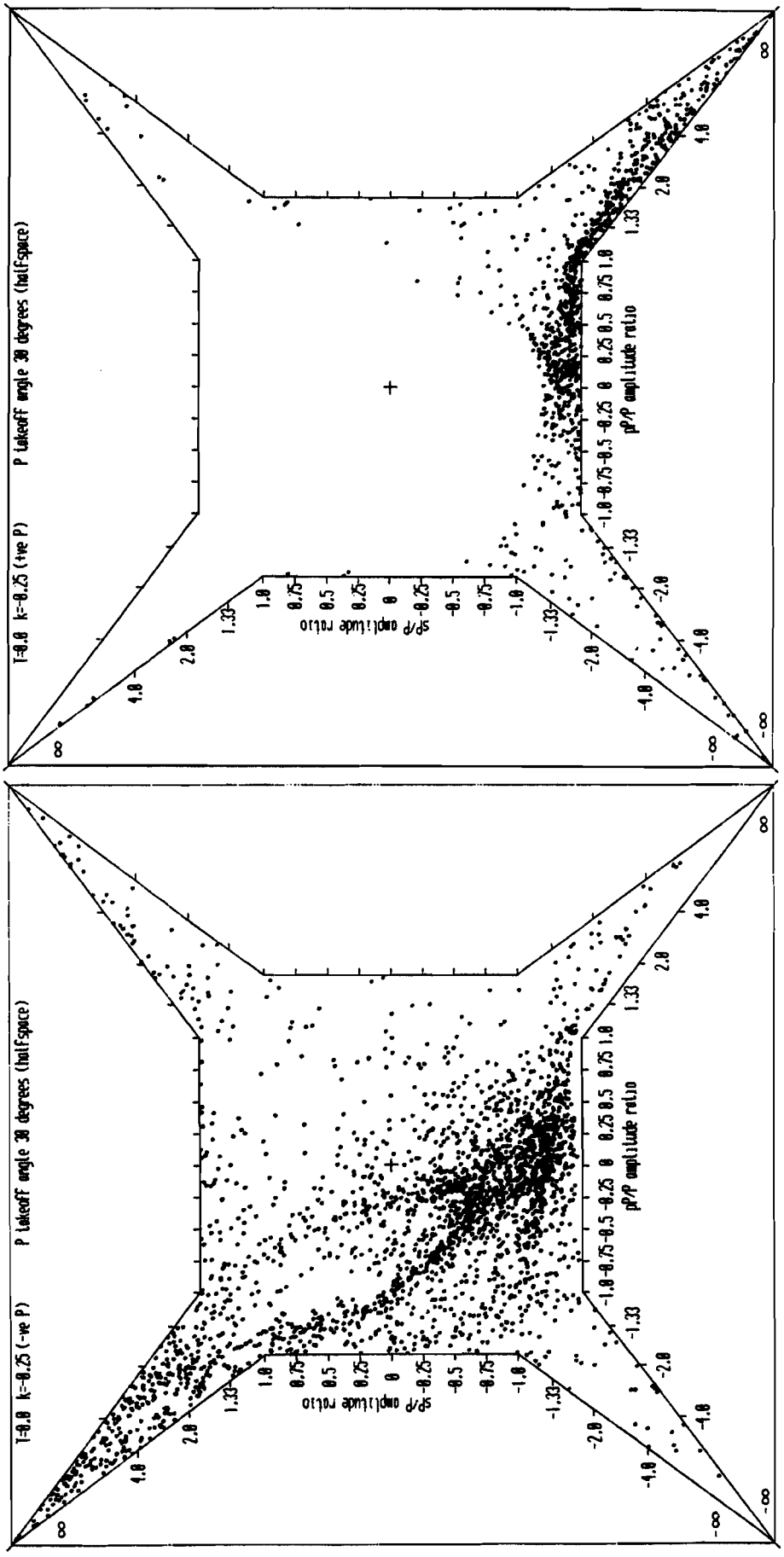
T=0.0 k=-0.25 (-ve P)
P takeoff angle 30 degrees (halfspace)
T=0.0 k=-0.25 (+ve P)
P takeoff angle 30 degrees (halfspace)
sP/P amplitude ratio
pP/P amplitude ratio
8
4.0
2.0
1.33
1.0
0.75
0.5
0.25
0
-0.25
-0.5
-0.75
-1.0
-1.33
-2.0
-4.0
-8

Figure 85

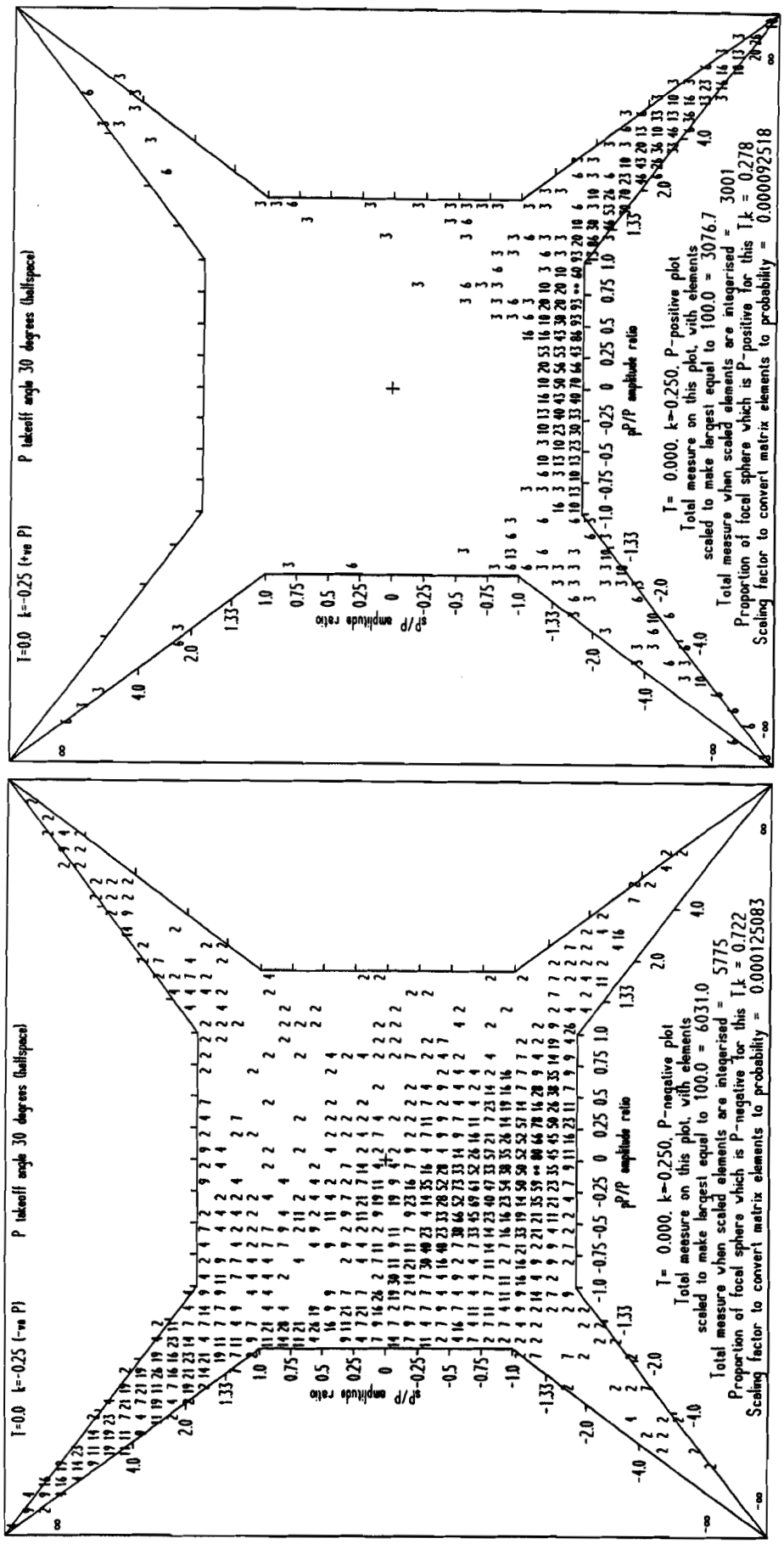

Figure 85 (continued)

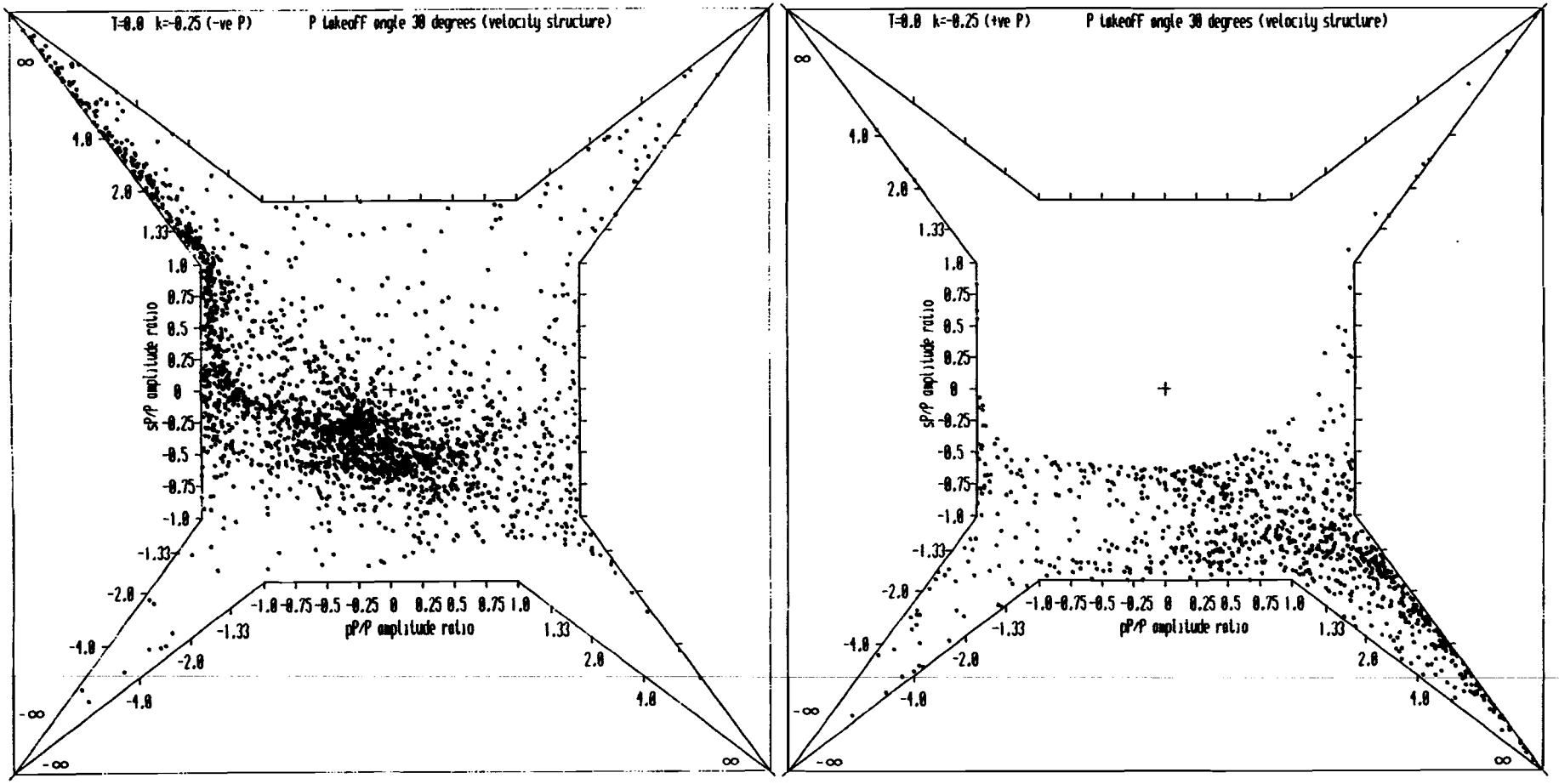
T=0.0 k=-0.25 (-ve P)
P takeoff angle 30 degrees (velocity structure)
sP/P amplitude ratio
pP/P amplitude ratio
T=0.0 k=-0.25 (+ve P)
P takeoff angle 30 degrees (velocity structure)
sP/P amplitude ratio
pP/P amplitude ratio

Figure 86

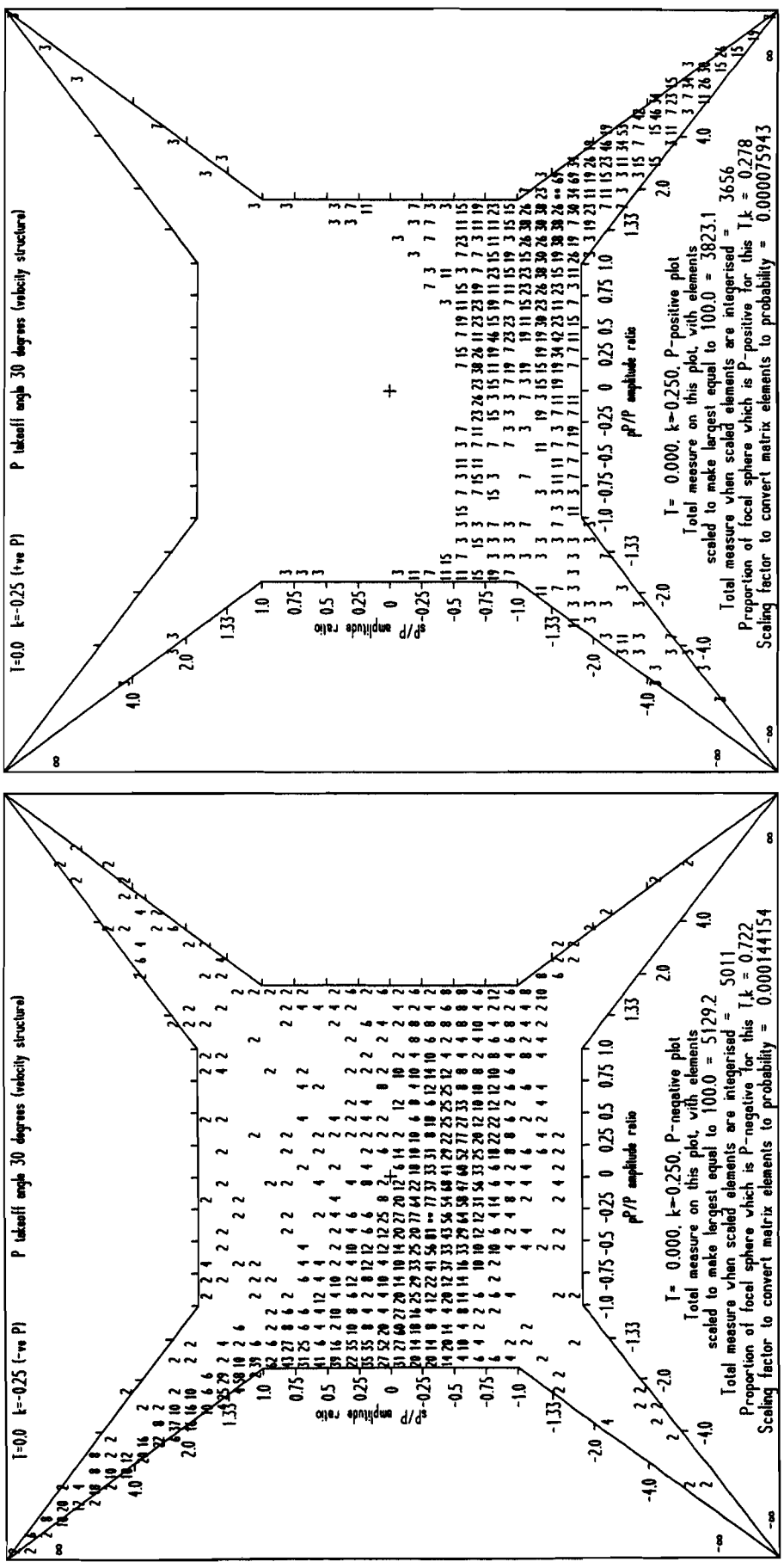

Figure 86 (continued)

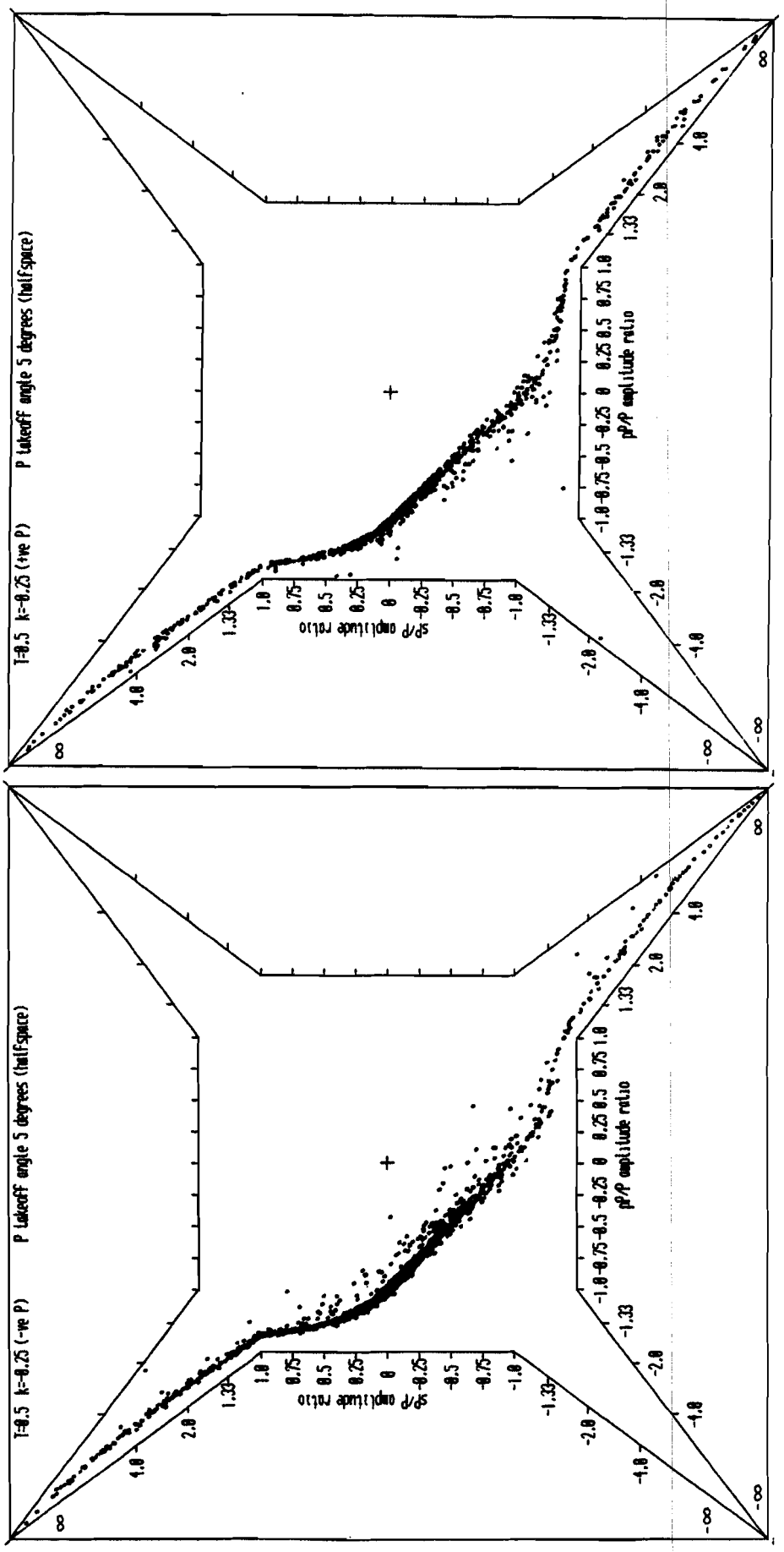
T=0.5 k=-0.25 (-ve P)
P takeoff angle 5 degrees (halfspace)
T=0.5 k=-0.25 (+ve P)
P takeoff angle 5 degrees (halfspace)
sP/P amplitude ratio
pP/P amplitude ratio

Figure 87

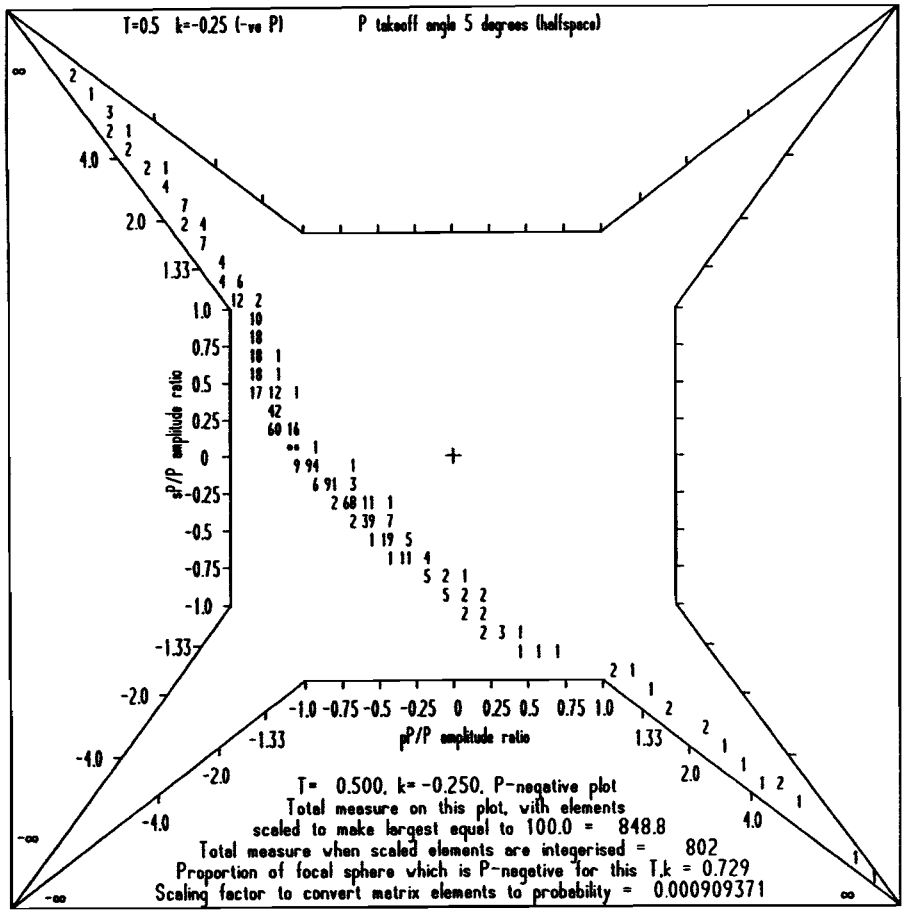

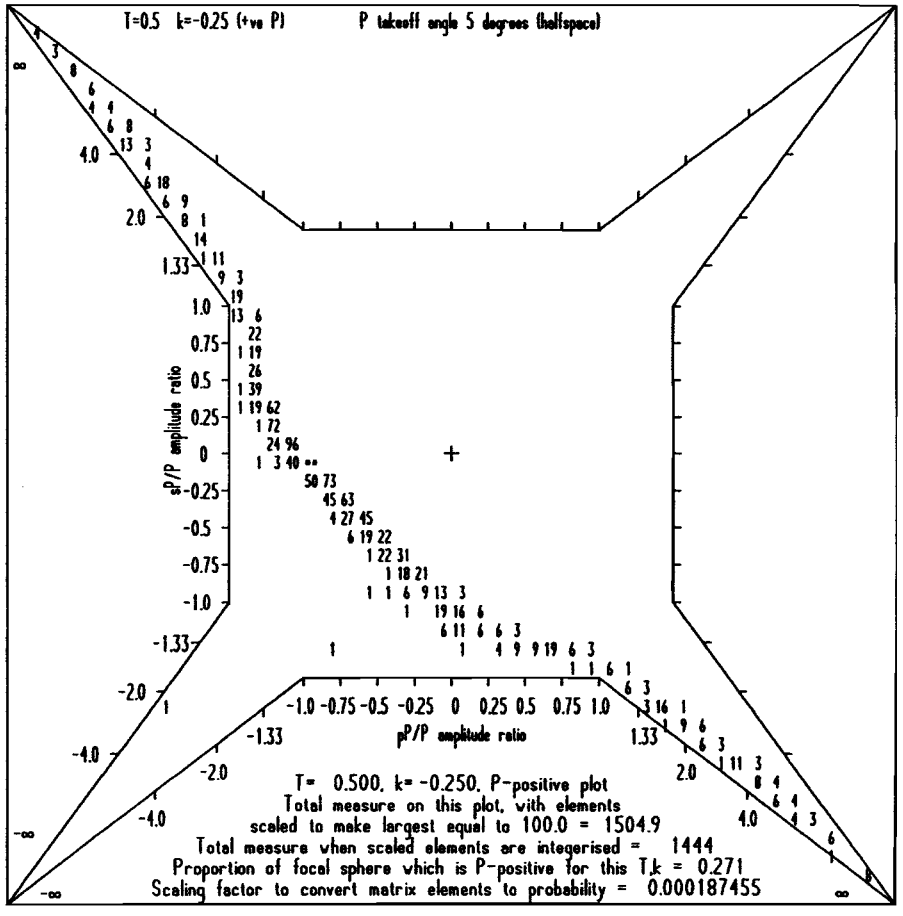

Figure 87 (continued)

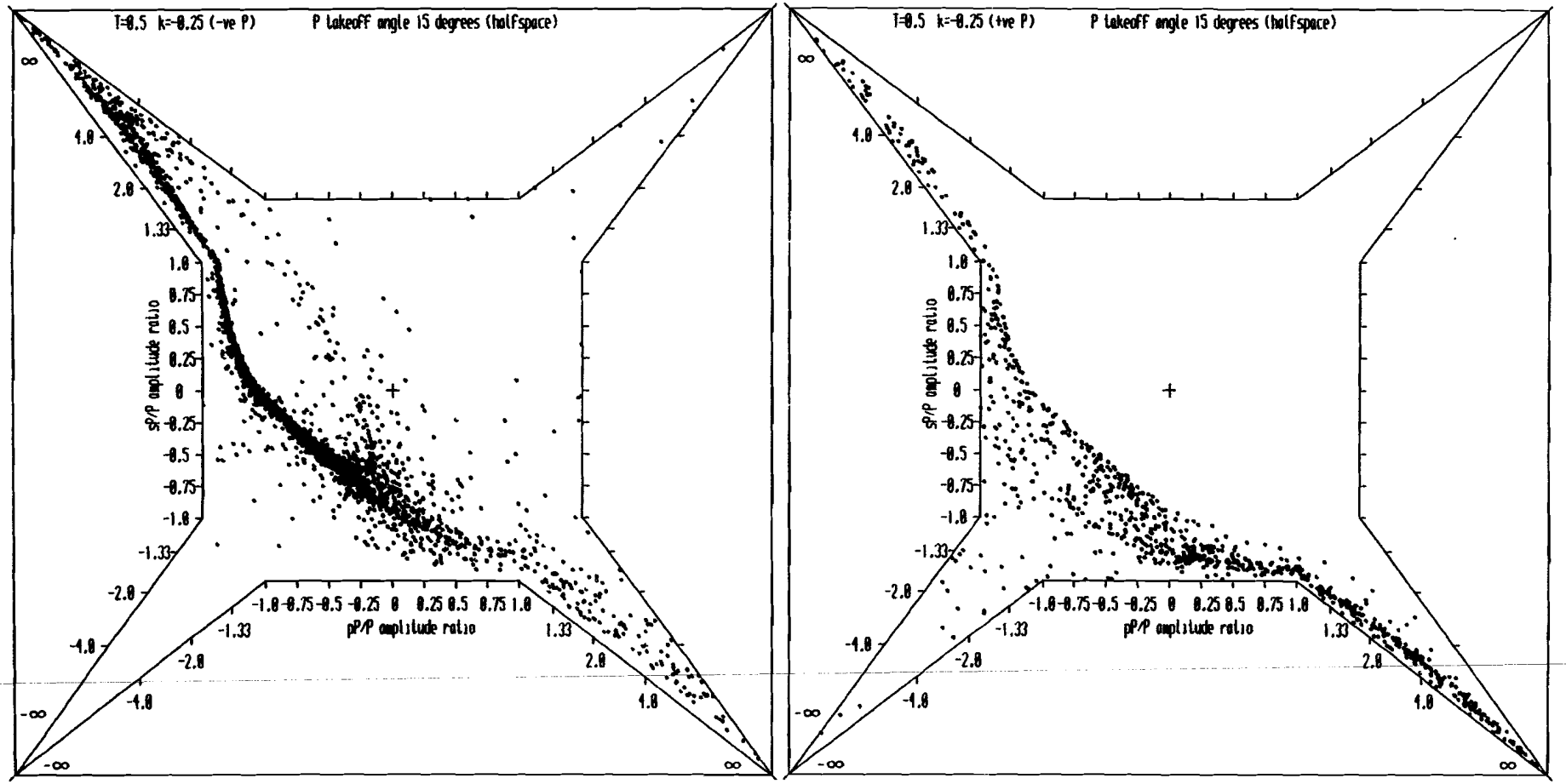
T=0.5 k=-0.25 (-ve P)
P takeoff angle 15 degrees (halfspace)
sP/P amplitude ratio
pP/P amplitude ratio
T=0.5 k=-0.25 (+ve P)
P takeoff angle 15 degrees (halfspace)
sP/P amplitude ratio
pP/P amplitude ratio

Figure 88

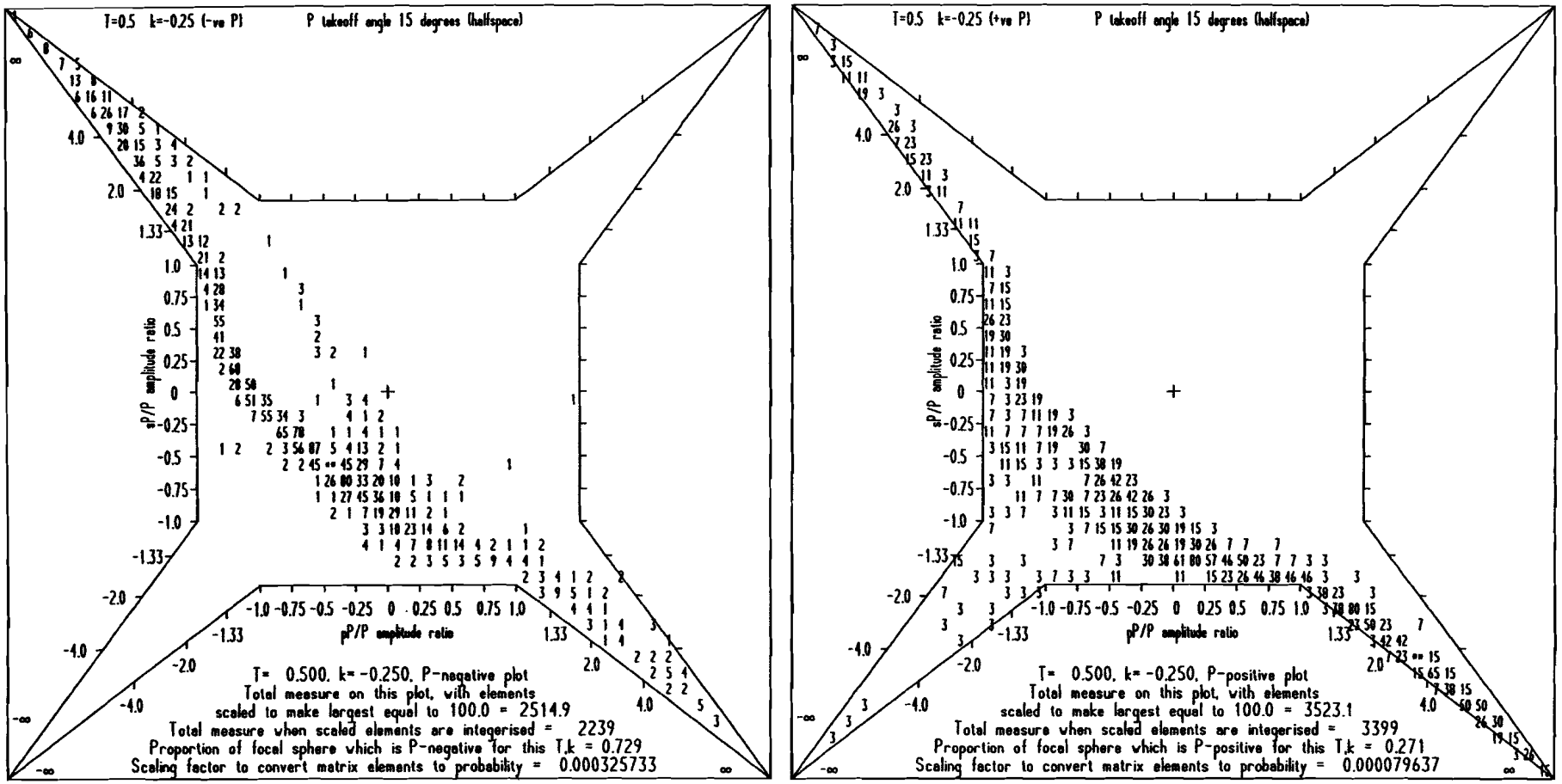

Figure 88 (continued)

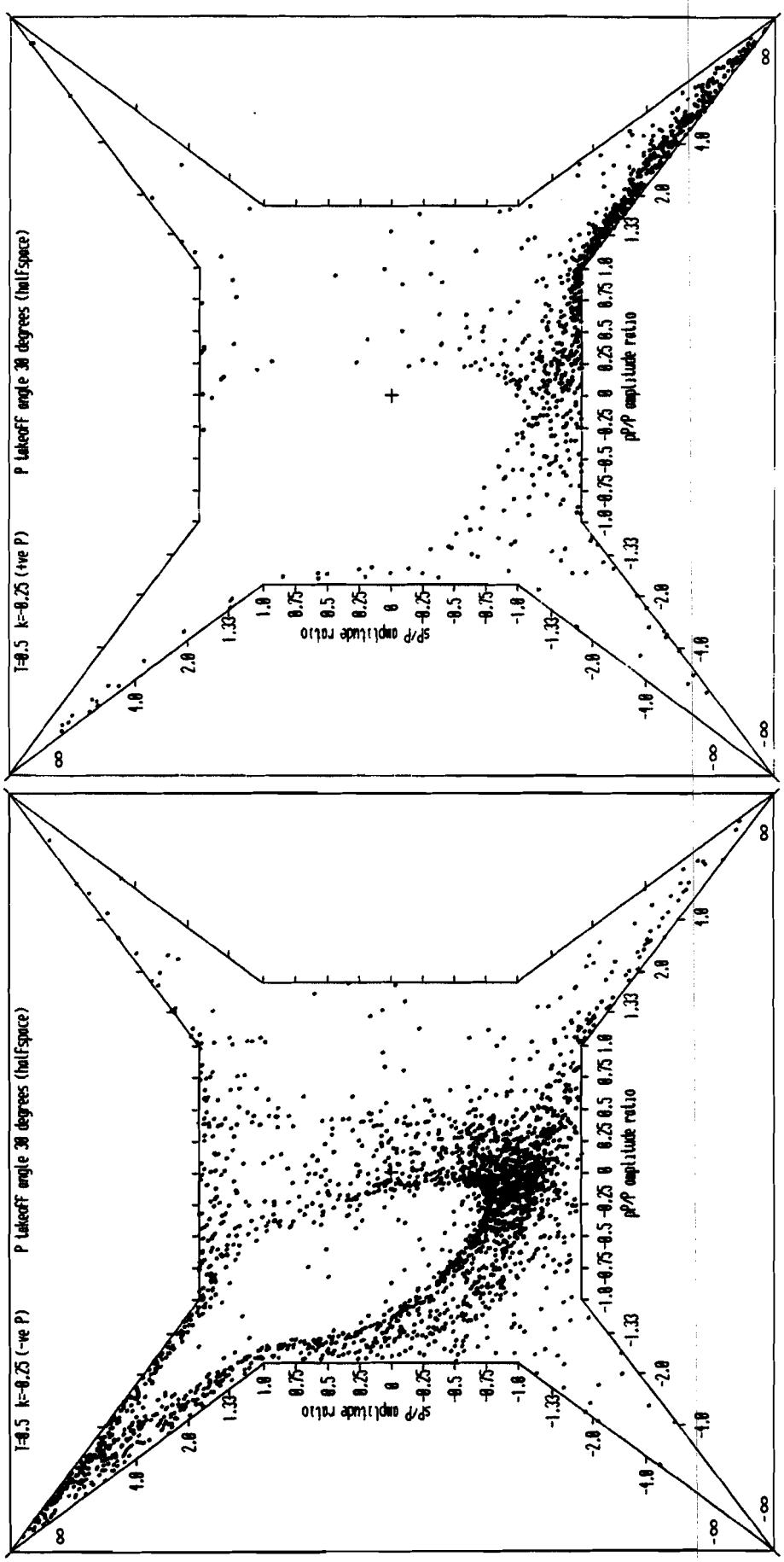
T=0.5 k=-0.25 (-ve P)
P takeoff angle 30 degrees (halfspace)
T=0.5 k=-0.25 (+ve P)
P takeoff angle 30 degrees (halfspace)
sP/P amplitude ratio
pP/P amplitude ratio

Figure 89

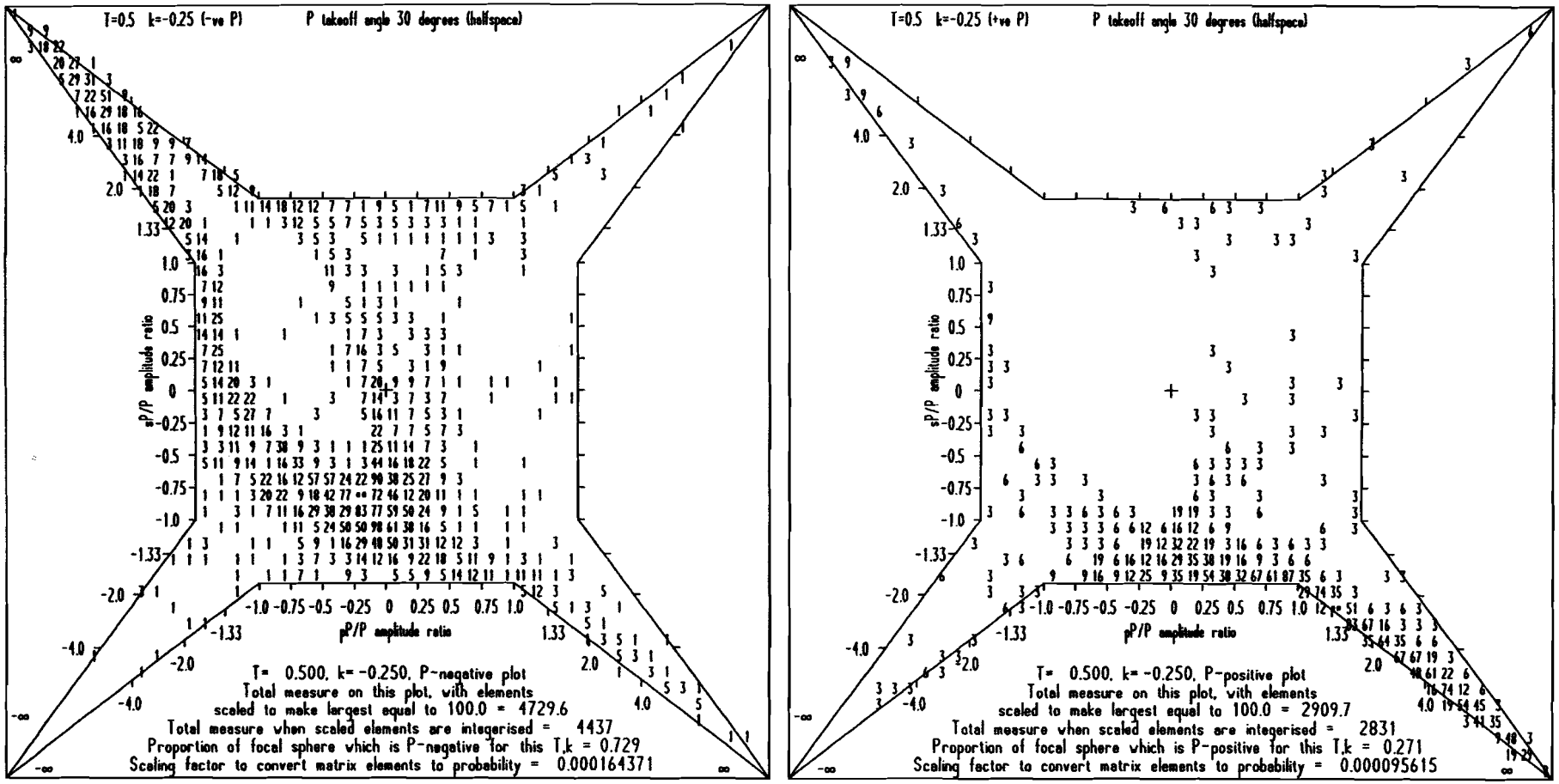

Figure 89 (continued)

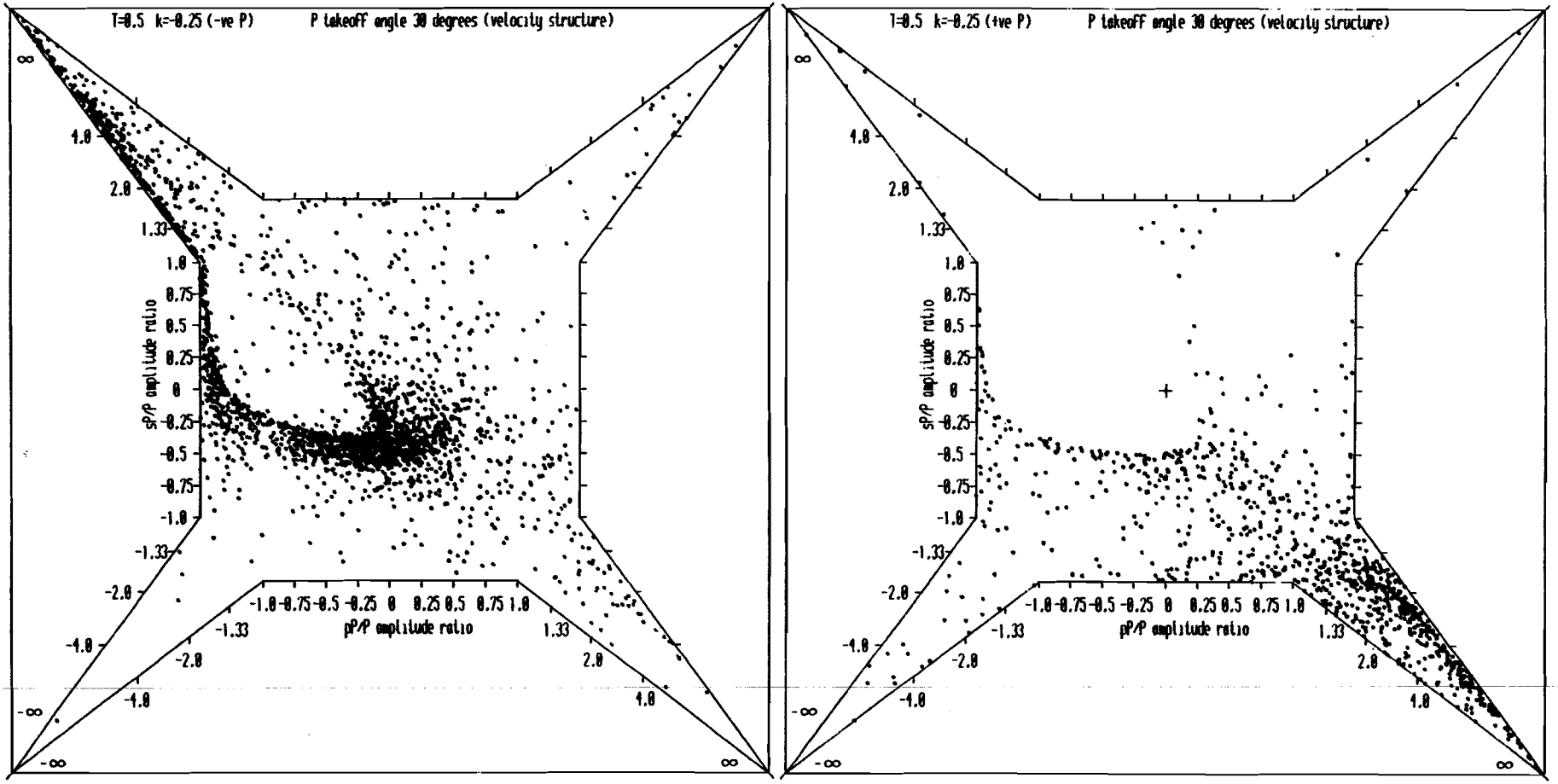
T=0.5 k=-0.25 (-ve P)
P takeoff angle 30 degrees (velocity structure)
sP/P amplitude ratio
pP/P amplitude ratio
T=0.5 k=-0.25 (+ve P)
P takeoff angle 30 degrees (velocity structure)
sP/P amplitude ratio
pP/P amplitude ratio

Figure 90

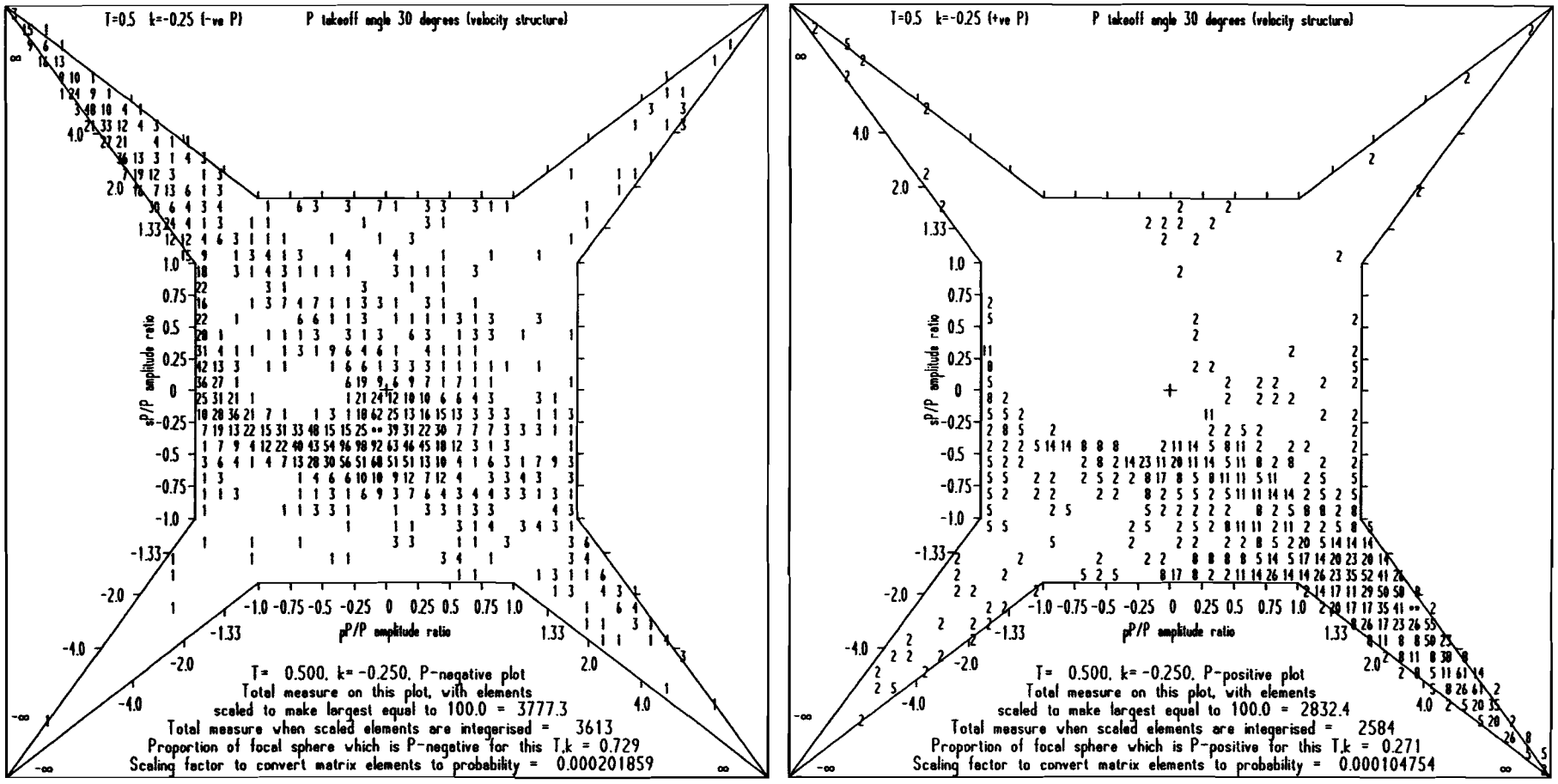

Figure 90 (continued)

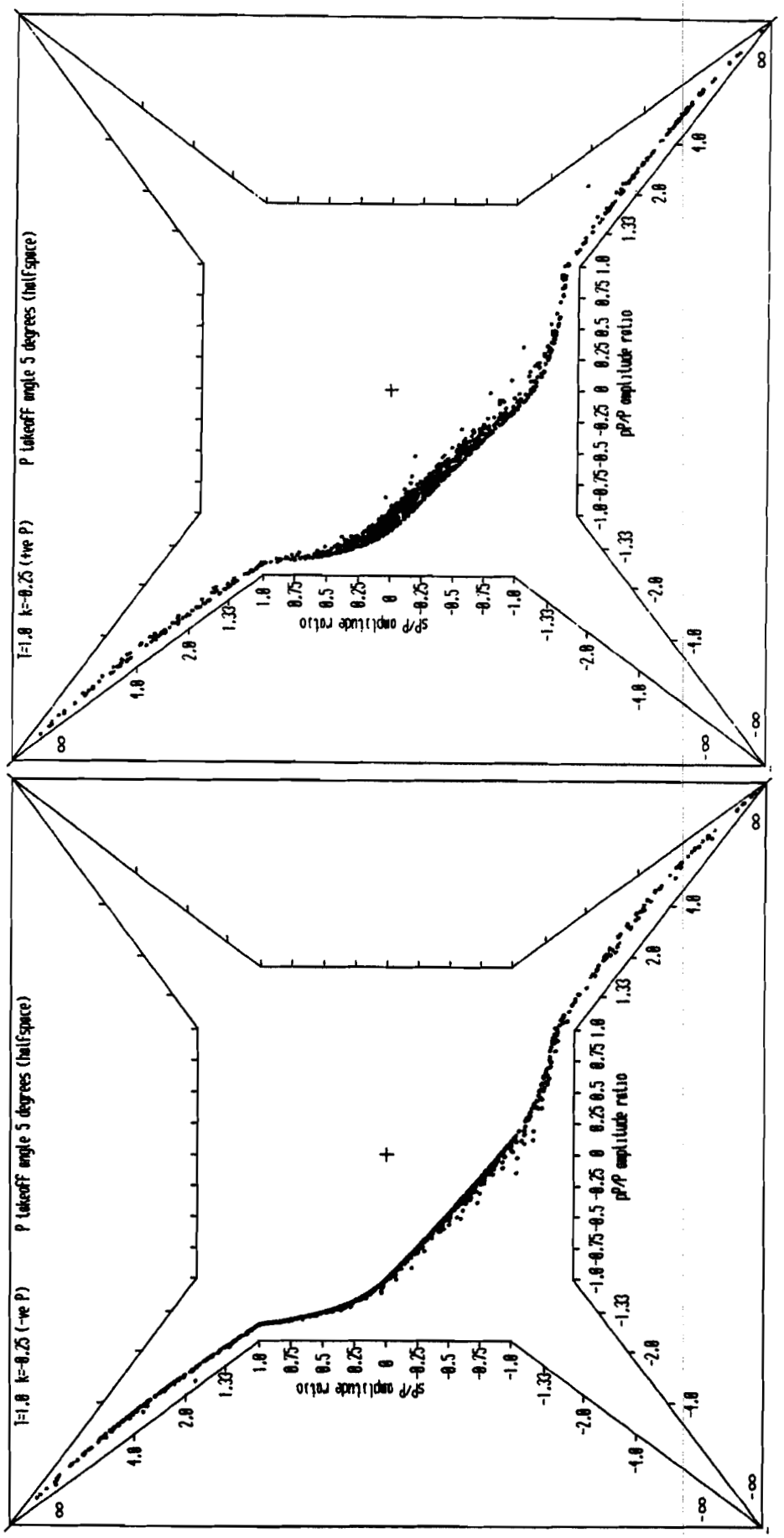
I=1.0 k=-0.25 (-ve P)
P takeoff angle 5 degrees (halfspace)
I=1.0 k=-0.25 (+ve P)
P takeoff angle 5 degrees (halfspace)
sP/P amplitude ratio
pP/P amplitude ratio

Figure 91

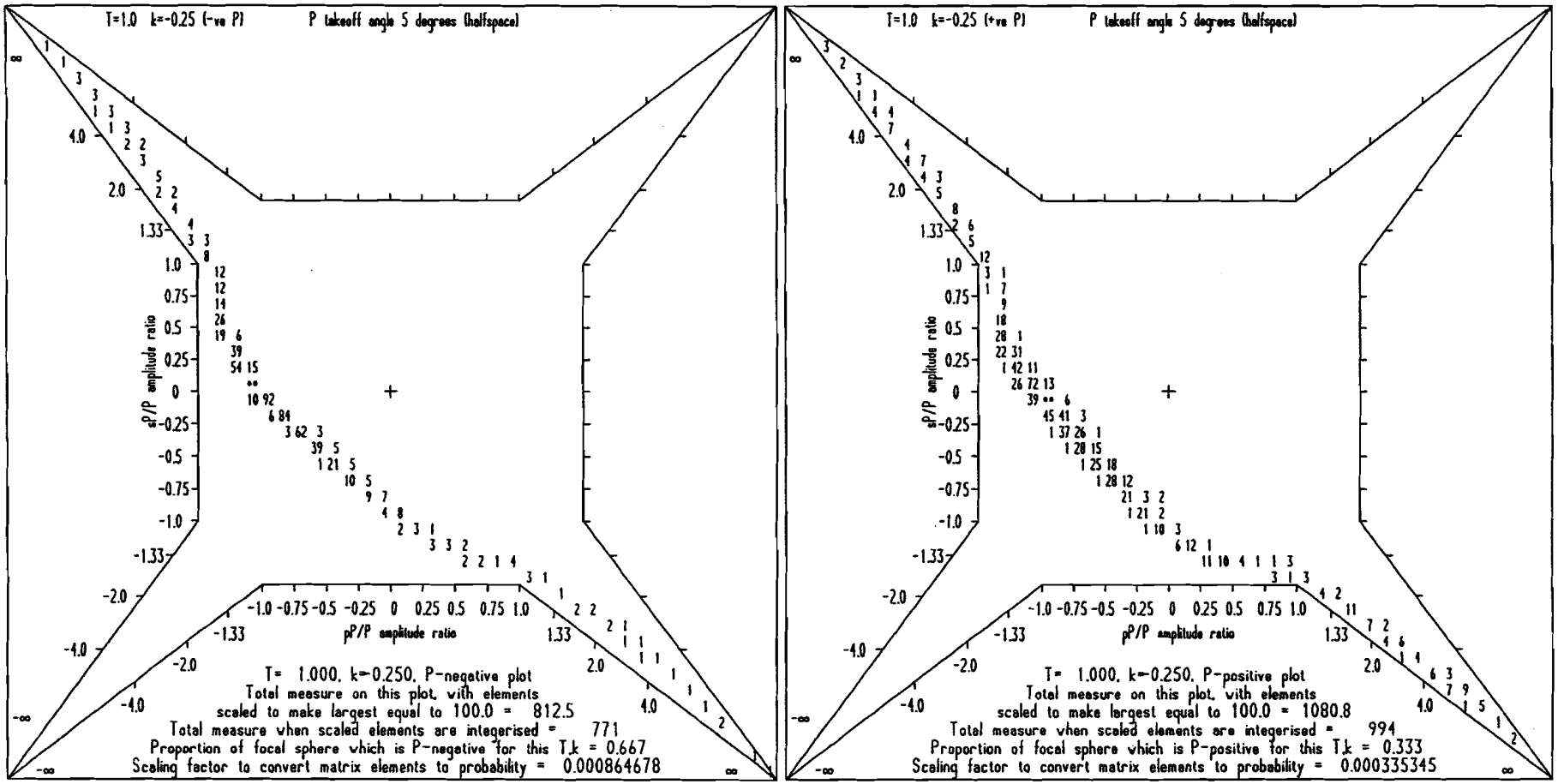

Figure 91 (continued)

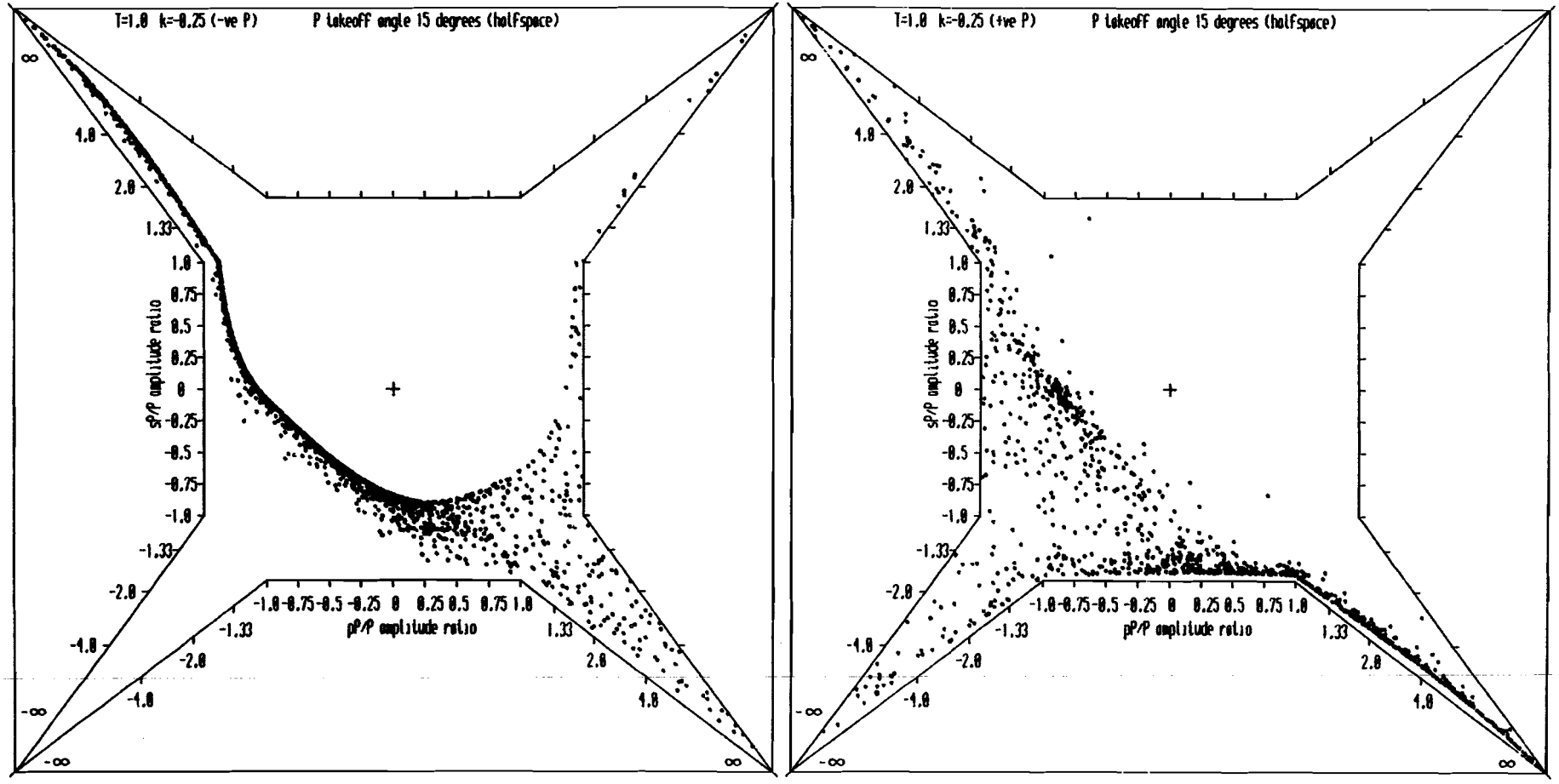
T=1.0 k=-0.25 (-ve P)
P takeoff angle 15 degrees (halfspace)
sP/P amplitude ratio
pP/P amplitude ratio
T=1.0 k=-0.25 (+ve P)
P takeoff angle 15 degrees (halfspace)
sP/P amplitude ratio
pP/P amplitude ratio

Figure 92

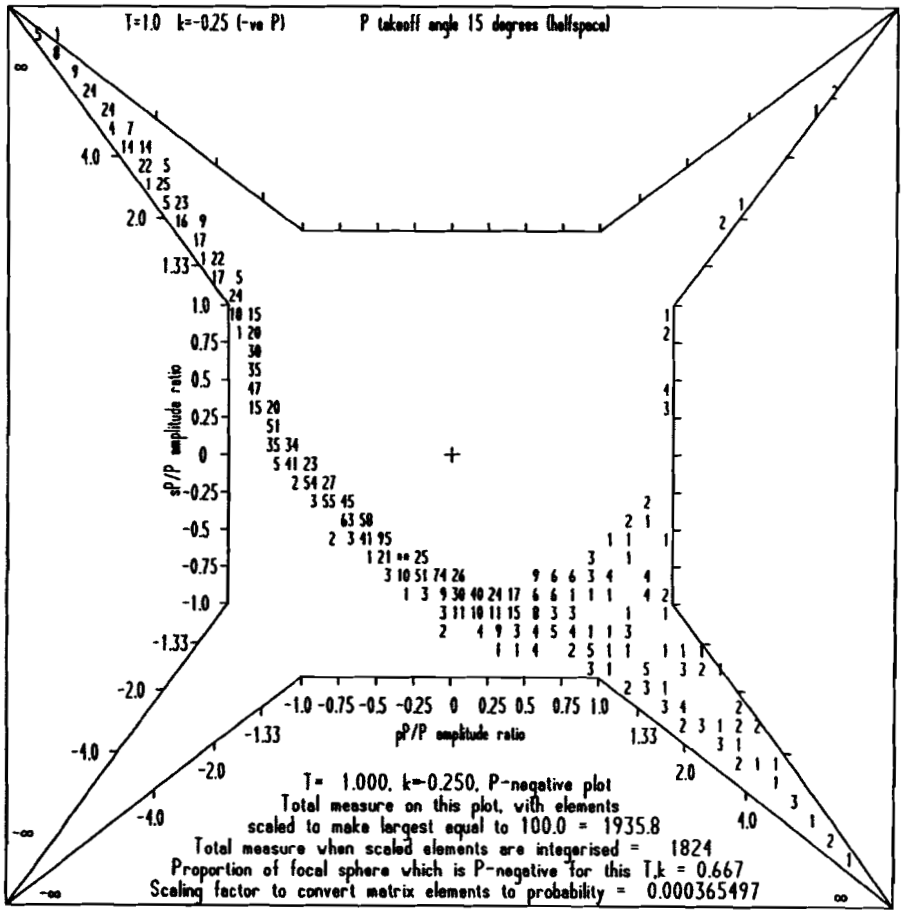

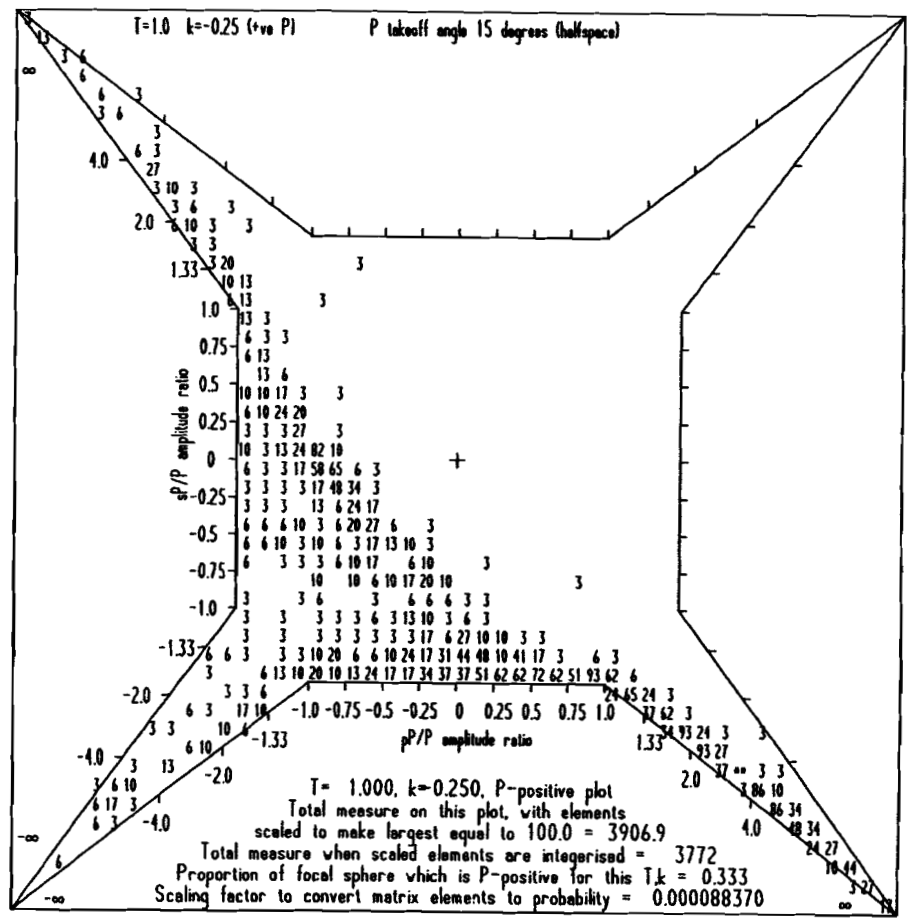

Figure 92 (continued)

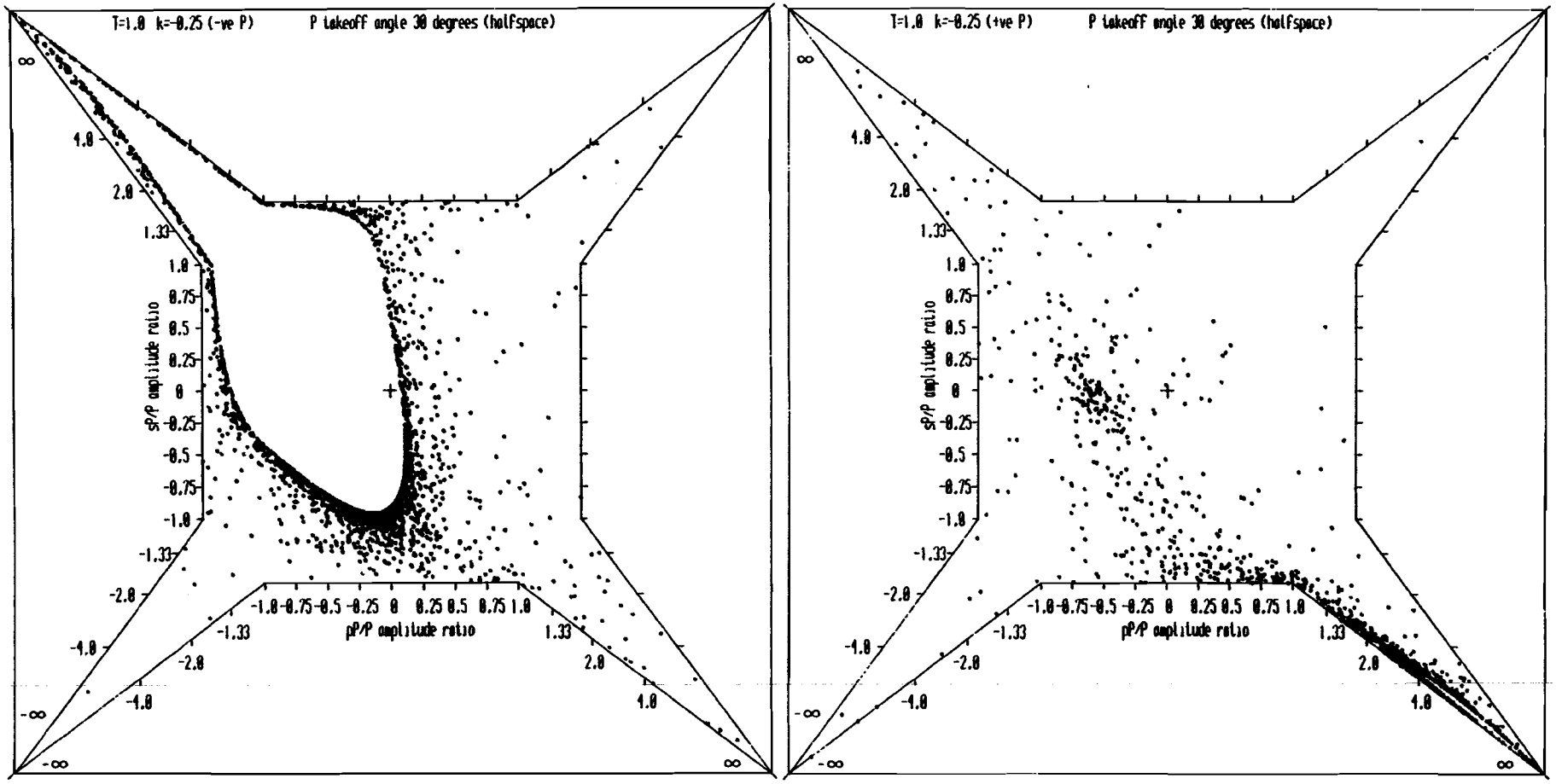
T=1.0 k=-0.25 (-ve P)
P takeoff angle 30 degrees (halfspace)
sP/P amplitude ratio
pP/P amplitude ratio
T=1.0 k=-0.25 (+ve P)
P takeoff angle 30 degrees (halfspace)
sP/P amplitude ratio
pP/P amplitude ratio

Figure 93

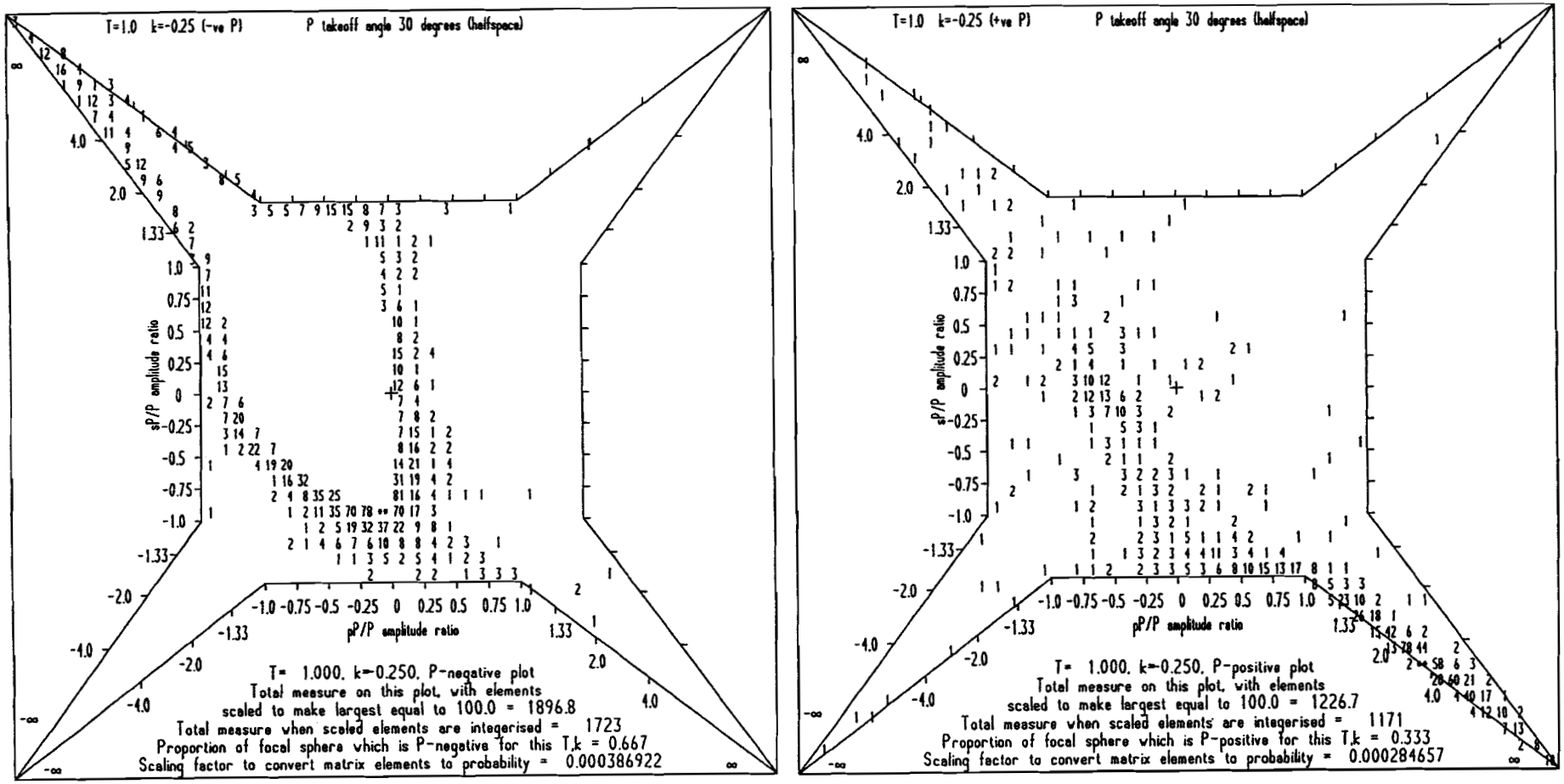

Figure 93 (continued)

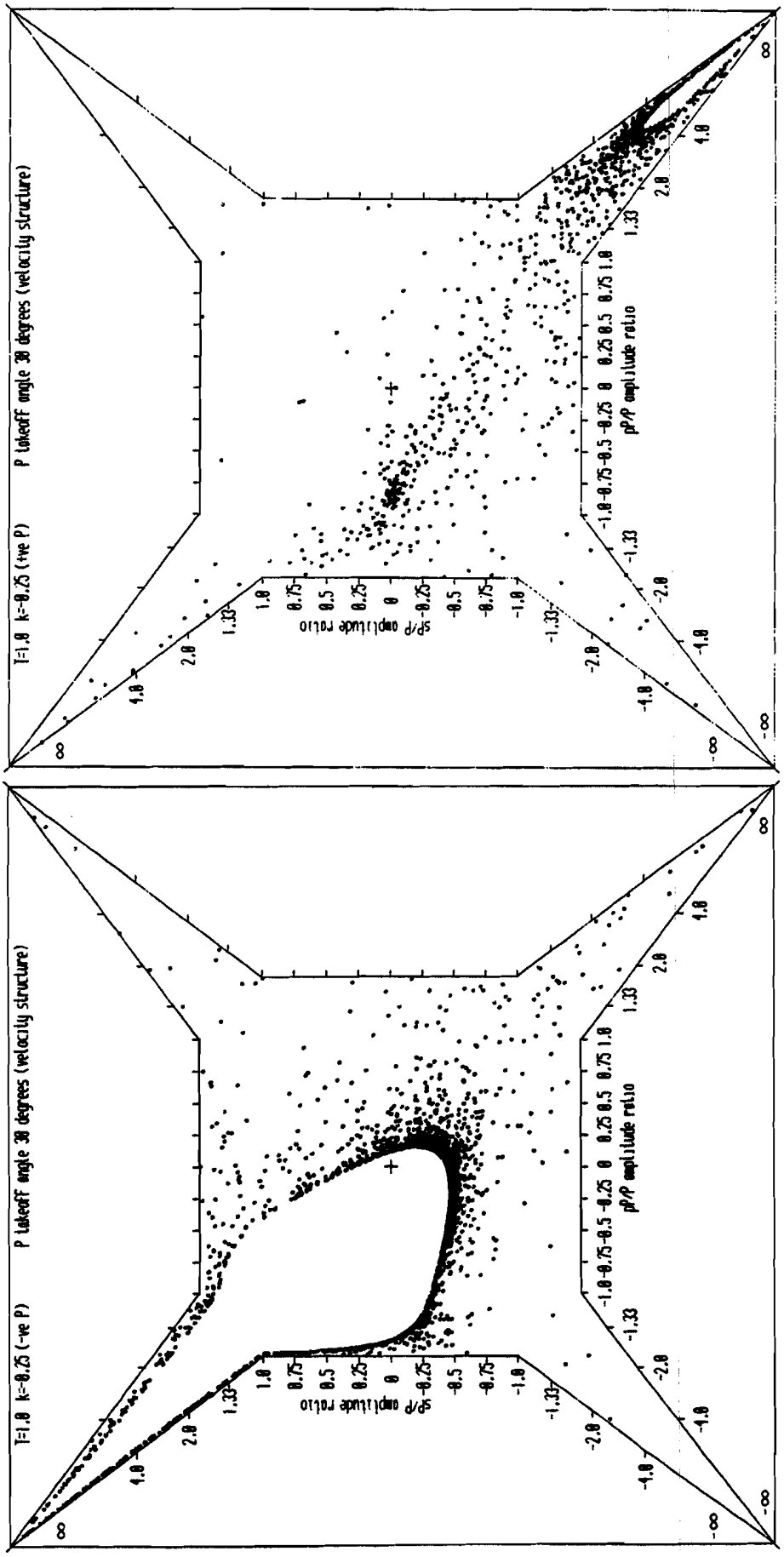
I=1.0 k=-0.25 (+ve P)
P takeoff angle 30 degrees (velocity structure)
sP/P amplitude ratio
pP/P amplitude ratio
I=1.0 k=0.25 (-ve P)
P takeoff angle 30 degrees (velocity structure)
sP/P amplitude ratio
pP/P amplitude ratio

Figure 94

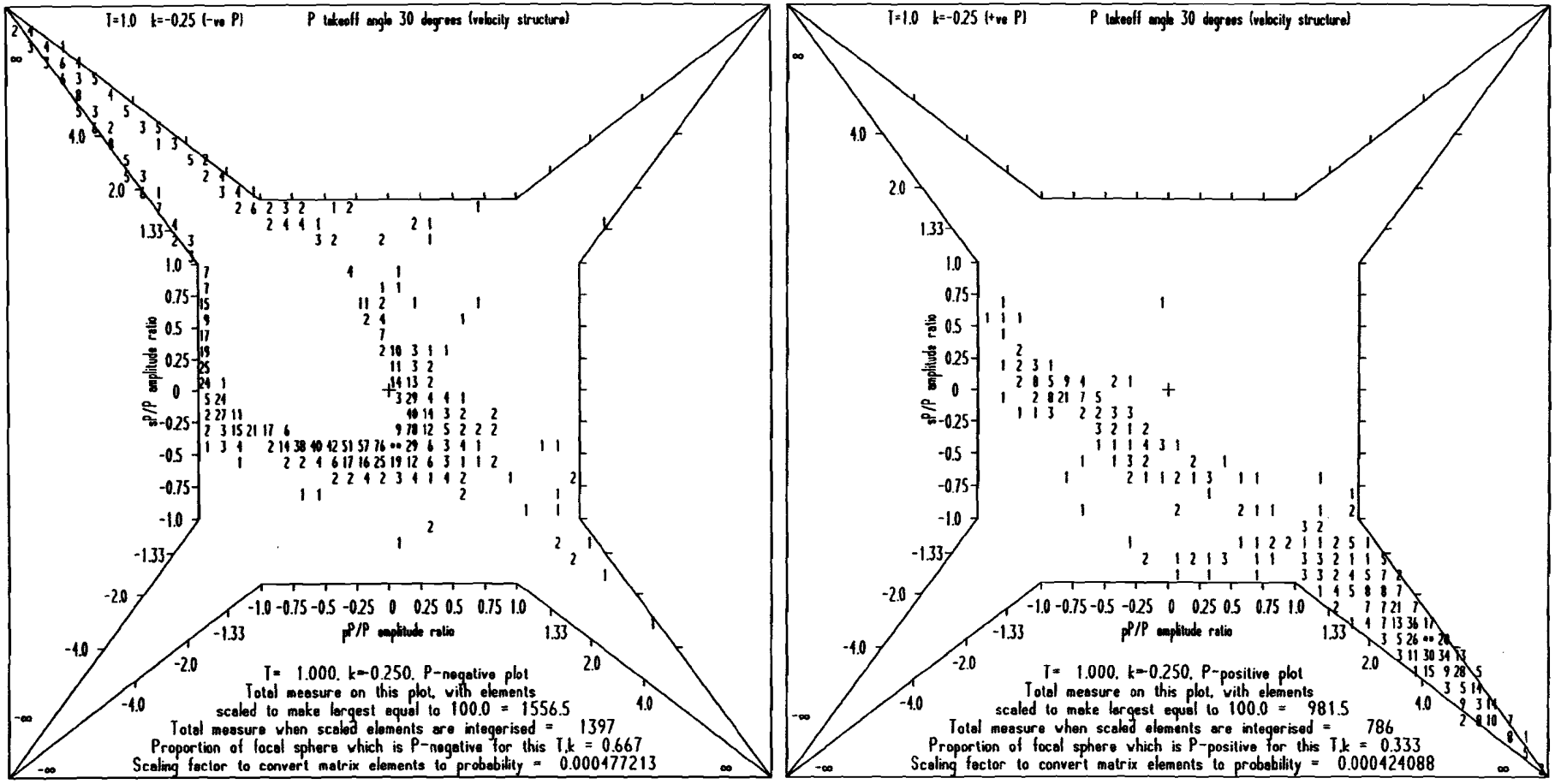

Figure 94 (continued)

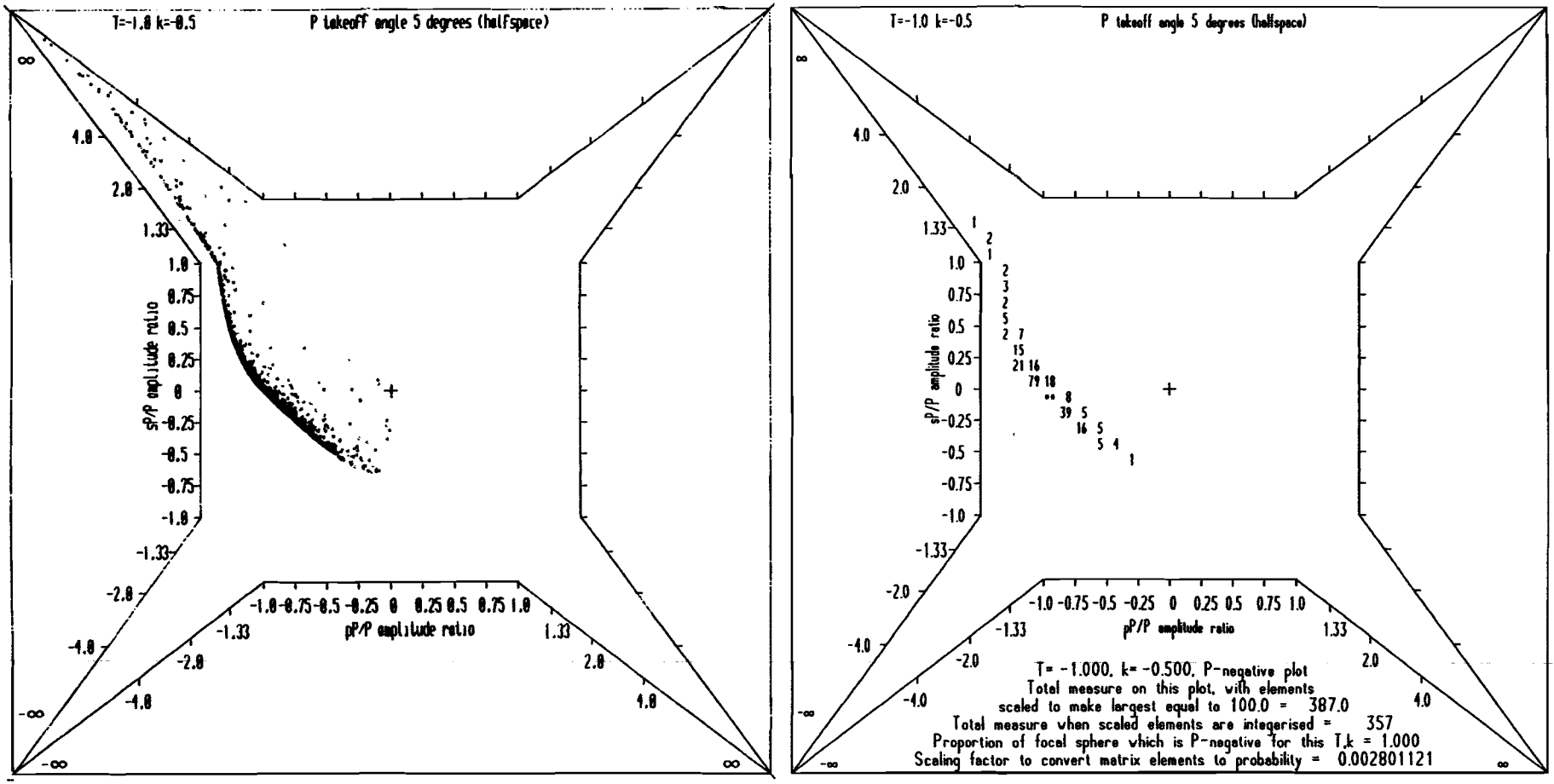
T=-1.0 k=-0.5
P takeoff angle 5 degrees (halfspace)
sP/P amplitude ratio
pP/P amplitude ratio
T=-1.0 k=-0.5
P takeoff angle 5 degrees (halfspace)
sP/P amplitude ratio
pP/P amplitude ratio
T= -1.000, k= -0.500, P-negative plot
Total measure on this plot, with elements
scaled to make largest equal to 100.0 = 387.0
Total measure when scaled elements are integerised = 357
Proportion of focal sphere which is P-negative for this T,k = 1.000
Scaling factor to convert matrix elements to probability = 0.002801121

Figure 95

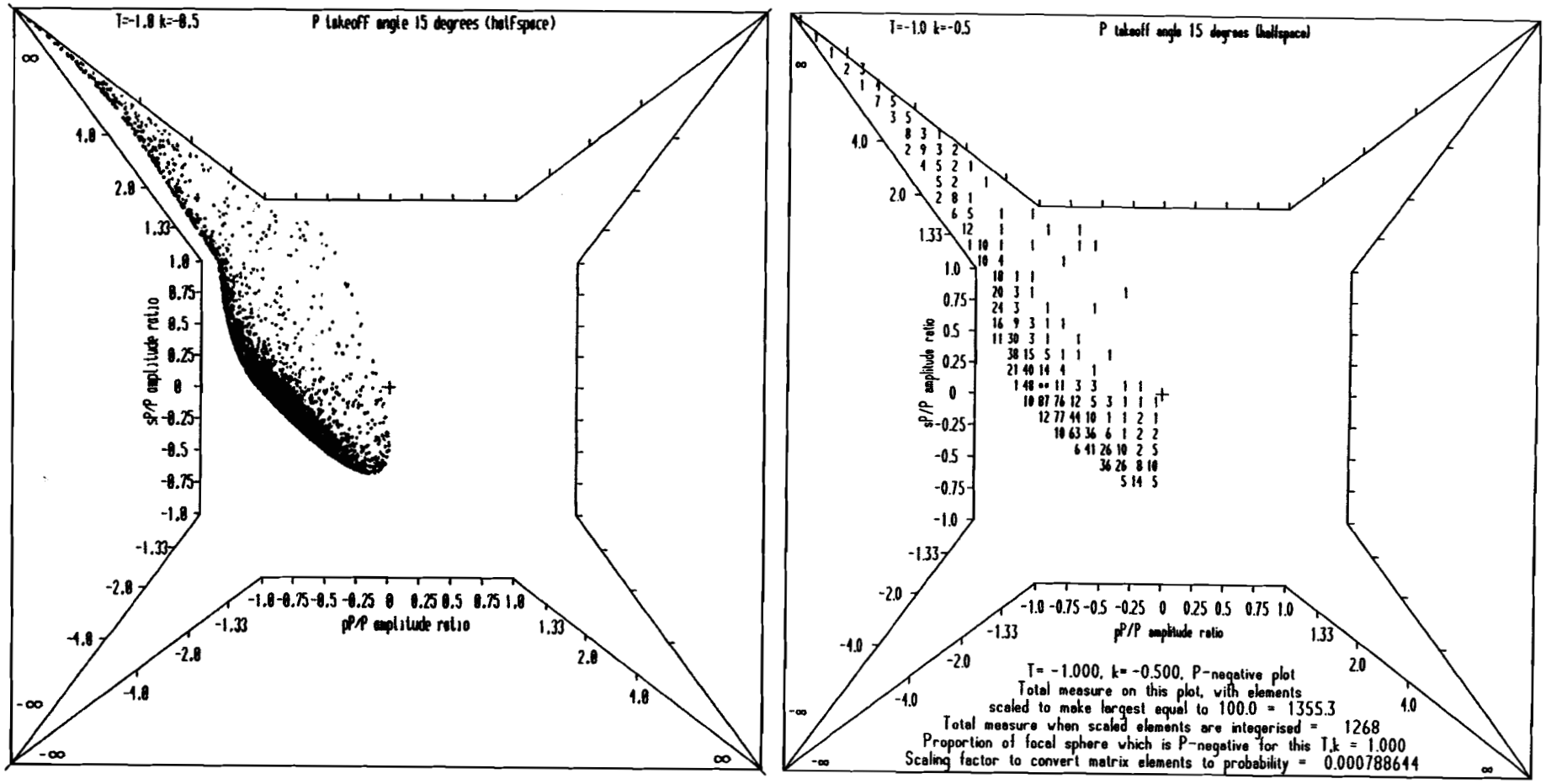
T=-1.0 k=-0.5
P takeoff angle 15 degrees (halfspace)
sP/P amplitude ratio
pP/P amplitude ratio
T= -1.000, k= -0.500, P-negative plot
Total measure on this plot, with elements
scaled to make largest equal to 100.0 = 1355.3
Total measure when scaled elements are integerised = 1268
Proportion of focal sphere which is P-negative for this T,k = 1.000
Scaling factor to convert matrix elements to probability = 0.000788644

Figure 96

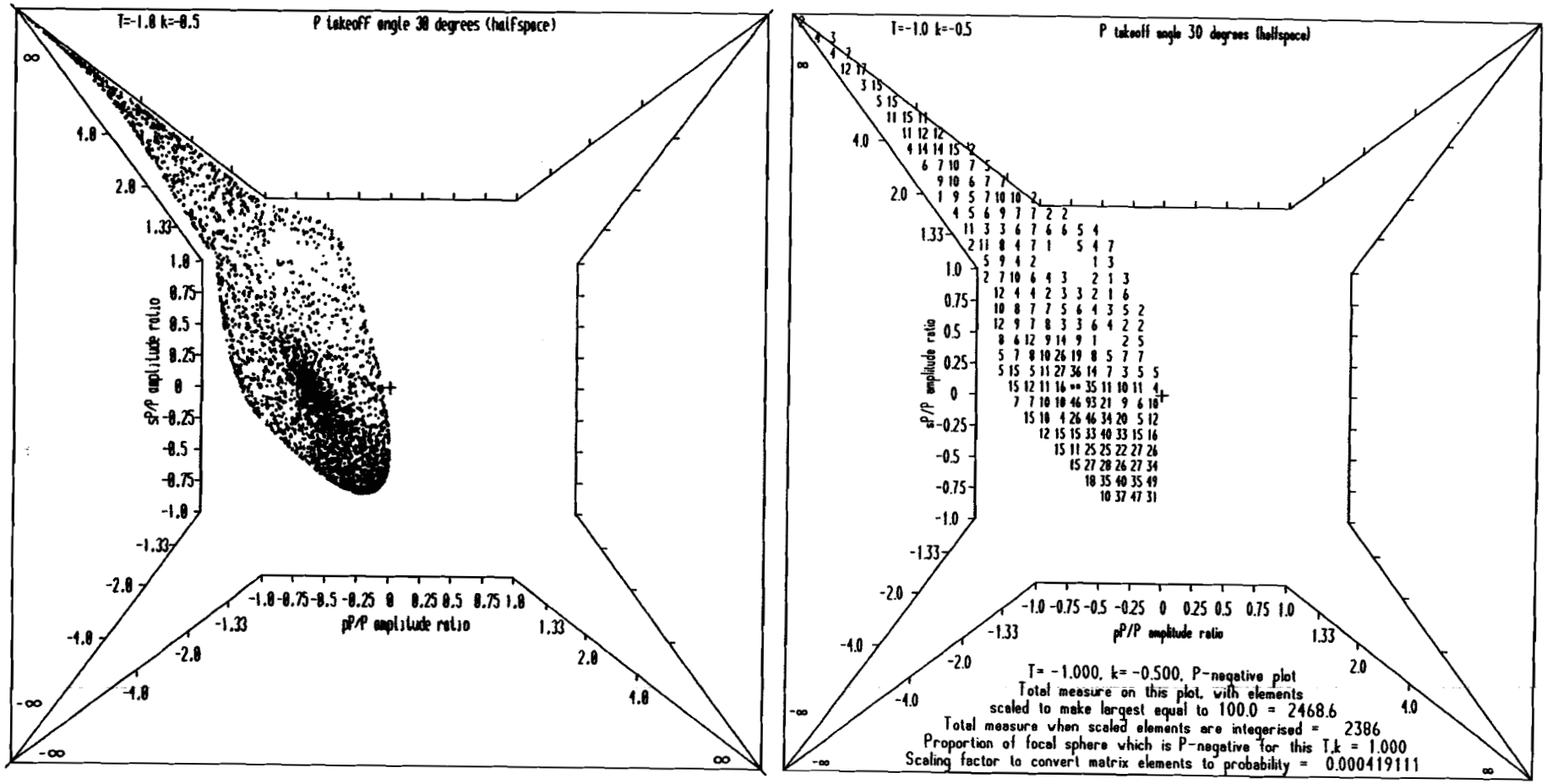
T=-1.0 k=-0.5
P takeoff angle 30 degrees (halfspace)
sP/P amplitude ratio
pP/P amplitude ratio
T= -1.000, k= -0.500, P-negative plot
Total measure on this plot, with elements
scaled to make largest equal to 100.0 = 2468.6
Total measure when scaled elements are integerised = 2386
Proportion of focal sphere which is P-negative for this T,k = 1.000
Scaling factor to convert matrix elements to probability = 0.000419111

Figure 97

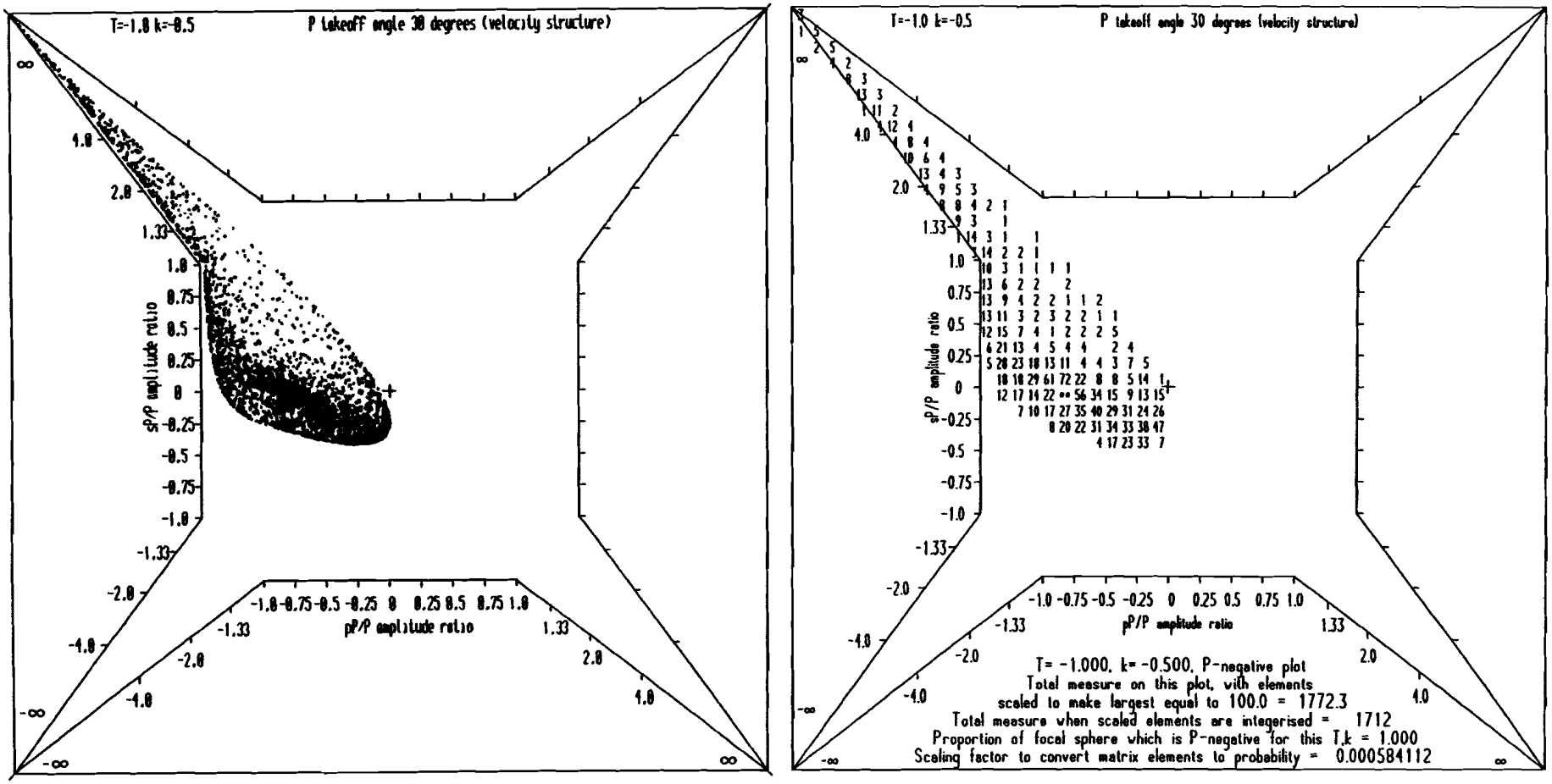
T=-1.0 k=-0.5
P takeoff angle 30 degrees (velocity structure)
sP/P amplitude ratio
pP/P amplitude ratio
T= -1.000, k= -0.500, P-negative plot
Total measure on this plot, with elements
scaled to make largest equal to 100.0 = 1772.3
Total measure when scaled elements are integerised = 1712
Proportion of focal sphere which is P-negative for this T,k = 1.000
Scaling factor to convert matrix elements to probability = 0.000584112

Figure 98

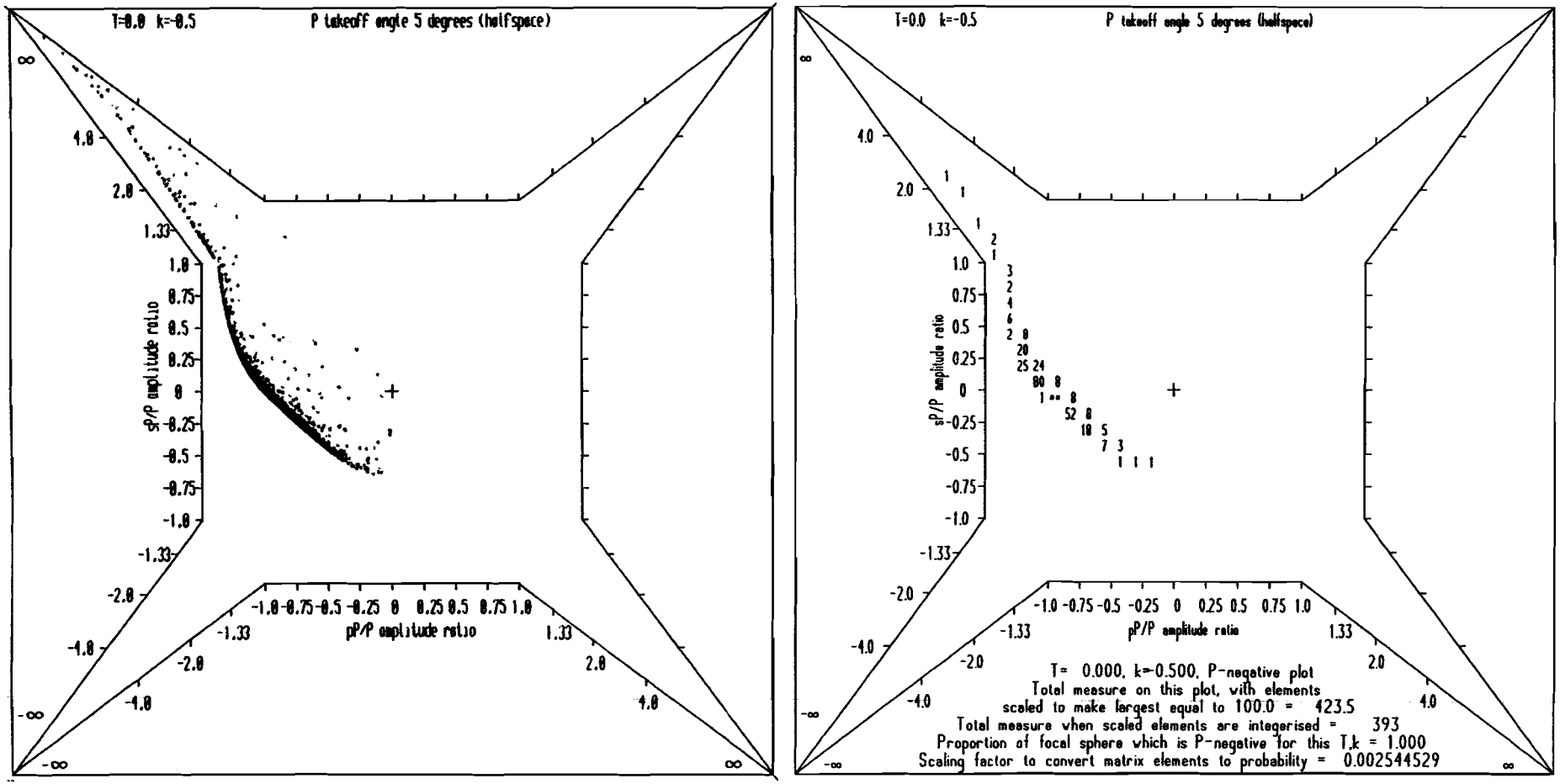
T=0.0 k=-0.5
P takeoff angle 5 degrees (halfspace)
sP/P amplitude ratio
pP/P amplitude ratio
T=0.0 k=-0.5
P takeoff angle 5 degrees (halfspace)
sP/P amplitude ratio
pP/P amplitude ratio
T= 0.000, k=-0.500, P-negative plot
Total measure on this plot, with elements
scaled to make largest equal to 100.0 = 423.5
Total measure when scaled elements are integerised = 393
Proportion of focal sphere which is P-negative for this T,k = 1.000
Scaling factor to convert matrix elements to probability = 0.002544529

Figure 99

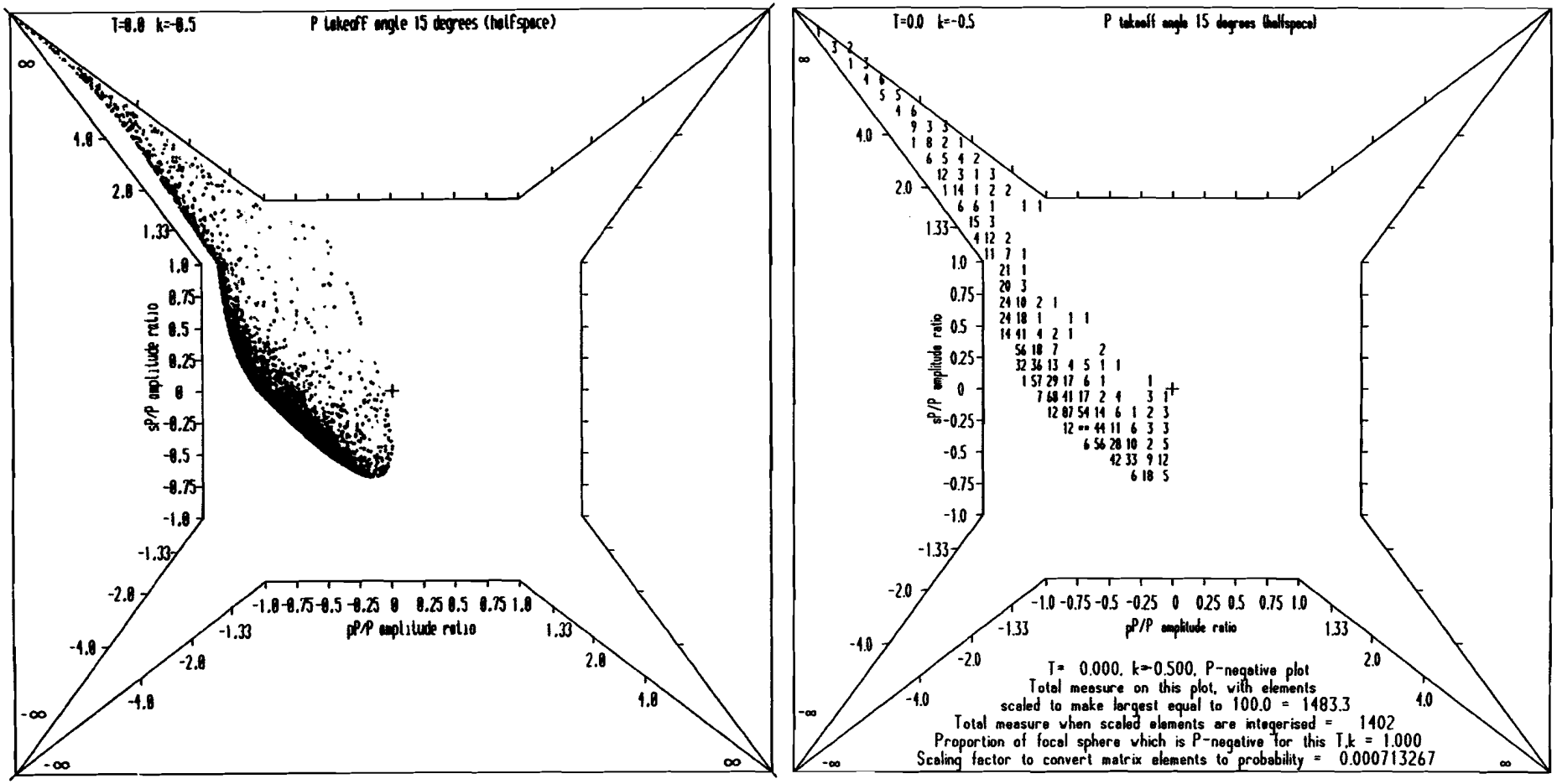
T=0.0 k=-0.5
P takeoff angle 15 degrees (halfspace)
sP/P amplitude ratio
pP/P amplitude ratio
T= 0.000, k=-0.500, P-negative plot
Total measure on this plot, with elements
scaled to make largest equal to 100.0 = 1483.3
Total measure when scaled elements are integerised = 1402
Proportion of focal sphere which is P-negative for this T,k = 1.000
Scaling factor to convert matrix elements to probability = 0.000713267

Figure 100

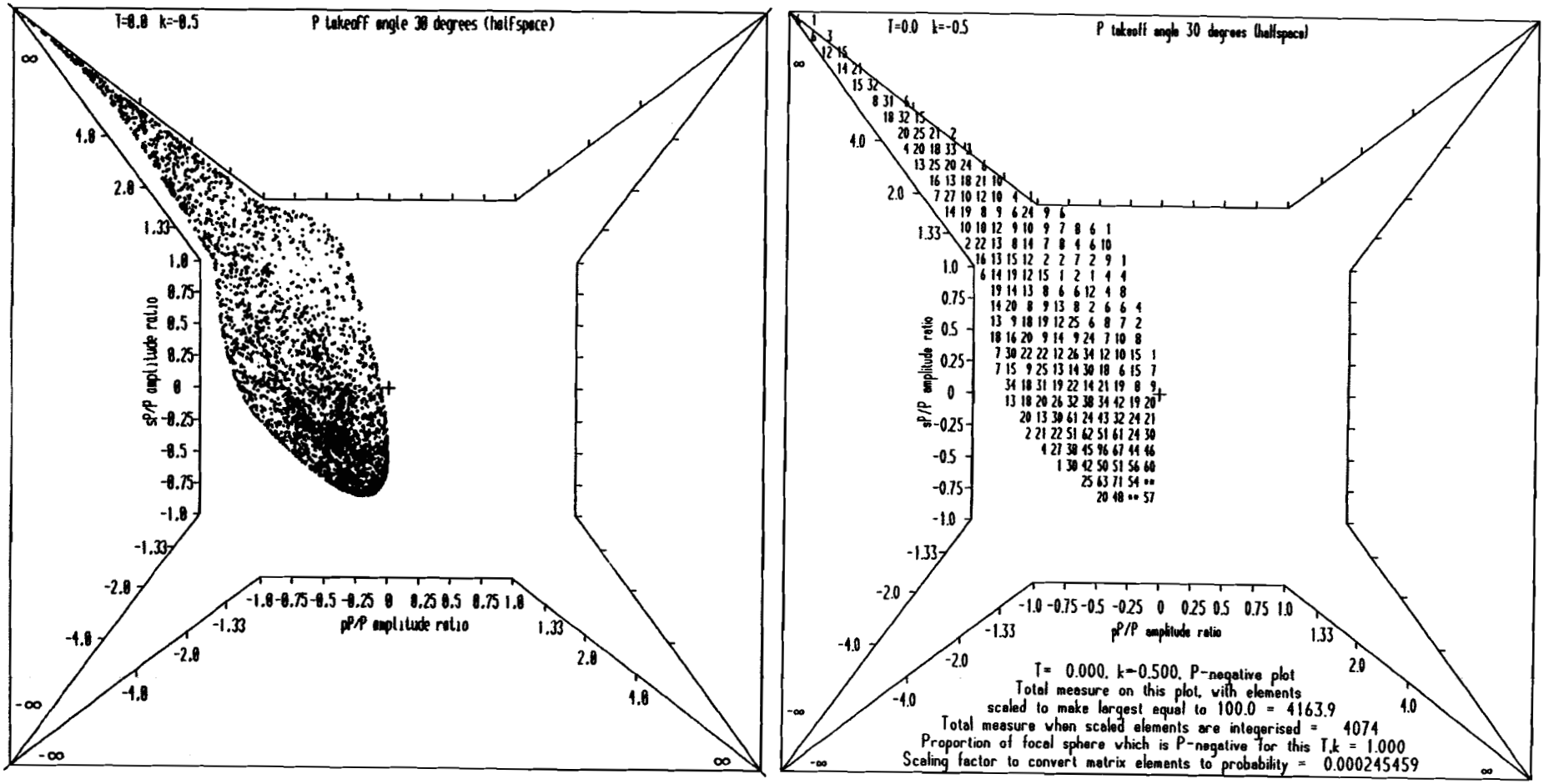
T=0.0 k=-0.5
P takeoff angle 30 degrees (halfspace)
sP/P amplitude ratio
pP/P amplitude ratio
T= 0.000, k=-0.500, P-negative plot
Total measure on this plot, with elements
scaled to make largest equal to 100.0 = 4163.9
Total measure when scaled elements are integerised = 4074
Proportion of focal sphere which is P-negative for this T,k = 1.000
Scaling factor to convert matrix elements to probability = 0.000245459

Figure 101

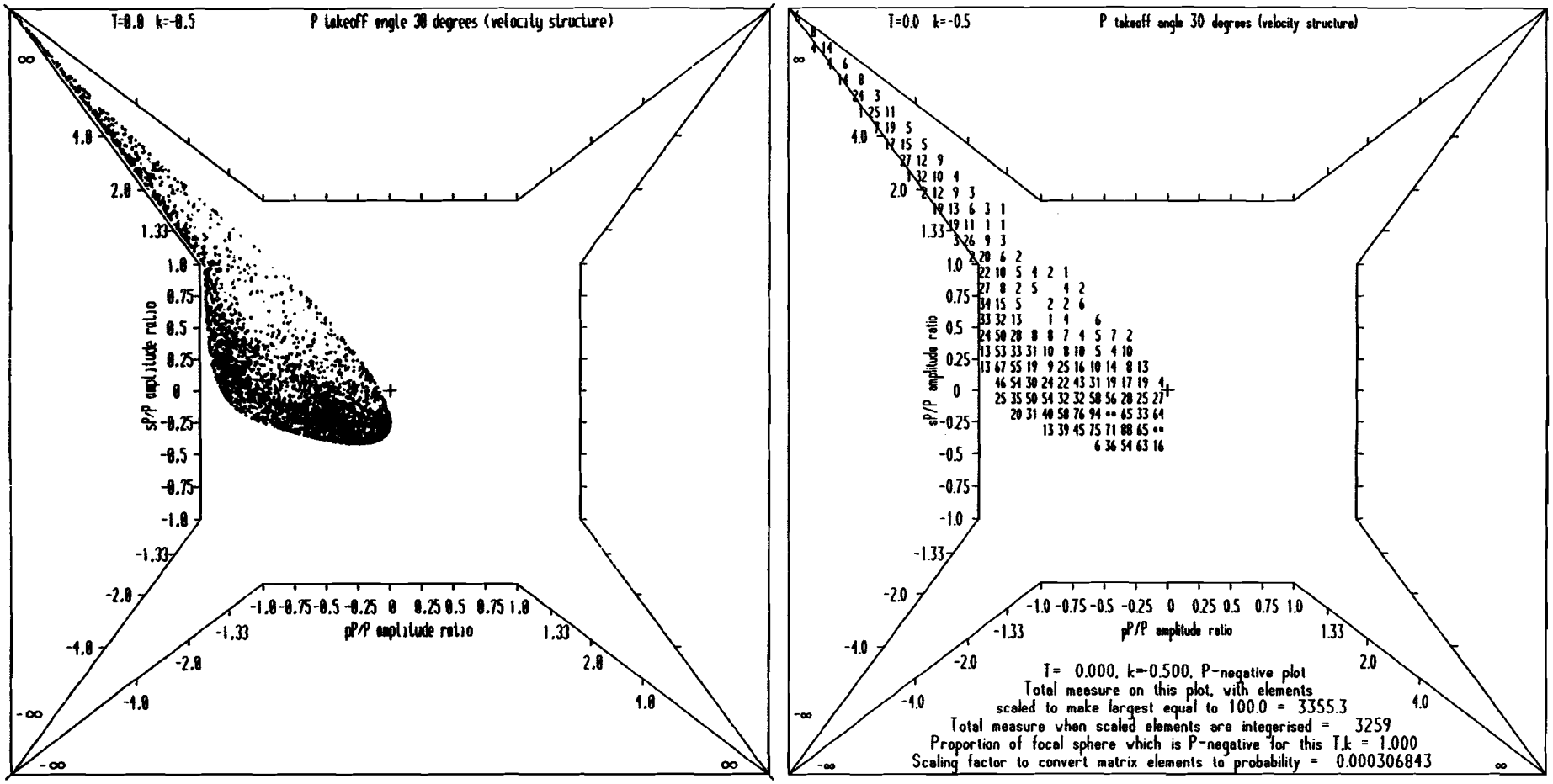
T=0.0 k=-0.5
P takeoff angle 30 degrees (velocity structure)
sP/P amplitude ratio
pP/P amplitude ratio
T= 0.000, k=-0.500, P-negative plot
Total measure on this plot, with elements
scaled to make largest equal to 100.0 = 3355.3
Total measure when scaled elements are integerised = 3259
Proportion of focal sphere which is P-negative for this T,k = 1.000
Scaling factor to convert matrix elements to probability = 0.000306843

Figure 102

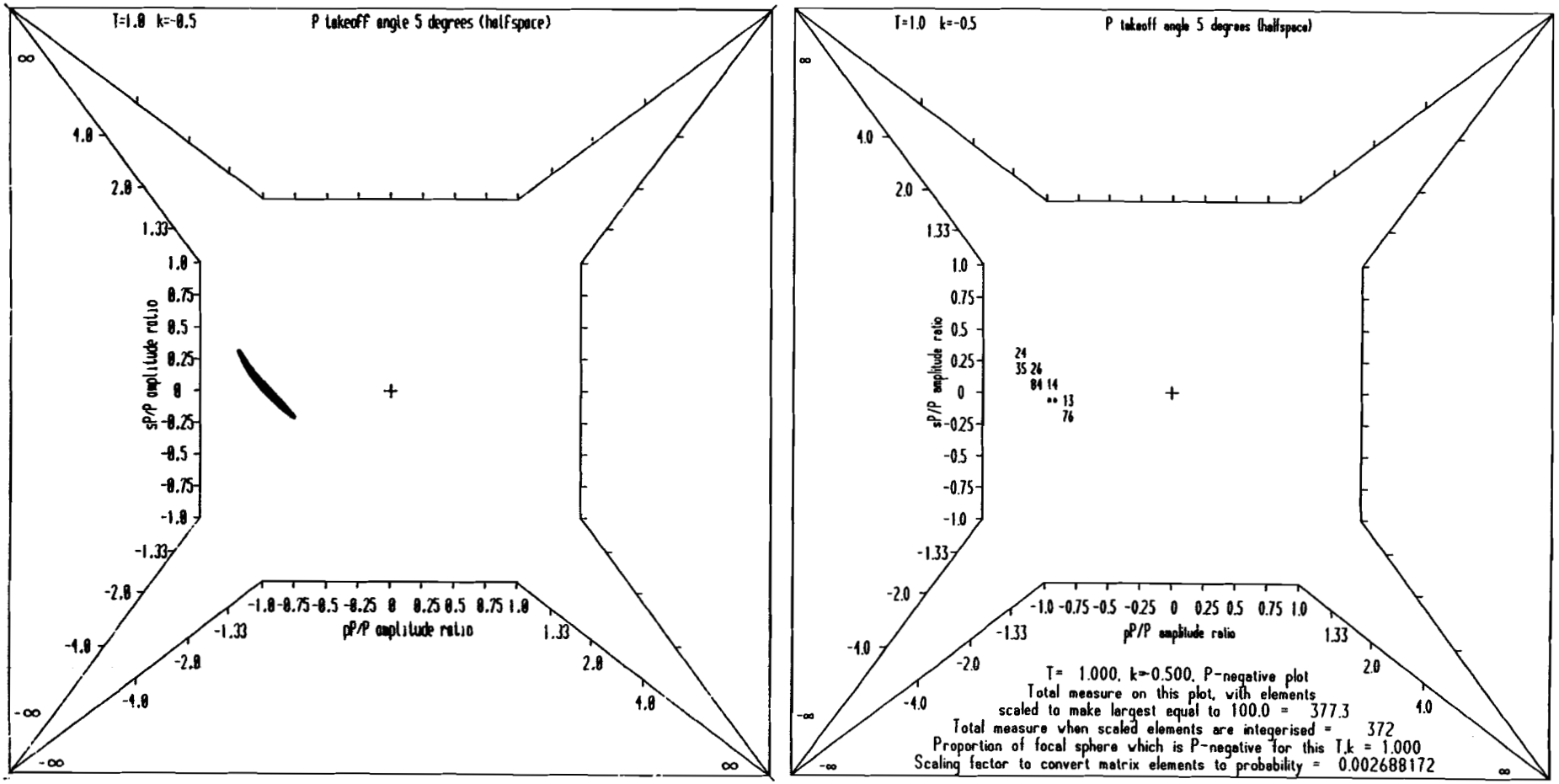
T=1.0 k=-0.5
P takeoff angle 5 degrees (halfspace)
sP/P amplitude ratio
pP/P amplitude ratio
T= 1.000, k=0.500, P-negative plot
Total measure on this plot, with elements
scaled to make largest equal to 100.0 = 377.3
Total measure when scaled elements are integerised = 372
Proportion of focal sphere which is P-negative for this T,k = 1.000
Scaling factor to convert matrix elements to probability = 0.002688172

Figure 103

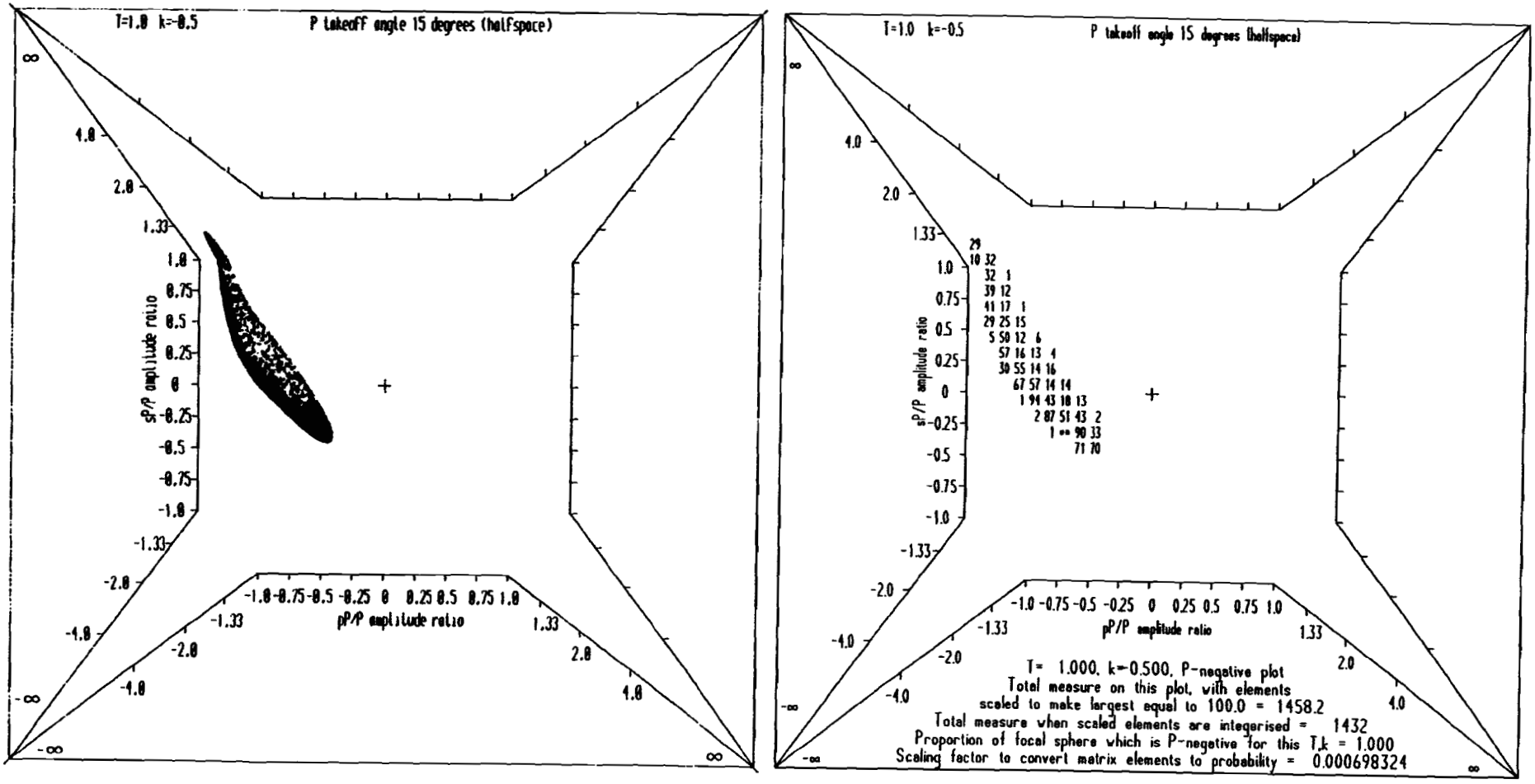
T=1.0 k=-0.5
P takeoff angle 15 degrees (halfspace)
sP/P amplitude ratio
pP/P amplitude ratio
T=1.0 k=-0.5
P takeoff angle 15 degrees (halfspace)
sP/P amplitude ratio
pP/P amplitude ratio
T= 1.000, k=-0.500, P-negative plot
Total measure on this plot, with elements
scaled to make largest equal to 100.0 = 1458.2
Total measure when scaled elements are integerised = 1432
Proportion of focal sphere which is P-negative for this T,k = 1.000
Scaling factor to convert matrix elements to probability = 0.000698324

Figure 104

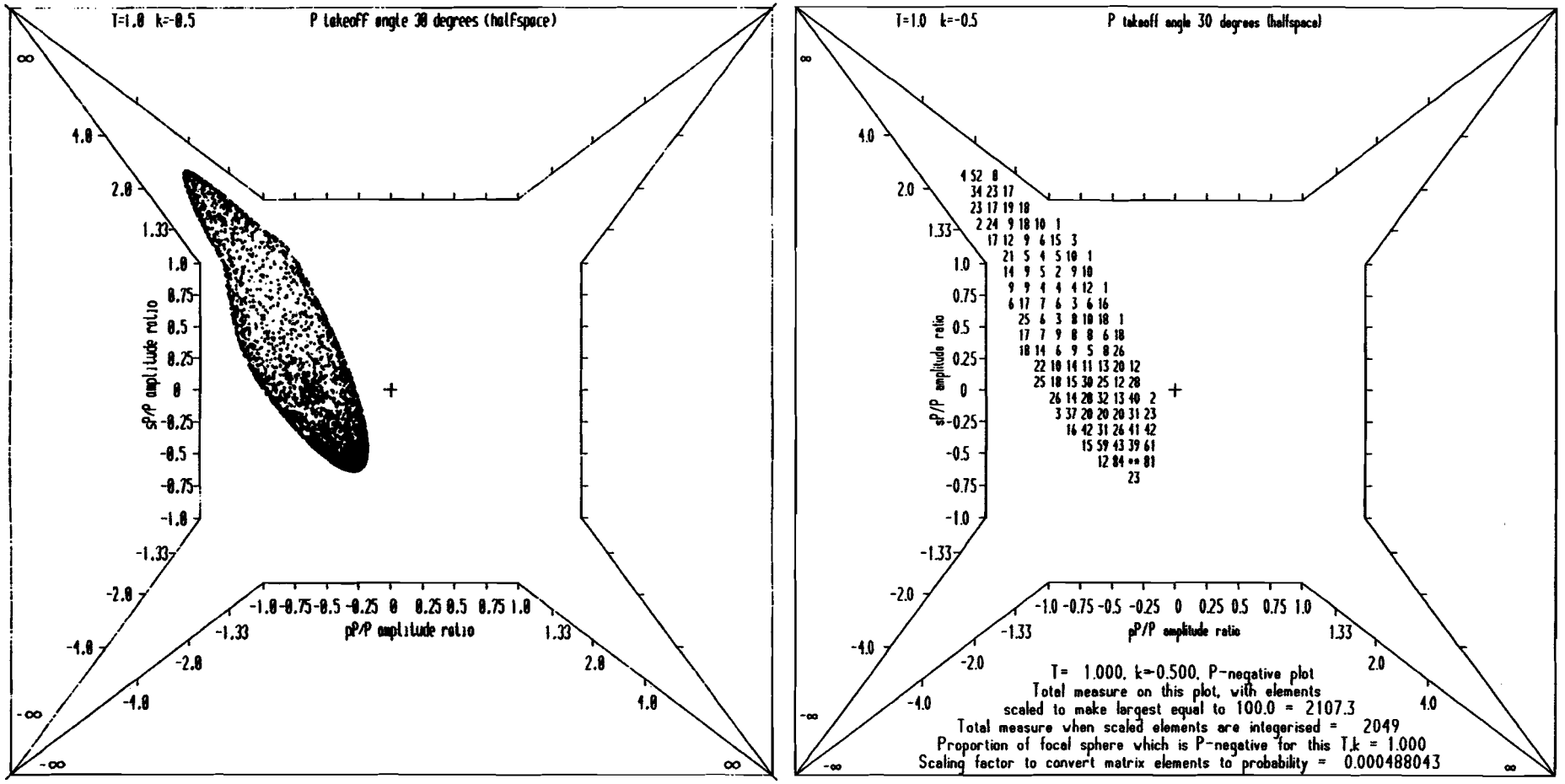
T=1.0 k=-0.5
P takeoff angle 30 degrees (halfspace)
sP/P amplitude ratio
pP/P amplitude ratio
T= 1.000, k=-0.500, P-negative plot
Total measure on this plot, with elements
scaled to make largest equal to 100.0 = 2107.3
Total measure when scaled elements are integerised = 2049
Proportion of focal sphere which is P-negative for this T,k = 1.000
Scaling factor to convert matrix elements to probability = 0.000488043

Figure 105

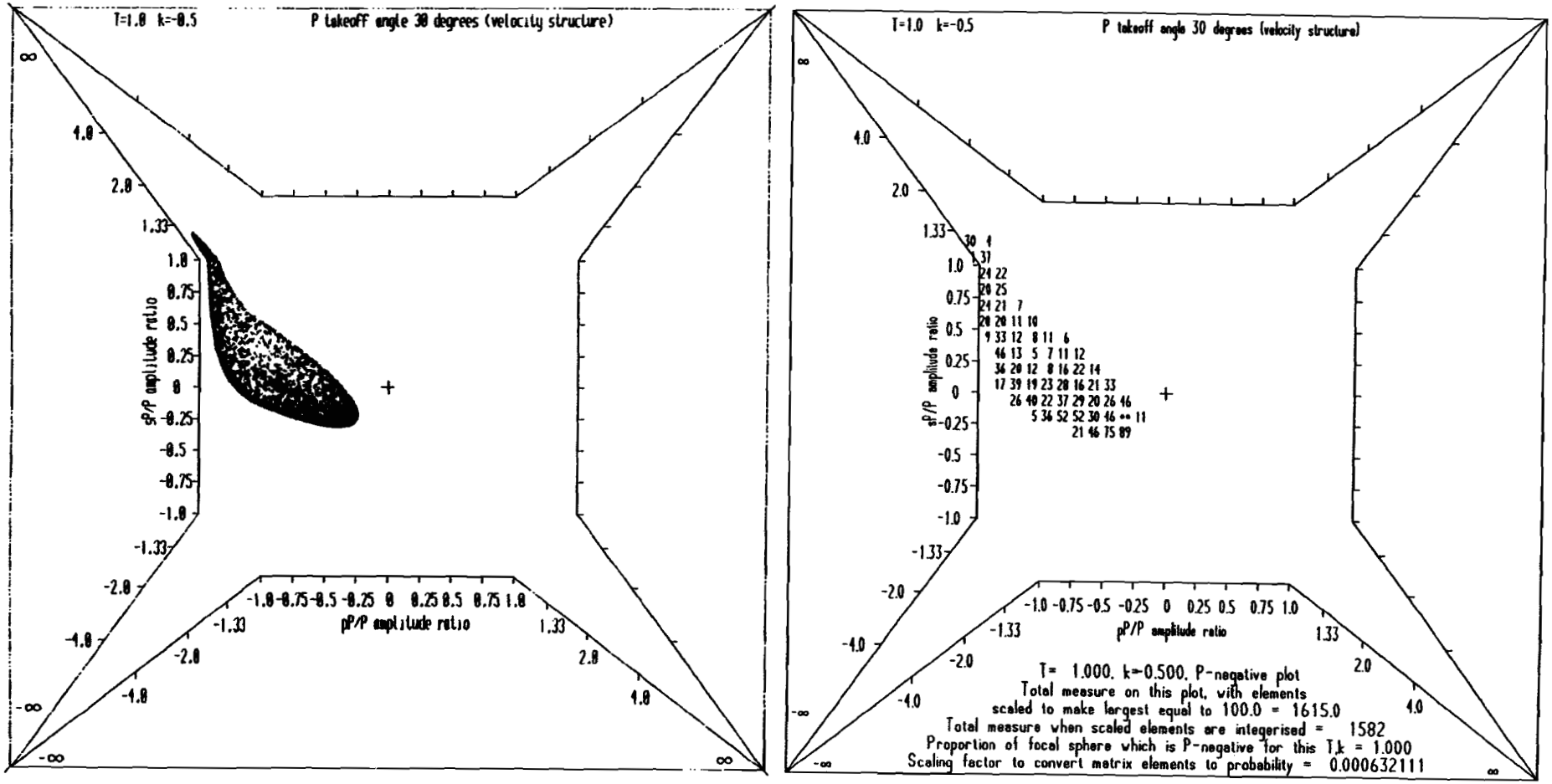
T=1.0 k=-0.5
P takeoff angle 30 degrees (velocity structure)
sP/P amplitude ratio
pP/P amplitude ratio
T= 1.000, k=0.500, P-negative plot
Total measure on this plot, with elements
scaled to make largest equal to 100.0 = 1615.0
Total measure when scaled elements are integerised = 1582
Proportion of focal sphere which is P-negative for this T,k = 1.000
Scaling factor to convert matrix elements to probability = 0.000632111

Figure 106

Available from

HER MAJESTY'S STATIONERY OFFICE

49 High Holborn, London W.C.1
71 Lothian Road, Edinburgh EH3 9AZ
9-12 Princess Street, Manchester M60 8AS
Southey House, Wine Street, Bristol BS1 2BQ
258 Broad Street, Birmingham B1 2HE
80 Chichester Street, Belfast BT1 4JY
or through a bookseller.

ISBN-0-85518206-7

Printed in England

UK UNLIMITED